JOURNAL OF APPLIED PHYSICS

JOURNAL OF APPLIED PHYSICS

Vol. 21, No. 6 JUNE, 1950

In This Issue

Special Issue on High Polymers

Page

Random Noise in Dielectric Materials R. F. Boyer 469
Emulsion Polymerization with Ultrasonic Vibration A. S. Ostroski and R. B. Stambaugh 478
Transitions in High Polymeric Materials Rolf Buchdahl and Lawrence E. Nielsen 482
Mechanical Properties of Oriented Polystyrene Film Lawrence E. Nielsen and Rolf Buchdahl 488
Non-Destructive Mechanical Test for Animal Fibers Harris M. Burte 494
Equivalent Effects of Time and Temperature in the Shear Creep and Recovery of Elastomers F. S. Conant, G. L. Hall, and W. James Lyons 499
Studies in Plasticization of Polyvinyl Chloride. I. Physical Changes and Their Measurement M. L. Dannis 505
Studies in Plasticization of Polyvinyl Chloride. II. Plasticizer Variations in PVC-Plasticizer Systems M. L. Dannis 510
Mechanical Properties of Substances of High Molecular Weight. VIII. Dispersion of Dynamic Rigidity and Viscosity in Concentrated Polyvinyl Acetate Solutions John D. Ferry, W. M. Sawyer, George V. Browning, and Arthur H. Groth, Jr. 513
Stress Phenomena from the Respective Viewpoints of Solid-State and High Polymer Physics Maurice L. Huggins 518
Some Theoretical Considerations of Dynamic-Property Data on Textile Specimens W. James Lyons 520
Equation of State for High Polymers R. S. Spencer and G. D. Gilmore 523
Behavior of Granulated Polymers under Pressure R. S. Spencer, G. D. Gilmore, and R. M. Wiley 527

Regular Contributed Original Research

Application of the Membrane Analogy to the Solution of Heat-Conduction Problems L. H. Wilson and A. J. Miles 532
Work Functions of the Elements Herbert B. Michaelson 536
Compilation of Body Wave Velocity Data for Cubic and Hexagonal Metals Louis Gold 541
Light Energy and Spectral Distribution for Some Important X-Ray Screens Holger Sköldborne 546
Unbalanced Terminations on a Shielded-Pair Line K. Tomiyasu 552
Shear Stress in a Turbulent Boundary Layer Donald Ross and J. M. Robertson 557
Propagation of the TM_{01} Mode in a Metal Tube Containing an Imperfect Dielectric David L. Hetrick 561
Ultra Speed Tensile of Rubber and Synthetic Elastomers D. S. Villars 565
Relations Concerning Wave Fronts and Reflectors K. S. Kelleher 573
Effect of an Obstacle in the Fresnel Field on the Distant Field of a Linear Radiator G. A. Woonton 577
Second-Order Transition Temperatures and Related Properties of Polystyrene. I. Influence of Molecular Weight Thomas G. Fox, Jr. and Paul J. Flory 581
Electrical Breakdown in CSF_5 Ronald Geballe and Fred S. Linn 592
Effect of Cold-Work Distortion on X-Ray Patterns B. E. Warren and B. L. Averbach 595
Quantized Theory of Strain Hardening as Applied to the Cutting of Metals Milton C. Shaw 599
Mechanical and Electrical Properties of Plasticized Vinyl Chloride Compositions Lawrence E. Nielsen, Rolf Buchdahl, and Rita Levreault 607
Letters to the Editor:
X-Ray Tube Producing a Beam of X-Rays Convergent to a Point C. H. Bachman and S. J. Silverman 615
On Turbulent Jet Mixing in Two-Dimensional Supersonic Flow D. Bershader and S. I. Pai 616
Use of Brightness Temperatures in Richardson Plots Henry F. Ivey 616
Stroboscopic Mapping of Time-Variable Fields L. Marton and D. L. Reverdin 617
Announcement 618
Index to Advertisers xxvi

BOARD OF EDITORS
Elmer Hutchisson, *Editor*

Associate Editors
Howard H. Aiken
Otto Beeck
James Hillier
W. James Lyons
Philip Morrison
Eric Reissner
Raymond J. Seeger
Frederick Seitz
Charles S. Smith

Publication of the American Institute of Physics

OFFICERS
George R. Harrison, *Chairman*
George B. Pegram, *Treasurer*
John T. Tate, *Adviser on Publications*

GOVERNING BOARD
J. W. Beams
C. Paul Boner
Wallace R. Brode
W. F. Fair, Jr.
J. B. Fisk
G. P. Harnwell
George R. Harrison
W. V. Houston
Rudolph Kingslake
Paul Kirkpatrick
Paul E. Klopsteg
F. W. Loomis
Philip M. Morse
J. R. Oppenheimer
George B. Pegram
Harold K. Schilling
Francis G. Slack
John C. Steinberg
John T. Tate

Consultant on Printing
Melvin Loos

ADMINISTRATIVE STAFF
Henry A. Barton, *Director*
Wallace Waterfall, *Executive Secretary*
Theodore Vorburger, *Assistant Treasurer and Comptroller*
Ruth F. Bryans, *Publication Manager*
Betty Hofstadter, *Assistant Secretary*
Eileen B. Neuberger, *Circulation Manager*

The Journal of Applied Physics, published monthly at Prince and Lemon Sts., Lancaster, Pa., is devoted to physics in its role as the science basic to other natural sciences and to the arts and industries. Previous to 1937 this publication was known as Physics. The Journal of Applied Physics publishes editorials and reviews, as well as technical papers of applied physics. Articles appearing in it are indexed regularly, according to their field, by Physics Abstracts, Chemical Abstracts, Engineering Index, Inc., Industrial Arts Index, etc.

Manuscripts should be submitted to Elmer Hutchisson, Editor, Case Institute of Technology, Cleveland 6, Ohio. Unless otherwise stated, submission of a manuscript is a representation that it has been neither copyrighted, published, not submitted for publication elsewhere. The authors' institutions are requested to pay a **publication charge** of $8 per page which, if honored, entitles them to 100 reprints without further charge. Instructions will be sent with galley proofs.

Subscriptions, renewals, and orders for back numbers should be addressed to the American Institute of Physics, 57 East 55 Street, New York 22, New York.

Subscription Price	U.S. and Canada	Elsewhere
To members and associate members of the American Institute of Physics	$7.00	$ 8.00
To all others	9.00	10.00

Back Number Prices

Yearly back number rate when complete year is available: $10.00. Single copies: $1.00 each.

Changes of address should be sent to the American Institute of Physics; **corrected proofs** should be sent to the Publication Manager, American Institute of Physics. **Advertising rates** supplied on request. Orders, advertising copy, and cuts should be sent to the American Institute of Physics.

Entered as second class matter January 22, 1937, at the Post Office at Lancaster, Pennsylvania, under the Act of March 3, 1879. Accepted for mailing at the special rate of postage provided for in paragraph (d-2), section 34.40, P. L. & R. of 1948, authorized May 2, 1932.

Journal
of
Applied Physics

Volume 21, Number 6 June, 1950

Special Issue on High Polymer Physics

The following thirteen papers were presented at the meeting of the Division of High Polymer Physics of the American Physical Society in New York City, February 2–4, 1950.

Random Noise in Dielectric Materials

R. F. Boyer
The Dow Chemical Company, Midland, Michigan

When thin films of polar plastic materials are subjected to d.c. potentials of 10 to 300 volts per mil they exhibit current fluctuations (with frequencies in the range of 60 to 1000 c.p.s.) which last for minutes and which even persist for a few seconds on removing the voltage. These fluctuations are about 1000 fold above the noise level of the circuit and are about 1 percent of the steady d.c. current. They eventually die out but can usually be restored by reversing the polarity. This noise is greater the more polar the nature of the polymer and the higher its moisture content. The effect seems to arise from water or impurity ions which can jump whenever a hole opens between polymer chains and is thus an activated rate process sufficiently slowed down by the highly viscous nature of the polymeric medium to be readily observable. On an oscillograph screen it is possible to see both the forward and the backward diffusion. This noise is most pronounced in Cellophane, Nylon, and copolymers of vinylidene chloride with acrylonitrile, but also appears with polystyrene stored at 86 percent relative humidity. Films of methylcellulose do not show the effect. Numerically the effect seems to arise from the random motion of groups of several hundred ions as a unit. As an extension of these ideas it is suggested and demonstrated that the moisture vapor diffusion constants for a series of polymers increase with the frequency of the loss factor maximum while the moisture vapor permeability increases with the direct current conductivity.

INTRODUCTION

WHEN a direct current potential of the order of 100 volts/mil is applied to a thin film of dielectric material, as in making a resistivity test, it is always observed that there is an initial high current which drops off rapidly to an approximately steady value. Thus it is customary to measure the current after one minute duration and use this value in computing the specific resistivity. We find however that this "steady" current actually fluctuates in a seemingly random manner. The magnitude of these fluctuations is usually about one percent or less of the average current flow. The duration of this random current is a matter of minutes and in some cases up to an hour or more: depending on the kind of material, moisture content, thickness of sample, and applied voltage.

It is the purpose of this paper to discuss in a general way the main features of this random noise effect; to relate it with the general mechanism of moisture vapor transmission through polymers; and to show how the moisture vapor transmission is numerically related to the d.c. conductivity and the a.c. loss factor of the polymer. Since this random noise effect is apparently a new one, there are many aspects of it which are still obscure to us.

HISTORY

In 1945 R. H. Campbell of the Webster Electric Company informed us that samples of Saran film (vinylidene chloride—10 percent vinyl chloride copolymer) used in condenser A of the high gain circuit of Fig. 1 caused a plopping noise in the loudspeaker whereas polystyrene did not show this effect. Mr. Campbell suspected moisture. We considered it a possible dipole analog of the Barkhausen effect wherein whole regions of dipoles would rotate as a unit. Indeed we tried to look for such effects on a 1000-cycle bridge circuit which used a cathode ray oscillograph as a null indicator, but we were unsuccessful. Two years ago it was decided to repeat Mr. Campbell's observations by using an identical circuit except that the input resistance of our amplifier was 5 meg. We checked his findings. Moreover, we also connected the amplifier output to a Brush recording

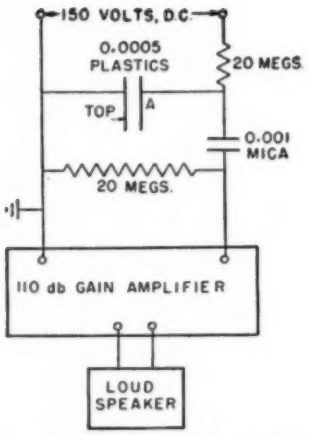

FIG. 1. Circuit used for noise studies. A is the experimental condenser. The amplifier has a 5-megohm input resistance, and cuts off below 30 cycles. In later studies the 0.001 mica blocking condenser was eliminated and the experimental condenser substituted in its place to simplify the circuit.

oscillograph[1] and obtained a permanent record of these plops. They were relatively weak and only a factor of two above the basic noise of the circuit which was estimated to be about a microvolt.

We next tried some other types of vinylidene chloride copolymers, particularly the ones with high acrylonitrile content[2] which would have a high dipole moment. These proved to be quite noisy, with voltage fluctuations of several millivolts. A number of other plastic materials such as Nylon, rubber hydrochloride, paper, Cellophane, plasticized polyvinyl chloride, etc., were then checked. Each of these proved to be more noisy than the original saran sample, although each had a characteristic noise. In fact, it could be said that both the "noise" in the loudspeaker and the pattern drawn by Brush recorders were characteristic of a material. For example, Saran gave an occasional dull plop, Nylon a hissing or frying noise, polyvinyl chloride a scratchy noise. We realize the inadequacy of such verbal descriptions but an examination of typical records may clarify these descriptions. There was, as will be seen later in Fig. 6, a difference in the tracings made by the 60- and 120-cycle pen arms of the Brush recorder. Obviously each "noise" has a frequency distribution spectrum: the Brush oscillograph measures predominantly the low frequency component (say up to 100 cycles); the loudspeaker responds well up to 10,000 cycles, etc. In some instances visual observation of the screen of a fast cathode-ray oscillograph was employed to study the high frequency components in more detail.

Figure 2 shows a time sequence on a sample of coated Cellophane 1.5 mils thick to which 150 volts was applied. Each horizontal line represents one foot of record or one minute of elapsed time while the numbers at the end of the line represent the number of feet of record which has been deleted. The symbols along the chart indicate various operations: B-150 signifies the application of 150 volts d.c. with the bottom electrode negative. The vertical scale is voltage, the maximum peaks representing about 25 mv. At B^+ the polarity on the sample was reversed, leading to considerable noise. Reversal of the voltage as in line 3 leads to a gradual diminution of the noise; the reversal to B^+ in line 6 restores the noise to full intensity with little inclination to die off. Reversal in line 7 again leads to a decaying noise.

The various details of Fig. 2 are characteristic of the behavior of most of the materials, the variation from material to material lying in the direction of intensity of the noise, duration under a given applied voltage, and what we might call the general random behavior of the noise. The main features of Fig. 2, generalized to include most of our experience, are as follows.

1. The noise is usually small at the beginning and its onset may require either a fixed voltage applied for some seconds, or several reversals of the voltage, or increasing the applied voltage to a high value—say 300 volts until the noise starts, and then reducing the voltage.

2. There are usually directional effects in the films. This is quite understandable in a coated Cellophane whereas with a material such as Nylon it might be presumed that manufacturing operations give a different structure to the two surfaces.

3. The noise usually dies out with time but can be restored in general by reversal of the polarity or by increasing the applied voltage. Eventually however, most samples become dead and nothing will restore the

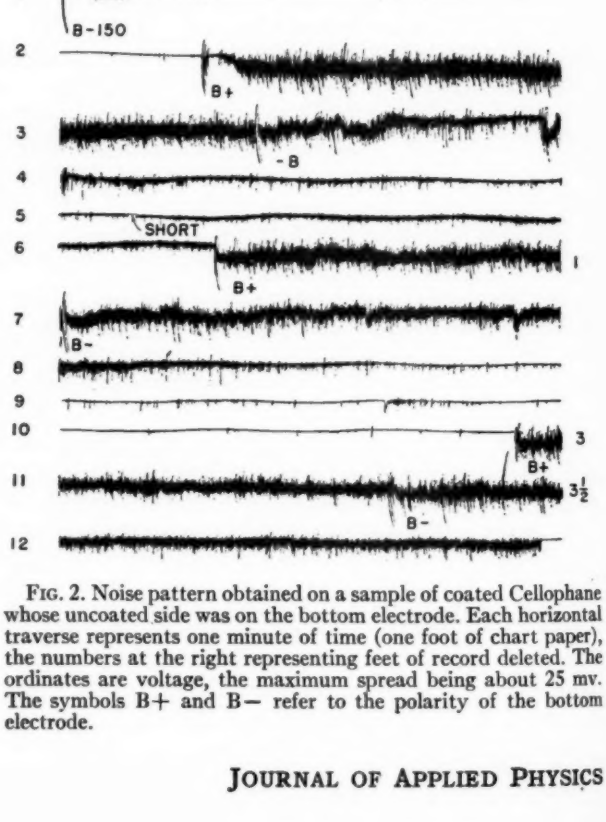

FIG. 2. Noise pattern obtained on a sample of coated Cellophane whose uncoated side was on the bottom electrode. Each horizontal traverse represents one minute of time (one foot of chart paper), the numbers at the right representing feet of record deleted. The ordinates are voltage, the maximum spread being about 25 mv. The symbols B+ and B− refer to the polarity of the bottom electrode.

[1] The Brush Development Company, Cleveland, Ohio.
[2] United States Patent 2,238,020.

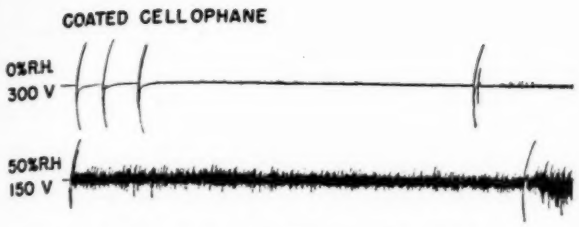

FIG. 3. Effect of relative humidity at which sample was stored on noise pattern of coated Cellophane.

noise. This abrupt termination of the noise is frequently preceded by a particularly loud burst of noise, and one gets the impression of actual dielectric breakdown although we have never noted any visual signs of breakdown.

4. One further effect was noted especially on polyethylene at 86 percent R.H. and 300 volts: the noise level was generally low but at almost regular intervals would increase at least fivefold, persist for a few cycles, and then resume its low level. These bursts would repeat themselves. At low voltages a normal noise pattern similar to that of Fig. 6 (c and d) appears.

In the early work, before these various effects were completely understood, many seeming anomalies were noted, such as apparent failure of the noise to occur with certain types of metal electrodes. We now believe that the single most important variable is the relative humidity at which the sample has been stored. In general the intensity of noise increases with the moisture content and polarity of the sample.

Figure 3 illustrates the effect of relative humidity on coated Cellophane. At zero percent R.H. the sample showed very little activity even at 300 volts and the few displacements which were observed were mostly in one direction with respect to the base line of the recording. At 50 percent relative humidity and with the voltage decreased to 150 volts, the noise has increased tremendously, and the pattern is distributed on both sides of the zero. Figure 4 shows similar behavior for a copolymer of 60 percent vinylidene chloride—40 percent acrylonitrile where the humidity has been carried to 86 percent. At 86 percent R.H. and 250 volts, the loudspeaker was emitting a siren-like noise of gradually increasing pitch and intensity. Figure 5 shows the effect of relative humidity on Nylon; in this case, at 86 percent R.H., the voltage was dropped to 67 volts and still gave a pronounced effect. Here again it is particularly evident that the character of the noise changes markedly on increasing the voltage: low voltages give records symmetrical about the zero line, high voltages gave a more assymmetric recording. This effect will be discussed in the theoretical section.

It should be emphasized that the relative humidity values just given refer to those at which the samples had been stored for 24 hours or more. The measuring electrodes (with associated resistances and capacitors) were housed in a brass case for good electrical shielding. When

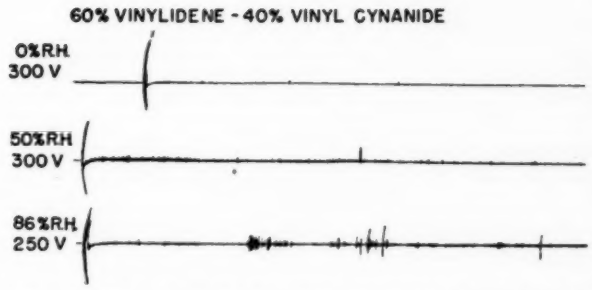

FIG. 4. Effect of relative humidity on current fluctuations in a 60 percent vinylidenechloride — 40 percent vinylcyanide copolymer. The fluctuations are unsymmetrical about the axis at high voltage, become symmetrical at higher humidities and lower voltages. The loud speaker emitted a siren-like noise while the bottom line was being recorded.

the film sample was removed from its humidity chamber and placed in the measuring apparatus, where ambient conditions prevailed, the sample either lost or gained moisture. This fact accounts for some but not all of the anomalous behavior which was found. Since the relative humidity of the room was around 20–30 percent for many of these measurements, the very active samples of high moisture content tended to dry out and lose activity. However, Cellophane has an equilibrium moisture content of about five percent even at 20 percent R.H. and hence still has fairly high activity at all times. We noted one case in which the voltage remained on a Cellophane sample overnight; in the morning the sample showed no noise until the voltage was reversed, when it was extremely noisy.

We might conclude this section with a brief description of several additional experiments. Various types of electrodes were tried, such as aluminum, brass, lead and silver, with no appreciable differences as long as a fresh sample of plastic was taken each time from the humidity chamber. Brass was the standard electrode material and was used for all curves given in this report. In general a one-inch diameter electrode was used unless otherwise noted.

A sevenfold range of sample thickness (0.0004 to 0.0028 in.) at a constant potential gradient of 15 volts per mil on a 60 percent vinylidene chloride—40 percent acrylonitrile copolymer at 50 percent R.H. was studied. Each sample was run on one polarity until the noise

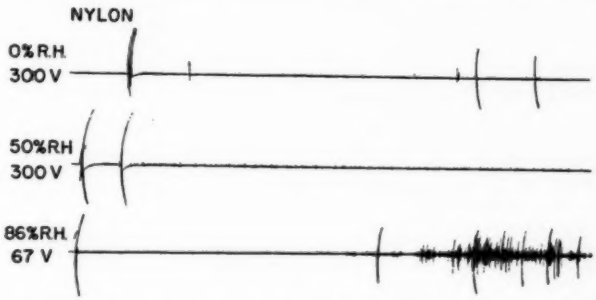

FIG. 5. Effect of relative humidity on Nylon noise pattern. The time scale here as in Figs. 3 and 4 is one minute per horizontal traverse.

stopped. This end point was naturally somewhat arbitrary, but in general the duration of the noise increased linearly with the thickness.

Some of the more noisy materials such as Cellophane were run between two films of polystyrene. They still gave a characteristic noise diminished in intensity. Polystyrene alone did not show this effect unless it had been conditioned first at 86 percent R.H. Films of water soluble methylcellulose were run but did not give any noise apparently because of their extremely high conductivity. If, however, a methocel film was sandwiched between two sheets of polystyrene, it did give a reproducible pattern both on applying and removing the potential, although this pattern does not have the character of a noise but rather of an oscillatory discharge.

We are reserving until a later time studies of the effect of temperature on these noise phenomena. It will be necessary to vary the temperature while keeping the moisture content of the sample approximately constant.

Before concluding this experimental section we wish to call attention to some of the prior literature where analogous effects have been described. Haworth and Bozorth[3] in studying pre-breakdown phenomena in glass observed that the current is "noisy," and occurs in pulses which grow in magnitude as the field intensity increases. Von Hippel[4] has also observed similar effects. Tykociner, Brown, and Paine[5] observed oscillations associated with oil-impregnated paper at high field strengths, and arising from voids in the dielectric. Austen and Hackett[6] ascribe similar effects to the sudden discharge of a local region of the dielectric of lower electric strength than the dielectric in series with it: This discharge may give the appearance of an oscillating current if the circuit constants are of the correct magnitude. Quite recently Glass[7] has studied leakage noise in a number of dielectric materials, both ceramic and organic, at high humidities and high applied voltages. His principle source of noise was surface leakage at the high relative humidity of the samples. Teflon and fluorothene were the only materials free from such effects.

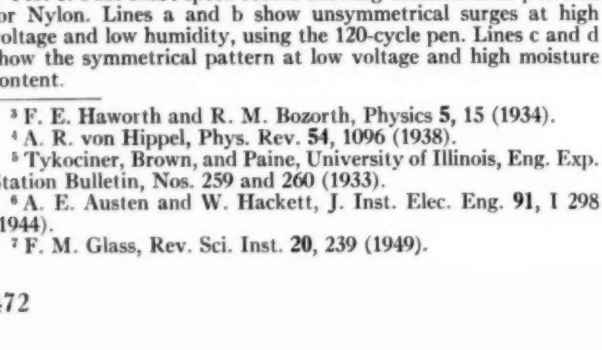

FIG. 6. Fast chart speed record showing detailed noise patterns for Nylon. Lines a and b show unsymmetrical surges at high voltage and low humidity, using the 120-cycle pen. Lines c and d show the symmetrical pattern at low voltage and high moisture content.

[3] F. E. Haworth and R. M. Bozorth, Physics **5**, 15 (1934).
[4] A. R. von Hippel, Phys. Rev. **54**, 1096 (1938).
[5] Tykociner, Brown, and Paine, University of Illinois, Eng. Exp. Station Bulletin, Nos. 259 and 260 (1933).
[6] A. E. Austen and W. Hackett, J. Inst. Elec. Eng. **91**, I 298 (1944).
[7] F. M. Glass, Rev. Sci. Inst. **20**, 239 (1949).

Seitz has given a general theory[8] of electron multiplication processes in crystals, which lead to the current avalanches that precede and eventually cause dielectric breakdown. The effects described in the present paper occur at voltages from 15 to 300 volts per mil, whereas the dielectric strengths of the various materials studied range from about 500 to 5000 volts per mil.

Incidentally, some years ago Whitehead and Nethercot[9] studied dielectric breakdown in cellulose acetate, which they called a moist dielectric. They found that this material did not obey Ohm's law but that the conductivity increased linearly with voltage up to 140,000 volts/cm, and even more rapidly at still higher voltages. They spoke of "ion avalanches" as occurring at these higher voltages and actually preceding dielectric breakdown.

More recently Whitehead[10] has presented oscillograph tracings showing the current resulting from applying an alternating potential to polyethylene. There is good evidence on these tracings for what we would call a noise pattern.

THEORETICAL DISCUSSION

The general effects just described in Figs. 2–5 might arise from surface or volume ionic conduction or from rotation of large regions of dipoles. It seems quite possible that several of these effects might be operating together. We are inclined to rule out dipole rotation first on the basis of some of the long-time effects observed, and secondly, because of the marked effect of moisture on polymers such as saran which one would not expect to be markedly plasticized by the absorption of a few hundredths of a percent of water. The cooperative movement of large groups of dipoles would likely be confined to crystalline polymers. Surface conduction, while possibly important at high relative humidities, cannot be of any appreciable importance for samples stored at zero percent R.H., where the noise is still observable at high voltages. We did not use a guard ring on the electrodes. Surface conduction would certainly follow a different mechanism than that of volume conduction, and probably would not place as great dependence on the size of the diffusing ion.

We are thus strongly inclined to view the various phenomena discussed in this paper as arising from the migration of ions through the polymer under the applied electric field. The ions are presumably those of H^+ and OH^- although in the case of saran it is quite possible that Cl^- ions are also present while each of the other polymers may have characteristic impurity ions, both organic and inorganic.

[8] F. Seitz, Phys. Rev. **76**, 1376 (1949).
[9] S. Whitehead and W. Nethercot, Proc. Phys. Soc. **47**, 974 (1935).
[10] S. Whitehead, Trans. Faraday Soc. **42A**, 66 (1946).

According to Stearn and Eyring,[11,12] the migration of ions in an electric field is susceptible to the usual absolute reaction rate treatment whereby the observed ionic currents are the net resultant of a forward movement of the ions in the direction of the applied field and a backward diffusion because of the concentration gradient of ions thus established. Or

$$\text{Net rate} = (NDc\varphi ze/kT) - NDdc/dx. \qquad (1)$$

N=Avogadro number. D=Diffusion constant of ion. c=Concentration of ion. φ=Potential gradient. z=Valence of ion. e=Electronic charge. dc/dx=Concentration gradient. k=Boltzmann constant. T=Absolute temperature.

Under high potential gradients the second term is almost negligible and the observed current fluctuations are primarily in one direction as may be seen in Fig. 6(a and b) for Nylon film of 0.9 mil thickness at zero percent R.H. and 280 volts applied potential. At higher relative humidities where the fluctuations are much greater and the voltages are greatly reduced, then these fluctuations occur on either side of zero, as can be seen in Fig. 6(c and d) for the same Nylon film.

It might be pointed out that these current fluctuations are frequently of such magnitude as to cause an observable shift in the "steady" current. This can be seen, for example, in line 3 of Fig. 2 where the entire noise pattern shifts its center. Such effects can also be seen on the cathode-ray oscillograph where the base line moves up or down with large fluctuations. It would be desirable, obviously, to record this d.c. component simultaneously with the noise pattern.

We believe these fluctuations arise because of the nature of the medium in which the ionic conduction occurs. One is quite familiar with the mechanism for moisture vapor transmission through polymers as pictured by Barrer and others in terms of absolute reaction rate theory. This theory pictures that as a result of segmental motion of the polymer chains holes occasionally open through which the water molecules can diffuse. This segmental motion presumably has a natural frequency corresponding to that of the peak in the loss factor *vs.* frequency curve for various polymers.

If we apply a similar picture to ionic migration, it will be recognized that on a molecular scale the movement of ions in the direction of the field will be sporadic and that fluctuation phenomena might occur at about the usual frequency for dielectric response. Thus the highly viscous nature of the polymeric medium presumably slows down hole formation to a convenient rate for observation, and makes the measurement of conduction current through such a specimen a convenient tool for the study of this internal molecular process.

If, however, the energy acquired by an ion in the applied field is not too large as compared with kT, then the backward jumps of the ions, as indicated by Eq. (1) will become important. This backward rate must also occur at a rate governed by the frequency of motion of the chain segments. Moreover, it seems likely, especially if H^+ and OH^- ions only are involved, that both types of ions will be subject to the forward and backward jumps, each at its own characteristic rate. Thus the observed noise will be a composite resultant of the random motions

TABLE I. Distribution of amplitudes of noise.

Ordinate in mm	No. of intersections on 60-cycle pen tracing: Cellophane 180 v 50% R.H. 5 mm = 10 mv	Nylon 200 v 50% R.H. 5 mm = 1 mv	Nylon 12.5 v 86% R.H. 5 mm = 1 mv
0	2	2	2
1	4	6	4
2	6	10	8
3	6	12	12
4	8	14	14
5	14	21	16
6	18	25	25
7	26	32	33
8	38	39	38
9	62	44	62
10	88	52	74
11	94	58	88
12	114	70	101
13	102	70	111
14	86	63	102
15	70	63	104
16	64	58	88
17	40	50	68
18	24	45	56
19	18	34	48
20	16	30	34
21	6	20	24
22	2	14	14
23	2	14	10
24	2	6	7
25	—	4	4
26	—	2	2
27	—	2	—
	942	860	1149
Time of observation	1 sec.	0.6 sec.	1 sec.
Root-mean-square deflection	3.9 mm	5.4 mm	4.5 mm
Root-mean-square voltage deviation Δv_{rms}	7.8 mv	1.08 mv	0.9 mv
Root-mean-square current deviation Δi_{rms}, in electronic charge units	12.5×10^9	1.8×10^9	1.4×10^9
Resistance of sample, ohms	1.5×10^8	1.5×10^9	5×10^7
Calculated average current, i_0, in electronic charge units	8×10^{12}	10^{12}	1.6×10^{12}
$(ei_0/t)^{\frac{1}{2}}$	2.8×10^7	10^7	1.3×10^7
Ratio: $\Delta i_{rms}/(ei_0/t)^{\frac{1}{2}}$	4.5×10^2	1.8×10^2	1.1×10^2
Ratio: $\Delta i_{rms}/i_0$	1.5×10^{-3}	1.8×10^{-3}	1×10^{-3}

[11] A. E. Stearn and H. Eyring, J. Phys. Chem. **44**, 976 (1940).
[12] Glasstone, Laidler, and Eyring, The Theory of Rate Processes, (McGraw-Hill Book Company, Inc., New York, 1941), p. 552 ff.

of the ions, which motion depends on the internal mobility of the system, on the size of the ions, on the temperature, and on the applied field.

Some numerical calculations to illustrate orders of magnitude may be helpful at this point. For example, a potential of 250 volts applied to a 1-mil film is 100,000 v/cm which corresponds to an energy of 1.6×10^{-7} erg per cm. Assuming that an ion jumps a distance of 5×10^{-8} cm each time, it acquires an energy of 8×10^{-15} erg. kT is 4×10^{-14} erg and hence at 250 volts the electrical energy is 20 percent of kT. Thus the energies we are using vary from about 1 to 20 percent of kT which accounts already for the characteristic difference in the patterns of Fig. 6(a and c).

Next some estimate of the magnitude of these current fluctuations may be of interest. Thus, in a typical example, Nylon film at 50 percent R.H. and 200 volts gave an extreme fluctuation range of 5 mv. From the nature of the circuit one can calculate that this would correspond to about 10^{-10} electronic charges per burst. Many of the smaller bursts would involve only a tenth of this amount. The steady current, calculated from specific resistivity, is about 10^{12} electronic charges. Additional calculations are given in Table I.

We wish to return now to Fig. 6, which represents studies on nylon at high and low voltages at full chart speed. Lines a and b represent zero percent R.H. and 280 volts with reversal of polarity. In line a the strong surges are seen to be going down with only minor surges in the upward direction; whereas in line b with reversed polarity the strong surges are upward. This conductivity in Nylon at zero percent relative humidity may arise from mobile hydrogen atoms, according to the mechanism suggested by Baker and Yager.[12a] Lines c and d at 86 percent R.H. and 12½ volts illustrate the surges uniformly distributed on either side of the zero line. Line c was recorded with the 120-cycle pen which shows more fine detail than does line d which is on the 60-cycle pen. These two traces are shifted slightly with respect to each other (as can be seen at the right hand side) because of different lengths of the pen arms. It is possible to note the same events on each record and to see that while they do have the same general features yet they actually differ in details.

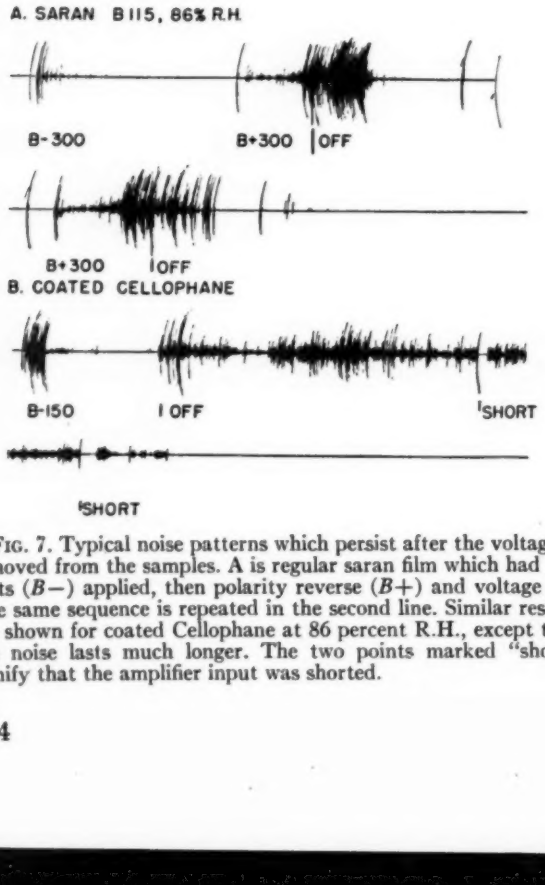

FIG. 7. Typical noise patterns which persist after the voltage is removed from the samples. A is regular saran film which had 300 volts ($B-$) applied, then polarity reverse ($B+$) and voltage off. The same sequence is repeated in the second line. Similar results are shown for coated Cellophane at 86 percent R.H., except that the noise lasts much longer. The two points marked "short" signify that the amplifier input was shorted.

The curves of Fig. 6(c and d) illustrate a principle which is common in fluctuation phenomena, namely, that when the disturbing force is small (low voltage in this case) the fluctuations appear to follow roughly the natural frequency of the system. Thus 6c has about a frequency of 120 cycles, while line 6d corresponds more closely to 60 cycles. Kappler observed this type of behavior with galvanometer mirrors when the ambient pressure was reduced to a low value.[12b] This behavior does not affect the root-mean-square deviation.

Tracings of the kind shown in c and d were obtained both on Nylon and coated Cellophane, using a cross-sectioned recording paper having one millimeter squares supplied with the recorder. These records facilitated statistical studies of the nature of the noise record. For example, by counting the number of intersections of lines parallel to the time axis with the curve, as recommended by Furth[13] and recently applied by Furth and MacDonald,[14] we obtained the distribution data listed in Table I. The 60-cycle pen tracing was used in each case, and the bottom-most point reached by any tracing was taken as zero millimeters for the ordinate scale. It was a coincidence that each of these occupied roughly 25 mm since the actual voltage range was 10-fold greater for the Cellophane. Finally, a similar statistical study was made of the events in line d of Fig. 6, for a period of one second.

It is evident from the distribution data of Table I that the noise peaks are symmetrical about the zero line even up to 200 volts applied potential under conditions when the average current through the film tends to be large. Then the second term of Eq. (1), Ddc/dx, is apparently large and the backward current is appreciable. If, however, as indicated by lines a and b of Fig. 6 the voltage is high and the moisture content low, ideal conditions prevail for observing unsymmetrical surges. In other words, there are presumably so few ions present that the concentration gradient, dc/dx, of ions cannot acquire a large value.

We must now examine in more detail the question of the random nature of these fluctuation currents.[14a] We

[12a] W. O. Baker and W. A. Yager, J. Am. Chem. Soc. **64**, 2177 (1942).
[12b] E. Kappler, Ann. I. Physik **11**, 233 (1931).
[13] R. Furth, Ann. d. Physik **53**, 177 (1917).
[14] R. Furth and D. K. C. MacDonald, Proc. Phys. Soc. **59**, 388 (1947).
[14a] R. B. Barnes and S. Silverman, Rev. Mod. Phys. **6**, 162 (1934).

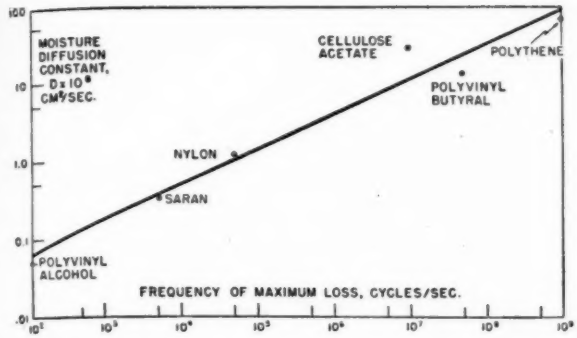

FIG. 8. Diffusion constant for moisture vapor as a function of the frequency at which the electrical loss factor of the polymer is a maximum.

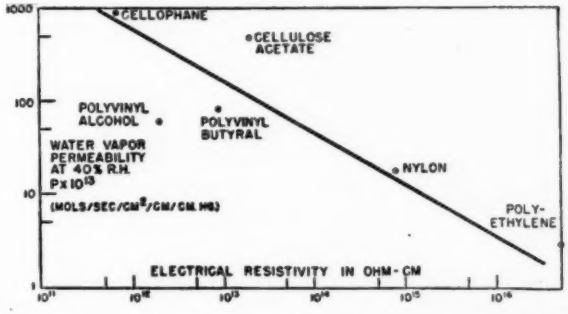

FIG. 9. Correlation between moisture vapor permeability (which is the product of diffusion constant and solubility) and the direct current resistivity of a series of polymers.

have been assuming that the conduction current is composed only of current pulses arising from ion jumps in the dielectric medium, and that these jumps occur at random. If we observe the net current (or a potential drop across a resistance) in the time interval, t, then the root-mean-square current fluctuation, Δi_{rms} is

$$\Delta i_{\text{rms}} = (ei_0/t)^{\frac{1}{2}}. \tag{2}$$

Where e is the electronic charge in coulombs, i_0 is the average current, and t is the time interval. t is, for the 60-cycle Brush oscillograph pen, approximately 0.01 sec. Hence, for a typical case i_0 is 10^{-9} amp. or 10^{10} electronic charges per second. For this case one calculates $\Delta i_{\text{rms}} = 10^6$ electronic charge units per second. Alternately, one may use the Schottky expression

$$\Delta i_{\text{rms}} = (2ei_0\Delta F)^{\frac{1}{2}} \tag{3}$$

where ΔF is the band width and the other symbols have their previous significance. Assuming ΔF as 100 cycles, then the numerical value used above of $i_0 = 10^{-9}$ amp. gives $\Delta i_{\text{rms}} = 1.4 \times 10^6$ electronic charges per second, which differs from the preceding value only by the factor $(2)^{\frac{1}{2}}$. The several average and statistical quantities are given in the appropriate columns of Table I. It is seen that Δi_{rms} is from 110 to 450 times the value one would calculate from the average current if normal shot effect conditions applied. Also Δi_{rms} is seen to vary from 0.2 to 5 percent of the steady current. It must be re-emphasized that these values are probably indicative only until we can make simultaneous measurements of the actual steady current.

The fact that these Δi_{rms} values are at least a hundred times larger than one would calculate from the steady current requires a revision of our original premises. The simplest revision is to assume that groups of ions move randomly in the form of "avalanches." Normally the term "avalanche" implies the cumulative building up of a large number of ions by successive collisions. Such a meaning is not intended here. Rather, it seems more likely that if a "hole" opens through the dielectric, it may persist long enough to permit a large number of ions to move through. This may be particularly marked at high moisture contents where small pockets of water exist within the dielectric. It is further possible that the passage of a few ions between a certain pair of chain segments may generate sufficient local heat to keep a path open for additional ions.

Moreover, there is an additional aspect of Eq. (1) which has unique significance for a polymeric dielectric. In any normal electrolysis experiment it does not seem likely that appreciable concentration gradients of ions will exist. However, trapping mechanisms in a high polymer may well give rise to some extremely large concentration gradients. Also, the average current, i_0, which one observes consists of the difference between a forward and backward current,

$$i_0 = i_f - i_b. \tag{4}$$

It is conceivable that the two directional currents, i_f and i_b, could both be large with respect to i_0. The fluctuating current should be based on these individual currents i_f and i_b. Hence the observed fluctuations in current may well seem extremely large in comparison to the average current.

AFTER EFFECTS

There is one final effect which should be mentioned: This noise will frequently persist for a few seconds after the voltage has been removed from the sample. Figure 7 shows some typical records.

According to Maxwell's rule, the relaxation time, τ, for an arbitrary distribution of charge in a solid, is given by $\tau = \epsilon'/\sigma$ where ϵ' is the dielectric constant and σ is the conductivity in m k sec units. Thus a material of dielectric constant 5 and resistivity of 10^{12} ohm-cm should have a relaxation time of 0.4 sec. Some of these observed times are of the order of one minute. Pollissar has discussed conduction in liquids on the basis of a cage model.[15] It seems that in a solid plastic, particularly one that can crystallize, the concept of ions trapped in local cages acquires a high probability. It may well account for some of the long-time constants observed here after the voltage is removed. A highly viscous medium, and especially one in which motion of the ions proceeds in discrete steps, is an ideal one for trapping ions. Two

[15] M. J. Polissar, J. Chem. Phys. **6**, 833 (1938).

TABLE II. Correlation of moisture vapor transmission with dielectric properties of plastics.

Material	Moisture[a] diffusion constant $D\times10^9$ in cm²/sec.	Moisture[a] vapor permeability $\times10^{13}$ in moles/sec. cm²/cm/unit pressure differential	Frequency[b] of power factor maximum in cycles/sec.	D.C.[b,c] resistivity in ohm-cm
Polyvinyl-alcohol	0.05	60	$<10^3$	2×10^{12}
Vinylidene-chloride-acrylonitrile copolymer	0.32	0.7	10^3	7×10^{16}
Nylon	1.2	18	5×10^4	8×10^{14}
Polyvinyl-butyral	13	83	4×10^7	9×10^{12}
Cellulose acetate	30	500	10^7	2×10^{13}
Polyethylene	68	2.9	10^9	$>5\times10^{16}$
Cellophane		900		7×10^{11}

[a] From Hauser and McLaren at 40 percent relative humidity.
[b] From von Hippel.
[c] At 30 percent R.H.

pockets of ions of opposite sign may either move further in the paths toward their respective electrodes, or may mutually discharge each other, giving rise to considerable current surges in the backward direction. It might be noted that the sudden stoppage of an "avalanche" of ions would have the appearance of a surge in the reverse direction.

An inspection of the circuit will indicate that the effective time constant becomes much longer when the potential is removed, based on the discharge of the 0.001 mica condenser to ground through the sample. Thus the time constant can be of the order of several seconds, depending on the actual leakage resistance of the experimental condenser. However, some of these persistent aftereffects last much longer and are the result, we believe, of trapped ions.

RELATIONSHIP OF THIS NOISE TO MOISTURE VAPOR TRANSMISSION

If our picture of this noise is correct: i.e., arising from the activated diffusion of ions where the rate-controlling step is the speed with which chain segments can rotate, then there should be an intimate correlation between these noise effects and moisture vapor transmission. According to Barrer[16–19] the transmission of water through a plastic membrane is given by the expression

$$P=D\cdot S \qquad (5)$$

where D is the diffusion constant in cm²/sec. and S is the solubility of the water molecule in the polymer medium while P is the observed permeability constant in moles per cm² per sec. per unit thickness per unit differential water vapor pressure. Now the diffusion rate should be controlled, among other factors, by the speed with which the segments can open. Hence one would expect a direct relationship between the diffusion constant, D, and the frequency of the maximum in the dielectric response curve, i.e., the frequency at which the loss factor is a maximum. Figure 8 based on the moisture diffusion data of Hauser and McLaren[20] and the dielectric data of von Hippel and associates[21] shows that this is approximately true. Polyethylene itself has no dipoles to give rise to loss so that the observed value of 10^9 cycles presumably arises from impurity groups such as carbonyl. It will be recognized of course that each dielectric material has a differently shaped loss factor *vs.* frequency curve and that the length of the segment engaging in the dielectric response will vary. In some cases also it is mainly a side group rather than a segment of the main valence chain which responds to the applied electric field. Moreover, in Fig. 8 the slope is 0.5, indicating that D increases only as the square root of the segmental frequency.

Nevertheless, we believe the general features of Fig. 8 to be essentially correct and extremely illuminating. It is seen from Table II that Saran and polyethylene represent extreme cases as regards diffusion even though they are relatively close on the final moisture vapor transmission. The outstandingly low moisture vapor transmission of Saran would, in this point of view, be ascribed to the fact that the large chlorine groups have slowed down chain segment rotation to a relatively low frequency. Polyvinyl alcohol is an even more extreme case than saran as far as diffusion at low relative humidities, and here it is presumably both the size of the OH group and hydrogen bonding which slows down dielectric response.

We might mention that results similar to those of Fig. 8 also hold for the diffusion of nitrogen and butane through a series of vulcanized rubbers, using the diffusion data of Barrer and Skirrow[19] and the dielectric data of Scott, McPherson, and Curtis.[22] So far as we know, the seemingly obvious relation between diffusion and dielectric response frequency has not hitherto been noted. However, Levi[23] has already noted that the activation energies and entropies for dielectric relaxation and for moisture vapor transmission follow essentially the same pattern. A further extension of Fig. 8 would be to seek a correlation between the noise frequency spectrum and the dielectric response curve. We have observed qualitatively, on a fast cathode-ray oscillograph, that polyethylene does have higher frequence noise effects than does saran.

Next, if we return to a consideration of Eq. (1), we see from the first term that the electrical conductivity arising from a direct current field is proportional to the product $D\cdot c$ where D is the diffusion constant of the ion

[16] R. M. Barrer, Trans. Faraday Soc. **34**, 849 (1938); **35**, 628, 644 (1939); **36**, 1235 (1940).
[17] R. M. Barrer, Diffusion in and through Solids (Cambridge University Press, New York City, 1941).
[18] R. M. Barrer and G. Skirrow, J. Polymer Sci. **3**, 549 (1948).
[19] P. Doty, J. Chem. Phys. **14**, 244 (1946).
[20] P. M. Hauser and A. D. McLaren, Ind. Eng. Chem. **40**, 112 (1948).
[21] A. R. von Hippel, "Tables of dielectric materials," Laboratory for Insulation Research, M.I.T., Vol. II (June, 1945).
[22] Scott, McPherson, and Curtis, Bur. Stand. J. Research **11**, 173 (1933).
[23] D. L. Levi, Trans. Faraday Soc. **42A**, 152 (1946).

and c is the concentration of ions. But these are precisely the two factors on which moisture vapor permeability depend: except that moisture diffusion refers to the whole electrolyte molecule rather than its constituent ions. However, there is an intimate relation between the diffusion of an electrolyte and the diffusion of its constituent ions. Hence, one is led to predict a relationship between the moisture vapor permeability of polymer films and their direct current conductivities or resistivities. Figure 9, using the data collected in Table II, shows that this relationship holds surprisingly well.

Actually, in the usual electrical resistivity test the sample has been equilibrated in an atmosphere of constant humidity and has a uniform water content throughout its thickness; in a moisture vapor test the water content varies through the film. In addition, different samples were used for the two types of tests. Also, various impurity ions may be present from sample to sample. These various uncertainties may account for the fact that the slope of Fig. 9 is not quite unity.

One may ask now whether or not water vapor diffusion proceeds in part or entirely by an ionic mechanism. For example, a hydrogen ion, having a higher mobility, might diffuse forward and then pull along the slower $-OH$ ion. This is probably the source of the electric currents which Fischer and Muller[24] found to accompany the diffusion of water through plastic films until the steady state was reached. They found that the electrical current passed through a maximum whose height was greater the larger the moisture vapor permeability of the film, and then fell to zero under steady-state moisture transmission. Since the net charge transport would be zero such currents would depend on the difference in velocities of the hydrogen and hydroxyl ions.

[24] C. Fischer and F. Horst Muller, Kolloid Zeits. **101**, 43 (1942).

SUMMARY

This report is concerned with a description and preliminary interpretation of random fluctuation currents which accompany the application to thin films of moist dielectrics voltage gradients which are higher than those used in normal electrolysis experiments and lower than those leading to dielectric breakdown. These fluctuating currents are believed to arise from the fact that both the forward motion of the ions in the direction of the field and their backward movement because of concentration gradients thus established are regulated by the segmental motion of the polymer chains. It appears now, at least for the low frequency part of the noise spectrum which we analyzed, that groups of ions rather than single ions are acting as the random charge carriers.

This present report must be recognized as a preliminary study of the problem. The following are some of the many experiments which must be performed to elucidate fine details: effect of temperature; simultaneous recording of the average current, especially as it depends on applied voltage; study of the noise frequency spectrum; evaluation of surface *vs.* volume conductivity effects; a study of various ion types other than those of water, such as ammonium, chloride, etc.; and a more detailed study of aftereffects. Finally, a more complete theory needs to be developed. It is interesting to note that Richardson has developed a theory of fluctuations arising from diffusional mechanisms to account for noise developed at electrical contacts.[25]

It is a pleasure to acknowledge the assistance of Herbert Bauss who built the apparatus and aided in making the observations; to F. Towsley for discussions about noise problems in electronic circuits; and to E. B. Baker and L. A. Matheson for helpful discussions about the general significance of these results.

[25] J. M. Richardson, Bell Sys. Tech. J. **29**, 117 (1950).

Emulsion Polymerization with Ultrasonic Vibration

A. S. Ostroski and R. B. Stambaugh
*The Goodyear Tire and Rubber Company, Akron, Ohio**

Emulsion-type polymerization reactions have been accelerated by irradiation with ultrasonic energy.

A magnetostriction oscillator at 15 kc gave essentially the same results as a piezoelectric oscillator at 500 kc. The rate of formation of polystyrene was doubled and higher final yields obtained using about 0.03 watt of vibrational power per cc of latex. Experiments were made to separate local heating effects from those due to vibrational energy.

A thermostatted stainless steel cell was developed for irradiating butadiene emulsions under pressures up to 60 p.s.i. About ½ watt of vibrational power per cc of latex doubled the rate of reaction for GR-S, Redox, and Redsol formulas.

The ultrasonic intensity apparently must exceed a critical value before any appreciable accelerative effect is observed. Above the critical intensity, the time to reach a given yield of polymer is approximately inversely proportional to the power used.

I. INTRODUCTION

While the more spectacular phenomena associated with intense ultrasonic radiation have been described by many observers, very little information about practical applications of this energy has been published.[1] Colloidal systems[2] may be affected as to rate of emulsification, particle size and stability, and certain chemical reactions[2,3] are accelerated by the action of ultrasonic waves. The breakdown or de-polymerization of polymers in solution has been studied,[1,4] and the polymerization of acetic acid by treatment with ultrasonic power has been reported.[1] Apparently nothing has been published on the effects of ultrasonic vibration on emulsion polymerization systems such as are used in the production of synthetic rubber and with which the present investigation is concerned.

II. MAGNETOSTRICTION APPARATUS

Both a magnetostriction type of oscillator, operating at 15 kc, and a piezoelectric oscillator, operating at 500 kc, were used as sources of vibrational energy. The magnetostriction oscillator consisted of a laminated nickel bar, 6 in. long and ¾ in. square, excited by a coil made up of 28 turns of ⅛-in. copper tubing through which water was forced for cooling. The coil carried both a d.c. polarizing current and an a.c. current of about 15 to 20 amp. at 400 volts, the latter being supplied by a variable frequency vacuum tube oscillator capable of about 1000 watts output. The bar was supported by a spider inside the insulated coil, and the assembly immersed in the emulsion to be treated. The liquid was maintained at the desired temperature by rapid stirring and the circulation of thermostatically controlled fluid in the jacketed walls of the stainless steel vessel. The chamber was covered and a stream of nitrogen was piped in to prevent contamination by oxygen. A block diagram of this system is shown in Fig. 1, and a photograph of the apparatus is shown in Fig. 2.

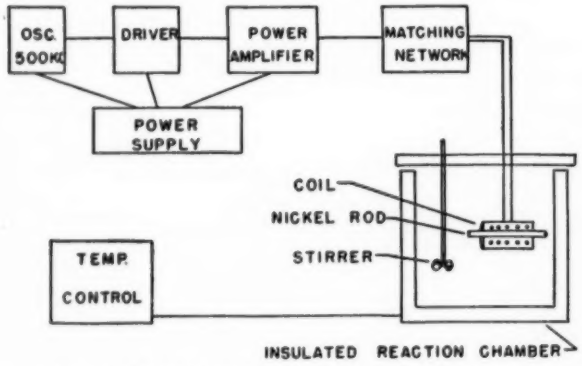

Fig. 1. Block diagram of magnetostriction vibrator.

The reaction was run at atmospheric pressure, and a simple styrene formula was used, containing: 100 parts (by wt.) of styrene monomer; 180 parts, distilled water; 5 parts, soap; 0.6 part, potassium persulfate. Samples were extracted by means of a pipette at intervals during each run so that the course of the reaction could be followed. The polystyrene in each sample was precipitated out in alcohol, dried, and weighed. Figure 3 shows some typical curves obtained with the bath at 50°C with 600- and 1200-cc batches. The percent of the original monomer transformed into polymer (yield) is plotted against the time elapsing after the styrene and soap solution, separately preheated to the bath tempera-

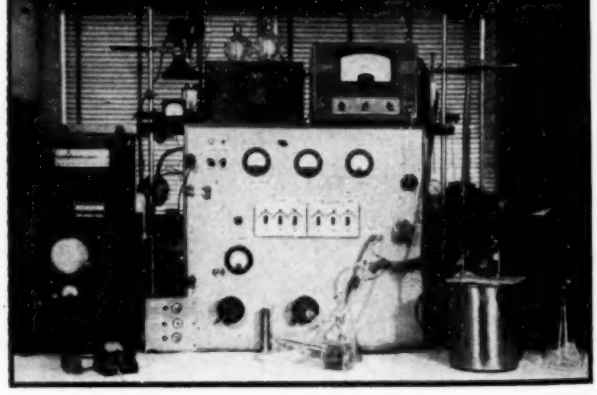

Fig. 2. Photograph of magnetostriction system.

* Contribution No. 174 from the Goodyear Tire and Rubber Company Research Laboratory.

[1] A list of references is given by Karl Sollner in his chapter on "Sonic and ultrasonic waves in colloid chemistry" in *Colloid Chemistry* (Reinhold Publishing Corporation, New York, 1944), edited by J. Alexander, Vol. 5. Also see D. Thompson, Chem. Eng. Progress **46**, 3 (1950).

[2] R. W. Wood and A. L. Loomis, Phil. Mag. **4** (7), 417 (1927).

[3] A. Kling and R. Kling, Comptes Rendus **223**, 33 (1946).

[4] H. Mark, J. Acous. Soc. Am. **16**, 3, 183 (1945).

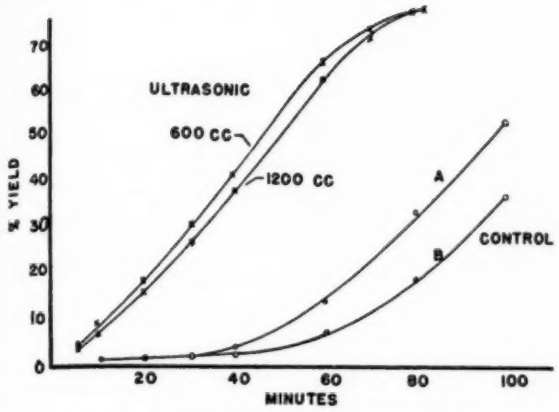

FIG. 3. Conversion of styrene at 50°C, 15 kc.

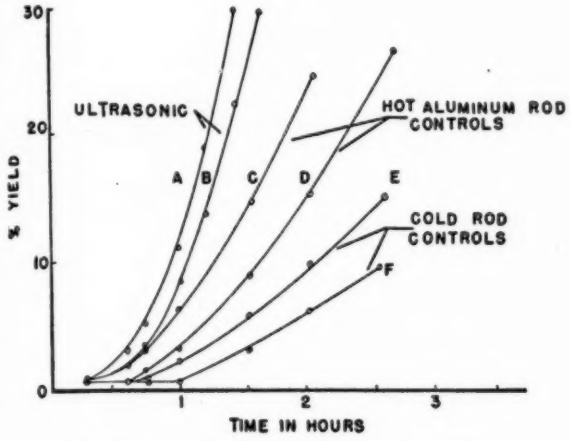

FIG. 4. Conversion of styrene at 40°C, 15 kc.

ture, were poured together into the vessel. Controls were run in the same apparatus without current in the coil.

The principle effect of the ultrasonic agitation appears to be the elimination of the induction period, with only a slight increase in the actual rate of the reaction as given by the slope of the curves.

At 40°C, the effect of the irradiation is much more pronounced. As illustrated in Fig. 4, the two curves A and B, obtained with the nickel rod excited, show a much more rapid conversion of the styrene than for curves E and F, when the rod was not energized. Due to magnetic and elastic hysteresis and eddy current losses, a great deal of heat is generated in the rod during a run. This results in a higher temperature in the emulsion immediately around the rod even though rapid stirring is maintained.

In order to show that the acceleration of the reaction was not due solely to this temperature rise, an aluminum rod was substituted for the nickel rod. This was heated by eddy currents to the same temperature as reached by the magnetostriction rod during a run, as measured by thermocouples welded to the surface of the middle section. Runs made with this hot aluminum rod produced curves C and D which show that the rod temperature does have some effect, but not sufficient to explain the rapid reaction of curves A and B which must be attributed to the ultrasonic agitation.

The nickel bar is very inefficient as a source of vibrational energy. The best estimates of actual acoustic power obtained with a kilowatt input to the amplifier were about 50 watts. This fact, combined with the difficulty of designing an enclosed system which could be operated under a relatively high pressure, made it desirable to use a piezoelectric crystal for further measurements.

III. QUARTZ OSCILLATOR

An X-cut quartz crystal was used for a source of energy at 500 kc, powered by a radiofrequency oscillator having a plate input of up to 300 watts. The crystal was 3.81 cm in diameter, having about 8 sq. cm of usable radiating area in contact with the emulsion. An estimated 100 watts of ultrasonic energy was realized with 200 watts plate input to the oscillator which was the usual power level. A few runs were made with 300 watts plate input, but several crystals were shattered in attempts to go above this level.

The crystal was mounted in the special reaction cell pictured in Fig. 5 which could be run at internal pressures of 60 lb./sq. in. This consisted of a stainless steel block through which a 2-in. diameter hole was drilled for the reaction chamber. A number of $\frac{1}{4}$-in. holes were drilled parallel to this chamber for circulation of temperature controlling fluid. The crystal was mounted against a hole cut through the bottom of the reaction

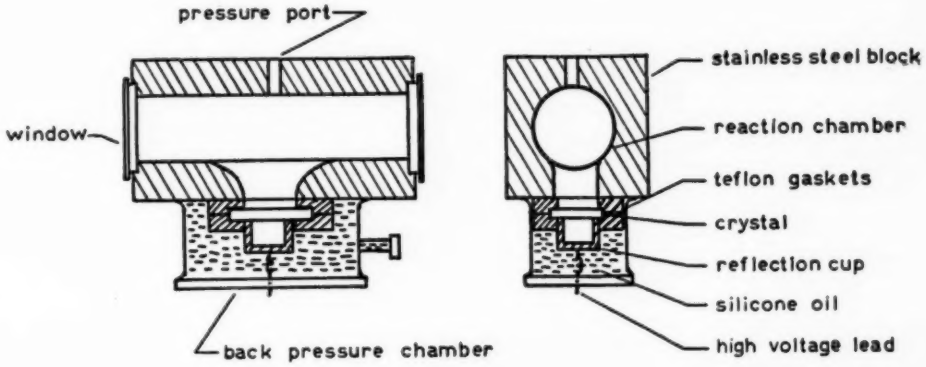

FIG. 5. Stainless steel reaction cell.

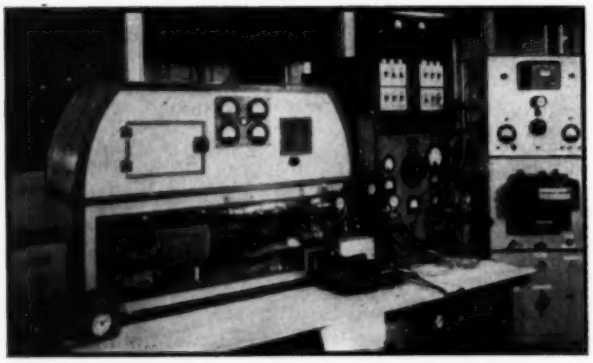

FIG. 6. Photograph of piezoelectric system.

chamber. It was held in place and insulated with Teflon gaskets. The high voltage side of the crystal was surrounded with silicone oil in a steel chamber welded to the block, having a polystyrene lid bolted to a flange on the bottom. The high voltage lead passed through this lid and made a spring contact to the brass, air-filled back-reflection cup which contacted the silvered back face of the crystal.

In the top of the block, a stainless steel pipe and valve was screwed into a threaded hole for filling and emptying the chamber and for insertion of a thermocouple. A pressure gauge was mounted on a side arm off this pipe. Heavy glass windows at each end of the cell provided means for observing the emulsion while it was being irradiated. These could be removed for cleaning the cell.

The photograph of Fig. 6 shows this apparatus with the associated recording and controlling systems for temperature, pressure, and power. The reaction cell in the center foreground is mounted in a cradle with a pneumatic piston beside it which rocked it constantly to prevent layering of the immiscible components of the charges.

When operating with high pressures in the cell, the oil in the chamber on the bottom side of the quartz crystal was automatically maintained at an equal pressure so that there was no tendency for the gaskets holding the crystal to leak. Furthermore, bending and damping of the crystal was minimized.

Since the reaction chamber was limited to charges of 200 cc or less, in order to treat large volumes of styrene at essentially atmospheric pressure, the cell was connected to a thermostatted ten-liter reservoir and a circulating diaphram pump by means of flexible metal hoses. The system was evacuated, the charge sucked in, and nitrogen forced in until the pressure was a few pounds per square inch above atmospheric. Samples of the latex could be removed at any time by means of a pet-cock.

The curves shown in Fig. 7 were obtained using the simple styrene formula given above in four-liter batches at 50°C with 200 watts plate input. As found with the magnetostriction oscillator, the main effect at this temperature was a decrease in the induction period and a somewhat higher final yield, although the actual rate of conversion was very little faster with the ultrasonic power on.

Figure 8 shows some results obtained at 40°C and, again, as found with the magnetostriction oscillator, there is a much more pronounced effect. Each of the three curves drawn in this plot was obtained with a different power concentration which was varied by changing the plate input to the oscillator or by changing the size of the batch.

No accurate method for measuring the actual ultrasonic power was available. Although a number of measurements were made on heating effects and radiation pressures, the figures obtained were unreliable. Probably about 50 percent of the plate input power was available as vibrational energy. However, to avoid the issue, the plate-input power was used as a basis for comparisons.

Figure 9 is a plot of the time required to reach a given yield of polystyrene as a function of the power concentration. These curves show that the reduction in time is approximately proportional to the power used. As the power is increased to very high concentrations, a minimum time to reach a given yield is approached. For

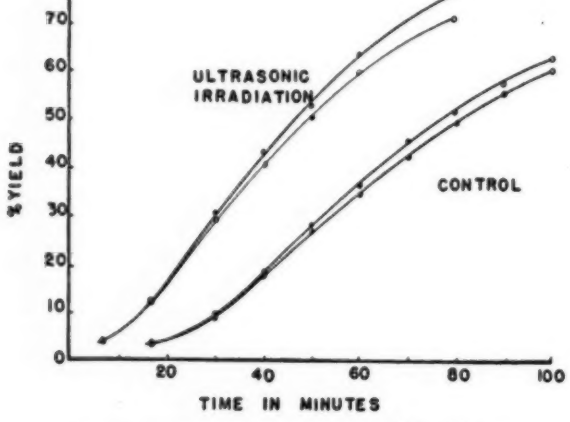

FIG. 7. Conversion of styrene at 50°C, 500 kc.

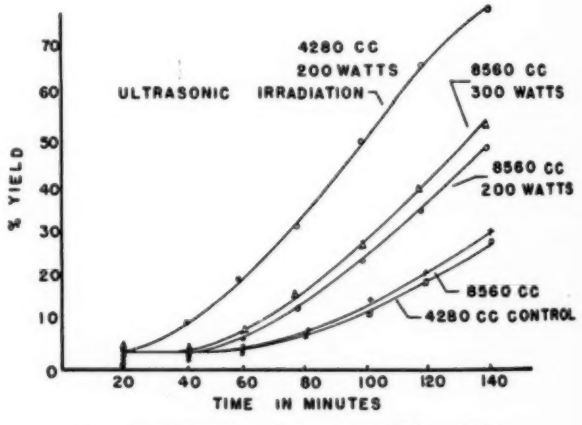

FIG. 8. Conversion of styrene at 40°C, 500 kc.

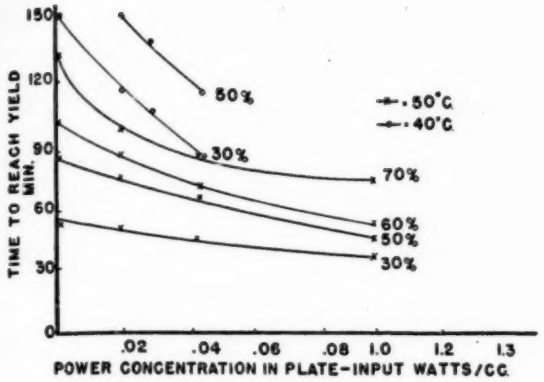

FIG. 9. Effect of power on conversion of styrene. (500-kc irradiation.)

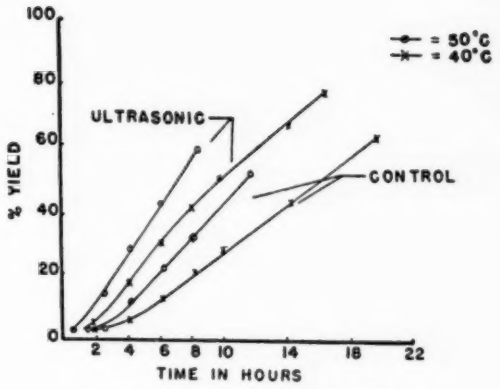

FIG. 10. Conversion of GR-S at 500 kc.

instance, at one watt per cc, 25 min. at 50°C is required to reach 70 percent yield.

As the power concentration is reduced to low levels by increasing the amount of latex in the batch, the curve intercepts the axis at the correct value as obtained from control runs with no power. However, if the batch is held at the same volume and the power concentration reduced by decreasing the plate input, a point is reached when no cavitation is produced. Below this critical intensity, the reaction rate is the same as the control, indicating that cavitation may be a necessary condition for the acceleration of the reaction.

IV. SNYTHETIC RUBBER POLYMERIZATION

For butadiene polymerization reactions, requiring 40 to 60 lb. pressure it was necessary to cut off the reservoir and circulating pump from the system, so that the batch size was limited to the reaction chamber. Figure 10 shows the results obtained for GR-S at 40° and 50°C. This was the standard mutual formula with a small amount of sulfuric acid added: 37.5 g of butadiene; 14.5 g of styrene; 90.0 g of distilled water; 2.5 g of soap; 0.15 g of potassium persulfate; 1.5 cc of 2.1*N* H_2SO_4; 1 to 2 drops of modifier (mercaptan).

The sulfuric acid solution was added to bring the *p*H down to 8.2 which was necessary to prevent foaming and consequent loss of ultrasonic power absorption by the latex. Control runs were made on the identical formula both in the reaction chamber without excitation of the crystal, and in standard glass bottles in a water bath. Samples were taken from the cell at definite intervals by means of a special hypodermic needle inserted through a gasket. The plate input was 200 watts, so that about 1 watt per cc (or about $\frac{1}{2}$ watt of vibrational power per cc) is required to double the yield in a given reaction time at either 40° or 50°C. This is a much larger power requirement than observed for the polymerization of styrene.

Essentially the same results were obtained with both a Redox "cold rubber" recipe at 41°F, as shown in Fig. 11, and a Redsol formula. The GR-S polymer produced with ultrasonic irradiation was apparently the same as the control product. Viscosity and density measurements showed no differences, and the infra-red absorption spectra were the same within the limits of spectrometer reproducibility.

V. DISCUSSION

The exact role of the ultrasonic agitation in accelerating these reactions is not understood. Apparently, cavitation is required, so that the high instantaneous pressures and temperatures produced upon collapse of the cavitation bubbles must be the principal cause of the effects. If higher localized temperatures at the cavitation centers are the cause, the polymer produced should have the characteristics of the control polymer made at higher temperatures. While no differences in the properties have been found as yet, the effects would be small and a more careful analysis of the properties may show these differences. If it were the high pressures (rather than temperatures) produced at the cavitation centers which were responsible for the rapid polymerizations, the properties of irradiated polymers should be compared to those special control polymers made at very high pressures. No such information is available at present.

In the case of the styrene polymerizations, the reduction of the induction period can be explained by the faster and better emulsification produced by the ultra-

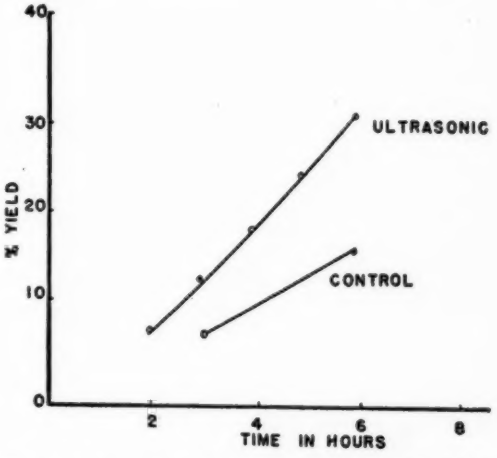

FIG. 11. Conversion of "cold rubber" at 41°F, 500 kc.

sonic agitation, a well-known phenomenon. In addition, several observers[3] have noted the ability of ultrasonic radiation to increase the rate of oxidation and produce peroxides. Since the induction period is usually caused by free oxygen in the system,[5] the rapid removal of this oxygen would permit the polymerization to start much sooner.

The increase in the actual rate of the reaction could be attributed to either increased rate of formation of free radicals by the persulfate reaction, or increased activity of the styrene in the polymer particles. The rate of reaction is usually considered to be established by the number of polymer particles formed initially. This is not greatly affected by irradiation (from particle size measurements) and the reaction cannot be "triggered" by the ultrasonic power. Several runs with both styrene and GR-S were made in which the ultrasonic power was cut off after a definite time. In these cases the reaction rate dropped to that of the control for the rest of the run.

The irradiated runs made with styrene usually proceeded to much higher yields (80 or 90 percent) before the reaction rate dropped off, while most control runs leveled off at 60 to 70 percent. This suggests that an important role of the ultrasonic radiation may be to oxidize inhibiting impurities which prevent the reaction from going to completion.

[5] I. M. Kolthoff and W. J. Dale, J. Am. Chem. Soc. **69**, 441 (1947).

ACKNOWLEDGMENT

The authors wish to express their thanks to the Goodyear Tire and Rubber Company and to Dr. H. J. Osterhof for permission to publish this work. This investigation was carried out under the sponsorship of the Office of Rubber Reserve, Reconstruction Finance Corporation, in connection with the Government Synthetic Rubber Program.

Transitions in High Polymeric Materials

ROLF BUCHDAHL AND LAWRENCE E. NIELSEN
Monsanto Chemical Company, Plastics Research Laboratory, Springfield, Massachusetts

The evidence for and against the interpretation of the "second-order" transition in polymers in terms of a thermodynamic transition of the second order is reviewed and some new experimental data concerning transition in mixtures of polymers are presented. It is shown that the relaxation theory is insufficient to explain the transition, as observed by mechanical, electrical and thermal measurements. The usual objections which are raised against the assumption of a thermodynamic transition are shown to be invalid. Various molecular processes responsible for a thermodynamic transition are discussed and it is shown that the general mechanism of "hindered" rotation (changes in rotational configuration) is the most likely.

I

EMBRITTLEMENT has long been recognized as one of the characteristic phenomena of all polymeric materials and, from a phenomenological point of view, can best be described by the change of dynamic elastic modulus (E) and mechanical damping with temperature[1–4,*] as shown schematically in Fig. 1. Embrittlement occurs at a temperature, T_b, where the modulus has reached its maximum value. As the temperature is raised, the modulus undergoes a drastic change within a relatively narrow temperature range (the transition or "leathery" region) and then levels off again at higher temperatures where the material usually displays all the typical properties of an elastomer. In the transition the mechanical damping goes through a maximum, as can be seen from Fig. 1. Whether or not a material is classified at room temperature as a "plastic" or as a "rubber" depends only, from this point of view, on the position of the transition region on the temperature scale.

Two important characteristics of a damping temperature curve are the transition temperature defined as the temperature of maximum damping and the width. Within the transition region, as defined by dynamic mechanical measurements, many other physical properties change also in a more or less discontinuous manner. The specific heat undergoes a rather sudden increase as shown in Fig. 2; the thermal expansion coefficient[5] and the refractive index[6] changes, in most cases, in a discontinuous manner; the dielectric constant increases rapidly, and the electrical loss factor goes through a maximum.[7–9] (The dispersion in the electrical case is much more dependent on frequency than in the mechanical case.) Finally, in a few cases, it has been found

[1] A. W. Nolle, J. Polymer Sci. **5**, 1 (1950).
[2] Nielsen, Buchdahl, Levreault, J. App. Phys. **31**, 607 (1950).
[3] J. W. Liska, Ind. Eng. Chem. **36**, 40 (1940).
[4] R. F. Clash, Jr. and R. M. Berg, Symposium on Plastics A.S.T.M. (1944).
[*] In references 3 and 4 a static modulus is used instead of the dynamic modulus.

[5] R. F. Boyer and R. S. Spencer, *Advances in Colloid Science II* (Interscience Publishers, Inc., New York, 1946), pp. 1–55.
[6] R. H. Wiley and G. M. Brauer, J. Polymer Sci. **3**, 455 (1948).
[7] R. Fuoss, J. Am. Chem. Soc. **61**, 2334 (1939); **63**, 2401, 2410, 2832 (1941); **64**, 283 (1942).
[8] Davies, Miller, and Busse, J. Am. Chem. Soc. **63**, 361 (1941).
[9] Wurstlin, Kolloid Zeits. **105**, 9 (1943).

that the compressibility[10] and thermal conductivity[11] undergo rapid changes in a narrow temperature region.

On the basis of the experimental evidence available, there can be no doubt that polymers undergo a transition which can be detected by numerous methods; there exists, however, a considerable amount of disagreement concerning the nature and origin of this transition. This problem can be stated quite simply as follows: (1) Is the transition a real one from the thermodynamic point of view? (2) If it is a real one, what is its origin? (3) If it is not real, in the thermodynamic sense, how can it be interpreted in a satisfactory manner? The fact that the transition has been referred to as a "second-order" transition indicates that the interpretation has, at times, been considered in terms of a real thermodynamic transition of the second order.[12] A thermodynamic second-order transition is defined as a transition extending over a small but finite temperature range ΔT with a heat of transition given by the integral $\int \Delta C dT$ where ΔC denotes the excess of specific heat at the transition.[13] However, during recent years the prevalent opinion has been that the transition is an apparent one and can be interpreted as the temperature "point where the rate of attainment of equilibrium is of the same order of magnitude as the time scale of ordinary physical experiments."[14] This conclusion is based on two separate but related experimental findings: The transition as measured by volume expansion shows strong time effects and when equilibrium conditions are approached tends to disappear (at least in the case of polystyrene);[15] the transition region shifts with frequency when measured by the response to an alternating mechanical or electrical force. According to this point of view, the transition is due to the existence of a relaxation spectrum[16] and corresponds to an isoviscous state.[17] Recently, however, several investigators[18–20] have emphasized the fact that the concept of relaxation is not sufficient to give a satisfactory interpretation of these transitions in high polymers and that it is necessary to assume some sort of thermodynamic transition. In the following sections we intend to show in a qualitative manner† (1) why such an assumption is necessary; (2) that the existence of a thermodynamic transition of the second order is in agreement with experimental findings and does not invalidate the existence of dispersion (or rate) effects; and finally we state the molecular process involved in the transition.

II

Before discussing the major limitations of any relaxation or isoviscous theory, it is necessary to consider the results Spencer and Boyer[20a] obtained in their study of the thermal expansion coefficient (α) of polystyrene. They concluded that, at least for polystyrene, the transition is a rate phenomenon and not a thermodynamic singularity. Polystyrene is a typical amorphous material where the mechanical properties are not further complicated by the presence of crystallites, and has only a single transition at about 105°C which is independent of molecular weight above $M_\omega \sim 150{,}000$;[21] it is important to clarify this point because it has frequently been used as the most powerful argument in favor of the relaxation theory. A careful examination of the published data does not seem to justify a linear relationship without a discontinuity between 20 and 150°C as claimed by the authors, unless the precision of the measurements is much lower than indicated. It seems that the discontinuity persists, irrespective of the time allowed to obtain equilibrium. It should be pointed out that the existence of a discontinuity is not a necessary criteria for the existence of a second-order transition; Fowler and Guggenheim have shown[22] that α above and below the transition temperature (T_t) is given by the

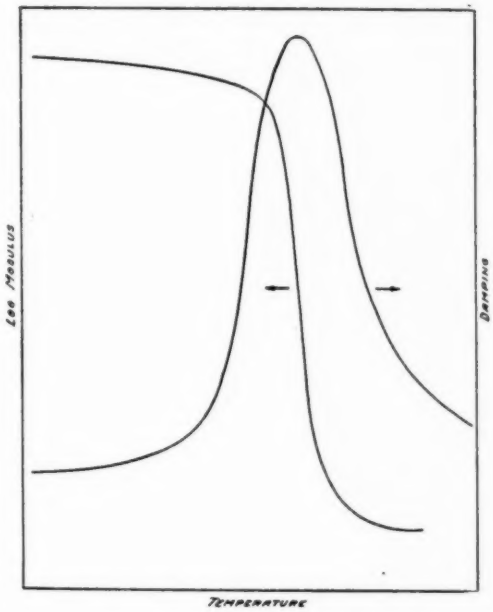

FIG. 1. Generalized dynamic modulus and damping curves as a function of temperature.

[10] A. H. Scott, J. Research Nat. Bur. Stand. **4**, 99 (1935).
[11] A. Schallamach, Proc. Phys. Soc. London **53**, 214 (1941).
[12] M. Ruhemann and F. Simon, Zeits. f. physik. Chemie **A138**, 1 (1928).
[13] J. Frenkel, *Kinetic Theory of Liquids* (Oxford University Press, New York, 1946).
[14] Alfrey, Goldfinger, and Mark, J. App. Phys. **14**, 700 (1943).
[15] R. S. Spencer and R. F. Boyer, J. App. Phys. **17**, 398 (1946).
[16] T. Alfrey, Jr., *Mechanical Behavior of High-Polymers* (Interscience Publishers, Inc., New York, 1946).
[17] R. F. Boyer and R. S. Spencer, J. App. Phys. **16**, 594 (1945).
[18] Stein, Krimm, and Tobolsky, Phys. Rev. **75**, 1301 (1949).
[19] E. Guth and H. M. James, Phys. Rev. **75**, 1314 (1949).
[20] Merz, Nielsen, and Buchdahl, J. Polymer Sci. **4**, 605 (1949).
† The quantitative formulation of such a theory will be published in the near future.

[20a] R. S. Spencer and R. F. Boyer, J. App. Phys. **17**, 398 (1946).
[21] Merz, Buchdahl, and Nielsen, Ind. Eng. Chem. (to be published).
[22] *Statistical Thermodynamics*, Cambridge University Press, London (1939), p. 607.

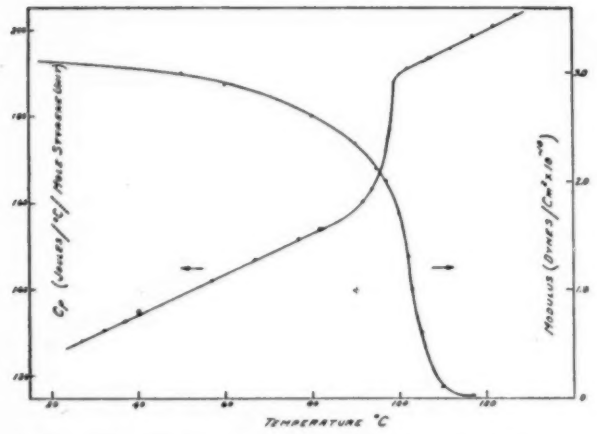

FIG. 2. Dynamic Young's modulus and specific heat as a function of temperature (the specific heat data were obtained by the N.B.S.).

following equations:

$$\alpha-\alpha_0=-\beta^0(3/2)(w/kT_t^2)(dw/dv)(0<T_t-T\leq T_t)$$
$$\alpha-\alpha_0=0(T>T_t),$$

where α_0 = expansion coefficient of the disordered state and w is the energy of unmixing. It will be noticed that a discontinuity in α at T_t only exists when dw/dv is different from zero or not negligibly small. There might well exist cases where the change in this energy with volume is sufficiently small or actually zero so that a discontinuity will not be found despite the existence of a thermodynamic transition.

One of the major difficulties encountered by the relaxation theory is the temperature dependance of the rate constant τ, near or in the transition region. It is generally assumed that τ varies exponentially with temperature: $\tau=C\cdot e^{W/RT}$, where W has the meaning of an activation energy. Such activation energies have been determined from measurements of electrical[23] or mechanical[1,24] damping, or from stress relaxation curves;[25] the values usually found are between 10 and 50 kcal. and appear to be closely related to the activation energies of viscous flow of high polymers.‡ However, these activation energies are much too low to account for the marked changes in the modulus in the transition region (as observed at low frequencies); in other words, the activation energy becomes itself a function of the temperature as the transition temperature is approached. As a matter of fact, Frenkel[13] has pointed out that the equation given above for τ must be modified by assuming $W=\text{const.}\,eu/RT$ in order to be in agreement with experimental data; and that such an increase of the activation energy is due to a change of the structure which can be specified by an order-disorder parameter, s. It would seem more reasonable to postulate the following relationship for $\tau=\text{const.}\,eW/[R(T-T_t)]$ for $T\geqq T_t$. It is therefore quite evident that the relaxation theory by itself cannot give a satisfactory interpretation of the strong temperature dependance of the modulus or damping, which in the case of unplasticized polyvinyl chloride is about 180 kcal., in terms of an activation energy, in the transition region.

Another difficulty arises when one considers the interrelationship between frequency (V) and temperature (T) with respect to the dynamic modulus and damping. On the basis of the relaxation theory there exists a definite interrelationship which can most easily be expressed by the proportionality

$$\frac{\ln V_1'}{\ln V_2'}\sim\frac{T_2}{T_1},$$

i.e., a lowering of the temperature has the same effect as increasing the frequency, and $E(T)$ and $E(V)$ are closely related functions. Again, in the case of electrical measurements of simple low molecular weight materials in *non*-polar solvents, theory and experiment are in good agreement.[26] The extensive electrical studies by Fuoss[7] on various polymer-plasticizer systems also seem to be in harmony with a relaxation theory when a relaxation spectrum instead of a single relaxation time is assumed. It should be pointed out, however, that this agreement with theory might be somewhat fortuitous in view of the results obtained by Schallamach[27] on the dielectric relaxation of mixtures of dipolar liquids. When one now considers the available data[28,1] on mechanical damping or modulus as a function of frequency and temperature, it becomes immediately apparent that the agreement between theory and experiment is not good: (1) The frequency dependance is such that one has to assume a continuous relaxation spectrum extending over 10 decades or more; an assumption whose physical significance is—to say the least—somewhat doubtful. (2) An upper frequency limit of the modulus has never been experimentally established with certainty. (3) The interdependance between temperature and frequency is not very pronounced and certainly does not hold in the transition region. It will be shown in the next section that the dispersion effects can be interpreted as the consequence of the existence of a thermodynamic transition.

Finally, we wish to consider briefly the difficulties which arise with respect to the dependance of the transition temperature on plasticizer concentration on the basis of a relaxation or isoviscous state theory. ¶The

[23] W. Kaufmann, Rev. Mod. Phys. **14**, 12 (1942).
[24] Alexandrov and Lazurkin, Acta Physicochimica (U.S.S.R.) **12**, 647 (1940).
[25] A. Tobolsky and H. Eyring, J. Chem. Phys. **11**, 125 (1943).
‡ On the basis of Debye's theory of relaxation $W_\tau=W_\eta$. Although this relation holds well for short and compact low molecular weight compounds in solution, it has been shown by Schallamach (Trans. Faraday Soc. **42**, 495 (1946)) to be inapplicable in the case of non-polymeric chain molecules.

[26] P. P. Debye, *Polar Molecules* (Chemical Catalog Company, Inc., New York, 1929).
[27] A. Schallamach, Trans. Faraday Soc. **42A**, 180 (1946).
[28] Sack, Lamb, and Work, J. App. Phys. **18**, 450 (1947).
¶ This problem is intimately related to the general theory of plasticization which we plan to discuss in detail at a later date.

lowering of the transition point is explained in terms of a lowering of the internal viscosity so that upon addition of a plasticizer the isoviscous state (or the equivalent relaxation spectrum) has been shifted toward a lower temperature.[28a, 29] This concept implies that there can be only one transition point upon addition of a plasticizer. However, investigations of the dielectric losses in swollen rubber[30] show that one can obtain, under certain conditions, more than one maximum. Similar results have been found in the case of a mixture of two polymers (polystyrene and 40:60 percent butadiene-styrene copolymer) as can be seen in Fig. 3. Furthermore, a survey of reliable transition temperature data as a function of plasticizer concentration[2, 7, 8, 31] has shown that the transition temperature is a linear function of the volume fraction of plasticizer over a wide concentration range provided certain conditions are fulfilled[32, 2] (see Fig. 4). Recent investigations on the dielectric properties of plasticized compositions[33] have shown that the $T_c - C_v$ relationship when extrapolated to 100 percent plasticizers gives a transition point for the plasticizer which agrees with the experimentally determined transition point. The relationship derived by Boyer and Spencer[28] ‖ on the basis of the theory of isoviscous state is not in agreement with the $T_t - C_v$ relationship which, for the simplest case, is determined only by the transition points of the two components and has to be modified depending on the mutual compatibility of the constituents.

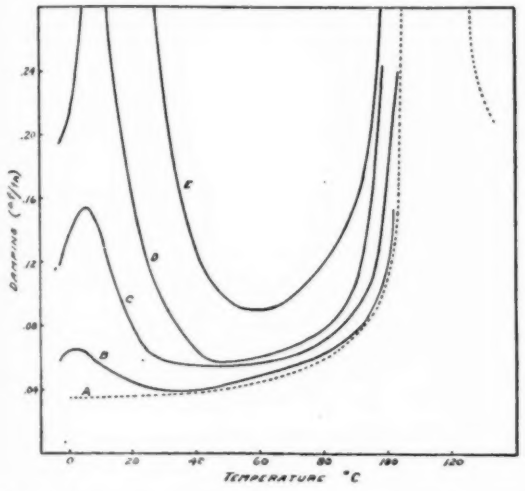

FIG. 3. Damping—temperature curves for polymer mixtures:

	Polystyrene	Styrene-butadiene copolymer
A	100	0
B	90	10
C	74	26
D	60	40
E	40	60

[28a] R. F. Boyer and S. Spencer, J. Polymer Sci. **2**, 157 (1947).
[29] H. Jones, J. Soc. Chem. Ind. **67**, 415 (1948).
[30] A. Schallamach, Trans. Faraday Soc. **45**, 605 (1949).
[31] L. Nielsen and R. Levreault, Nature **164**, 317 (1949).
[32] W. R. Richard and P. A. S. Smith, J. Chem. Phys. **18**, 230 (1950).
[33] A. J. Warner, A.S.T.M. Bulletin (April, 1950).
‖ In view of the fact that the Flory equation of viscous flow of polymers has recently been found to hold only over a limited molecular weight range, the agreement with experimental data is probably accidental.

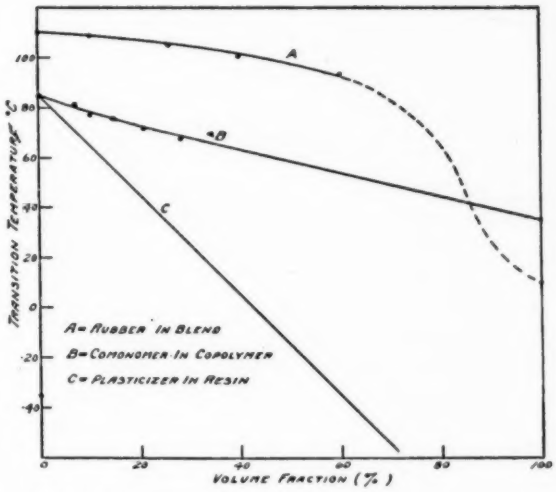

FIG. 4. Transition temperature as a function of volume fraction.

III

It is clear from the preceding discussion that the application of the relaxation concept to the transition phenomenon under consideration is insufficient to explain the salient features of such transitions. The necessity of assuming a real thermodynamic transition becomes, therefore, almost inescapable even when one approaches the problem at first from the relaxation point of view, as has been pointed out by several investigators.[1, 13] On the other hand, an interpretation on the basis of a thermodynamic transition has, in the past, encountered some difficulties because certain experimental findings appeared to be in disagreement with the concept of a true transition. These findings are (a) the apparent disappearance of the discontinuity of the thermal expansion coefficient in the case of polystyrene; (b) the shape of the specific heat curve in the transition region, and (c) the effect of time (or frequency) on the position and magnitude of the transition.

It has already been pointed out that the experimental data on equilibrium volume expansion of polystyrene confirm the existence of a discontinuity; in the one case where similar measurements were made on glass,[34] the discontinuity also persisted. Furthermore, recent measurements[35] of the volume expansion of various polystyrene fractions indicate that in some instances α goes through a maximum at the transition, similar to the specific heat changes observed in second-order transitions of simple low molecular weight compounds or metallic alloys.

At a second-order transition the specific heat changes in a characteristic manner: as the transition point is

[34] A. Winter, J. Am. Ceram. Soc. **26**, 189 (1943).
[35] R. W. Raetz, Monsanto Chemical Company (unpublished data).

approached, it increases more and more rapidly; at the transition point, the specific heat falls back, in the case of small and simple compounds, to a value not much above the one it had many degrees below the transition temperature (λ-transition). Published data on the specific heats of polymers, such as the one shown in Fig. 2, are somewhat different; the specific heat increases rather abruptly in the transition region[36] but fails to return to a low value beyond the transition point. It has been argued[12,37,38] that specific heat curves of this type are characteristic of non-equilibrium conditions. This argument, however, overlooks the fact that, as a result of a second-order transition, additional degrees of freedom of the system might become operative, and the appearance of new degree of freedoms are not the cause but the result of the transition. As a consequence of this, the specific heat remains high and the discontinuity disappears, although very precise measurements over a very narrow temperature region within the transition range might or might not reveal a discontinuity; such data are not yet available for polymers. It should be pointed out that even in low molecular weight materials the transition is frequently not too sharp and that the diffuseness of the specific heat-temperature curve usually, but not necessarily, increases as the molecule becomes larger and more complex. Measurements on C_2F_6[39] illustrate this point very nicely and recent studies of hindered rotation on the same material[40] by means of the line width due to nuclear magnetic moments have shown conclusively that the specific heat change is due to a second-order transition.

Finally, there remains the effect of time or frequency on the position and magnitude of a second-order transition. Second-order transitions are usually free of relaxation effects, that is to say, the transition region or the transition temperature remain unaffected when the transition is studied by the application of external forces of different frequencies. In the case of polymers and glasses this is not so. Increasing the frequency shifts the transition temperature to higher values and also makes the transition region broader. This effect is easily understood when one remembers that the transition in polymers leads to a rubber, which on the basis of many extensive theoretical and experimental investigations[41–47] is the relaxing system par excellence; that is to say, its mechanical properties can quite satisfactorily be explained by a set or distribution of relaxation times. It is obvious, therefore, that as the material goes through the transition into the rubbery state, the relaxation effects will immediately become apparent. One should therefore expect that the transition is sharp when measurements are made at low frequency and becomes more diffuse for higher frequencies, because once the system has gone through the transition one deals with a rubber which will respond to forces of a given frequency according to its relaxation spectrum. This interpretation also explains the poor correlation between temperature and frequency in the transition region discussed in the previous section. The frequency dependance of the transition temperature is therefore not in conflict with the assumption of a true second-order transition but is due to the fact that the mechanical properties of one of the "phases" is determined by a widespread of relaxation times.

IV

It now remains to identify the thermodynamic transition with a reasonable molecular process. The absence of simultaneous electrical, mechanical and thermal data on one polymer makes it impossible to come to a definite conclusion on this point at the present time. However, there are a good many indications which point to one molecular process in preference to several others which *a priori* might be possible. These processes are: (1) melting of crystallites; (2) disappearance of long-range order as in the case of metallic alloys,[48] in ferromagnetic substances,[49] and possibly in some polar crystals;[12,50] (3) hindered rotation.[51,**]

The melting of crystallites can be ruled out as the cause of the transition for the following reasons. No latent heat of fusion has ever been found at the transitions under consideration, which means that no sharp discontinuity has been observed in the specific heat and the transition is not of the first order. It should be pointed out, however, that in the case of partly crystalline polymers, one does observe a transition in the mechanical properties;[52] this transition occurs though at considerably higher temperatures than the second-order transition point. Furthermore, in a study of the volume expansion coefficient (α) of amorphous and partly crystalline rubber, it has been shown[53] that the change in α of the latter material at the melting point is only a fraction of the change occurring in α at the second-order transition point, and that the change in α of the amorphous rubber is equal to the sum of the two

[36] Rands, Ferguson, and Prather, J. Research Nat. Bur. Stand. **33**, 63 (1944).
[37] P. S. Ehrenfest, Comm. Leiden Supplement **75b** (1933).
[38] E. Justi and M. Laue, Zeits. J. Tech. Physik **12**, 521 (1934).
[39] E. L. Pace and J. G. Aston, J. Am. Chem. Soc. **70**, 566 (1948).
[40] H. S. Gutowsky and G. E. Pake, J. Chem. Phys. **18**, 162 (1950).
[41] P. Flory, Chem. Rev. **35**, 51 (1944).
[42] H. M. James and E. Guth, J. App. Phys. **15**, 294 (1944).
[43] M. S. Green and A. V. Tobolsky, J. Chem. Phys. **14**, 80 (1946).
[44] G. Kirkwood, J. Chem. Phys. **14**, 41 (1946).
[45] A. V. Tobolsky and R. D. Andrews, J. Chem. Phys. **13**, 3 (1945).
[46] M. D. Stern and A. V. Tobolsky, J. Chem. Phys. **14**, 93 (1946).
[47] Mooney, Wolstenholm, and Villars, J. App. Phys. **15**, 324 (1944).
[48] F. C. Nix and W. Shockley, Rev. Mod. Phys. **10**, 1 (1938).
[49] R. Becker and W. Doring, *Ferromagnetismus* (Edwards Brothers, New York, 1943).
[50] R. Frohlich, *Theory of Dielectrics* (Oxford University Press, New York, 1949).
[51] L. Pauling, Phys. Rev. **36**, 430 (1930).
** The term "hindered rotation" is used here in the broadest possible sense, including, for example, *cis-trans*-isomerism.
[52] L. Nielsen, Monsanto Chemical Company (unpublished data).
[53] N. Bekkedahl, J. Research Nat. Bur. Stand. **13**, 411 (1934).

separate changes in the partly crystalline material. In other words, the fraction of material which has entered into a crystalline structure does not contribute significantly to the second-order transition at lower temperature. No noticeable change in the x-ray diffraction pattern has been observed in the transition region.

The disappearance of long-range order as a cause of the transition is most unlikely because a transition of that kind presupposes the existence of a "superlattice" for which there exists no experimental evidence in high polymers, at the present time. The rather marked change in the volume expansion coefficient at the transition is another argument against long-range-short-range order transition. Finally, the frequency dependance of the transition—the fact that the transition becomes sharper at lower frequencies and appears to approach a limiting value as $V \to 0$—argues against a transition based primarily on cooperative phenomena.[19]

This leaves the process of hindered rotation[22, 51, 54]—applied here in a very general sense—as the cause of the second-order transition. Experimental evidence available so far and analogies with similar transitions in low molecular weight compounds all favor an interpretation on this basis. First of all, we should recall the volume expansion data on amorphous and partially crystalline rubber, referred to. The non-crystalline phase has its transition at the same temperature and the change in α is of the same type in the amorphous region as it is in the crystalline region. At a given temperature there occurs an "internal" or molecular freezing.[55] This phenomenon has been observed repeatedly in a great many low molecular weight compounds.[54, 56] Such transitions, of which there can be more than one in one compound, are a characteristic property of all solid matter. The close similarity between low and high molecular weight materials is brought out very clearly by the concentration dependance of the transition temperature in polymer-plasticizer compositions.[7, 8, 31, 33, 57] It has already been stated that for several plasticizers transition points have been found experimentally which agree well with extrapolated values from the linear portion of the $T_t - C_v$ curves. It is fortunate that the dielectric and thermal properties of one of these plasticizers, camphor, has been studied extensively[58, 59] where it has been shown that the transitions of this and similar compounds is definitely due to hindered rotation. These studies on camphor furthermore reveal how strongly the transition temperature and the shape of the dielectric constant-temperature curve is affected by slight differences in molecular structure such as *cis-trans*-isomerism. The same has been observed in polymers. Unvulcanized rubber and gutta percha are considered *cis-trans*-isomers exhibiting brittle points at $-58°C$ and $-23°C$, respectively; similarly, the isomers discovered by Schildknecht[60] show characteristic differences in their mechanical properties at room temperature which is indicative of different transition temperatures. It is also of interest to point out that vulcanization leads to an increase in the transition temperature.[5] This has recently been interpreted by Nolle[1] as due to a decrease of the effective chain length between "hindrances." Although vulcanization leads undoubtedly to a large number of crosslinks, it is not the reduced chain lengths which increases the transition temperature, but the increased hindrances which are introduced by sufficiently large amounts of crosslinking.

It appears, therefore, that all available data can be satisfactorily interpreted on the basis of a second-order transition which is due to hindered rotation of complex molecules. The detailed knowledge of the molecular potential which will permit the establishment of a reliable qualitative theory will require more extensive investigation of mechanical, electrical, and thermal properties. The recently developed method of magnetic nuclear resonance[40, 61] should be particularly beneficial.

[54] C. P. Smyth, Chem. Rev. **19**, 329 (1936).
[55] K. Uberreiter, Zeits. f. angew Chemie **53**, 247 (1940).
[56] A. Eucken, Zeits. f. Elektrochemie **45**, 126 (1939).
[57] M. C. Reed and J. Harding, Ind. Eng. Chem. **41**, 675 (1949).
[58] W. A. Yager and S. O. Morgan, J. Am. Chem. Soc. **57**, 2071 (1935).
[59] A. H. White and S. O. Morgan, J. Am. Chem. Soc. **57**, 2078 (1935).
[60] Schildknecht, Gross, and Zoss, Ind. Eng. Chem. **41**, 1998 (1949).
[61] Gutowsky, Kistiakowsky, Pake, and Purcell, J. Chem. Phys. **17**, 972 (1949).

Mechanical Properties of Oriented Polystyrene Film

LAWRENCE E. NIELSEN AND ROLF BUCHDAHL
Monsanto Chemical Company, Plastics Research Laboratory, Springfield, Massachusetts

Cast films of polystyrene were oriented by stretching at temperatures above the softening temperature of the material and then cooled. A factorially designed experiment was carried out in which the amount of stretching, temperature of stretching, time held in the stretched state before cooling, and effect of several cycles of stretching before cooling were investigated as they affect the birefringence, the stress-strain properties, dynamic modulus and damping, and the softening temperature of polystyrene.

The values of many of the mechanical properties are more closely related to the birefringence than to the amount of hot stretching. In general, the value of the stress-strain properties in the direction of hot stretch, the dynamic modulus, and the birefringence all increase with an increase in the amount of stretching, a decrease in temperature, an increase in rate of cooling after stretching, and a decrease in the number of times the film was stretched before finally cooling. The softening temperature is decreased in direct proportion to the birefringence. Annealed films give higher softening temperatures than films which have been stretched and then allowed to shrink before cooling.

IT is quite well known that often remarkable changes in the physical properties of a high polymeric substance may be brought about by stretching the material while it is at a temperature above its softening point and then cooling it down.[1–3] However, practically no quantitative data have been published showing how the mechanical properties such as the stress-strain characteristics are changed by such a treatment.

This stretching process undoubtedly causes the high polymer molecules to become oriented or arranged in a configuration different from their normal arrangement. On cooling after stretching, the material changes from a soft rubber-like state to a rigid state, thereby "freezing" the molecules in an oriented condition. These lined up molecules, which have different characteristics parallel and perpendicular to their long dimension, give an anisotropic behavior to many physical properties. For instance, the stretched material may show optical anisotropy or birefringence, and the mechanical properties such as ultimate strength may differ greatly parallel and perpendicular to the direction of stretch.

Orientation phenomena are very complex in nature not only because there are many variables such as the amount of stretch and the temperature at which stretching took place but also because of the fact that there are different kinds of orientation. In this investigation only stretching in one direction will be considered. Furthermore, all the data and discussion to follow except on birefringence apply only to the direction of stretch and not to the direction perpendicular to it. It is to be expected that entirely different properties will be found in the direction perpendicular to the stretch.

The problem of quantitatively measuring the degree of orientation arises. On the basis of past work it appears that the birefringence is one of the best methods of measuring the orientation. The amount of hot stretching is not satisfactory because of the tendency of the molecular segments to assume an unoriented condition. Therefore, for a given amount of hot stretching the number of oriented molecular segments found in the cooled sample depends upon the temperature of stretching, how fast the specimen was stretched, and how long it took the specimen to cool down.

All oriented specimens were made up according to the factorial design given in Table I. A factorially designed experiment was chosen because several variables were to be studied and it was desirable to know to what extent these variables interact with one another. In addition it is possible to obtain the largest amount of

TABLE I. Design of experiment on oriented polystyrene films.

Elongation percent	50				150				300			
After treatment	Chilled		Relaxed		Chilled		Relaxed		Chilled		Relaxed	
Amount of working	O	X	O	X	O	X	O	X	O	X	O	X
Temperature	105 115	105 115	105 115	105 115	105 115	105 115	105 115	105 115	105 115	105 115	105 115	105 115
Specimen No. 1	1CO11 1CO21	1CX11 1CX21	1RO11 1RO21	1RX11 1RX21	2CO11 2CO21	2CX11 2CX21	2RO11 2RO21	2RX11 2RX21	3CO11 3CO21	3CX11 3CX21	3RO11 3RO21	3RX11 3RX21
Specimen No. 2	1CO12 1CO22	1CX12 1CX22	1RO12 1RO22	1RX12 1RX22	2CO12 2CO22	2CX12 2CX22	2RO12 2RO22	2RX12 2RX22	3CO12 3CO22	3CX12 3CX22	3RO12 3RO22	3RX12 3RX22

[1] J. Bailey, India Rubber World **118**, 225 (May, 1948).
[2] H. Müller, Kolloid Zeits. **95**, 138, 306 (1941).
[3] H. Müller, Wissenschaftliche Veröffentlichungen aus den Siemens Werken **19**, 110 (1940).

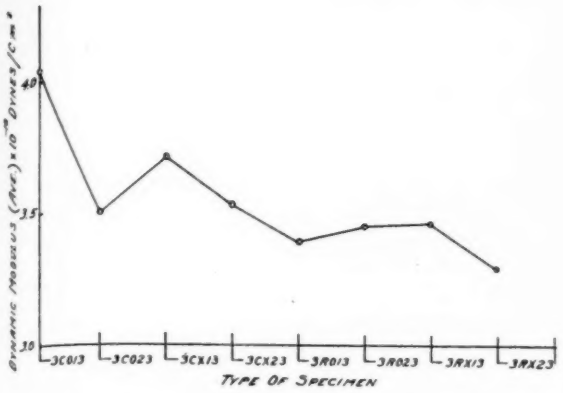

FIG. 1. Dynamic Young's modulus of oriented polystyrene films at 25°C.

information with the smallest amount of work with this type of experiment. All specimens were made from strips of film which before stretching were one inch wide and roughly 0.015-inch thick. These films had been cast from methyl ethyl ketone and were carefully dried and annealed for several days as previously described.[4] Studies were made at three levels of elongation—50 percent, 150 percent, and 300 percent hot stretch. Two types of after-treatment were used. In the one case the film was immediately chilled to below the softening temperature after stretching. In the other case the film was held at its final length for 200 seconds before cooling. It has been shown[5] that the birefringence and retractive force of the film are greatly decreased from their initial value after 200 seconds, even though the length has been held constant. Therefore, it was important to be able to separate effects due to elongation from those determined primarily by birefringence or "frozen in" stresses. From our previous work,[5] it had been found that such properties as creep depend upon whether the film had been used previously for such a test. Therefore, for lack of a better term the effect of "working" was investigated. In Table I "O" stands for stretching with no previous working while X means the sample was twice stretched and then allowed to shrink to nearly its original length before the film was stretched again and then cooled. Stretching was carried out at two different temperature levels. At 105°C the film is quite stiff and only slightly rubber-like in nature while at 115°C the polystyrene films are very much like a rubber. In the code numbers to designate the specimens the first numbers 1, 2, and 3 stand for 50 percent, 150 percent, and 300 percent elongation, respectively. Figures 1 and 2 in fourth position of the code numbers indicate 105°C and 115°C, respectively. The number of the sample is given by the last number of the code. For example, a code number 2CO13 would mean the sample had been elongated 150 percent and immediately chilled without working at a temperature of 105°C and that it was the third such specimen prepared. In addition to these 24 types of oriented films some experiments for comparison were made on annealed unoriented films and worked unoriented films. These latter were prepared by stretching and shrinking the film twice before cooling down with no stretching. Actually in most cases the worked films did not completely shrink to their original length; the birefringence, though, was either zero or very small compared to the oriented films.

The following measurements were made on these films: birefringence, tensile stress-strain tests, softening temperature, dynamic Young's modulus, and mechanical damping.

DYNAMIC MECHANICAL TESTS

Since it was suspected that the dynamic Young's modulus and mechanical damping were not radically changed by orientation in the case of polystyrene, only specimens elongated 300 percent were studied. The dynamic properties were determined with an electromagnetic reed vibrator.[4,6–8] The modulus was calculated from the resonance frequency and the damping from the half-width of the resonance peak. (The half-width of the resonance peak may be expressed as the ratio of the imaginary to real part of Young's modulus by dividing the half-width by $\sqrt{3}$.) The results at 25°C and 30 c.p.s. are summarized in Table II and Fig. 1. Results on annealed and worked films are also included.

Figure 2 compares the damping (half-width of resonance peak) for annealed, worked, and typical oriented (3RX23) films as the temperature is varied.

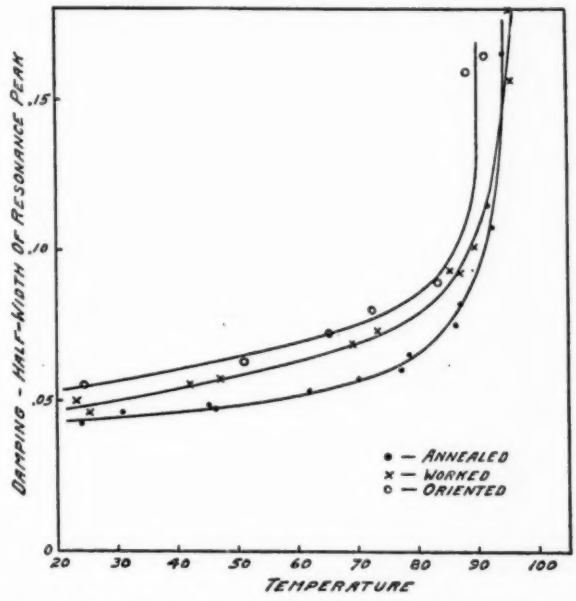

FIG. 2. Mechanical damping as a function of temperature for annealed, worked, and typical oriented polystyrene films.

[4] Merz, Nielsen, and Buchdahl, J. Polymer Sci. **4**, 605 (1949).
[5] L. E. Nielsen and R. Buchdahl, J. Chem. Phys. **17**, 839 (1949) and J. Colloid Sci. (to be published).
[6] L. E. Nielsen, A.S.T.M. Bulletin **165**, 48 (1950).
[7] A. W. Nolle, J. App. Phys. **19**, 753 (1948).
[8] J. Ballou and J. Smith, J. App. Phys. **20**, 493 (1949).

TABLE II. Dynamic mechanical properties of oriented and unoriented polystyrene films at 25°C.

Type of film	Birefringence A/mil (av.)	Dynamic Young's modulus (dynes/cm²)	Half-width of resonance peak	No. of specimens tested
Annealed	0	$3.24\pm0.10\times10^{10}$	0.046 ± 0.002	5
Worked	~0	$3.18\pm0.14\times10^{10}$	0.049 ± 0.0015	4
3CO13	4500	$4.04\pm0.20\times10^{10}$	0.054 ± 0.002	6
3CO23	2640	$3.50\pm0.09\times10^{10}$	0.049 ± 0.001	3
3CX13	4280	$3.71\pm0.19\times10^{10}$	0.053 ± 0.004	3
3CX23	1970	$3.53\pm0.24\times10^{10}$	0.051 ± 0.002	4
3RO13	2090	$3.39\pm0.08\times10^{10}$	0.051 ± 0.002	3
3RO23	864	$3.45\pm0.13\times10^{10}$	0.056 ± 0.004	3
3RX13	1580	$3.46\pm0.12\times10^{10}$	0.050 ± 0.004	3
3RX23	814	$3.29\pm0.16\times10^{10}$	0.056 ± 0.000	3

On the basis of these results, it is seen that orientation increases the modulus of polystyrene. Comparison with birefringence data indicates the dynamic modulus varies in about the same way as the birefringence. Damping also increases with orientation but only slightly and part of this increase may be attributed to the effect of working which automatically takes place during the process of stretching the film. Both orientation and working lower the transition temperature range where the damping increases very rapidly with temperature.

BIREFRINGENCE AND STRESS-STRAIN DATA

The birefringence and stress-strain data are given in Table III. The notation is the same as used in Table I. Duplicates were made of all the specimens.

The birefringence was measured by a Babinet compensator using polarized light. Figure 3 indicates how the average birefringence changes with the different types of specimens. The birefringence of films stretched at 105°C is always considerably higher than that of films stretched at 115°C, the other conditions being held constant. Chilling the film immediately after stretching gives a higher birefringence than if the film is held in the stretched state for 200 seconds before cooling. Of course, the greater the elongation the greater is the birefringence if the other variables are held constant. Working has very little effect. An analysis of variance[9] was carried out on these data and the effects of the variables temperature, amount of stretching, and after-treatment were found to be significant at the 99.9 percent level of confidence. There seems to be no interaction of the variables in the case of birefringence.

The stress-strain data were obtained on an Instron machine[10] using a crosshead speed of 0.2 inch/minute and a specimen length of 2 inches between the clamps. The tests were conducted at a temperature of 25°C under a relative humidity of 50 percent. Table III also contains data on unoriented annealed and unoriented worked films for comparison; these data are the average

TABLE III. Birefringence and stress-strain data on oriented polystyrene films.

Specimen	Birefringence (A per mil $\times10^{-3}$)	Modulus (psi $\times10^{-5}$)	Elongation at yield (percent)	Elongation to break (percent)	Yield stress (psi)	Ultimate strength (psi)	Energy to break (arbitrary units
1CO11	11.2	2.68	7.40	7.40	10480	10480	3670
1CO12	13.2	3.08	—	5.80	—	10420	4790
1CO21	3.35	2.88	4.75	4.75	7600	7600	2090
1CO22	4.72	2.49	4.65	4.65	8560	8560	2130
1CX11	9.03	3.72	—	5.00	—	9580	2660
1CX12	11.3	2.85	—	4.90	—	9620	2730
1CX21	3.20	2.17	—	3.70	—	7850	1610
1CX22	5.07	2.79	—	4.25	—	7870	1990
1RO11	2.64	2.73	—	3.85	—	7700	1740
1RO12	3.91	2.79	—	4.00	—	7730	1760
1RO21	1.24	3.03	3.25	4.00	7130	6850	1880
1RO22	2.01	3.46	—	3.60	—	7300	1510
1RX11	2.45	2.91	—	3.90	—	7600	1650
1RX12	3.29	3.03	—	3.70	—	7460	1550
1RX21	1.18	2.97	3.25	3.50	6680	6620	1360
1RX22	1.86	2.70	4.40	4.40	6440	6440	1750
2CO11	32.2	4.17	4.65	4.90	10850	10650	3620
2CO12	28.4	3.45	5.55	6.85	10820	8870	5280
2CO21	10.7	3.52	5.20	5.30	10400	10400	3460
2CO22	12.8	3.51	5.25	5.60	10100	9380	3920
2CX11	24.0	3.74	5.30	5.60	11250	11250	4000
2CX12	26.8	3.68	4.75	5.00	10380	9820	3240
2CX21	9.22	3.52	—	4.00	—	9120	2180
2CX22	12.2	3.40	4.85	5.50	10900	9320	3670
2RO11	8.42	3.33	5.10	5.10	10250	10250	3310
2RO12	9.69	3.25	5.10	5.10	10240	10240	3310
2RO21	4.48	3.11	4.00	4.90	8770	8550	2290
2RO22	5.16	3.11	—	3.85	—	8940	2150
2RX11	10.0	3.49	—	4.00	—	9350	2170
2RX12	8.68	3.42	—	4.25	—	10180	2390
2RX21	4.95	3.22	4.20	4.20	8590	8590	2170
2RX22	4.89	3.15	—	3.45	—	8740	1630
3CO11	50.6	3.74	4.60	6.35	10100	9540	4720
3CO12	65.8	4.81	4.50	6.20	10810	10000	2170
3CO21	41.2	4.64	4.35	5.35	11770	9700	4380
3CO22	31.4	3.75	4.75	7.50	10350	8290	5730
3CX11	47.0	4.25	4.40	5.70	10950	10420	4470
3CX12	35.7	3.63	4.25	4.95	10340	9740	3450
3CX21	22.3	3.68	4.40	5.05	9730	9170	3460
3CX22	33.2	3.51	4.25	5.05	10560	9340	3590
3RO11	23.4	3.46	4.50	5.75	10300	9160	4080
3RO12	18.5	3.61	4.60	9.25	10780	7330	6960
3RO21	11.0	3.71	4.30	4.60	10360	10100	3220
3RO22	10.9	3.70	4.25	4.25	10640	10640	2900
3RX11	17.9	2.98	4.25	4.75	9310	8660	2770
3RX12	29.7	3.63	4.25	4.70	10570	8850	3270
3RX21	10.3	3.22	—	4.20	—	9800	2290
3RX22	8.55	3.66	4.05	4.05	10000	10000	2530
Annealed (av.)	0	2.66	—	2.53	—	6170	
"Worked" (av.)	0.35	2.70	3.00	3.00	6720	6720	

of 3 specimens each. The blank spaces in the columns for yield data arise from the fact that not all of the

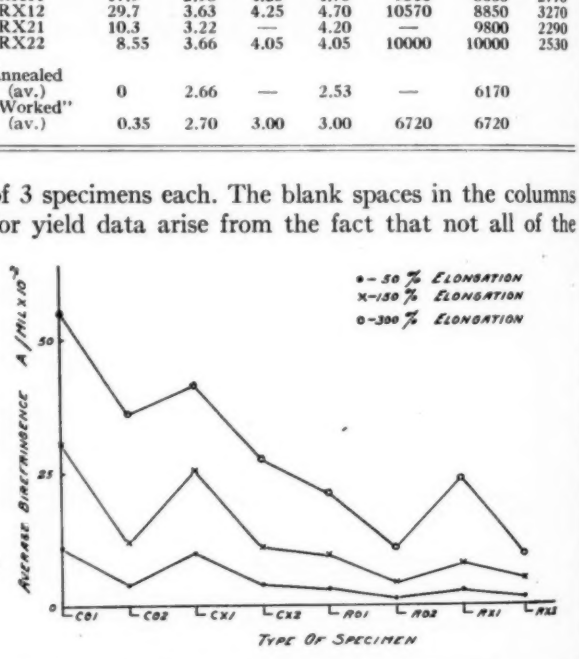

FIG. 3. Birefringence of oriented polystyrene films prepared under various conditions. The types of specimen are designated by the code given in Table I.

[9] K. A. Brownlee, *Industrial Experimentation* (Chemical Publishing Company, Inc., Brooklyn, New York, 1947).
[10] G. S. Burr, Electronics **22**, No. 5, 101 (1949).

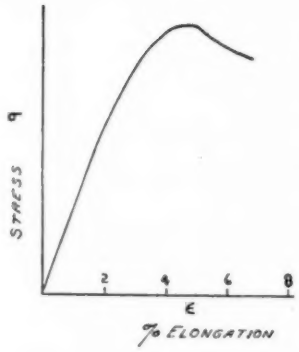

FIG. 4. A typical stress-strain curve for oriented polystyrene films.

specimens gave a yield value. A typical stress-strain curve is given in Fig. 4.

The variation in Young's modulus for the different types of samples is illustrated in Fig. 5. It will be noted that the modulus shows some of the same general trends as the birefringence. The modulus increases with the amount of hot stretching and usually decreases with temperature. However, the analysis of variance indicates the effects of these variables to be at only about a 90 percent level of significance and are largely covered up by a large interaction between elongation and after-treatment. The effect of working and after-treatment on the modulus is not significant. All the oriented films have higher moduli than annealed or unoriented worked films.

The analysis of the data on elongation to break the specimens indicates the elongation increases with the amount of stretching (99 percent level of significance), it decreases with increase in temperature (99 percent level of significance) and it decreases with working (99.9 percent level of confidence). The elongation to break is greater for chilled than relaxed specimens with a level of confidence of 99.9 percent. There are no interactions between the variables for the data on elongation to break. During the tests it was noted that if a yield point was reached, all further elongation took place near this yield point in a small band across the specimen. Much larger elongations would have been observed if all the specimen had elongated as much as that portion near the original point of yielding.

The energy to break a specimen, that is, the area under the stress-strain curve, is relatively free of interactions between the variables also. The more the specimen is stretched while soft the greater is the energy to break (99.9 percent level of significance). Increasing the temperature decreases the area under the stress-strain curve (99 percent level of significance). The values are larger for chilled than relaxed specimens (99.9 percent level of significance). Working decreases the energy to break (99 percent level of significance). The energy to break also shows the same general trends as the birefringence.

The ultimate strength is a complex function of the variables studied, although all the oriented specimens gave higher values than the unoriented ones. The analysis of variance indicated the most significant factor was a very strong interaction between the three variables, amount of stretch, after-treatment, and temperature. Undoubtedly, some of this complexity is brought about by the fact that some of the specimens had yield points and others did not. Most of the specimens which did show yield points gave low values of tensile stress once the yield point was passed, as is shown in Fig. 4. Those films with the greatest amount of hot stretching in general gave yield values while the films with the least amount of stretching broke at the yield point or before. Therefore, the expected increase in ultimate strength with amount of stretching was not picked up.

An analysis of variance was not made on the elongation at yield and the stress at the yield point since some of the films did not show a yield point. Certain general conclusions may be made though. The greater the amount of hot stretching the greater is the possibility of reaching a yield point. Most of the films with 50 percent stretching broke at the yield point or before it was reached. Neither the elongation at yield nor the yield stress depends to any great extent on the temperature of stretching, after-treatment, or working. Although none of the unoriented annealed films gave a yield point, all the unoriented worked films did, surprisingly enough.

In the cases where there are no interactions of the variables as shown by the analysis of variance, it is possible to calculate quite accurately the variation of the properties as the variables are changed. These results are summarized in Table IV.

Since many of the mechanical properties appear to vary in the same manner as the birefringence, correlation coefficients were determined. The results are summarized in Table V. These correlation coefficients were found for the following equations:

$$10^{-5}E = 2.50 + 0.85 \log B$$
$$\epsilon_b = 3.26 + 1.65 \log B$$
$$\sigma_b = 5708 + 3510 \log \log B$$
$$\log(A - 3.00) = 0.13 + 0.32 \log B.$$

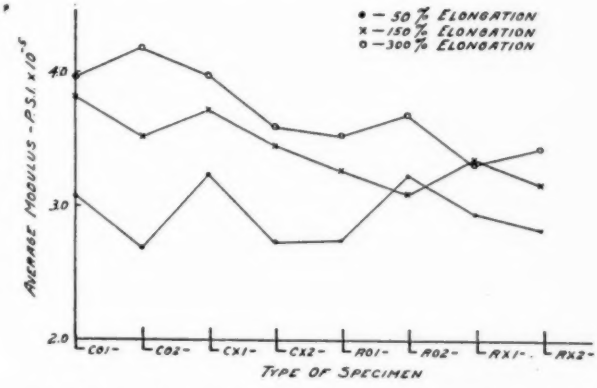

FIG. 5. Young's modulus calculated from the initial slope of the stress-strain curves of oriented polystyrene films. The code designating the types of specimens is given in Table I.

TABLE IV. Relative value of properties on changes of variables.[a]

Property	ϵ_2/ϵ_1	ϵ_3/ϵ_1	T_2/T_1	t_2/t_1	W_2/W_1
Birefringence	2.76	5.74	0.52	0.39	1.0
Elong. @ break	1.09	1.23	0.86	0.83	0.84
Energy to break	1.40	1.72	0.80	0.73	0.77

[a] The reference values are: ϵ_1=50 percent hot stretch; T_1=105°C; t_1=chilling after stretching; W_1=no working. The other variables are: ϵ_2=150 percent; ϵ_3=300 percent; T_2=115°C; t_2=relaxed before cooling; W_2=working.

TABLE V. Correlation of birefringence with stress-strain properties.

Variables	Correlation coefficient
Birefringence and Young's modulus	0.813
Birefringence and elongation	0.717
Birefringence and tensile strength	0.802
Birefringence and energy to break	0.864

In these equations B=birefringence in A/mil$\times 10^{-2}$, E=Young's modulus in pounds/square inch, ϵ_b=percent elongation at break, σ_b=tensile strength in pounds/sq. in., and A=the energy to break in arbitrary units.

Table V shows that the stress-strain properties of oriented polystyrene films are very closely related to their birefringence. It is known that birefringence is a fairly good quantitative measure of orientation, and it appears that the mechanical properties are primarily dependent also upon this degree of orientation. The effects of such variables as temperature, after-treatment, and working are, to a first approximation, important only to the extent they change the birefringence. However, the importance of these other variables cannot be completely overlooked in interpreting the stress-strain properties of oriented polystyrene.

SOFTENING TEMPERATURES

One of the most important properties of plastics from the practical standpoint is a softening temperature. This softening temperature may be defined in various ways, but in all cases it gives an indication of the temperature range where the material goes through a transition from a hard, rigid substance to a soft, rubbery one.

If an oriented film is placed in an oven in which the temperature is gradually increasing, the length of film will remain nearly constant until the softening temperature is reached. Over a very narrow temperature range, the film will then rapidly shrink in length as the orientation starts to disappear. Müller[3] has shown that the softening temperature is lowered as the birefringence of the oriented films increases. This has been checked using films whose birefringence has been varied by different amounts of stretch, stretching at different temperatures, and by different after-treatments. Results are given in Table VI and Fig. 6. The softening temperature was arbitrarily defined as that temperature at which the specimen had shrunk one percent. The temperature of the oven was increased at the rate of about ½°C per minute.

TABLE VI. Change in softening temperature with birefringence.

Film No.	Birefringence A/mil.	Softening temperature °C
2RX23	400	95.3
2CO23	1020	93.5
2CX13	2150	91.0
3CO13	5950	83.2

From these results, it is obvious that the lowering of the softening temperature is primarily dependent upon the birefringence and not upon other possible variables such as elongation or after-treatment.

The softening temperature is also altered by an externally applied force[11] or by working. The effect of stress was verified by gradually heating the specimens to which tensile loads of different sizes were applied by hanging weights from clamps. The length of specimen remains nearly constant till a very sudden increase in length takes place on reaching the softening range. Some of the data are illustrated in Fig. 7, where the softening temperature was again taken as the temperature where the total elongation was 1 percent. The worked films give a softening temperature several degrees lower than annealed films. Since some working automatically takes place in the process of orienting the films by stretching, it is to be expected that the softening temperature extrapolated to zero birefringence (see Fig. 6) would be lower than the softening temperature obtained by extrapolating to zero external force (see Fig. 7). This turns out to be the case, the values being 96.6°C and 98.0°C respectively.

DISCUSSION

On the basis of the data presented here and in the past,[3,5] it has been shown that orientation or the

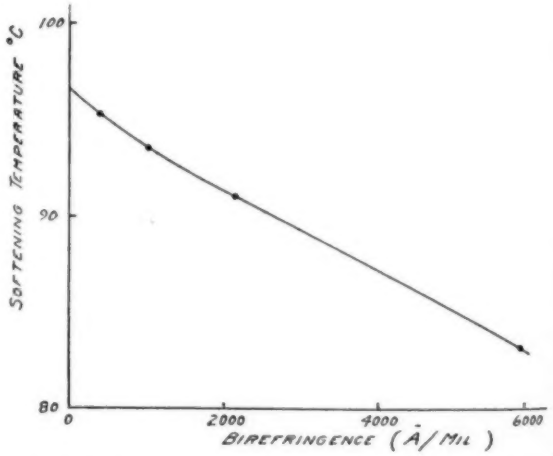

FIG. 6. Variation of softening temperature with the birefringence of oriented films.

[11] R. F. Boyer and R. S. Spencer, J. App. Phys. **16**, 594 (1945).

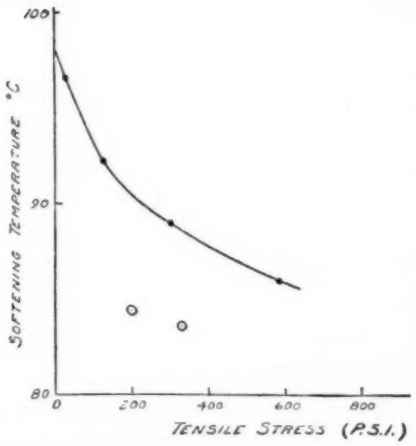

FIG. 7. Variation of softening temperature with tensile load for annealed polystyrene films. The two points enclosed in circles are for unoriented worked films.

lining up of molecular segments is far more accurately measured by birefringence than by the amount of hot stretching in the case of polystyrene. Widely different values of birefringence may be obtained with the same amount of stretching by changing the temperature at which stretching takes place, or by holding the hot film in the stretched state for some time to allow some of the molecular segments to resume their normal relaxed state. Such properties as the softening temperature, and elastic modulus reflect the changes in birefringence which are brought about by these different treatments.

We attribute the decreased birefringence and changes in mechanical properties which accompany an increase in the stretching temperature as due primarily to the molecules being able to assume a relaxed or unoriented condition more rapidly as the temperature increases. Similarly, most of the changes brought about by the after-treatments, such as chilling immediately after stretching or allowing some time to elapse before cooling, may be explained in terms of the degree of orientation "frozen" into the cooled films.

Some of the phenomena which appear to be influenced by "working" may be due to the partial destruction of the network structure of entangled and intertwined molecules found in polystyrene.[5] Other effects such as the lowering of the softening temperature are believed to be due to non-equilibrium conditions existing in worked films. In an annealed film the molecules have had time to assume their most probable shapes and configurations. However, on stretching and shrinking a film, many molecular segments are forced into positions and shapes not most favorable for them; this working would then be expected to decrease the density of the material over that found under equilibrium conditions existing in annealed films. This slight increase in the average distance between molecules of the worked films would be expected to lower the softening temperature somewhat.

We wish to express our appreciation to Mr. C. H. Adams and to the Fabrics Research Laboratory for their help in securing the stress-strain data and to Mr. E. C. Harrington who carried out the statistical analysis of the data.

A Non-Destructive Mechanical Test for Animal Fibers

HARRIS M. BURTE*
The Textile Research Institute and the Department of Chemical Engineering, Princeton University, Princeton, New Jersey

The slope of the force-extension curve in the Hooke's law region can be measured non-destructively, for animal fibers, at three to fifteen minute intervals. The change of this Hookean slope with time is used to follow the course of the heterogeneous reaction between wool and a reagent.

Data are presented on the interaction between concentrated neutral salt solutions and wool fibers. These results indicate that wo processes occur: (a) Relatively rapid hydration or dehydration of the fiber until equilibrium with the activity of water in the salt solution is attained; (b) Relatively slow absorption of salt ions by the fiber. Very concentrated salt solutions dehydrate the fiber so completely that absorption of salt ions is not possible. Swelling experiments and experiments involving other mechanical properties confirm these hypotheses. The interaction between wool fibers and aqueous solutions of large organic molecules follows a similar pattern.

MOST natural high polymers are chemically and morphologically quite complex. A study of the mechanisms and kinetics of their reactions using the classical methods of chemical analysis is frequently a laborious task. Their mechanical properties, however, are easily measured, and usually are strongly affected by chemical treatment. The investigation of chemical reactions by using a mechanical property as the measured parameter has therefore attained some popularity. The present work is concerned with a further extension of these mechano-chemical methods[1] in the field of animal fibers, e.g. hair and wool.

Speakman[1] has developed a non-destructive mechanical test with which he and others have investigated many of the changes resulting from treatment of wool fibers. The basis of the method is the fact that if a wool fiber is rapidly stretched to not more than 30 percent extension in cold water, contracted and allowed to rest 24 hours in cold water before re-extending, the second force-extension curve will closely duplicate the first. Thus, if a chemical reaction were carried out on the fiber just before the second test, the difference between the first and second force-extension curves would be due solely to the effect of the chemical reaction. The initial extension to 30 percent coupled with the rest in water was a non-destructive test. The advantages of such a test are very great; since both measurements are made on a single fiber, the need for cross-sectional area or denier measurements is eliminated and the problem of fiber-to-fiber variance is largely circumvented.

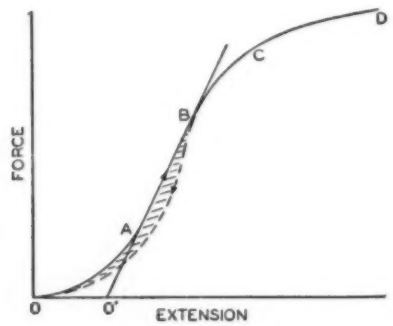

FIG. 1. Typical force-extension curve in the low range of extensions.

One objection to the test described above is the long time necessary between successive measurements. Furthermore, in order to follow the change of mechanical properties with time of treatment, a series of fibers must usually be used with the introduction of errors due to fiber-to-fiber differences. Speakman[1] points out that 30 percent extension is merely a general limit applicable to most animal fibers, and that for special conditions less drastic extensions might be needed. In the present work attention was focused on the Hooke's law region of the force-extension curves. Figure 1 shows a typical force-extension curve for a single wool fiber. In the region O–A the crimp of the fiber is being removed, in the region A–B (Hooke's law region) the force is linear with extension, in the region B–C the curve begins to depart from linearity and at some position, C, the yield point is reached. Extension of the fiber is usually measured from point O′, and C generally occurs at from one to two percent extension. The slope of the curve in the linear region A–B will be called the Hookean slope. The fiber is not acting like a true Hooke's law spring in this region, since the contraction curve (dotted line) is always of initially steeper slope than the extension curve and a hysteresis loop (cross hatched) is formed. The Hookean slope is, however, a perfectly definite property that can be measured quite accurately. Dividing it by the cross-sectional area of the fiber will give a quantity analagous to Young's modulus.

Woods[2] has measured the Hookean slope for wool and hair as a function of relative humidity. He states that "under a very wide range of conditions an extension of the fibre by one percent or so involves no change in the fibre properties." The conditions under which the Hookean slope measurement is non-destructive were more closely investigated in the present work.

EXPERIMENTAL TECHNIQUE

Measurements of all mechanical properties were made with the Instron Tensile Tester.[3] Usually, the fiber was

* Research Fellow of the Textile Research Institute.
[1] J. B. Speakman, J. Textile Inst. **38**, T102–126 (1947).
[2] H. J. Woods, Proc. Leeds Phil. and Lit. Soc. (Sci.) **3**, 577–583 (1940).
[3] H. Hindman and G. S. Burr, Trans. Am. Soc. Mech. Eng. **71**, 789–796 (1949).

extended slightly into the region B–C, and immediately contracted. For sample lengths of one to three inches, the rate of extension used was 0.10 in. per minute. Depending upon the fiber type and conditions of testing, it was possible to make a measurement of the Hookean slope every 3 to 15 min. without any dependence of the Hookean slope on the number of determinations. The shorter time intervals were for water soaked fibers; as the relative humidity of the air surrounding the fiber decreased, the longer time intervals were needed. If the time intervals between measurements were too short, successive values of the Hookean slope would show a slight increase. The fact that both of the above observations are due to imperfect elasticity of the fiber, even when it is extended only one to two percent, is shown in Fig. 2. The time interval between extensions was three to four minutes, the amount of semi-permanent set caused by the first extension was only 0.125 percent, yet it caused an increase in the Hookean slope of 7.3 percent (i.e., from 33.1 to 35.5 g/cm). When a sufficient time interval was allowed, successive measurements were reproducible to about ± 1 percent. Furthermore, the test is non-destructive when performed on chemically treated fibers, whereas an extension to 30 percent would often cause a permanent change in fiber properties. Therefore, it is possible to use a *single* fiber to follow the change of Hookean slope as a chemical reaction with the fiber proceeds, and the change in Hookean slope will be due solely to the effect of the reaction. Tobolsky and Andrews[4] have performed similar experiments with rubber, calling the method "intermittent relaxation."

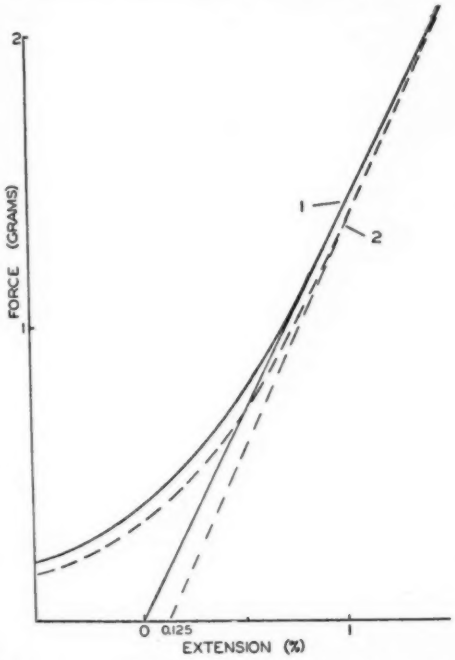

FIG. 2. Two successive measurements of the Hookean slope. (Three to four minute interval between extensions. R.H.=65 percent.) 1—First extension, Hookean slope=33.1 g/cm. 2—Second extension, Hookean slope=35.5 g/cm.

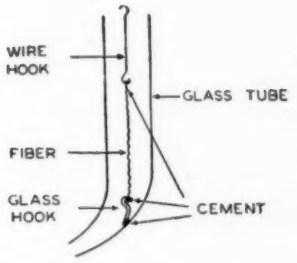

FIG. 3. Single fiber mounted for testing.

THE INTERACTION BETWEEN WOOL AND CONCENTRATED NEUTRAL SALT SOLUTIONS

As an example of the use of the non-destructive Hookean slope technique, some work on the heterogeneous reaction between single wool fibers and concentrated neutral salt solutions will be described.

Sookne and Harris[5] have shown that the mechanical properties of wool fibers immersed in concentrated solutions of neutral salts are not the same as the properties when in an atmosphere in equilibrium with these solutions. Neither are they the same as the properties of the fiber in pure water. In the present work, fibers at different initial conditions were treated with various concentrated neutral salt solutions. The change of Hookean slope with time of treatment was measured, and was plotted as k/k_0 *vs.* time, where k is the Hookean slope at any time after the reaction has started, and k_0 is the Hookean slope at zero time. The dimensionless quantity (k/k_0) is Woods' "relative Young's modulus."[2]

The fibers studied were from a sample of Columbia ewes wool, 56's grade, which had been cleaned by successive ether extractions and water washings. Single fibers were mounted in suitable containers by means of small hooks and de Khotinsky cement (Fig. 3). The container was attached to the Instron crosshead, the wire hook to the Instron load cell. All values of the Hookean slope were corrected for the small error introduced by the deflection of the load measuring element of the Instron Tester.

The curves of relative modulus (or relative Hookean slope) *vs.* time, for initially wet fibers that were treated with saturated salt solutions, are given in Fig. 4. The following explanation is proposed:

(a) Since the diffusion of water into, and out of, the fiber is probably much more rapid than the diffusion of salt ions, the first process to occur on immersing the fiber in a salt solution will be a dehydration or hydration of the fiber (depending upon its initial state) to a state in equilibrium with the activity of water in the salt solution. For the present purposes, the activity of the water can be indicated by the relative humidity over the solution. Woods[2] and Speakman[6] have shown that

[4] A. V. Tobolsky and R. D. Andrews, J. Chem. Phys. **13**, 3–27 (1945).

[5] A. M. Sookne and M. Harris, American Dyestuff Reporter **26**, 659–666 (1937); **27**, 171–173 (1938).

[6] J. B. Speakman, J. Soc. Chem. Ind. **49**, 209T (1930).

FIG. 4. Relative modulus *vs.* time after adding saturated salt solutions to an initially wet fiber.

dehydration of the fiber will cause the Hookean slope to increase.

(b) Concurrently, a slower process of absorption of the salt ions by the wool fiber occurs. These ions form lyospheres around charged centers in the fiber which are probably the acidic and basic side chains. Lundgren and co-workers[7] have proposed a very similar scheme to account for the effect of salts on synthetic feather keratin fibers. Absorption of the salt ions decreases the Hookean slope by either breaking salt linkages, or increasing the separation of the long polypeptide molecular chains of which the wool is composed. Both mechanisms may be important.

(c) If the activity of water in the salt solution is very low, the consequent rapid dehydration of the fiber may reduce the swelling to such an extent that the slower subsequent diffusion of the salt ions into the wool fiber is greatly hindered. Speakman[8,9] has shown that a wet fiber will absorb molecules that are too large to diffuse into a dry fiber.

Thus, when the fiber was treated with a saturated solution of either sodium chloride or sodium bromide (Fig. 4) the first process was one of dehydration causing the relative modulus to increase. Note that, as expected, the lower the relative humidity over the solution, and thus the greater the dehydration, the greater was the initial increase in relative modulus. The concurrent

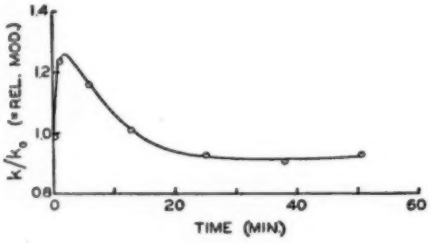

FIG. 5. Relative modulus *vs.* time after adding a lithium chloride solution (one vol. saturated solution, 2 vol. water) to an initially wet fiber.

[7] Lundgren, Stein, Kearn, and O'Connell, J. Phys. and Colloid Chem. **52**, 180–206 (1948).
[8] J. B. Speakman, J. Soc. Chem. Ind. **48**, T321–324 (1929).
[9] J. B. Speakman, Proc. Roy. Soc. **132A**, 167–191 (1931).

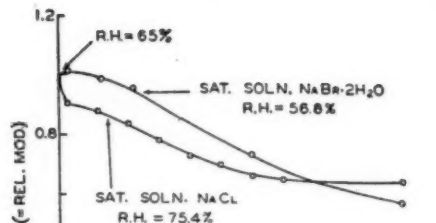

FIG. 6. Relative modulus *vs.* time after adding saturated salt solutions to a fiber initially at 65 percent R.H.

slower absorption of salt ions caused the decrease after the maximum. The bromide causes a greater decrease than the chloride, but the reason for this is not clear. The upper curve, obtained with the saturated lithium chloride solution with a very low partial pressure of water vapor over it, shows no evidence of the absorption of salt although some absorption undoubtedly took place in the early stages of dehydration before the molecular network was sufficiently dehydrated to forbid further diffusion of the salt ions. It might be pointed out that all the curves of Fig. 4 were obtained on the same fiber. It had previously been found that prolonged washing in water would remove all of the absorbed salt, and leave the fiber in its initial state. As might be expected, when a fiber in equilibrium with a saturated sodium bromide or sodium chloride solution was immersed in water, the relative modulus-time curve was found to go through a minimum as first water diffused into the partially dehydrated fiber and then the salt ions diffused out.

For an unsaturated lithium chloride solution, the dehydration of the fiber should not be great enough to prevent absorption of the salt ions, and a maximum in the relative modulus-time curve should be observed. In Fig. 5 this effect is shown for a different fiber from the one illustrated in Fig. 4. Note that, for this concentration of lithium chloride the Hookean slope finally decreased below the initial value in water. This action might be expected, since Alexander[10] has pointed out that lithium salts will cause hydrogen bond breakdown, which would be in addition to the salt effect described above.

When a fiber initially conditioned at 70°F, 65 percent R.H. was brought into contact with a saturated sodium chloride solution the relative modulus-time curve (Fig. 6) decreased rapidly at first as water was absorbed to bring the fiber to equilibrium with the higher activity of water, corresponding to a relative humidity of 75.4 percent, in the salt solution. This decrease was followed

[10] P. Alexander, Research **2**, 246–247 (1949).

by another slower one as salt ions were absorbed. When, however, a different fiber initially at 65 percent R.H. was immersed in a saturated sodium bromide solution (R.H.=56.8 percent) the relative modulus-time curve went through a slight maximum as the two effects of slight further dehydration of the fiber and absorption of salt ions opposed each other. Eventually, the relative modulus decreased as the ions were absorbed. When this fiber was then removed from the bromide solution and allowed to come to equilibrium with a 65 percent R.H. atmosphere, a slight further decrease of the relative modulus was noted. The latter decrease resulted from the fact that water could be absorbed from the atmosphere (which was at a higher relative humidity than that corresponding to the saturated sodium bromide solution), but the salt ions could not escape. On washing the fiber with water and once more allowing it to stand at 65 percent R.H., the initial value of the Hookean slope was recovered, i.e. the relative modulus became 1. The experiment just described proves that the fiber absorbs salt ions from the solution and that this absorption affects its mechanical properties.

In Fig. 7 are given the relative modulus *vs.* time curves for a series of initially wet fibers which had been treated with a saturated sodium bromide solution. The striking fact is the large fiber-to-fiber variance. It is obvious that, lacking the Hookean slope non-destructive test wherein a *single fiber can be used to follow the entire course of the reaction*, a relatively large number of samples would have had to be tested to clearly indicate the reaction mechanism.

THE INTERACTION BETWEEN WOOL AND GLYCERINE SOLUTIONS

The behavior of the fiber in concentrated salt solutions is in many respects similar to what one would expect in aqueous solutions of large polar organic molecules. Speakman[9] has described such systems (e.g. glycerine-water-wool). If a dry fiber is treated with the anhydrous liquid, the molecular network of wool is too tight for many glycerine molecules to diffuse into the fiber. If, however, an aqueous solution of glycerine is used, the water swells the fiber to an extent permitting absorption of the glycerine molecules. In the first case,

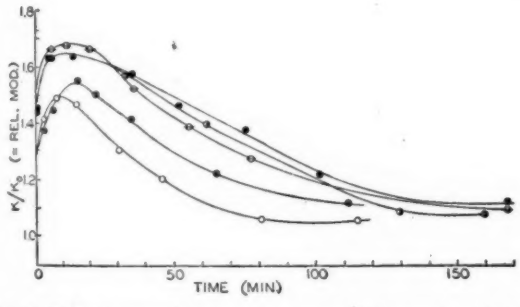

FIG. 7. Relative modulus *vs.* time curves illustrating the large fiber-to-fiber variance (initially wet fibers treated with a saturated sodium bromide solution).

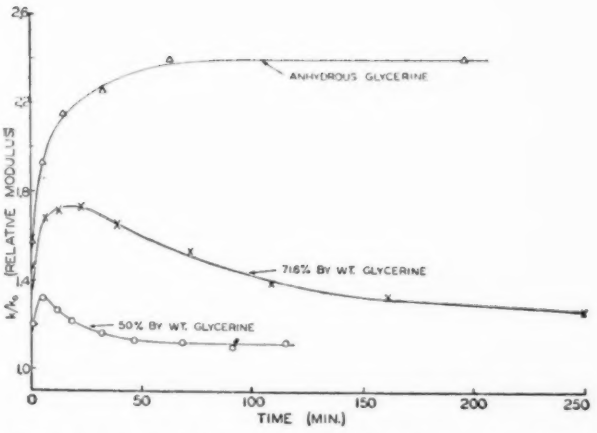

FIG. 8. Relative modulus *vs.* time after adding glycerine solutions to an initially wet fiber.

the behavior should correspond to that for a saturated lithium chloride solution. In the second case, on adding an aqueous glycerine solution to an originally wet fiber, the relative modulus-time curve should go through a maximum. The data of Fig. 8 bear out these hypotheses. The curves for the aqueous solutions are for the same fiber, but that for the anhydrous glycerine is for a different fiber.

USE OF OTHER MECHANO-CHEMICAL METHODS

Extension to 30 Percent

The non-destructive test involving a 30 percent extension was also used for a comparison with the results using the Hookean slope. Figure 9 shows force-extension curves on a human hair fiber extended 30 percent of its original length. A 24-hour rest period in water was allowed to elapse between each extension. Curve *a* is the initial extension in water. Curve *b* is an extension after the fiber had been standing in a saturated sodium chloride solution for 42 min. Curve *c* is a re-extension in water after the salt had been washed out. The reaction occurring in *b* was reversible, and the fiber could in this case be reused. Curve *d* resulted after the fiber had been standing in saturated salt solution for 15.5 min. It is evident that the curve of energy to extend 30 percent *vs.* time must go through a maximum. Also, if the amount of semi-permanent set resulting from extending to 30 percent and then contracting at the same rate were plotted against time, the curve would go through a maximum. Both of these facts are in accord with the explanation developed by using the Hookean slope measurement.

Repeated Cycling Technique

One further mechanical testing technique will be mentioned. When a wet wool fiber is subjected to repeated extensions to a fixed elongation, the force-extension curve is shifted progressively lower on the force axis, (Fig. 10). (The rate of extension used here was about 50

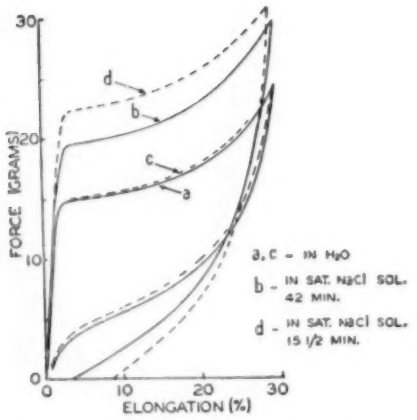

FIG. 9. Force-extension curves to 30 percent extension.

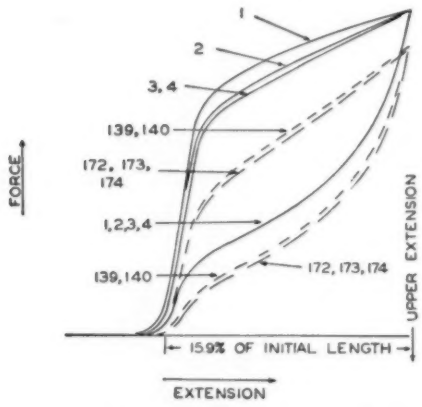

FIG. 10. Successive extension-contraction cycles on a wet wool fiber.

percent per minute.) After a number of cycles, however, the rate of change with number of cycles becomes very slow (compare cycles 140 and 172 of Fig. 10). If, at such a point, some substance which interacts with wool is introduced, the entire change in the force-extension curve should be due substantially to the effect of the extraneous substance on the wool fiber. With the Instron Tester the repeated cycling of the fiber can be made automatic. There are, however, several limitations to this method. (a) The effect of the reaction on a mechanically degraded, rather than the initial undamaged fiber, is being studied. (b) The continued cycling may cause further breakdown due to the repeated stressing of the reacted fiber, whereas it would not do so with the original fiber. This may obscure the main value of the experiment which is to measure the progressive change of mechanical properties of wool with time of reaction. (c) The force-extension curves become somewhat difficult to interpret if practically 100 percent elasticity is not displayed.

In spite of these limitations the method has some value as shown by the results of its application to the interaction between wool and a saturated salt solution (Fig. 11). The repeated cycling technique gave much the same information as the non-destructive extension to 30 percent method in a fraction of the experimental time. The saturated salt solution was sodium chloride and the fiber was subjected to 175 extension-contraction cycles before the solution was added.

Swelling Experiments

In accord with the results of the mechano-chemical experiments, White and Barnard[11] of this laboratory have shown that, when an initially wet hair fiber is immersed in a concentrated salt solution, the swelling *vs.* time curve goes through a minimum. When very concentrated solutions such as saturated lithium bromide are used, the swelling decreases and does not thereafter increase.

WORK IN PROGRESS

If a fiber is initially conditioned to the relative humidity existing over a salt solution before being

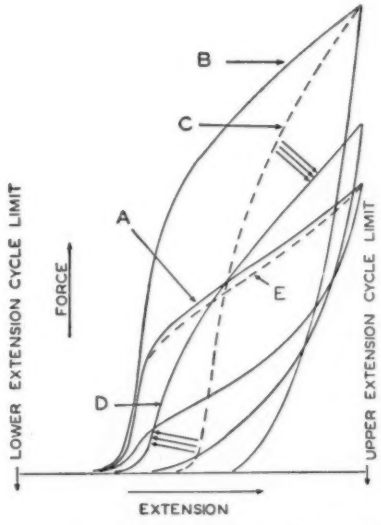

FIG. 11. Repeated cycling technique applied to the interaction between a wool fiber and a saturated sodium chloride solution. A—in water before adding salt solution; B—first cycle after adding sodium chloride solution; C—second cycle in salt solution; D—54 min. after adding salt solution; and E—first cycle after replacing salt solution with water.

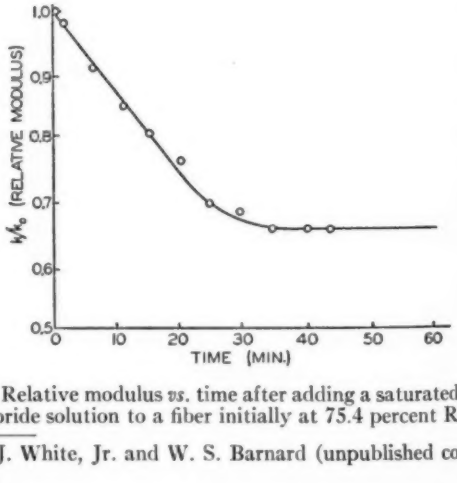

FIG. 12. Relative modulus *vs.* time after adding a saturated sodium chloride solution to a fiber initially at 75.4 percent R.H.

[11] H. J. White, Jr. and W. S. Barnard (unpublished communication).

treated with the solution, the initial hydration or dehydration will be eliminated, and the only effect measured should be that of the absorption of the salt ions. Figure 12 shows the relative modulus-time curve for a fiber, initially conditioned in a stream of air which had been bubbled through a saturated sodium chloride solution, and then immersed in a saturated sodium chloride solution. By making use of such curves, the rate of absorption of sodium chloride from its saturated solution is being studied as a function of animal fiber type and diameter.

SUMMARY

(1) An investigation has been made of the conditions under which the slope of the force-extension curve in the Hooke's law region may, for animal fibers, be non-destructively measured.

(2) A *single* fiber can be used to investigate a chemical reaction by measuring the change of Hookean slope with time of reaction.

(3) The usefulness of this technique is illustrated by its application to the heterogeneous reaction between wool and concentrated neutral salt solutions. The heterogeneous reaction between wool and aqueous glycerine solutions was also studied.

(4) Other mechano-chemical methods as well as swelling experiments are described. They give results consistent with those for the Hookean slope technique.

(5) A mechanism consistent with the experimental results is presented.

ACKNOWLEDGMENT

The author wishes to thank Professor J. C. Whitwell under whose direction this work was done and Dr. J. H. Wakelin for their many helpful suggestions. It is also a pleasure to acknowledge the support, in the later stages of this work, of the various organizations sponsoring the "International Wool Project" being carried out in the Textile Research Institute Laboratories. These organizations include The Wool Bureau, Inc., representing both the American Wool Council and the International Wool Secretariat, the U. S. Department of Agriculture, the Office of Naval Research and a group of American wool manufacturers.

Equivalent Effects of Time and Temperature in the Shear Creep and Recovery of Elastomers

F. S. Conant, G. L. Hall, and W. James Lyons
Chemical and Physical Research Laboratories, Firestone Tire and Rubber Company, Akron Ohio

An explicit relationship is set forth for the time-temperature dependence of the *viscoelastic* phenomena in the superelastic polymers. An empirical equation that was found to represent adequately the above-mentioned relationship over the entire multiple-temperature curve is of the form: $\log t_c=[C_\alpha/(T-b)]+C_\beta$. Experimental verification is given for the equivalent influence of time and temperature on the creep and recovery of compounds based on Hevea, GR-S, Neoprene GN, Butaprene, and butyl rubber. A comparison of the empirical equation with that of a theoretical reaction-rate equation of Tobolsky and Eyring indicates a temperature dependence of the energy of activation.

INTRODUCTION

THE dependence of creep phenomena on temperature in high polymers is well known, having been observed and discussed by a number of investigators.[1] The experiments show that, for a given time interval, the viscoelastic strain (or recovery) tends generally to rise to a higher level with an increase in the temperature of the experiment. The present series of experiments have disclosed that for rubber-like materials a consistent elevation of the strain-time curves with an increase in temperature is obtained, if corrections are made for the Gough-Joule effect. While a number of empirical relationships describing the dependence of *viscous* flow on temperature have been proposed and analyzed theoretically, no clear-cut, explicit relationships have been set forth for the temperature-dependence of *viscoelastic* phenomena in the superelastic polymers. The closest approach to such a relationship appears to be one based on a temperature function for viscosity, quoted by Leaderman.[1]

The observed nature of the dependence of viscoelastic behavior on temperature implies that it should be experimentally possible to duplicate the strain S_v attained in time t_1 at temperature T_1 with an equal strain S_v attained in time t_2 at T_2. As has been indicated, a series of creep or recovery experiments on a given material, each conducted over the same time interval, but at different T, will yield a family of creep (or recovery) curves; for increasing values of T the curves will lie higher and higher along the S direction. From these considerations emerges the possibility of selecting a series of temperatures for these experiments such that each curve at its termini in the selected time interval will match the termini of the curves obtained at the next higher and lower temperatures. Each terminus provides

[1] For a review of these studies see H. Leaderman, *Elastic and Creep Properties of Filamentous Materials and Other High Polymers* (Textile Foundation, Washington, 1943), pp. 30–33, 75 ff.

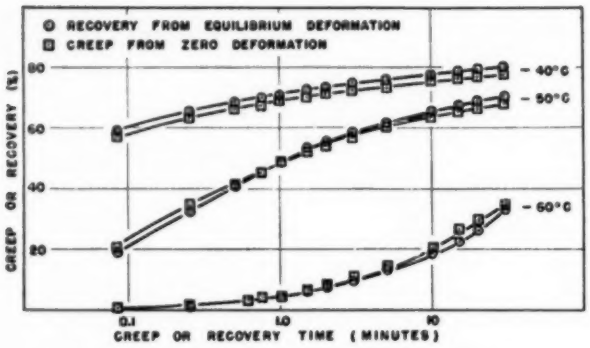

FIG. 1. Equivalence of creep and recovery, Hevea, 35.6-lb./sq. in. load.

the *particular* S_v which, given by one combination t_1 and T_1, can be duplicated by another combination t_2 and T_2. Plotted end-to-end the curves will become segments of one over-all multiple-temperature curve. Tobolsky and Andrews[2] observed such a continuous relationship in analogous stress relaxation tests and proposed an implicit relationship among time, temperature, and stress. Without a knowledge of the time-temperature function, however, it does not appear possible to predict whether the general, synthetic graph will be a smooth curve without discontinuities at the junctions of the segments.

With the aim of testing the foregoing theory, as well as deriving an analytical expression for the relationship between time and temperature, observations in creep and recovery on Hevea, GR-S, Neoprene GN, Butaprene, and Butyl rubber were undertaken.

APPARATUS AND METHODS

The test apparatus used has been described previously.[3] Essentially, it consists of a means of applying a shear stress to a double sandwich-type of specimen, and of observing the deformation of the specimen as test conditions are varied. The test specimens used were also based on the same compounding formulas and cures as given in the above reference.

In the creep tests performed, the unstressed test specimen was first brought to thermal equilibrium at the desired temperature. Twenty minutes conditioning time was allowed after a thermocouple in the center metal web of the specimen indicated that the test temperature had been reached. A shear stress of 35.6 p.s.i. was then applied quickly and the consequent deformation noted at appropriate intervals from 5 sec. to 30 min. after loading. In general, the measurements were made first at the lowest test temperature. After completion of the test the load was removed and the temperature of the test chamber raised. Recovery was usually found to be complete, after conditioning at the next higher test temperature.

In the recovery test the specimen was conditioned overnight (16 hr.) at 35°C under load. At the end of this time, deformation had proceeded to essentially an equilibrium state. The temperature was then gradually lowered to the lowest test temperature, during which time the deformation increased because of the Gough-Joule effect. A curve of equilibrium deformation *vs.* temperature was obtained during the cooling. As soon as thermal equilibrium was reached at the lowest test temperature the load was removed and the recovery noted at appropriate intervals from 5 sec. to 30 min. At the end of this time the load was reapplied and the temperature raised to the next test temperature. The reestablishment of equilibrium deformation was shown by the approach of the deformation to that of the equilibrium curve previously obtained.

In a study of creep or recovery it is often advantageous, if not necessary, to compensate for the Gough-Joule effect, through a normalization of the data. Unless this is done it is found that after a sufficient creep or recovery time the deflection at a low temperature exceeds that at a higher temperature, because of

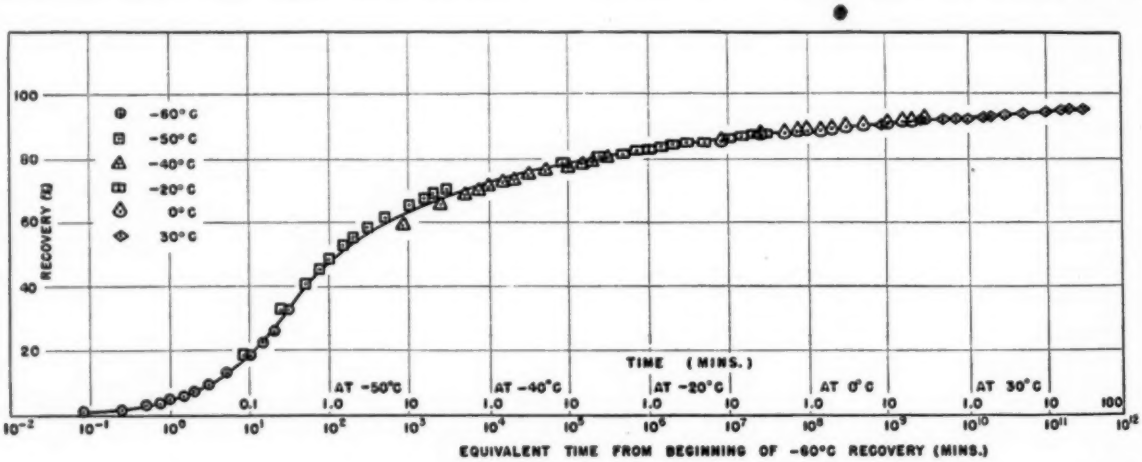

FIG. 2. Recovery from equilibrium deformation, Hevea, 35.6-lb./sq. in. load. Test temperatures taken at multiples of 10°C.

[2] A. V. Tobolsky and R. D. Andrews, J. Chem. Phys. **13**, 3 (1945).
[3] Conant, Hall, and Thurman, J. App. Phys. **20**, 526 (1949).

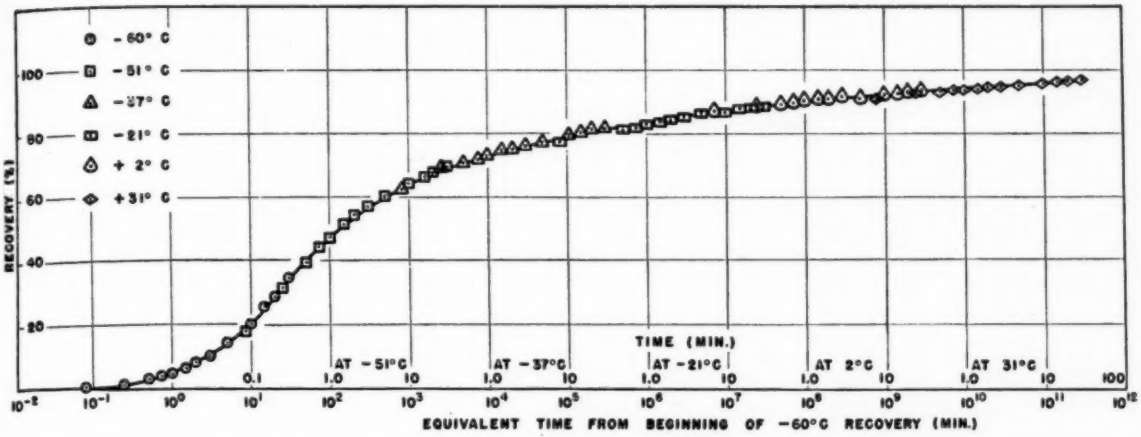

FIG. 3. Recovery from equilibrium deformation, Hevea, 35.6-lb./sq. in. load; adjusted temperature intervals.

this effect. The data presented here were normalized by presenting each creep datum as a percentage of the equilibrium deformation for that temperature and each recovery as a percentage of complete recovery.

Both creep and recovery curves were obtained on all of the stocks in the present series. The normalized data for each showed the two to be equivalent within the experimental error of either. Figure 1 shows a typical example of the close correspondence of the two types of data. Only the recovery data will be presented for the other stocks in the series.

JOINING OF RECOVERY CURVES OBTAINED AT DIFFERENT TEMPERATURES

From data such as those shown in Fig. 1, it appears that the creep or recovery curves at different temperatures might be joined end-to-end to form such a continuous, synthetic curve as was projected in the introduction. Such a continuous curve is meaningless, of course, unless the segments are matched so that the logarithmic time scale is continuous. Brief reflection will disclose that it is not necessary actually to procure a continuous locus of experimental points (such as could be obtained only by a fortuitous choice of temperatures) in order to secure a smooth multiple-temperature curve. When a series of parallel curve segments, obtained at reasonably well-scattered temperatures, and overlapping on the time scale, are available, the general continuous curve can be derived by drawing it parallel to these segments. This procedure is illustrated in Fig. 2 which shows 30-min. recovery data for Hevea stock B. The data at some of the temperatures are seen to be displaced from the smooth continuous curve.

The smooth curve of Fig. 2 strongly implies the existence of a continuous functional relationship between normalized creep or recovery time and temperature. Tentatively assuming its correctness, the curve may be used to supply numerical data for a set of simultaneous equations to test various t-functions of T. Following this procedure an empirical equation of the following form has been found to represent adequately the data over the entire viscoelastic region.

$$\log t_c = [C_\alpha/(T-b)] + C_\beta, \qquad (1)$$

where t_c = creep or recovery time, T = absolute temperature, and C_α, b, and C_β are arbitrary constants. The resemblance of Eq. (1) to the Arrhenius formula for the temperature-dependence of rate processes, will be recognized.

While an estimate may be made from data such as those in Fig. 2, of the temperatures at which tests should be made in order that the experimental curve segments should be on the continuous line, it is preferable, by way of testing Eq. (1), to use it to derive the appropriate temperatures. Using the equation and the data in Fig. 2, temperatures of $-60°$, $-51°$, $-37°$, $-21°$, $+2°$, and 31°C were selected for test. Figure 3 shows that recovery curves obtained at these selected temperatures do, indeed, form a continuous multiple-temperature curve.

An additional confirmation of the equivalence of time and temperature is provided by the data in Fig. 4. The experimental points show the recovery at -60°C, while the curve shows the joined recovery curves of the same specimen (Hevea stock B). The two are seen to be very nearly equivalent, for the 16-hr. period of test at -60°C.

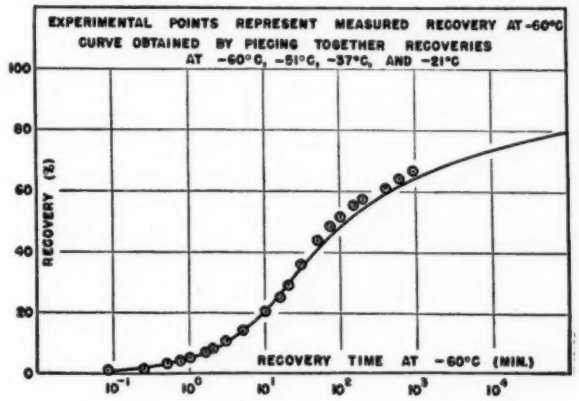
EXPERIMENTAL POINTS REPRESENT MEASURED RECOVERY AT -60°C
CURVE OBTAINED BY PIECING TOGETHER RECOVERIES AT -60°C, -51°C, -37°C, AND -21°C
RECOVERY (%)
RECOVERY TIME AT -60°C (MIN.)

FIG. 4. Recovery from equilibrium deformation, Hevea, 35.6-lb./sq. in. load.

TABLE I. Values of empirical parameters in Eq. (1) for 50 percent recovery from equilibrium shear deformation of various elastomers.

Stock	C_α	C_β	b	Derived test temp. (°C)
Hevea	1780	−17.5	122	−60, −51, −37, −21, 2, 31
GR-S	3121	−19.1	100	−50, −40, −27, −20, −4, 30
Neoprene GN	480	−7.52	193	−40, −32, −20, 0, 40[a]
Butyl rubber	5040	−23.52	33	−60, −46, −38, −30, 0, 40
Butaprene	720	−8.82	183	−30, −18, −10, 0, 30

[a] This is the derived test temperature for the material in the same crystalline state as it was at lower temperatures. In the test made at 30°C some of the crystals had probably melted, resulting in a higher recovery than that calculated. This same singularity appeared in the creep curves for Neoprene GN.

A continuous multiple temperature recovery curve for a GR-S stock is shown in Fig. 5. Test temperatures were selected by an application of Eq. (1) to previous data obtained at even decade temperature intervals. This curve is quite different in shape from that in Fig. 3 for Hevea, reflecting the more sluggish response of GR-S to low temperature stress.

Figures 6–8 show joined together recovery curves at even decade, temperature intervals on motor mounting-type stocks of Neoprene GN, Butyl rubber, and Butaprene. (Formulas are given in reference 3.) Each curve is characteristically sigmoidal. Only the Neoprene GN, however, shows the sharp increase in deformation with time that was evident in the Hevea stock. The Neoprene GN curve also shows a slight upturn at high temperatures, possibly because of the disappearance of a slight degree of crystallization.

An application of the above empirical formula to the data is shown in Table I which gives the constants and derived test temperatures. These calculations were based on the time required for 50 percent recovery at each temperature. The constant C_β is affected by the degree of recovery chosen. The constants C_α and b appear to be properties of the material tested and are independent of the reference point. Values of T and $\log t_e$ were substituted in Eq. (1) at three different temperatures for which the data were on the smooth curve. Solution of the resulting simultaneous equations gave the constants C_α, C_β, and b. The derived test temperatures given in Table I were obtained by an application of Eq. (1) to data obtained at even decade, temperature intervals. If the data shown in Figs. 6–8 had been obtained at the derived test temperatures, then all experimental points should have been on the curves, as they were in Figs. 3 and 5.

The interdependence of time, temperature, stress, and strain in the viscoelastic phenomena is well known. Mullins[4] recognized the need for a test that would use time as a parameter in determining low temperature serviceability. He also stated the need for a simple expression relating time with modulus. Many of the low temperature tests, such as Gehman's torsion test,[5] the Young's modulus test of Conant and Liska[6] and the cold compression set test[7] recognize time only to the extent that they specify a particular loading time in making their measurement. The above-mentioned tests are valuable in that they give the temperature below which, because of change in a particular physical property, the product can no longer be considered serviceable. However, time is not directly included as a parameter in these tests. The T-50 test[8] is arbitrary in that both time and temperature are varied simultaneously. Equation (1) does give a simple relationship between time and temperature, thus enabling time to be used as a parameter in determining low temperature serviceability.

The applicability of the data in Table I in conjunction with Eq. (1) to determine a low temperature serviceability index is readily apparent. For example, one can obtain the temperature at which a stock will recover 50 percent in 1 min. On this basis the stocks tested give the

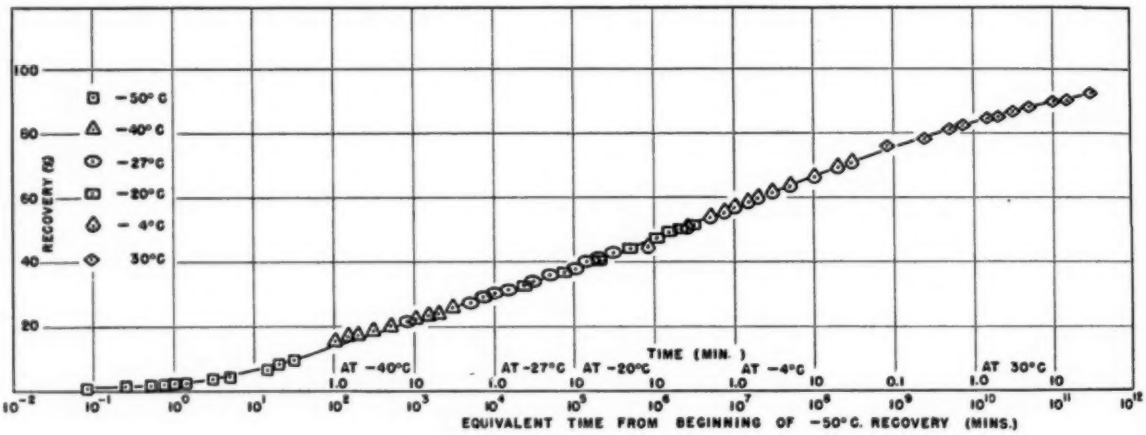

FIG. 5. Recovery from equilibrium deformation, GR-S, 35.6-lb./sq. in. load; adjusted temperature intervals.

[4] L. Mullins, Trans. I. R. I. **21**, 247 (December, 1945).
[5] Gehman, Woodford, and Wilkinson, Ind. Eng. Chem. **39**, 1108 (1947).
[6] F. S. Conant and J. W. Liska, J. App. Phys. **15**, 767 (1944).
[7] Morris, Hollister, and Mallard, India Rubber World **112**, 455 (July, 1945).
[8] W. S. McCortney and J. V. Hendrich, Ind. Eng. Chem. **33**, 579 (1941).

following indices: Hevea −49.5°C; GR-S −10°C; Neoprene GN −16°C; Butyl rubber −26°C; and Butaprene −6°C. The particular conditions selected for defining the index would, of course, be determined by the use for which the rubber was intended.

THEORETICAL CONSIDERATIONS

In an application of the reaction-rate theory of the mechanical properties of polymers to creep under constant stress, Tobolsky and Eyring[9] arrive at the equation

$$S=\frac{f}{G_1}+\frac{1}{B_2G_1}\ln A_2B_2G_\mu+\frac{1}{B_2G_1}\ln t, \qquad (2)$$

where S = strain in the specimen; f = total stress; G_1 and G_μ are appropriate elastic moduli associated with strains of the primary and secondary network bonds; and t = duration of creep experiment. The quantities A_2 and B_2 are defined by the equations

$$A_2=2n_2\lambda_2(kT/h)\exp(-\Delta F/kT), \qquad (3)$$

and

$$B_2=\lambda_2/2N_2kT, \qquad (4)$$

where k and h are Boltzmann's and Planck's constants, respectively; T is the absolute temperature; F is the free energy of activation for the deformation process; and n_2, λ_2, and N_2 are theoretical quantities related to the unit or elementary process.

If Eq. (2) is written out in full and certain terms are canceled, where possible, we arrive at the equation

$$S=\frac{f}{G_1}+\frac{2NkT}{G_1\lambda_2}\left[\ln\left(\frac{2n_2\lambda_2}{h}\cdot\lambda_2\frac{G_\mu t}{2N_2}\right)-\frac{\Delta F}{kT}\right]. \qquad (5)$$

k and h are well recognized as universal constants. Furthermore, we shall accept the material and structural characteristics, G_1, G_μ, λ_2, and ΔF as being time- and temperature-independent. The parameter N_2, however, Tobolsky and Eyring have deduced, decreases with a rise in temperature, though they do not give an expression for the relationship. We shall assume that the inverse variation of N_2 with absolute temperature is a

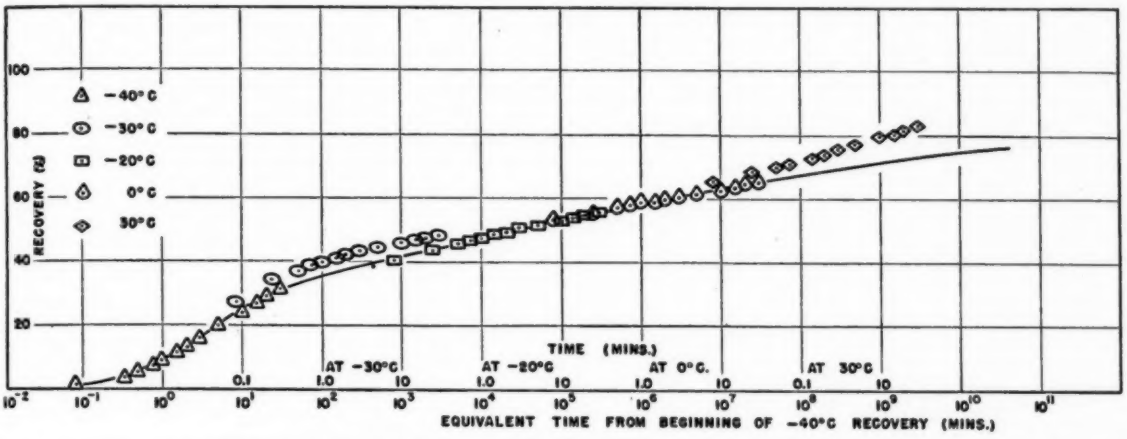

FIG. 6. Recovery from equilibrium deformation, Neoprene GN, 35.6-lb./sq. in. load. Test temperatures taken at multiples of 10°C.

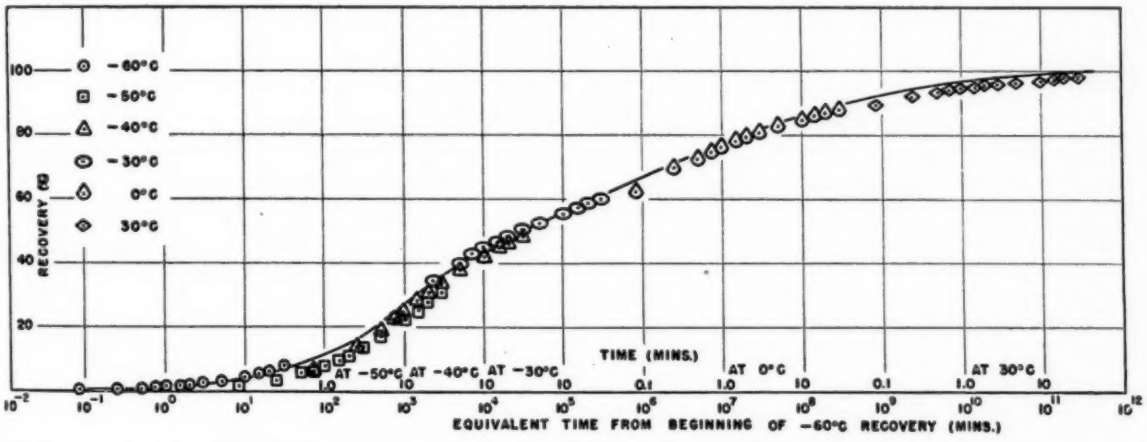

FIG. 7. Recovery from equilibrium deformation, Butyl rubber, 35.6-lb./sq. in. load. Test temperatures taken at multiples of 10°C.

[9] A. Tobolsky and H. Eyring, J. Chem. Phys. **11**, 125 (1943).

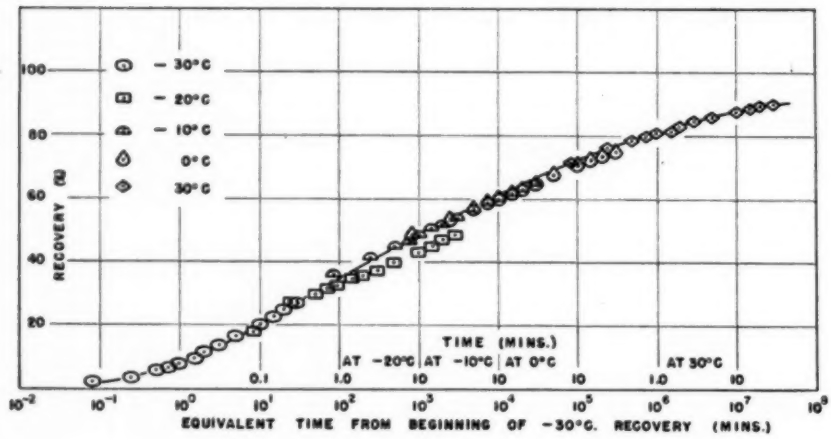

FIG. 8. Recovery from equilibrium deformation, Butaprene, 35.6-lb./sq. in. load. Test temperatures taken at multiples of 10°C.

good approximation, and also, that n_2 effectively varies inversely as the temperature over the range covered by the present experiments. The assignment of this functional dependence to N_2 and n_2 is admittedly quite arbitrary, from the theoretical point of view. However, if the network of secondary bonds can be regarded as behaving like an ideal gas, the assigned dependence on T becomes entirely reasonable, for N_2 represents the number of secondary bonds per unit area, while n_2 is the number of elementary deformation processes per unit length.*

Thus we obtain for the viscoelastic component of the deformation

$$S_v \equiv S - f/G_1 = C_1 \log C_2 t - C_3/T \tag{6}$$

involving the three parameters

$$\begin{aligned} C_1 &= \text{const.} \cdot 2.30(2k/G_1\lambda_2), \\ C_2 &= \text{const.} \cdot \lambda_2^2 G_\mu/h \end{aligned} \tag{7}$$

and

$$C_3 = \text{const.} \cdot 2\Delta F/G_1\lambda_2.$$

By rearranging terms, and selecting a fixed value for S_v, Eq. (6), placing $t = t_c$, may be written with a new set of constants

$$\log t_c = (C_\alpha/T) + C_\beta \tag{8}$$

where

$$C_\alpha = C_3/C_1; \quad C_\beta = (S_v/C_1) - \log C_2.$$

Equation (8) is seen to bear a close resemblance to the empirical Eq. (1), the difference being in the absence of the "correction" term, b on the temperature T, which appears in Eq. (1). The presence of the b in the empirical equation may be interpreted as an indication that the activation energies for the deformation processes involved in these experiments are not independent of temperature, but rather, are functions of temperature, of a form which gives decreasing values with increasing temperature:

$$\Delta F = \text{const. } T/(T-b). \tag{9}$$

Evidence for the temperature-dependence of the activation energy for *flow* in liquids has been recognized by Ewell,[10] though in this case indications were that the activation energy was an increasing function of temperature.

ACKNOWLEDGMENTS

The constructive interest of Dr. George R. Thurman, and his discussions with the authors, have produced valuable suggestions. The encouragement of the officials of the Firestone research organization, and their cooperation in making possible this contribution, is gratefully acknowledged.

* It may be remarked that attempts, before Eq. (1) was adopted for trial, to fit to the experimental data a working equation based on the assumption of the temperature-independence of N_2 and n_2, proved unsatisfactory.

[10] R. H. Ewell, J. App. Phys. **9**, 252 (1938).

Studies in Plasticization of Polyvinyl Chloride
I. Physical Changes and Their Measurement

M. L. Dannis
B. F. Goodrich Research Center, Brecksville, Ohio

The softening of a hard resin, polyvinyl chloride, by a liquid, dioctyl phthalate, is a set of processes occurring in sequence. Imbibition of the liquid is accompanied by volume reduction in the system. Dilatometer methods evaluate the amount and rate of volume decrease. The rate is temperature dependent, activation energy about 80 kcal. Solution of liquid into the resin follows with no further volume, but large dielectric change. Dielectric changes are measured on material in a cylindrical condenser, using a Schering bridge, and are rate dependent, activation energy about 110 kcal. Data are best described, assuming that segments of the polymer molecule "react" independently of one another.

I. INTRODUCTION

PLASTICIZED polyvinvyl chloride (Koroseal) is a material used widely in industrial or consumer goods because of its many excellent physical and chemical properties. Some of these properties such as electrical characteristics have been studied in detail,[1] since they were important to both the manufacturer and the consumer. In all studies published thus far, the material actually investigated was the final product, usually milled and pressed into the required physical form.

This paper concerns itself with a study of the reactions and processes that occur when this final material is made from the original raw materials. These changes are largely physical in nature, but do follow many of the rules of "rate-process" chemistry, permitting some evaluation of thermodynamic barriers in the reacting systems.

"Plasticization" is a term used to describe the softening of a hard resin, usually by means of a viscous liquid. Specifically, polyvinyl chloride, henceforth abbreviated PVC, which is a hard, brittle, horny material, may be softened to a resilient, rubbery material by the addition of appropriate amounts of esters such as di-2-ethylhexyl phthalate (DOP)[2] or *m*-tricresyl phosphate (TCP). The "reactions" accompanying this softening action are not simple and thoroughly understood, but at least three basic steps have been identified.

These steps are listed. (1) "Shrinkage"—believed to be a measure of plasticizer imbibition by the polymer. (2) "Dielectric Conversion"—believed to be a solution of the plasticizer into the resin. (3) "Fusion"—believed to be a simple physical consolidation.

II. SHRINKAGE

The specific volume of plasticized PVC is less than the volume of the components present.[3,4] This difference in volume has been studied as a rate-process phenomenon, using a dilatometer technique, described below.

About three grams of PVC powder or granules, as sold commercially, are weighed into a filter paper capsule. The capsule is inserted into a dilatometer bulb, followed by a glass plug. The plug partially protects the sample from overheating in subsequent glass sealing. The sample bulb is partially constricted just below the plug. Plasticizer fluid is put in the reservoir at the other end of the dilatometer. An oven is slipped over the bulb, vacuum connections made to both ends, and pumping begun. The oven is set at 60°C for one hour, and the liquid is gently boiled for a short time. The bulb is sealed off while the system is still evacuated, then cooled in ice water. The dilatometer is tipped, allowing the cool fluid to immerse the sample, still in ice water. After a few minutes the remaining

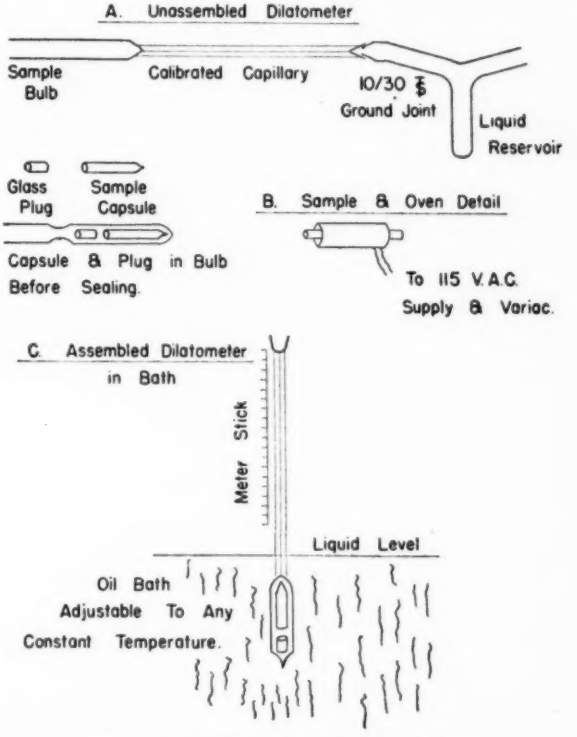

FIG. 1. Schematic dilatometer technique.

[1] Davies, Miller, and Busse, "Dielectric properties of plasticized polyvinyl chloride," J. Am. Chem. Soc. **63**, 361 (1941).
[2] T. L. Gresham, U. S. Patent 2,325,951 (August 3, 1943).
[3] Raymond M. Fuoss, "Electrical properties of solids. V," J. Am. Chem. Soc. **61**, 2334 (1939). The statement above Fig. 1 was later changed, to admit that slight volume loss in plasticizing PVC was always found.
[4] Raymond M. Fuoss, J. Am. Chem. Soc. **63**, 2401 (1941).

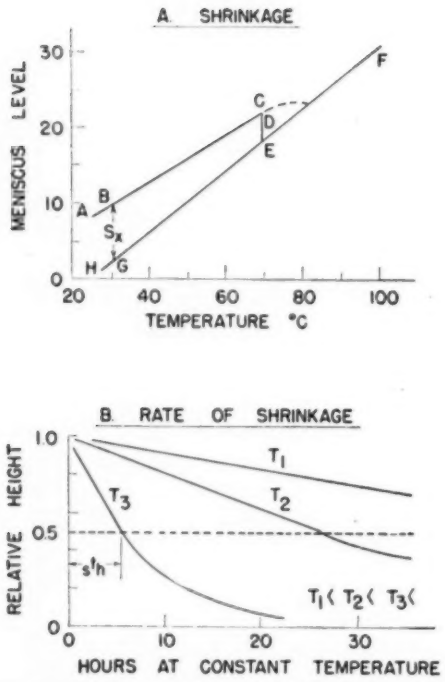

FIG. 2. Typical dilatometer characteristics. (A) Expansion and contraction. (B) Loss of volume at constant temperature.

vacuum connection is broken and the bulb removed from the ice bath. Excess fluid is sucked from the calibrated capillary by a smaller probe capillary. A meter stick is wired to the capillary, and the sample bulb put in a "constant" temperature bath. Typical apparatus is shown in Fig. 1, A, B, C.

The bath is held at a selected temperature long enough to establish thermal equilibration, about 5 minutes, and the meniscus level read. The bath temperature is then raised, thermal equilibration established, and the level read again. No correction is made for the thermal gradient between the bath and the portion of the capillary at room temperature. The bath is ultimately maintained constant at some predetermined value for periods up to 50 hours, and the meniscus level read as a function of time. The temperature of the bath is again raised, at intervals as before, up to a maximum about 100°C. The bath is then cooled in a manner similar to the heating cycle, until the system is at room temperature.

Data from a typical run are shown plotted in Fig. 2. The first portion of the warming, *AC*, up to the constant temperature, shows the characteristics of simple thermal expansion. The second portion, *CE, at constant temperature*, shows that the level decreases, or a net decrease in volume exists. Sufficient time may be allowed for all the possible change in volume to occur, but usually, at slower rates, the volume change is completed at more elevated temperature wherein the rate is faster. Further heating after the volume change is complete, and subsequent cooling and heating traces a reproducible path, *FH*. The cooling relationship is linear, but of different slope than the initial heating relationship. The difference in slope is indicative that the final material has a different coefficient of thermal expansion than the original. No attempt has been made to measure either coefficient.

Two quantities are evaluated from the dilatometer data. (1) S_x, defined as the extent of shrinkage, or loss in volume between initial and final states at 30°C. (2) $_st_h$, defined as the time when half the shrinkage is complete, at the temperature of measurement.

S_x, for a particular PVC with DOP, is 0.053±0.003 cc/cc of PVC. The second quantity, $_st_h$, is more easily visualized if the data are presented as in Fig. 2B. The shrinkage at the particular temperature of test is shown as "relative height," on which a value of unity represents no shrinkage, or the original thermal expansion line, and the value of zero, the final expansion and contraction line. On this presentation, $_st_h$ is the time when relative height is one-half.

The curves, so expressed, are reproducible within a few percent. The shape of the shrinkage curve has not been derived in any satisfactory manner. The slopes or half-times vary considerably with temperature, and may be plotted in the conventional Arrhenius manner, as in Fig. 3, evaluating an activation energy,

$$\Delta E^{**} = 80 \text{ kcal./mole.}$$

III. DIELECTRIC CONVERSION

An electrical method exists for following changes which occur in a plasticizing system. This method involves following the change in over-all dielectric constant of the system, as the change proceeds isothermally. Note that the dielectric constant[1] of plasti-

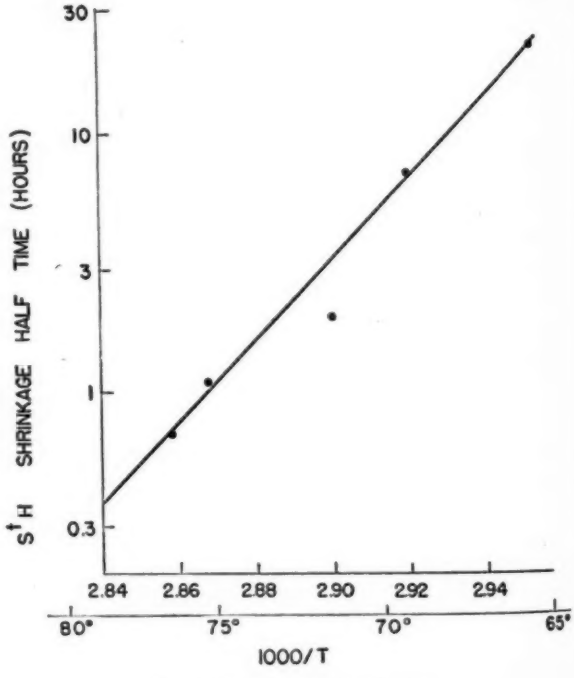

FIG. 3. Shrinkage rate change.

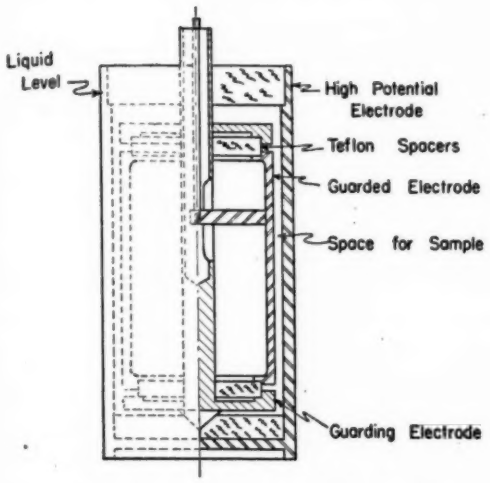

FIG. 4. Guarded cylindrical dielectric cell.

cized PVC is greater than the volume fraction summation of its components. Thus, conditions may be established such that this change in dielectric constant may be evaluated in detail. These conditions are established, and measurements made, by procedures generally labeled "dielectric rate studies."

The material studied is a mixture of PVC and plasticizer, proportioned such that the mixture is slightly oily and easily manipulated. Plasticizer ratios are commonly 80–95 PHR, but have been varied from 20 to 150 PHR. The mixture is loaded into a three-electrode, guarded cylindrical cell, shown in Fig. 4.

The cell is placed in an oil bath, controllable to 0.05°C. About $\frac{3}{4}$ hour is allowed for thermal equilibration, then the (over-all) dielectric constant and loss factor are evaluated, using a Schering bridge at audio-frequencies. In the original state, the measured dielectric constant at any particular frequency is very close to the volume fraction summation of the components, if due allowance is made for entrapped air. This relationship is a limiting case of the Bruggeman formula for small spheres in an inert fluid.[5]

The temperature of the bath is raised about 10°C, thermal equilibration established, and dielectric measurements made again. This procedure is repeated until the temperature reaches some predetermined value. At this constant temperature, measurements are made as a function of time, with intervals ranging from a half-hour to a day each. The measured dielectric constant changes from the value associated with the original mix to a value approaching that expected for plasticized PVC having the same space factor.

The change in dielectric constant is not uniform, but is rapid at first, becoming slower as time progresses. The manner of change is similar to the exponential decay of a source material into a product.

$$\epsilon_t = \epsilon_1(e^{-mt}) + \epsilon_2(1-e^{-mt}), \qquad (1)$$

where ϵ_t = dielectric constant of the mixture at time, t
ϵ_1 = dielectric constant of the mixture originally
ϵ_2 = dielectric constant of the mixture finally.

Equation (1) may be re-expressed.

$$\ln(\epsilon_2-\epsilon_1)/(\epsilon_2-\epsilon_t) = mt. \qquad (2)$$

This is usually plotted

$$\log\Delta\epsilon/\Delta\epsilon_t = m't, \quad \text{as shown in Fig. 5.} \qquad (3)$$

Define a half-life, $_dt_h$, a time such that the fraction doubles, or the logarithm increases by ln2. This half-life is the inverse of the slope of the lines shown, and is a good measure of (relative) dielectric change rate. The half-life is temperature dependent, and a conventional Arrhenius plot, such as Fig. 6, permits an evaluation of the activation energy.

$$\Delta E^{**} = 110 \text{ kcal./mole.}$$

The change in dielectric constant noted during thermal equilibration is only one of several physical changes occurring. The mixture has changed from an oily slurry to a dry, crumbly, non-coherent powder. This powder is believed identical with the material known as "preplasticized PVC."

If this changed material is the same as fully plasticized PVC the change in dielectric constant should be accompanied by appearance of a loss factor peak near room temperature.[1] A "cooling curve" taken on this material showed the required peak. It was noted that the loss factor of the material increased with a decrease in temperature, probably the most characteristic behavior of polar materials near an "absorption" peak.

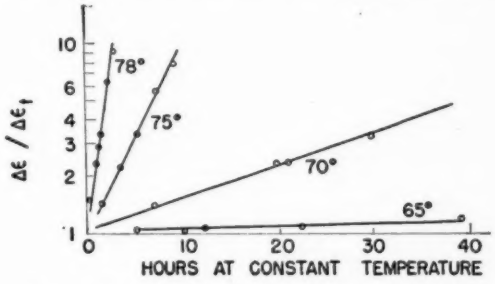

FIG. 5. Dielectric change in PVC-DOP systems.

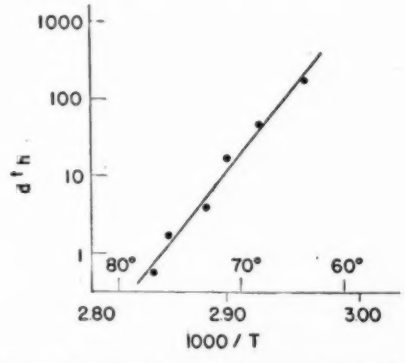

FIG. 6. Rate of change of dielectric properties with temperature.

[5] D. A. G. Bruggeman, Ann. d. Phys **24**, 636–64 (1935).

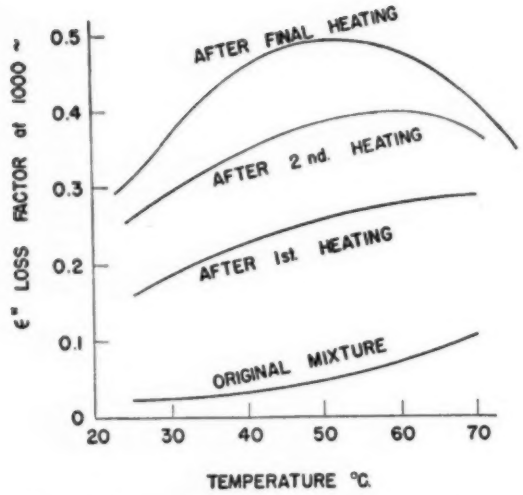

FIG. 7. Change of dipole peak during conversion.

IV. ASSOCIATED EXPERIMENTS

The dielectric data, as expressed by Eq. (2), imply that the final material is formed, as such, without any intermediate "dilution" steps or processes. This implication seemed so radical that other experiments were run to check this hypothesis. If the final material were so formed, it would be expected that the associated dipole peak would "grow" at a given temperature, for several investigators[1, 3] have shown that the temperature of the loss factor peak depends upon the amount of plasticizer associated with the PVC. Hence, an experiment was run to try to identify dipole peaks at intermediate stages of this change, i.e., an interrupted conversion run.

The dielectric properties of a mixture in the cell were measured while the cell was warmed. Conversion was allowed to proceed about one $_{d}t_{h}$ only. The mixture was cooled quickly, and a similar warm-up curve obtained. At the same constant temperature, equilibration was established for an additional $_{d}t_{h}$. Quick cooling was followed by the measurement of another warm-up curve. Final heating to complete conversion, and subsequent cooling measurements gave a final curve. The data are presented in Fig. 7. Note that the loss factor peak changes in thermal location, in contrast to concepts of "growing at one temperature."

Another experiment, contributing interesting data, referred to as the "dilution run" was performed as follows. A mixture of PVC and DOP of lower plasticizer content than previously studied was heat-treated to assure complete conversion, but no fusion, i.e., preplasticized PVC was made. This material was then mixed with further DOP and thermal-dielectric curves obtained. The data are presented graphically in Fig. 8.

Note that the dipole peak in the warming portion of the cycle is that for the original plasticized PVC. The dipole peak after additional heat treatment is that for the final mixture. Similarly, note that the dielectric constant of any one mixture increased during the heat treatment. The low absolute values of dielectric constant are due to the low space factor, i.e., the large amount of entrapped air, for which no correction was made. It is concluded that the plasticized PVC of low plasticizer contents "dilutes" further in the same manner as the PVC itself.

V. DISCUSSION

It is important to cite reasons and facts for believing that the shrinkage and dielectric phenomena are two separate "reactions," even though time related. (1) The time sequences are in a fixed order, i.e., shrinkage is essentially complete before dielectric conversion occurs. Note that at 65°C, for example, $_{s}t_{h} \approx 25$ hours, $_{d}t_{h} \approx 200$ hours. (2) The activation energies of shrinkage and dielectric conversion are different. (3) The shrinkage data cannot be expressed by the same relationships that "linearize" the dielectric data.

While "shrinkage" seems to be a distinct step in the plasticization process, the exact meaning of the measurements taken is not clear. It is believed that shrinkage measures the loss in volume of the system as plasticizer enters the PVC particle. However, the data do not fit the relationships derived upon the basis of plasticizer diffusing into a solid spherical polymer particle, simultaneously undergoing a loss in volume.

The large change in dielectric constant noted durin

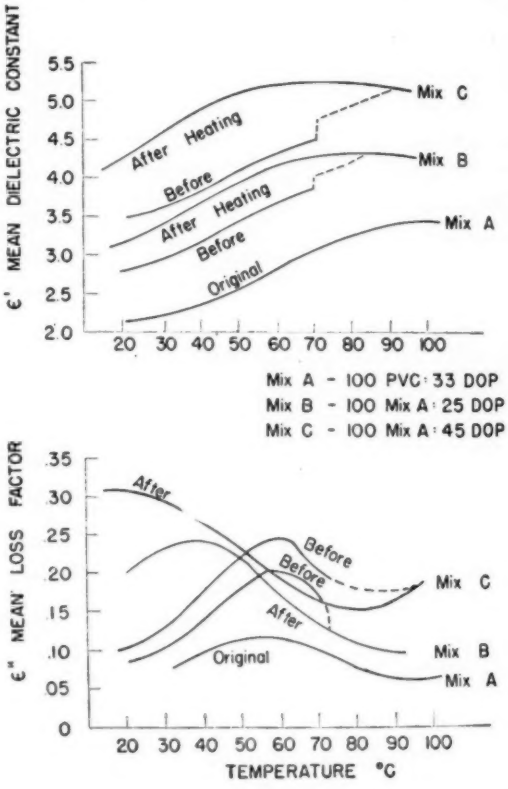

FIG. 8. Dielectric changes in dilution experiments. (A) Changes in measured dielectric constant. (B) Changes in measured loss factor.

plasticization is considered to be closely related to the other changes in physical properties. The assumption is made that these changes in properties are similar to those noted in simple liquids, as they change from solid to liquid phases. Thus, the increased dielectric constant of the plasticized PVC is due to the fact that part of the PVC is in its "liquid" form in which $\epsilon' \approx 11$, contrasted to $\epsilon' \approx 3$ in the "solid" form at room temperature. The "dilution data" suggest that a constant ratio of polymer may be converted from its "solid phase" to its "liquid phase," per unit of plasticizer, but that the plasticizer itself is unchanged in such a reaction. The concomitant effects of diluting the polymer in space allow the plasticizer to exhibit some of its own properties, such as color or viscosity, but such effects are secondary.

The changes in the real and complex part of the dielectric constant can be interpreted as follows. Discrete portions of the PVC chain, henceforth called "segments," have properties either "liquid" or "solid." While an individual segment may appear "liquid" or "solid," the composite behavior of two or more adjacent segments determines the loss factor. The segment is neither the polymerized monomer, nor the whole polymer molecule, but a portion of the chain about 10 vinyl groups or 20 carbon atoms long.

This segment concept of dielectric change leads to relationships identical with Eqs. (1), (2), and (3).

The segment is originally in the state wherein it shows a low dielectric constant. The change to the state wherein it shows the high dielectric constant follows rules of exponential decay, the rate constant depending upon plasticizer and temperature. Then, to a first approximation, the observed dielectric constant of a plasticized PVC system will be as in Eq. (4).

$$\epsilon = V_1\epsilon_1 + V_2\epsilon_2 \tag{4}$$

ϵ = experimentally observed dielectric constant
V_1 = volume fraction of PVC
V_2 = volume fraction of plasticizer
ϵ_1 = dielectric constant of PVC
ϵ_2 = dielectric constant of plasticizer.

In some cases ϵ_1 is apparently neither high nor low and Eq. (5) applies.

$$\epsilon_1 = V_\sigma\epsilon_\sigma + V_\lambda\epsilon_\lambda \tag{5}$$

ϵ_σ = low dielectric constant, about 3.5
ϵ_λ = high dielectric constant, about 11.5
V_σ, V_λ = relative fractions of each kind of PVC.

If an exponential decay process changes ϵ_σ to ϵ_λ, this may be expressed as

$$\epsilon_t = V_1[\epsilon_\sigma e^{-mt} + \epsilon_\lambda(1-e^{-mt})] + V_2\epsilon_2$$
$$\epsilon_t = V_1\epsilon_\sigma e^{-mt} + V_1(1-e^{-mt})\epsilon_\lambda + V_2\epsilon_2. \tag{6}$$

Then, using a procedure to derive a relationship similar to Eq. (2)

$$\ln\frac{V_1(\epsilon_\lambda - \epsilon_\sigma)}{(V_1\epsilon_\lambda + V_2\epsilon_2) - \epsilon_t} = mt. \tag{7}$$

Note that numerator of the fraction expresses the dielectric change in terms of concentration of PVC, and is independent of the kind of plasticizer. Similarly, the denominator expresses the difference between the final value and the instantaneous reading. Also note that the slope, m, or the half-life $_dl_h$, is independent of concentration, or of mix ratio of PVC and plasticizer.

The effect of plasticizer variation in the PVC-plasticizer system is expressed in a subsequent paper.[6]

VI. CONCLUSIONS

The plasticization of PVC by an ester such as DOP is a set of processes occurring in a definite sequence.

Two individual steps or processes have been identified, and labeled "shrinkage" and "dielectric conversion."

"Shrinkage" is a rate-process step not well understood.

"Dielectric conversion" is a rate-process step, which is independent of plasticizer-polymer mix ratio. The change in dielectric constant of a given mixture is related to the PVC content only. The change is assumed due to an unbinding of the PVC elementary segment, in the same manner normally accomplished by temperature alone.

VII. ACKNOWLEDGMENT

The author wishes to express his appreciation of the stimulating discussions with D. L. Loughborough concerning details of this work, and is indebted to the B. F. Goodrich Company for permission to publish the results of this investigation.

[6] M. L. Dannis, "Studies in plasticization of PVC. II. Plasticizer variations in PVC-plasticizer systems," J. App. Phys. **21**, 510 (1950).

Studies in Plasticization of Polyvinyl Chloride. II. Plasticizer Variations in PVC-Plasticizer Systems

M. L. Dannis
B. F. Goodrich Research Center, Brecksville, Ohio

Polyvinyl chloride resin is softened by certain liquids, called plasticizers, through a set of processes with high activation energies, 50–100 kcal. At fixed temperature, "reaction" rates are directly proportional to vapor pressure of the liquid. The dielectric change may be treated similarly to a chemical reaction between a solid and a vapor, and free energy of activation, ΔF^{**}, evaluated. ΔF^{**} is constant for various liquids with one resin. $\Delta E^{**}=\Delta H^{**}+L$ in this system, where ΔE^{**} is Arrhenius activation energy, ΔH^{**} energy barrier, L latent heat of vaporization of the liquid.

THE interaction of PVC and plasticizer (DOP) occurs in a complicated manner through a set of mechanisms apparently independent of concentration. Further information about these "reactions" was obtained in the study of the "reaction behavior" of PVC-plasticizer systems, varying the plasticizer composition as the major variable. The techniques and equipment used have been described previously.[1]

Since the introductory investigation had shown that the rate-curves and activation energy in both shrinkage and dielectric conversion were independent of mixing proportions, the mixes used in subsequent experiments were held constant within any one system, but varied as the plasticizer was changed, as determined by fluidity or compaction requirements.

The PVC used was a commercial polymer, Geon 101. Three different samples of resin were used, labeled *A*, *B*, and *G*. Samples *A* and *B* are believed to be identical. The plasticizers used were either commercial products of high purity, or laboratory prepared esters distilled in vacuum. All the liquids were used as received, with no further attempt at distillation or desiccation.

The systems studied as to shrinkage characteristics are listed subsequently in Table I. The data determining activation are shown in Fig. 1. The equations of the linear relationships shown, and the intercept with the 70°C ordinate, ${}_st_h$, are presented in Table I.

Note that in the systems with the plasticizers commonly considered the better "fluxing agents," the tendency is to "react" more easily. A fairly good comparison of relative shrinkage rates may be made by computing the shrinkage half-times at a particular temperature, since the slopes or activation energies are about the same magnitude. Note that the activation energies are relatively insensitive to molecular weight of the plasticizer, within the range $200<$M.W.<400. Note that the relative shrinkage rates, as measured by ${}_st_{70}$, are directly proportional to vapor pressure, as shown in Fig. 2. No other physical parameter of the plasticizer investigated, such as density, viscosity, molar volume, or surface tension gives a reasonable relationship.

The systems studied with respect to dielectric conversion characteristics are listed subsequently in Table II. The data for computing activation energies are shown in Fig. 3. The equations of the relationships shown are listed below in Table II, together with the ${}_dt_h$ value computed at 70°C, henceforth called ${}_dt_{70}$.

Note that in the systems with plasticizers commonly considered better "fluxing agents," the tendency is to convert more rapidly at a given temperature or the same speed at a lower temperature. Note that such "borderline" plasticizers as dilauryl phthalate and acetylated castor oil convert only slowly at elevated

TABLE I.

Shrinkage-rate equations:
$\log {}_st_h = A_s[(1000/T)-B_s]$
$\ln {}_st_h = \Delta E_s^{**}/RT - C_s/R$

${}_st_h$ = half-time in hours
T = absolute temperature
R = gas constant
ΔE_s^{**} = experimental activation energy cal./mole

System	A_s	B_s	ΔE_s^{**}	C_s	${}_st_{70}$
PVC-A, DOP	15.9	2.866	72×10^3	208	5.8
B, TCP	15.0	2.910	69	200	1.15
B, DBP	12.4	3.003	56	170	0.085
PVC-G, DOP	14.5	2.852	66×10^3	189	7.8
G, DMT	14.7	2.888	67	196	2.4
G, TCP	15.2	2.896	70	202	1.9
G, B-16	13.0	2.942	60	175	0.42
G, DBP	11.4	2.990	52	156	0.133

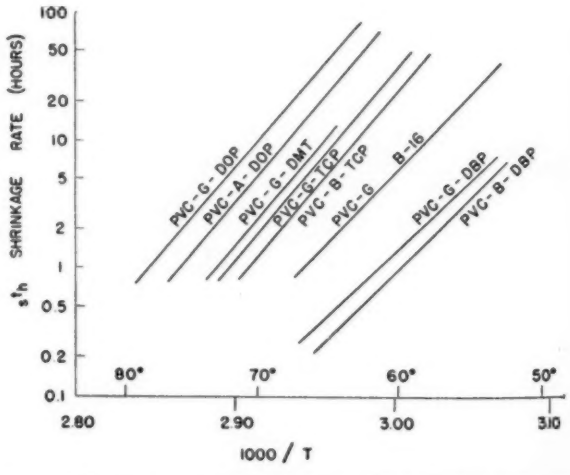

FIG. 1. Shrinkage rate characteristics in PVC-plasticizer systems.

[1] M. L. Dannis, "Studies in plasticization of PVC. I. Physical changes and their measurement," J. App. Phys. **31**, 505 (1950).

temperatures, i.e., above 80°C, or above the second-order transition temperature of the PVC.

Note that ΔE_d^{**}, as a measure of polymer plasticizer interaction tendency, does not correlate with other factors commonly used, namely, "compatibility" in a non-solvent (hexane) dilution test, or the Huggins-Flory "μ" value, as evaluated by Doty and Zable.[2] Note however, that the $_d t_{70}$ relationship is linear with vapor pressure, over four decades of the variables, as shown in Fig. 4. The vapor pressures used were taken from manufacturers' data, when possible.

THEORETICAL INTERPRETATION

Several facts have been presented about the dielectric conversion rates which classify this behavior as a new phenomenon. (1) The reacting system is two component, a liquid and a (solid) resin. (2) The initial reaction rate in any one system is independent of concentration or of mixing ratio. (3) The instantaneous reaction rate in any one system falls off in a simple exponential manner. (4) The reaction rate, in various systems at comparable conditions is proportional to the vapor pressure of the plasticizer.

The facts cited are consistent with the assumption of a reaction between a solid and a vapor. The concentration of plasticizer in the vapor state would be independent of the mix proportions of resin and plasticizer, but would depend greatly on the temperature. Similarly, the effective concentration of the solid would decay exponentially during the reaction, hence be the rate limiting step.

The dielectric conversion reaction has been expressed as Eq. (1) in the previous paper.[1]

$$\epsilon = \epsilon_1 e^{-mt} + \epsilon_2(1 - e^{-mt}). \tag{1}$$

The rate of change of dielectric constant, per unit change, is obtainable.

$$\frac{d\epsilon/(\epsilon_2 - \epsilon_1)}{dt} = me^{-mt}. \tag{2}$$

Impose the condition that t approaches zero,

$$\frac{d\epsilon/(\epsilon_2 - \epsilon_1)}{dt} = m. \tag{3}$$

So that m is the initial fractional rate of reaction of the system. This quantity has been evaluated experimentally, inasmuch as m is also the slope of the relationships presented previously in Fig. 5, of reference 1. Thus

$$m = \ln 2/3600 {}_d t_h. \tag{4}$$

From rate-process theory, as presented by Eyring, Glasstone *et al.*,[3,4] the "rate of reaction" of a system of two components is $C_A C_B k_r$, wherein C_A and C_B are the concentrations of the reactants, and k_r is the "specific reaction rate." k_r is defined

$$k_r = (kT/h) \exp(-\Delta F^{\circ **}/RT) \tag{5}$$

which is equivalent to the probability of finding a single activated complex in one cc of space, with a free energy of formation $\Delta F^{\circ **}$. Since actual experimental conditions do not involve the standard state, ΔF^{**} rather than $\Delta F^{\circ **}$, is the quantity discussed in further operations. Define the rate of reaction $= k_a$.

Then

$$k_a = C_A C_B k_r = m \tag{6}$$

if C_A and C_B are in appropriate units.

Since m has the dimensions of inverse time, C_A and

TABLE II. Dielectric conversion characteristics.

$\log {}_d t_h = A_d[(1000/T) - B_d]$
$\ln {}_d t_h = \Delta E_d^{**}/RT - C_d/R$

${}_d t_h$ = dielectric half-time in hours
T = absolute temperature
R = gas constant
ΔE_d^{**} = experimental activation energy—cal./mole

System	A_d	B_d	ΔE_d^{**}	C_d	${}_d t_{70}$
PVC-B-DnDP (Di-*n*-decyl phthalate)	19.0	2.807	87×10^3	244	110
PVC-A-DOP (Di-2-ethyl hexyl phthalate)	24.4	2.857	111	318	25
PVC-B-DnOP (Di-*n*-octyl phthalate)	22.4	2.862	103	294	15
PVC-B-TCP (*m*-tricresyl phosphate)	19.6	2.885	89	256	3.8
PVC-B-DMT (Dimethyl thianthrene)	22.7	2.899	104	302	2.3
PVC-B-B-16 (Butyl phthalyl butyl glycolate)	18.0	2.927	82	242	0.58
PVC-B-DBP (Dibutyl phthalate)	14.8	2.961	68	201	0.20
PVC-B-DEP (Di-ethyl phthalate)	17.6	3.020	80	243	0.0135
PVC-B-DMP (Dimethyl phthalate)	17.2	3.042	79	239	0.0063

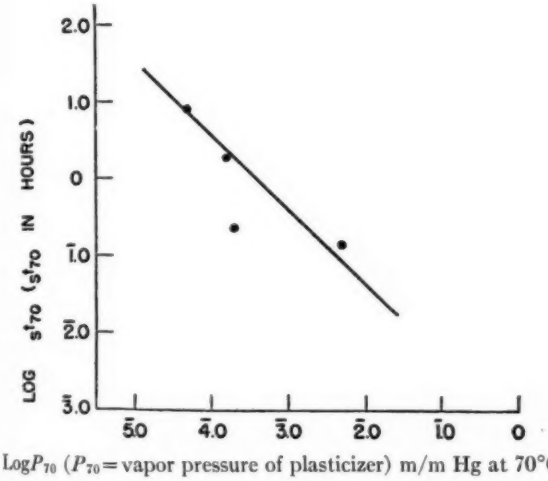

$\text{Log}P_{70}$ (P_{70} = vapor pressure of plasticizer) m/m Hg at 70°C

FIG. 2. Relationship of plasticizer vapor pressure to shrinkage rate.

[2] P. Doty and H. S. Zable, "Polymer-solvent interaction," J. Poly. Sci. 1, 90 (1946).

[3] Glasstone, Laidler, and Eyring, *Theory of Rate Processes* (McGraw-Hill Book Company, Inc., New York, 1941).

[4] S. Glasstone, *Textbook of Physical Chemistry* (D. Van Nostrand Company, Inc., New York, 1946), second edition.

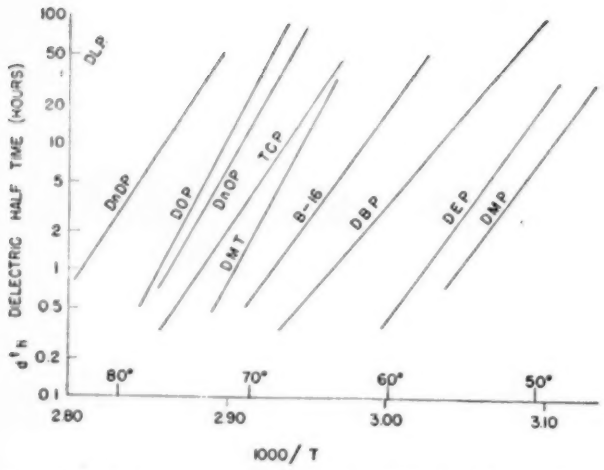

FIG. 3. Dielectric conversion rates in PVC-plasticizer systems.

C_B must be units of mole fractions. Evaluate ΔF^{**}

$$-\Delta F^{**}=RT[\ln(h/kT)+\ln(m/C_AC_B)]$$
$$\Delta F^{**}=-RT[\ln(h/kT)+\ln(\ln 2/3600C_AC_B\,d/h)]. \quad (7)$$

Since

$$\Delta F^{**}=\Delta H^{**}-T\Delta S^{**} \quad (8)$$

$$\Delta H^{**}-T\Delta S^{**}=-RT[\ln(h/kT)+\ln(\ln 2/3600C_AC_B\,d/h)]. \quad (9)$$

Evaluate (9) at T_1 and T_2, and subtract. Then

$$(-\Delta H^{**}/R)[(1/T_1)-(1/T_2)]=\ln(T_1/T)_2+\ln[(C_AC_B\,d/h)_1/(C_AC_B\,d/h)_2]. \quad (10)$$

But for small changes in temperature, $\ln(T_1/T_2)\approx 0$. C_A is the mole fraction of a solid, $(C_A)_2/(C_A)_1\approx 1$. C_B is the mole fraction of plasticizer vapor.

$$C_B=\left(\frac{P}{760}\times\frac{273}{T}\right) \quad \text{or} \quad (C_B)_2/(C_B)_1=\frac{(P/T)_2}{(P/T)_1}.$$

But the pressure of a vapor may be given by the Clapeyron equation

$$P_2=P_1\exp\{(L/R)[(1/T_1)-(1/T_2)]\}. \quad (11)$$

So

$$\ln[(C_B\,d/h)_2/(C_B\,d/h)_1]=\ln(T_1/T_2)-\ln[(d/h)_2/(d/h)_1]-(L/R)[(1/T_2)-(1/T_1)].$$

Thus

$$\ln[(d/h)_2/(d/h)_1]=(1/R)(-\Delta H^{**}+L)[(1/T_1)-(1/T_2)]. \quad (12)$$

Equation (12) is the method of evaluating ΔE^{**} in the usual Arrhenius plot of experimental activation energy. Thus

$$\Delta H^{**}=\Delta E^{**}-L-RT. \quad (13)$$

Note that Eq. (7) may be expressed as

$$\Delta F^{**}=\text{const}+\log P+\log d/h. \quad (14)$$

This relationship is shown experimentally by Fig. 4. Figure 4 also implies that ΔF^{**} is a constant from one reacting system to another, or that the mechanism of plasticization is independent of the kind of plasticizer. However, ΔH^{**} and ΔS^{**} do vary from one system to another, depending greatly upon the choice of plasticizer. The values of ΔE^{**}, ΔH^{**}, and ΔS^{**} are presented in Table III. Assuming C_A = unity, ΔF^{**} = 16,500 cal./mole at 70°C.

It is interesting to note that ΔS^{**} is the order of magnitude for dipole rotation of the PVC itself.[5]

No ordinary parameter of the molecule, such as molecular weight, molar volume, or viscosity seems to be related to these quantities in a simple manner.

Some data recently obtained, have shown that ΔF^{**} is a variable depending upon the history of the preparation of the PVC.

CONCLUSIONS

The interaction of plasticizer with PVC is markedly dependent upon the vapor pressure of the plasticizer used, and largely independent of all other variables, except temperature.

One part of the interaction process may be described kinetically as the reaction of a solid and a vapor.

The free energy of formation of the activated complex in the critical rate limiting step in plasticization is a

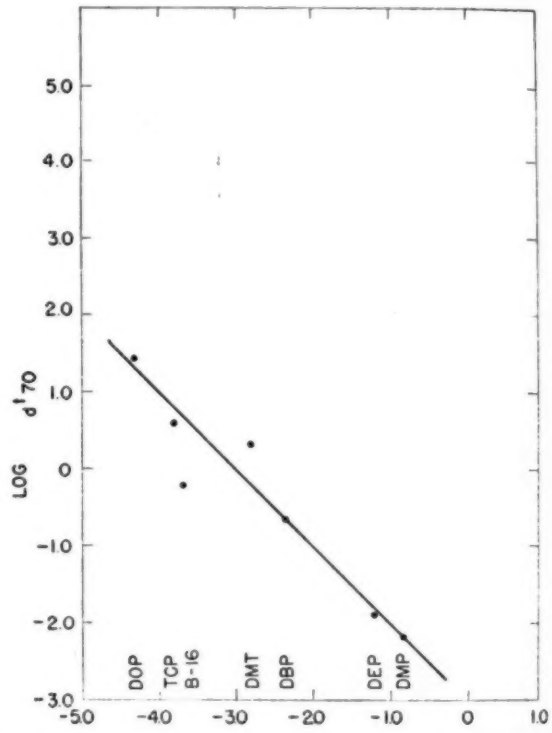

FIG. 4. Relationship of plasticizer vapor pressure to dielectric conversion.

[5] W. Kauzmann, "Dielectric phenomenon," Rev. Mod. Phys. 14, 16 (1942).

TABLE III. Thermodynamic constants of the activated complex in dielectric conversion.

System	ΔE^{**}	ΔH^{**}	ΔS^{**}
PVC-B, DnDP	87×10^3 cal./mole	59×10^3 cal./mole	125*EU*
A, DOP	111	83	196
B, DnOP	103	75	172
B, TCP	89	62	135
B, DMT	104	84	198
B, B-16	82	55	113
B, DBP	68	43	79
B, DEP	80	60	128
B, DMP	79	61	132

constant, regardless of kind of plasticizer used. This implies that the action of all plasticizers is fundamentally the same.

The Arrhenius activation energy, ΔE^{**}, obtained from a dielectric rate-plot, differs from the heat of activation, ΔH^{**}, by the latent heat of vaporization of the plasticizer used.

The interaction of plasticizer and PVC to form the "activated complex" leading to the plasticized material, does not depend on any simple, obvious property of the plasticizer, nor does it correlate with Huggins-Flory interaction coefficients previously evaluated for some of these systems.

ACKNOWLEDGMENTS

The author wishes to express his appreciation of the stimulating discussions with D. L. Loughborough concerning details of this work, and is indebted to the B. F. Goodrich Company for permission to publish the results of this investigation.

Mechanical Properties of Substances of High Molecular Weight. VIII. Dispersion of Dynamic Rigidity and Viscosity in Concentrated Polyvinyl Acetate Solutions*

JOHN D. FERRY, W. M. SAWYER,† GEORGE V. BROWNING,‡ AND ARTHUR H. GROTH, JR.
Department of Chemistry, University of Wisconsin, Madison, Wisconsin

The dynamic rigidities and viscosities of concentrated solutions of polyvinyl acetate in 1,2,3-trichloropropane have been obtained from transducer and wave propagation measurements. Two polymer samples with number-average molecular weights of 140,000 and 840,000 were studied in the lower audiofrequency range at concentrations from 3 to 40 percent and temperatures from −3 to 41°C. For each sample, when the reduced dynamic rigidity $G'T_0/Tc$ and the reduced dynamic viscosity η'/η were plotted against the reduced frequency, $\omega\eta T_0/Tc$, all the data superposed to give two composite dispersion functions. The distribution of Maxwellian relaxation times can be derived from the dispersion of either G' or η', and the two calculations are in reasonable agreement.

INTRODUCTION

STUDIES of wave propagation in concentrated polyvinyl acetate solutions have provided measurements of the wave rigidity, $\tilde{G}$, in several different solvents at various frequencies, temperatures, and concentrations, as reported in the preceding paper of this series.[1] In one solvent, 1,2,3-trichloropropane, the wave damping can be measured with sufficient accuracy to calculate also the dynamic rigidity, G', and dynamic viscosity, η', which can be more directly interpreted. These data are now presented and are supplemented by direct measurements of G' and η' using transducer methods,[2] which are applicable at lower concentrations. When reduced to a standard viscoelastic reference state by a treatment derived elsewhere,[3] the results can be combined to provide dispersion functions for G' and η' which extend over several cycles of logarithmic frequency. The two functions are interrelated through a distribution function of relaxation times.

MATERIALS AND METHODS

The two samples of polyvinyl acetate employed in this work have been described elsewhere.[1,4] The number-average molecular weights of the unfractionated material and of Fraction I (a cut comprising 13 percent of the unfractionated) were 140,000 and 840,000, respectively.

Values of the wave rigidity, reported previously in graphical form,[1] were combined where possible with measurements of the damping index, λ/x_0, to give the dynamic rigidity and viscosity by the equations[5]

$$G' = \tilde{G}\frac{4\pi^2[(4\pi^2-(\lambda/x_0)^2]}{[4\pi^2+(\lambda/x_0)^2]^2} \quad (1)$$

$$\eta' = \frac{\tilde{G}}{\omega}\frac{16\pi^3\lambda/x_0}{[4\pi^2+(\lambda/x_0)^2]^2}. \quad (2)$$

* Presented at the Seventh Meeting of the Division of High-Polymer Physics, American Physical Society, New York City (February 2–4, 1950).

† Present address: Shell Development Company, Emeryville, California.

‡ Present address: Standard Oil Company, Whiting, Indiana.

[1] W. M. Sawyer and J. D. Ferry, J. Am. Chem. Soc. (to be published).

[2] Smith, Ferry, and Schremp, J. App. Phys. **20**, 144 (1949).

[3] J. D. Ferry, J. Am. Chem. Soc. (to be published).

[4] G. V. Browning and J. D. Ferry, J. Chem. Phys. **17**, 1107 (1949).

[5] Ferry, Sawyer, and Ashworth, J. Polymer Sci. **2**, 593 (1947).

TABLE I. Dynamic rigidity and viscosity of solutions of unfractionated polymer from wave propagation measurements.

Conc., wt. percent	Temp. °C	ν	$G' \times 10^{-4}$ dyne/cm²	η' poises
23.8	0.1	250	9.7	35.0
		320	11.5	31.1
		400	15.1	29.2
		500	13.4	23.8
		630	15.9	21.8
		800	15.3	18.5
		1000	15.8	14.8
	10.5	250	8.0	31.8
		320	10.9	31.6
		400	10.7	20.6
		500	12.1	19.0
		630	11.7	16.8
		800	12.3	13.0
		1000	12.9	14.1
35.1	0.0	500	43.8	82.3
		630	46.8	65.0
		800	51.6	51.4
		1000	54.6	44.2
		1600	57.4	29.0
		2000	52.7	24.6
	10.4	500	35.5	68.5
		630	40.4	59.2
		800	40.8	38.6
		1000	43.0	29.7
		1250	47.6	26.7
		1600	49.7	24.0
	30.3	400	23.3	53.3
		500	27.2	41.5
		630	27.3	32.6
		800	28.3	23.2
		1000	29.6	20.6
		1250	29.0	20.0

TABLE II. Dynamic rigidity and viscosity of solutions of Fraction I from wave propagation measurements.

Conc., wt. percent	Temp. °C	ν	$G' \times 10^{-4}$ dyne/cm²	η' poises
14.3	0°	1000	6.9	7.0
17.0	0.4	200	6.6	32.8
		250	7.9	23.4
		320	8.1	18.2
		400	6.8	11.4
		500	8.7	11.2
		630	10.4	11.0
		800	11.5	9.2
		1000	11.5	8.6
		1250	12.0	7.6
		1600	11.7	6.7
	14.9	250	6.9	24.5
		320	7.6	15.8
		400	7.2	13.5
		500	8.3	12.2
		630	7.6	9.5
		800	8.9	8.8
		1000	9.8	8.4
		1250	8.0	6.8
	25.6	250	5.6	16.3
		320	6.6	12.6
		400	6.9	10.4
		500	6.8	8.3
		630	7.6	8.0
		800	7.6	7.0
		1000	8.3	6.0
		1250	8.1	5.7

Transducer measurements were made with the Model 2 transducer of Smith, Ferry, and Schremp.[2] The original experimental arrangement was improved by mounting the transducer in a box of sawdust, carefully shielding all leads, and replacing the a.c. operated decade amplifier by a Ballantine[6] Model 220 battery operated amplifier. An isolating transformer was substituted for the amplifier previously employed between the oscillator and impedance bridge. The bridge was calibrated. The mechanical resistance and reactance were calculated by the circle plot method, and the dynamic viscosity and rigidity were obtained from plots of these quantities against depth of immersion of the oscillating rod.[2]

EXPERIMENTAL RESULTS

The results of the wave propagation measurements on the two samples are given in Tables I and II, and those of the transducer measurements in Tables III and IV.

It has been shown[3] that if certain simple postulates regarding stress relaxation in concentrated polymer solutions are valid, dynamic data at various frequencies, temperatures, and concentrations should superpose to form two universal dispersion functions when the reduced dynamic rigidity, $G_r' = G'T_0/Tc$, and the reduced dynamic viscosity, $\eta_r' = \eta'/\eta$, are plotted against the reduced frequency, $\omega_r = \omega\eta T_0/Tc$. Here η is the steady flow viscosity (at small shearing stresses), c the concentration in g polymer per cc solution, T the absolute temperature, and T_0 a standard temperature, taken as 298°K. From the data of Tables I–IV, together with steady flow viscosities measured on these same solutions,[7] and values of c computed by assuming additivity of volumes of polymer and solvent,[1] the quantities G_r', η_r', and ω_r have been calculated and are plotted logarithmically for the two samples in Figs. 1 and 2. In each case the open circles are transducer data and the solid circles are wave propagation data from individual damping measurements. The heavy dashed curves for G_r' are obtained by applying a constant correction to the previously published composite curve for reduced dynamic rigidity,[1] $\bar{G}_r = \bar{G}T_0/Tc$; the ratio $G'/\bar{G}$ is fairly insensitive to the damping index when $\lambda/x_0 < 2\pi$, as shown by Eq. (1), and the variation of λ/x_0 is small enough over the ranges of frequency and concentration employed in the wave measurements so that a fairly good approximation is achieved by setting $G_r' = 0.90\bar{G}_r$.

The results of the two entirely different experimental methods fit together very well. By the use of reduced variables, the data for unfractionated polymer covering a range of concentrations from 5 to 40 percent and of

[6] Ballantine Laboratories, Boonton, New Jersey.

[7] Ferry, Browning, Sawyer, and Foster, J. Phys. Coll. Chem. (to be submitted).

TABLE III. Dynamic rigidity and viscosity of solutions of unfractionated polymer from transducer measurements.

Conc., wt. percent	Temp. °C	ν	$G' \times 10^{-4}$ dyn/cm²	η' poises
5.00	25.0	200	—	1.02
		320	—	1.20
		400	—	1.15
10.15	25.0	200	0.266	5.26
		250	0.318	4.62
		320	0.381	3.79
		400	—	3.69
	35.0	200	0.147	4.74
		250	0.255	3.88
		320	0.309	3.45
		400	—	3.15
15.8	25.0	200	1.40	11.2
		250	1.75	10.4
		320	1.98	9.8
		400	1.91	8.4
	35.0	200	—	12.9
		250	—	10.1
		320	1.34	9.1
		400	1.53	8.3
20.0	25.0	200	3.49	25.1
		250	3.90	20.4
		320	3.98	16.8
		400	4.19	15.2
24.1	25.0	200	7.25	35.6
		250	7.27	32.6
		320	7.50	24.2
		400	7.26	21.2
	35.0	200	5.25	31.8
		250	—	27.1
		320	6.60	22.8
		400	7.39	20.4

TABLE IV. Dynamic rigidity and viscosity of solutions of Fraction I from transducer measurements.

Conc., wt. percent	Temp. °C	ν	$G' \times 10^{-4}$ dyne/cm²	η' poises
3.0	25.0	200	—	1.20
		250	—	1.08
4.0	25.0	200	—	2.20
		250	—	1.74
		320	0.13	1.48
		400	0.22	1.45
5.0	25.0	200	—	3.02
		250	—	2.29
		320	—	1.95
		400	—	1.83
5.54	25.0	250	0.21	3.31
		320	0.23	2.71
		400	0.29	2.40
8.21	25.0	200	—	7.58
		250	0.76	6.41
		320	0.84	4.55
		400	0.85	4.10
11.3	25.0	250	1.78	8.70
		320	2.17	7.91
		400	2.28	6.48
14.35	25.0	250	3.95	13.1
		320	4.54	11.9
		400	4.81	10.2

temperatures from $-3°$ to 41°C superpose rather closely to give two universal dispersion curves, and the data for Fraction I superpose similarly over a somewhat smaller range of temperatures and concentrations. As the frequency increases by 10^5, the rigidity increases by about 10^2, while the viscosity falls off by about 10^{-4}.

The functions as represented in the figures are reduced to a hypothetical viscoelastic reference state of unit density (concentration) and unit steady flow viscosity (1 poise) at 298°K. Although this state is of course non-existent, it provides a convenient basis for combining data, and approximate dispersion curves for any real state of known temperature, concentration, and steady flow viscosity should be obtainable from Fig. 1 or 2 by adjusting the coordinates. If the postulates[3] that all relaxation mechanisms depend identically on temperature and concentration do not hold strictly, some distortion of the dispersion functions may arise from combining data in this way. However, here as in previous examples[3] the superposition is successful insofar as the data at different concentrations and temperatures overlap, and it is believed that any such distortion is slight.

It is of interest also to plot $\omega_r\eta_r'$ (which is the imaginary part of the reduced complex dynamic rigidity,[5] $G_r''=G''T_0/Tc$) and the mechanical loss factor, $G_r''/G_r'=G''/G'$, against the reduced frequency. These functions are shown in Fig. 3. In both samples G'', like G', increases rapidly with increasing frequency. Their ratio, however, falls off with increasing frequency and appears to approach a constant value of about 0.5.

An attempt to apply the complex plane plot of Cole and Cole[8] showed that the locus of $G'/(G'^2+G''^2)$ and $G''/(G'^2+G''^2)$ is not a circle.

THE RELAXATION DISTRIBUTION FUNCTION

The dispersion curves for G' and η' are not independent; a formulation of the relation between them can provide an additional experimental check. This is most conveniently written in terms of a distribution function of Maxwellian relaxation times, $F(\tau)$, such that each elastic contribution to the rigidity $F(\tau)d\tau$ is relaxed as though by a dashpot $\tau F(\tau)d\tau$.[9] The exact equations for G' and η' in terms of $F(\tau)$ are[10,11]

$$G'(\omega)=\int_0^\infty \frac{F(\tau)\omega^2\tau^2}{1+\omega^2\tau^2}d\tau; \quad \eta'(\omega)=\int_0^\infty \frac{\tau F(\tau)}{1+\omega^2\tau^2}d\tau. \quad (3)$$

[8] K. S. Cole and R. H. Cole, J. Chem. Phys. **9**, 341 (1941); A. W. Nolle, J. Polymer Sci. **5**, 1 (1950).

[9] Although a set of finite mechanisms is more convenient for discussing the effects of temperature and concentration on dispersion (see reference 3), the equivalent continuous distribution is more useful here.

[10] T. Alfrey and P. Doty, J. App. Phys. **16**, 700 (1945).

[11] Kuhn, Künzle, and Preissmann, Helv. Chim. Acta **30**, 307 (1947).

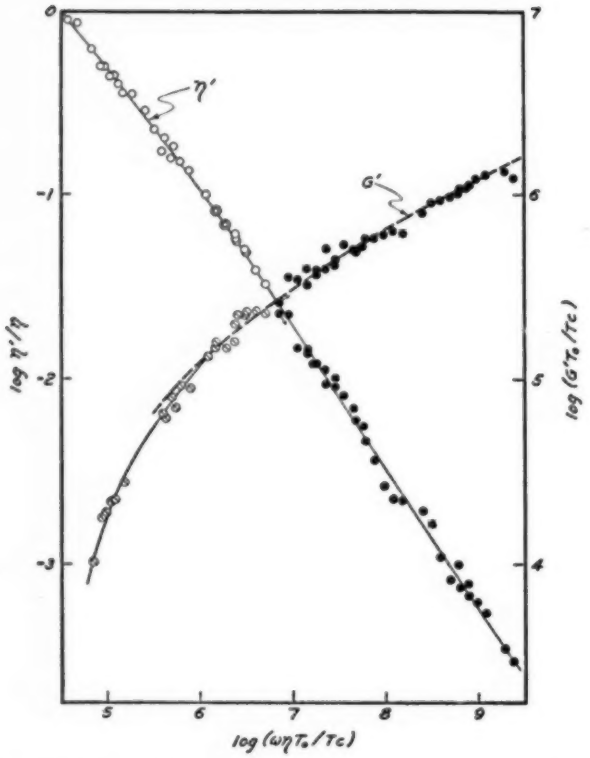

FIG. 1. Reduced dynamic rigidity and viscosity plotted against reduced frequency, for unfractionated sample. ○, η' from transducer measurements; ⊘, G' from transducer measurements; ●, η' and G' from wave propagation measurements with individual damping determinations; — —, displaced composite curve for $\bar{G}_r$, covering concentration range from 16 percent to 40 percent polymer (reference 1, Fig. 3), corresponding to the approximation $G_r' = 0.90\bar{G}_r$.

For a broad distribution we may use an approximation,

$$G'(\omega) = \int_{1/a\omega}^{\infty} F(\tau)d\tau; \quad \eta'(\omega) = \int_{0}^{1/a\omega} \tau F(\tau)d\tau \qquad (4)$$

such that those Maxwell elements with τ above a certain cut-off time $1/a\omega$ contribute only to the rigidity while those below contribute only to the viscosity. In the use of this approximation by Guth,[12] the numerical factor a was taken as unity; we must make it slightly different from unity to correlate the experimental values of G' and η'.

We define a logarithmic distribution function $\Phi(\ln\tau)d\ln\tau = F(\tau)d\tau$ and differentiate the definite integrals of Eqs. (4) with respect to their limits to obtain $dG'/d\ln\omega = \Phi(-\ln a\omega)$; $d\eta'/d\ln\omega = -(1/a\omega)\Phi(-\ln a\omega)$. For calculations from logarithmic plots such as Figs. 1 and 2, it is convenient to solve for Φ as follows:

$$\Phi(-\ln a\omega) = G'(d\log G'/d\log\omega) = -a\omega\eta'(d\log\eta'/d\log\omega). \qquad (5)$$

In terms of reduced variables, if Φ_r is defined as $\Phi T_0/Tc$, we have

$$\Phi_r(-\ln a\omega_r) = G_r'(d\log G_r'/d\log\omega_r) = -a\omega_r\eta_r'(d\log\eta_r'/d\log\omega_r). \qquad (6)$$

Thus Φ_r may be calculated either from the dispersion of G_r' or the dispersion of η_r'. Excellent agreement between the two methods is obtained for the unfractionated sample if a is taken as 0.77, as shown in Fig. 4, where Φ_r is plotted against $\log\tau_r$ (here $\tau_r = \tau cT/T_0\eta$). The same value of a applied to the data for Fraction I gives agreement at low τ_r but some divergence at high τ_r (Fig. 5). At high τ_r, the values from η' are considered to be more reliable.

The figures also show curves for $\tau_r\Phi_r$. The values of Φ_r and $\tau_r\Phi_r$ approach zero at high and low values of the abscissa, respectively, so that the integrals of Eqs.

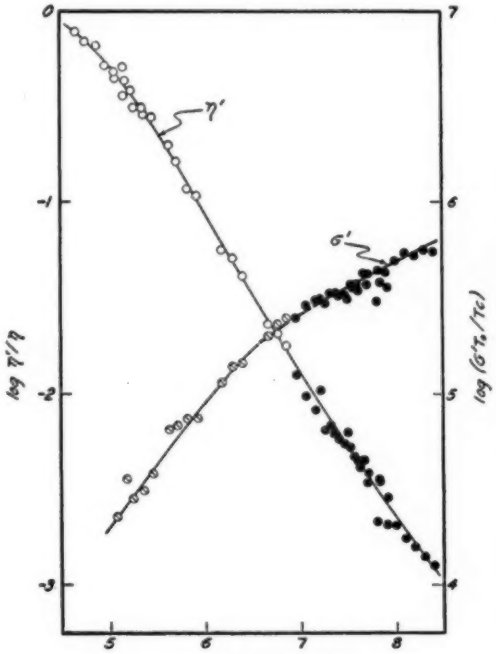

FIG. 2. Reduced dynamic rigidity and viscosity plotted against reduced frequency, for Fraction I. Key to symbols same as in Fig. 1. The displaced composite curve for $\bar{G}_r$ (reference 1, Fig. 8) includes concentrations of 14 percent and 17 percent polymer.

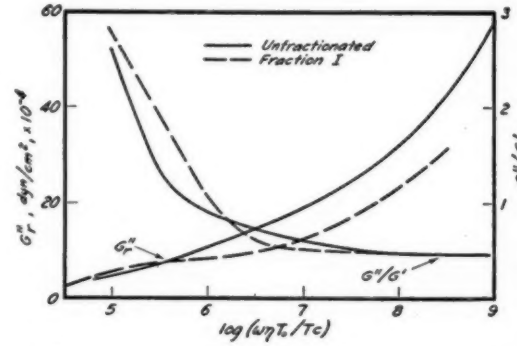

FIG. 3. Dispersion of G_r'' and G''/G', calculated from Figs. 1 and 2.

[12] Ivey, Mrowca, and Guth, J. App. Phys. **20**, 486 (1949).

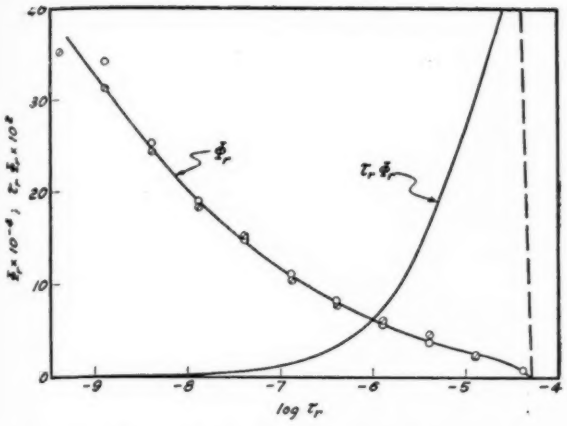

FIG. 4. Distribution functions Φ_r and $\tau_r\Phi_r$ for unfractionated sample, calculated from dispersion of $\eta'(\bigcirc)$ and dispersion of $G'(\varnothing)$.

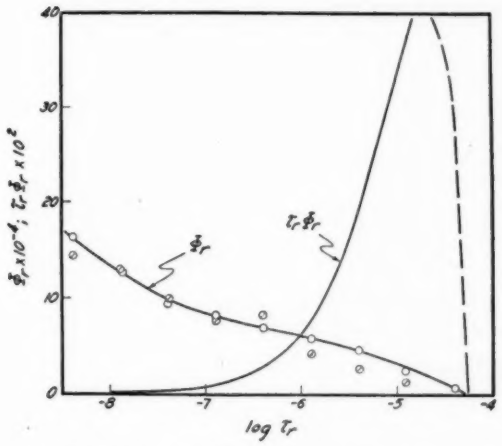

FIG. 5. Distribution functions Φ_r and $\tau_r\Phi_r$ for Fraction I. Key to symbols same as in Fig. 4.

(4) are convergent and may be used to calculate G_r' and η_r' at any desired frequency. Such calculations check the experimental values within graphical errors. The integral of $\tau_r\Phi_r d\ln\tau_r$ from $-\infty$ to ∞ must be unity because of the definitions of the reduced variables, and this is found graphically to be the case. Alternatively, G_r' and η_r' can be calculated from Φ_r by graphical integration of the exact Eqs. (3). These calculations check within about 10 percent, reflecting probably the degree of accuracy of the cut-off approximation. Thus a single empirical function Φ, together with data on the steady flow viscosity η, can provide an approximate description of the dynamic mechanical properties in small deformations over a wide range of frequencies, temperatures, and concentrations.

For the high molecular weight sample (Fig. 5), the function Φ is of the order of 10^5 dyne/cm^2 and, over several decades, has a relatively low slope. It is probable that the existence of such a plateau-like region in the relaxation function of high molecular weight polyisobutylene is responsible for the partial success of the box distribution approximation[11] in fitting stress relaxation data on this polymer.[13] For the low molecular weight polyvinyl acetate (Fig. 4), the slope of Φ is steeper, and it is not expected that the box approximation would be applicable to such a material. It would be of interest to obtain an extension of Φ in the direction of lower τ from high frequency measurements such as those of Mason and Baker.[14] The detailed shape of the function at the high τ end should be obtainable from stress relaxation measurements in concentrated solutions.[15]

ACKNOWLEDGMENT

This work was supported in part by the Research Committee of the Graduate School of the University of Wisconsin from funds supplied by the Wisconsin Alumni Research Foundation, and in part by a grant from Research Corporation.

[13] Andrews, Hofman-Bang, and Tobolsky, J. Polymer Sci. **3**, 669 (1948).

[14] Mason, Baker, McSkimin, and Heiss, Phys. Rev. **73**, 1074 (1948).

[15] F. W. Schremp and J. D. Ferry (unpublished work).

Stress Phenomena from the Respective Viewpoints of Solid-State and High Polymer Physics

MAURICE L. HUGGINS
Research Laboratory, Eastman Kodak Company, Rochester, New York

Flow and elastic properties are considered, in a qualitative manner, for the following types of materials: crystalline solids, simple liquids, glasses, and high polymers.

BY "stress phenomena" we mean here certain phenomena associated with the displacements of atoms or molecules relative to their neighbors when acted on by a shearing force or "shear stress." We are interested in the following: (1) The permanence of the displacements: On this basis we distinguish between elasticity, and flow or fracture. (2) The magnitude of the displacements, as related to the magnitude of the stress: Elastic moduli and stress-strain curves, for example, are expressions of this relationship. (3) The rate of displacement, as dependent on the stress: This is usually expressed by the fluidity or its reciprocal, the viscosity.

We are interested in the interpretation of these properties in terms of atomic and molecular structures and interatomic and intermolecular forces. Since the type of structure varies greatly in different classes of materials—crystals, liquids, glasses, high polymers, etc. —it is convenient to consider these classes separately.

In *crystalline solids* the chief effect of an applied stress is to shift all of the atoms or molecules slightly from their equilibrium positions in the crystal structure. Work is done against the interatomic or intermolecular forces; the energy of the system is increased. On removal of the stress, the atoms and molecules return to their equilibrium positions. The substance exhibits *short-range elasticity*.

If *flow* occurs at all, it takes place in jumps, one atom or molecule at a time. The structure after each jump is closely similar to that before the jump; hence the shifts are permanent and this is flow rather than elasticity. The jumps occur readily only where there are irregularities—departures from the perfectly crystalline arrangement—as at grain boundaries or regions where, for accidental reasons, there happens to be either a deficiency or an excess of atoms or molecules (per unit of volume) over the number required for the perfect crystal. Because of the crystalline arrangement, the shifts occur preferentially in certain directions, parallel to the atomic or molecular planes; hence the flow properties of the whole vary with direction.

To break or *fracture* a crystalline solid, the applied stress, greater than a certain "yield value," produces a shift of an atom or molecule to a less stable situation (e.g., one involving greater atomic separations); this shift facilitates a similar shift of a neighbor, such shifts then occurring autocatalytically across the crystal. This process is obviously also directional, the breaks tending to follow the planes of easiest cleavage in the crystal.

In simple *liquids*, irregularities of structure are numerous and irregularly distributed throughout the occupied volume. At some of these irregularities, shifts are constantly (or at least frequently) occurring, as a result of the temperature motions of the molecules. Without the application of an external stress, there is—within the errors of macroscopic observation—as much motion in any one direction as in the opposite direction; hence no over-all motion is observed. Application of a shear stress favors motions having a component in the direction of the stress and hinders those having a component in the opposite direction; *flow* is therefore observed. The rate of flow (hence the fluidity and its reciprocal, the viscosity) depends on the difference between the rate at which energy humps restricting molecular shifts are passed over in the forward and backward directions, and so on the magnitudes of these humps, their number, the temperature, and the applied stress. Unlike the crystalline case, the flow properties are independent of direction. For pure shear stress, there is (in a simple liquid) no "yield value"—an infinitesimal stress is sufficient to produce flow. *Elasticity* (short range) is observed for over-all compression, but not for shear.

Glasses are like liquids in having an irregular structure, but like crystalline solids in having (at ordinary temperatures) few or no atomic or molecular shifts occurring spontaneously—as a result of the temperature motions —or on the application of small shear stresses. Thus they exhibit *short-range elasticity*, and *flow* only with high stresses, long times, or high temperatures. The detailed interpretation of stress phenomena is complicated, for ordinary silicate glasses at least, by the fact that the structures contain charged ions, these being of a variety of chemical types, charges, sizes, and shapes. The existence of a substance in the glassy "state" is a result of the fact that the component atoms can be distributed in space in various ways of about equal stability, but with high energy humps hindering transitions from each such way to others.

High polymers are generally, like glasses, irregular in structure, although they frequently have regions which are more or less crystalline. The crystalline arrangement and many non-crystalline arrangements are usually of nearly equal energy. Moreover, the shifts of atoms needed to change a small non-crystalline region into a

crystalline one often do not require the breaking of any strong bonds—passage over large energy humps. On the other hand, to change a sample of a semicrystalline linear high polymer, in which many of the polymer chains run through two or more crystalline regions as well as amorphous intercrystalline regions, into a single crystal would require either the breaking of many strong bonds or the breaking up of many of the crystalline regions. This would involve passage over large energy humps, so large that the process would not occur at ordinary temperatures; at high temperatures the crystalline arrangement would not be stable relative to an amorphous structure. For these reasons, single crystals of linear high polymers have not been obtained.

Rotation around a single bond in an organic molecule, such as a linear high polymer, ordinarily involves only small changes in energy, of the order of magnitude of the average energy of temperature motion of the atoms. The polymer molecules can therefore change their shapes and their steric relations to their neighbors by motions of a few atoms at a time over relatively small energy humps. Both *flow* and *long-range elasticity* involve such changes. For flow, molecules must permanently shift their positions (e.g., their centers of gravity) relative to their neighbors—more of them shifting in the direction favored by the applied stress than in the opposite direction. In high polymers this shift rarely takes place all at once; it occurs, rather, as a succession of small shifts of portions of the molecule. The stress must be maintained over a time long enough for these successive shifts, and allowing for occasional shifts in the reverse direction—against the stress—in accord with the principles of equilibrium.

A single crosslink to an adjacent molecule can prevent the flow of a given molecule. The molecule can then change its shape, extending itself in the direction favored by the stress, but, on release of the stress, it will tend to revert to its original state, relative to its neighbors. This reversion may not be exactly achieved for a given molecule, but the average over all molecules of this sort will be such that there will be no permanent over-all shift, either in the forward direction or in the opposite direction. This reversible change of molecular shape is responsible for long-range elasticity.

The relative flow of adjacent molecules can be hindered or prevented by any intermolecular interactions of sufficient strength, such as hydrogen bonds or strong polar attractions. The cooperative action of many small forces is also effective. This occurs, for example, in crystalline regions: A portion of a chain molecule cannot be removed from such a region one segment at a time, a very large force being required to pull many segments simultaneously over their small energy humps. Even without crystallinity, a portion of a polymer chain which is extended as much as possible in the direction favored by the stress can move only as a unit. Motion of this unit obviously requires passage over a large energy hump—the summation of a series of small humps; it thus occurs less readily than motion of a smaller portion of the chain by itself.

Another factor to be considered is the extent to which a given shift of a segment in a polymer chain requires the pushing aside of neighboring regions, hence cooperating shifts in other molecules. This depends on the sizes, shapes and rigidities of the chain segments, including attached atoms or groups. Even the orientation, *cis* or *trans*, of the single bonds in a polymer chain adjacent to a chain double bond is important. With the *cis*-orientation (that in natural rubber), smaller segments may be shifted at a time and smaller volumes of the surroundings need to be rearranged, than with the *trans*-orientation (that in gutta percha). This is probably the explanation for the differences in long-range elasticity observed for natural rubber and gutta percha.

It is obviously possible for a material to exhibit both plastic flow and long-range elasticity at the same time. This is the case if, under the action of the applied stress, some of the molecules "flow" relative to their neighbors, while others merely change their shapes reversibly.

The forces restricting the motion of chain segments to give plastic flow and long-range elasticity are similar to those restricting the rotations of chains around the chain axes—the kind of motion which many types of chain molecules take up at their "second-order transition" temperatures, somewhat below the point at which they become fluid. The energy humps restricting both types of motion are similar in magnitude. The second-order transition point can therefore be used, for a given type of polymer at least, as a semiquantitative measure of its ability to undergo deformation of shape, either by plastic flow or by elastic extension, in the evaluation of plasticizers, for instance. For a better understanding of the plastic or elastic behavior of a substance or material, however, it is necessary to know something of the numbers of energy humps of different sizes—or, as some would prefer to express it, the distribution of "activation energies" or the "spectrum" of "relaxation times."

From the foregoing, it is evident that, although the same fundamental principles are involved in the different classes of substances considered, the application of these principles leads to widely different stress phenomena, as macroscopically observed.

Some Theoretical Considerations of Dynamic-Property Data on Textile Specimens

W. JAMES LYONS
Chemical and Physical Research Laboratories, The Firestone Tire and Rubber Company, Akron, Ohio

1. Early stretch-vibrometer data, of quite extensive character, on the frequency dependence of the internal friction μ of a Nylon monofil, has been found to conform to the relation

$$\mu=[\mu_2/(1+\omega^2\tau_2^2)]+\mu_3$$

which was deduced independently by Tobolsky and Eyring from considerations of molecular structure. Among other constants evaluated was the relaxation time for the secondary-bond network τ_2, which was found to have the value 9.3 sec.

2. By more sensitive graphing methods than had been used heretofore, it was confirmed by the Nylon data that the hyperbolic relationship between resonant frequency ω_0 and internal friction μ holds equally as well as the foregoing equation. The two relationships are shown to be nearly equivalent in the present experimental range. On evaluation of graphical parameters, the equation $\mu\omega_0=2.47\times10^9$ ergs/cm³ was obtained.

3. Using the same graphical method with a set of data on 11/4/2 cotton cord the relation $(\mu+0.9)\omega_0=7.05\times10^9$ ergs/cm³ was established.

INTRODUCTION

IN the application of a relaxation mechanism of the Kuhn type to dynamic experiments, Tobolsky and Eyring[1] indicate that under suitable conditions of load and frequency (in the range 20 to 200 c.p.s.) the modulus E and internal-friction coefficient μ, dynamically measured, are given by the equations

$$E=E_1+E_2, \tag{1}$$

and

$$\mu=[\mu_2/(1+\omega^2\tau_2^2)]+\mu_3, \tag{2}$$

where E_1 and E_2 are partial moduli governing the elastic deformation of the primary and secondary bonds, respectively; μ_2 and μ_3 represent friction, respectively, in the slippage of the secondary bonds, and in the motion of segments of the linear molecule relative to other parts of the chain; ω is the angular frequency of vibration, and τ_2 is the relaxation time for secondary-bond processes.

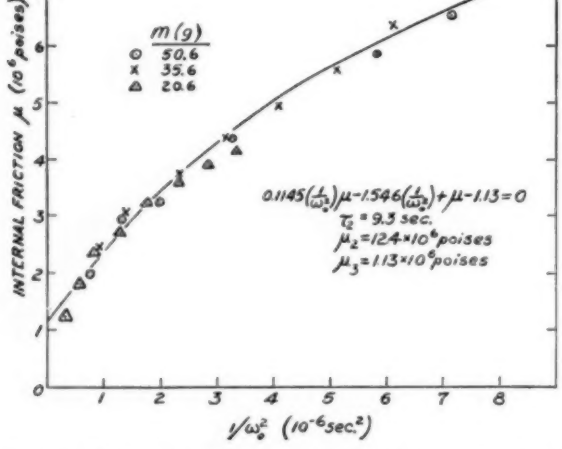

FIG. 1. Observed coefficient of internal friction of Nylon monofil as a function of $1/\omega_0$, at three vibrating masses m. Fitted to the data is a graph of Eq. (2).

[1] A. Tobolsky and H. Eyring, J. Chem. Phys. **11**, 125 (1943).

The partial moduli E_1 and E_2 being assumed to be material constants in this theory, the dynamic parameter E, according to Eq. (1), should be independent of frequency. In line with its earlier confirmation for rubbers at frequencies above the very lowest,[2,3] this theoretical conclusion has been confirmed on the textile stretch-vibrometer for samples of nine different textile materials,[4,5] up to frequencies between 300 and 400 c.p.s. At frequencies approaching, and in the supersonic range, the frequency-independence of E for textiles probably disappears, as it does for other high polymers.

It has been of further interest to investigate the validity of the internal-friction relation, Eq. (2). For this purpose the extensive data previously obtained on a high tenacity Nylon monofil were selected for treatment.

NYLON MONOFIL DATA

The calculated coefficients μ, obtained on the stretch-vibrometer for eight different lengths of the Nylon monofil, with three vibrating masses (reference 5, Fig. 8), were plotted as functions of $1/\omega_0^2$, $\omega_0(=2\pi f_0)$ being the resonant angular frequency at which the particular measurement was made. The result is shown in Fig. 1.

It can be readily verified that Eq. (2) can be written as an equation in $1/\omega^2$ and μ, as follows:

$$(1/\tau_2^2)\cdot(1/\omega^2)(\mu-\mu_2-\mu_3)+(\mu-\mu_3)=0, \tag{3}$$

where $1/\tau_2^2$, μ_2, and μ_3 are constants. The graph of this equation is a hyperbola having a μ-intercept of μ_3, and asymptotes $\mu=\mu_2+\mu_3$ and $1/\omega^2=-\tau_2^2$. It was recognized that the downward concavity of the pertinent branch of this curve coincided well with the distribution

[2] Gehman, Woodford, and Stambaugh, Ind. Eng. Chem. **33**, 1032 (1941).
[3] Dillon, Prettyman, and Hall, J. App. Phys. **15**, 309 (1944).
[4] W. J. Lyons and I. B. Prettyman, J. App. Phys. **19**, 473 (1948).
[5] W. J. Lyons, Textile Research J. **19**, 123 (1949).

of the experimental points in Fig. 1. Accordingly the three constants were evaluated to secure a good fit to these points. The resultant theoretical curve, for which $\tau_2=9.3$ sec., $\mu_2=12.4\times10^6$ poises, $\mu_3=1.13\times10^6$ poises, has been drawn in Fig. 1. The values of the constant coefficients in the equation set forth in Fig. 1 are those which are appropriate when $1/\omega_0$ is expressed in 10^{-3} sec.

DISCUSSION

The foregoing analysis has provided a value for the relaxation time τ_2 for secondary-bond processes. The value of 9.3 sec. is consistent with the conditions accepted by Tobolsky and Eyring in deriving Eq. (2), one of the conditions being that τ_2 is of the order of seconds.

If the familiar relation of Maxwellian relaxation theory, $\tau_i=\mu_i/E_i$, is considered as holding in intermolecular-bond processes, it is possible to estimate the value of the partial dynamic modulus E_2, for these processes. Thus

$$E_2=\mu_2/\tau_2$$
$$=(12.4\times10^6)/9.3=1.33\times10^6 \text{ dynes/cm}^2. \quad (4)$$

This value is practically negligible in comparison with the value of E which has been found for the Nylon sample: 8.0×10^{10} dynes/cm^2. It would appear then that in the type of longitudinal vibration to which the Nylon sample was subjected in the stretch-vibrometer, secondary bonds contribute very little to the over-all elasticity, and thus,

$$E\approx E_1. \quad (5)$$

The implication here that the primary bonds furnish practically all of the dynamic elasticity is at variance with the interpretation of Tobolsky and Eyring, who consider E_1 to be essentially the static modulus. Thus,

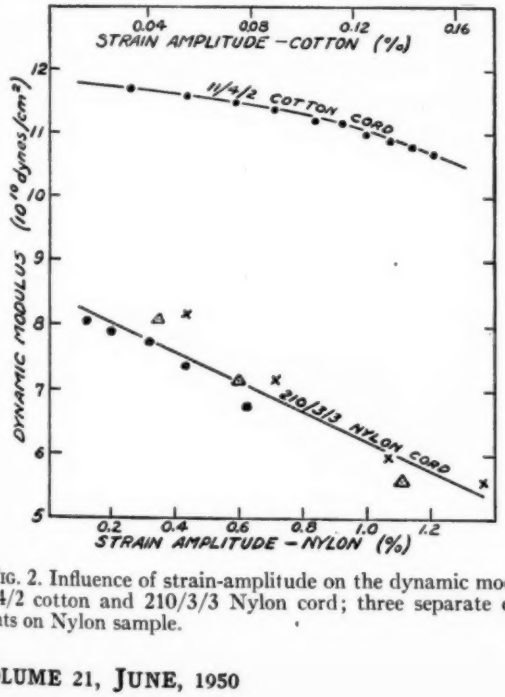

FIG. 2. Influence of strain-amplitude on the dynamic moduli of 11/4/2 cotton and 210/3/3 Nylon cord; three separate experiments on Nylon sample.

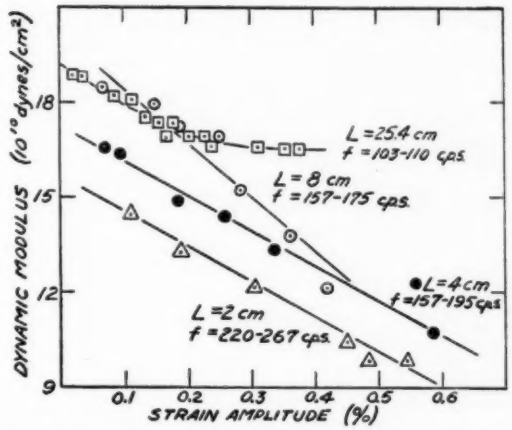

FIG. 3. Influence of strain-amplitude on the dynamic modulus of 1100/2 rayon cord; 2-kg load, at various free lengths of specimen, L.

on this view, E_1 and E_2 would be of the same order of magnitude, with E_1 being actually the smaller of the two, since this, quite generally, is what experiment indicates.

While the Tobolsky and Eyring analysis appears to be reasonable as applied to the rubber-like polymers, it is expected that in an oriented, linear fiber-forming polymer, such as the Nylon, being vibrated at a relatively small strain-amplitude, the basic dynamic, elastic processes could very well be restricted to the primary bonds. This behavior implies that the load is carried principally by the main valence chains, which view, for an oriented textile polymer such as high tenacity Nylon, is indeed tenable. In fact, Mark,[6] speaking of textile polymers, cellulose in particular, says "If any kind of van der Waals' forces were assumed to be responsible for the modulus of elasticity . . . the high values actually observed by various authors (would not be expected)." Secondary bonds, as represented by van der Waals' forces, are estimated to be smaller than primary valence forces by several orders of magnitude, in line with the relation found between E_1 and E_2 in the present analysis.

As the strains are carried to higher amplitudes it may be expected that more and more secondary bonds become involved, and the load is partially shifted over to them. This would result in an increase in the effective secondary-bond modulus E_2, and a decrease in the effective primary modulus E_1, but if replacement here is bond-for-bond, or even in the ratio of 100 for 1, the effect would be a decline in the over-all modulus E. This effect we have found in strain-amplitude studies on cotton, rayon and Nylon cords, as shown in Figs. 2 and 3.

Considered as an equation in μ and $1/\omega_0$, instead of $1/\omega_0^2$, Eq. (3) is a cubic. The graph of this cubic equation is plotted as a solid line in Fig. 4. By equating $d^2\mu/d(1/\omega_0)^2$ to zero the inflection point of the cubic is

[6] H. Mark, *Cellulose and Cellulose Derivatives* (Interscience Publishers, Inc., New York, 1943), edited by E. Ott, p. 995.

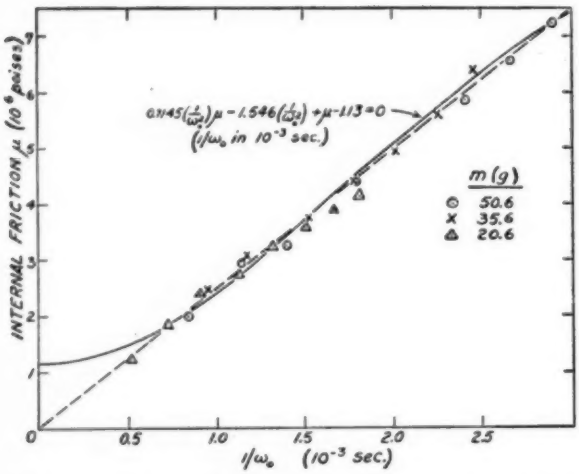

FIG. 4. Observed coefficient of internal friction of Nylon monofil as a function of $1/\omega_0$. Fitted to the data is the graph of Eq. (2) (solid line), as well as that of $\mu\omega_0 = \text{constant}$.

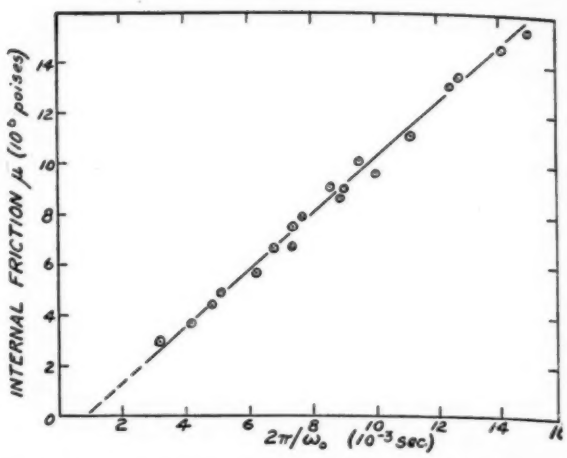

FIG. 5. Observed coefficient of internal friction of 11/4/2 cotton tirecord as a function of $2\pi/\omega_0$.

found to be at $1/\omega_0 = 1.7\times10^{-3}$ sec. The region of the inflection point of a cubic curve can be approximated by a straight line, and since the inflection point falls at about the middle of the array of experimental points in this study, the data themselves, as Fig. 4 shows, can be as well represented by a straight line as by the cubic. The equation of such a straight line is the hyperbolic relation

$$(\mu+\alpha)\omega_0 = \text{constant}, \tag{6}$$

with which, it has been demonstrated,[4,5] our data on a large number of textile samples are in apparent agreement. While Eq. (2) or (3) is not mathematically consistent with Eq. (6), the foregoing graphical analysis indicates why the data are in reasonably good agreement with both.

The straight line in Fig. 4, which is the most acceptable that could be drawn through the data points, has been extrapolated to the origin. The fact that a straight line passing through the origin fits the data, plotted on a $(1/\omega_0)\mu$-plane, demonstrates better than has been done heretofore that: (a) the relation between μ and ω_0 may be represented by a *true* hyperbola, and (b) the constant α is zero, and ω_0 has no additive constant. Furthermore, from Fig. 4 one is readily able to evaluate the constant in Eq. (6). Thus the data for the Nylon monofil, if they are regarded as representable by Eq. (6), lead to the relation

$$\mu\omega_0 = 2.47\times10^9 \text{ ergs/cm}^3. \tag{7}$$

An interesting sidelight emerges from the consideration of the constancy of the product $\mu\omega_0$, for, referring (5) to the equation

$$\mu = qF/s_m\omega_0, \tag{8}$$

it is seen that $\mu\omega_0 = \text{constant}$ implies that the displacement amplitude at resonance s_m is directly proportional to the amplitude of the applied force F, if the shape factor $q = L/2A$ remains constant. For a particular string, *strain*-amplitude is proportional to force-amplitude regardless of length L. Such a relationship appears entirely reasonable, though it is not part of the original dynamic theory. These considerations evidently place the product $\mu\omega_0$ in the role of a Young's modulus for the viscous component of the strain. This interpretation of $\mu\omega_0$ is brought out also (and without recourse to experiment) when the dynamics is expressed in complex notation.

COTTON CORD DATA

Following the latter treatment applied to the Nylon data, results on a cotton cord, taken from Fig. 6 of reference 4, have been plotted on a $(1/\omega_0)\mu$-plane, as shown in Fig. 5. Here again a straight line appears to represent the frequency dependence of μ. However, the line does not pass through the origin. The μ-intercept $(=-\alpha)$ is found to be -0.9. Evaluating the slope of the graph we get for the cotton sample,

$$(\mu+0.9)\omega_0 = 7.05\times10^9 \text{ ergs/cm}^3. \tag{9}$$

A natural question arises as to what theoretical interpretation is to be put on the finite value of α. In the light of the discussion on the Nylon data, it appears that no serious attempt to place a physical interpretation on α should be made. Evidently the vanishing of α in the Nylon case was quite fortuitous.

ACKNOWLEDGMENTS

The data upon which the present development rests are the results of the careful measurements and calculations of Mr. Irven B. Prettyman. The author has had the benefit of profitable discussions on the analytical aspects with Messrs. J. W. Liska and G. R. Thurman. The encouraging support of Firestone research management is gratefully acknowledged.

Equation of State for High Polymers

R. S. Spencer and G. D. Gilmore
The Dow Chemical Company, Midland, Michigan

In a former paper the authors suggested the following equation of state, $(P+\pi)(V-\omega)=RT$, where π is the internal pressure (or cohesive energy density) and ω is the volume at absolute zero. It was found that this equation was in good agreement with data on the thermal expansivity and isothermal compressibility of polystyrene.

The present paper reports isothermal compression measurements on polymethyl methacrylate, polyethylene, cellulose acetate-butyrate, and ethyl cellulose at temperatures within the fabrication range. The above equation of state is shown to apply equally as well to these thermoplastics as to polystyrene and values are given for the constants. The usefulness of this relationship is illustrated in a brief discussion of some phases of the injection molding process.

INTRODUCTION

In a former paper the authors suggested[1] the following modified van der Waals' equation of state,

$$(P+\pi)(V-\omega)=RT.$$

In this, P is the external pressure, π the internal pressure (or cohesive energy density), V is the volume, ω the volume at absolute zero, R the gas constant, and T the absolute temperature. It was found that this relationship was obeyed quite well by polystyrene, and served to correlate experimental observations of thermal expansion, isothermal compression, sound velocity, and cohesive energy density by swelling measurements.

This work was undertaken as part of a larger study of the fundamentals of the injection molding process, and most of our applications of this equation of state have been in that field. The desire to extend our findings to thermoplastics other than polystyrene has resulted in the present work, inasmuch as the equation of state is basic to further considerations in injection molding theory. This point will be illustrated briefly at the end of the discussion.

The pragmatic nature of our interest in this problem has limited considerably the scope of our investigation. No attempt was made to study the compressibility of these polymers below their apparent second-order transition temperatures, as the interest was centered on fabrication conditions. Preliminary attempts were made to observe time effects associated with pressure and temperature changes in the neighborhood of the apparent second-order transition,[2] but it was concluded that the apparatus used was unsuitable. It was noted, however, that polystyrene exhibits retarded isobaric volume changes, after a sudden change in pressure, as well as the retarded isothermal volume changes already reported.[2,3] It is hoped that this important phenomenon will be investigated further by other workers in the field.

We shall continue to use the hybrid units of reference 1 and express P and π in lb./sq. in., V and ω in cc/g, and T in degrees K.

[1] R. S. Spencer and G. D. Gilmore, J. App. Phys. **20**, 502–6 (1949).
[2] R. S. Spencer and R. F. Boyer, J. App. Phys. **17**, 398–404 (1946).
[3] Alfrey, Goldfinger, and Mark, J. App. Phys. **14**, 700 (1943).

EXPERIMENTAL METHODS

The basic apparatus used for isothermal compression measurements has been described elsewhere,[1] as follows: "It consists of a cylindrical specimen cavity, one square inch in cross-sectional area, with a close-fitting plunger for compressing the polymer. This plunger also contains a cavity which opens into a groove machined in the wall of the specimen cavity. This plunger cavity is filled with polymer, which is forced into the groove and acts as a seal for the sample in the main cavity. In operation, then, force is applied to the smaller central plunger, and the larger plunger directly contacting the sample *floats*."

Some slight changes have been made to facilitate operation. When it was desired to control temperature more closely than was possible with the electric heater the mold was placed inside a small insulated tank through which was pumped liquid from a thermostatted bath. The compression measurements were carried out with a Baldwin-Tate-Emery testing machine, which provided loads up to 20,000 lb. The compression strain was measured with a microformer-type (differential transformer) strain follower which operated the chart drive of a drum recorder. The pen movement was linked mechanically to the testing machine so as to record pressure. Thus, the recorder reproduced automatically the compression stress-strain curve. This arrangement effected a considerable speeding up of the measurements.

The polymethyl methacrylate used was a product of E. I. du Pont de Nemours and Company, designated as Lucite HM 140. The polyethylene was also a du Pont product, designated as P1000 PM 1. The cellulose acetate-butyrate was Tennessee Eastman's Tenite II, designated as 265-A. The ethyl cellulose formulation was a mixture of 15 percent plasticizer, 85 percent ethyl cellulose of degree of substitution 2.34. All of the samples were prepared by machining down cylinders to a firm press fit into the compressibility mold.

DISCUSSION

Broadly speaking, our measurements consist of parallel observations of pressure, P, and volume, V, at a fixed temperature, T. From such data we wish to deduce the probable values of the constants π, ω, and R.

TABLE I. Internal pressure of polymethyl methacrylate at 175°C.

$\bar{P}$	π
2500 p.s.i.	32,000 p.s.i.
3500	31,300
4500	31,700
5500	32,900
6500	30,100
7500	32,500
8500	27,200
9500	35,800
11,000	30,200
13,000	32,400
15,000	28,500
17,000	30,500
	Average = 31,300

TABLE II. Internal pressure of polyethylene at 178°C.

$\bar{P}$	π
1560 p.s.i.	46,500 p.s.i.
2500	47,700
3525	48,000
4605	47,400
5680	48,800
6600	46,400
7500	47,600
8540	47,600
9540	47,400
10,525	46,700
11,525	50,500
12,750	46,600
14,270	47,500
15,540	47,300
16,520	47,800
17,545	47,100
	Average = 47,600

This may be done, of course, by direct use of the equation of state in the form already given. However, there are experimental and theoretical advantages in considering only corresponding changes in pressure and volume, rather than absolute magnitudes. This procedure avoids the necessity of using the apparatus to measure thermal expansivity (for which it is not ideally suited), helps prevent the accumulation of errors, and is more sensitive in bringing out such things as the pressure-dependence of π.

In this differential method we eliminate ω, which can be calculated subsequently from a known value of the equilibrium volume at some temperature and pressure. The constants π and R remain to be determined from our data. If we knew the molecular weight, M, of an "interaction unit" of the polymer chain, we could calculate R, in our units, from our relationship $R=1206/M$. If the polymer is something like polystyrene or polymethyl methacrylate, having one bulky side-group per monomeric residue, it seems reasonable to assume that the interaction unit is just one residue. This appears to be true, within experimental error. Such polymers as polyethylene, with no side-groups, and cellulose derivatives, with several per residue, present much more ambiguous situations, however. It seems preferable, then, to begin by considering both π and R to be unknown constants. If the empirical value of R subsequently offers a suggestion as to the nature of the interaction unit, the data can be reworked accordingly.

The appropriate relationship to use in this approach is

$$[-T(\Delta P/\Delta V)]^{\frac{1}{2}}=[\pi/(R)^{\frac{1}{2}}]+[1/(R)^{\frac{1}{2}}]\cdot\bar{P}$$

where ΔV is the volume change resulting from a pressure change ΔP, and $\bar{P}$ is the average pressure over the interval ΔP. Probable values of the constants can be determined by drawing a straight line through a plot of $[-T(\Delta P/\Delta V)]^{\frac{1}{2}}$ *vs.* $\bar{P}$, or by a least-squares procedure, which was the method adopted.

If the monomeric residue is the interaction unit in polymethyl methacrylate, we should expect $R=12.05$. Applying a least-squares procedure to compression measurements at 175°C, we obtain $R=14.71$ and $\pi=35{,}300$ p.s.i. Assuming that the discrepancy in R is experimental error and taking $R=12.05$ as correct, the value of π can be computed over each pressure interval, as shown in Table I. The average value is $\pi=31{,}300$ p.s.i., the scatter is not excessive (there appears to have been an error in the volume of $P=9000$ p.s.i.) and there is no dependence of π on P over the range covered. The equilibrium volume-temperature coefficient would be $(\partial V/\partial T)_{P=0}=R/\pi=3.86\times10^{-4}$ cc/°C. The density at 25°C was 1.169 g/cc. Assuming this to be an equilibrium value, we calculate $\omega=0.740$ cc/g. If we calculate the density at the apparent second-order transition, using the data of Robinson, Ruggy, and Slantz,[4] and assume that to be a state of equilibrium, we obtain $\omega=0.734$. If we take the density at 30°C = 1.1818 g/cc, as given in reference 4, to be an equilibrium value, we get $\omega=0.728$. The last two values are probably preferable to the first one, only suitable equilibrium density measurements can resolve the question.

In the case of polyethylene at 178°C, the least-squares method gives $\pi=50{,}600$ p.s.i., $R=48.03$. This value of R is not far from 43.0, which corresponds to one ethylene residue as an interaction unit, so the latter value shall be taken as correct. Calculating for each pressure interval we obtain the results of Table II, which give as an average $\pi=47{,}600$ p.s.i. The equilibrium volume-temperature coefficient is $(\partial V/\partial T)_{P=0}=9.48\times10^{-4}$ cc/°C. The density at 25°C was found to be 0.9196 g/cc, from this $\omega=0.805$ cc/g. This is almost certainly not correct, however, due to the presence of considerable crystallinity at room temperature. Correcting the density to the melting point, using the data of Clash and Rynkiewicz,[5] we obtain $\omega=0.875$.

The least-squares values obtained with the data on ethyl cellulose at 196°C are $R=19.95$ and $\pi=34{,}800$ p.s.i. The value of R corresponds only to a fractional

[4] Robinson, Ruggy, and Slantz, J. App. Phys. **15**, 343-51 (1944).

[5] R. F. Clash, Jr., and L. M. Rynkiewicz, Ind. Eng. Chem. **36**, 279–82 (1944).

TABLE III. Internal pressure of ethyl cellulose at 196°C.

$\bar{P}$	π
1500 p.s.i.	34,700 p.s.i.
2500	34,900
3560	34,100
4560	35,600
5500	34,500
6500	35,300
7500	35,700
8500	33,700
9500	34,800
10,500	33,300
11,540	35,800
12,540	35,000
13,500	40,400
14,500	30,400
15,500	34,900
16,500	33,900
17,500	35,400
	Average = 34,800

TABLE IV. Internal pressure of cellulose acetate-butyrate at 181°C.

$\bar{P}$	π
1500 p.s.i.	41,800 p.s.i.
2500	40,000
3500	41,800
4500	42,500
5500	40,300
6500	41,800
7500	40,100
8500	41,000
9500	41,500
10,550	42,000
11,550	43,600
12,500	41,800
13,500	39,900
14,500	38,900
16,000	44,800
17,500	39,700
	Average = 41,300

part of a substituted glucose residue, as might be expected, therefore, we shall accept the least-squares value, having no better substitute. The scatter in the measurements is shown in Table III, where π is calculated for each pressure interval, using the above value of R. No trend of π with $\bar{P}$ may be noted. There appears to be an error in the volume observed at $P=14{,}000$. The equilibrium volume-temperature coefficient is $(\partial V/\partial T)_{P=0}=5.73\times10^{-4}$ cc/°C. The density at 25°C was observed to be 1.115 g/cc, giving $\omega=0.725$. Correcting to the apparent second-order transition, using the data of Wiley,[6] gave $\omega=0.720$.

In the case of cellulose acetate-butyrate at 181°C the least-squares values are $R=22.18$ and $\pi=41{,}300$ p.s.i. As with ethyl cellulose, the value of R corresponds to a fractional residue and will be accepted as given. In Table IV are shown the values of internal pressure for each pressure interval, calculated with the above value of R. The scatter and lack of dependence upon applied pressure are very much as has been noted in the preceding tables. The equilibrium volume-temperature coefficient is $(\partial V/\partial T)_{P=0}=5.37\times10^{-4}$ cc/°C. The density at 25°C was 1.17 g/cc, giving $\omega=0.695$. Correcting to equilibrium, using the data of Clash and Rynkiewicz,[5] gives $\omega=0.688$.

The equation of state constants which have been determined to date are summarized in Table V, together with activation energies for viscous flow, taken from various sources.[4,7,8] The activation energy for flow seems to rise with increasing cohesive energy density, as might be expected, with the glaring exception of polyethylene. This exception is apparent rather than real, however. The units of π are energy per unit volume, while the units of activation energy are energy per mole. Taking the residue molecular weights into account, a fair correlation is found between cohesive energy per mole and activation energy per mole for all five polymers. In Eyring's picture of viscous flow[9] this would be interpreted as signifying that the number of residues per kinetic chain segment is roughly a constant for the different polymers. We estimate that it is in the general neighborhood of 15 residues per segment.

The order in which the polymers arrange themselves on the basis of cohesive energy density is not too surprising, again with the exception of polyethylene. Considering only chemical structure, one would be tempted to guess, *a priori*, that polyethylene would have a lower cohesive energy density than the other polymers, and just the reverse is true, of course. However, the polyethylene molecule exhibits a quality which the others do not, and that is great regularity of structure and the ability to form close-packed arrangements. It is just this factor which permits polyethylene to crystallize in spite of its non-polar nature. Thus, polyethylene contains many more monomeric residues per cc than the other polymers. If we calculate the cohesive energy per residue, or per interaction unit, the apparent discrepancy disappears.

In discussing a few examples of the important role which the equation of state plays in injection molding theory it will be necessary first to present a somewhat simplified picture of what occurs in an injection molding cycle.[10] In the more usual type of molding press the polymer is fed in at room temperature and is heated to molding temperature in the machine. In a subsequent cycle this hot polymer is forced through the channels of the press and mold, eventually filling the mold cavity. It is customary to maintain pressure on the ram of the press for some time after the mold is filled. During this interval several things are going on. The pressure in the mold builds up fairly rapidly to a

[6] F. E. Wiley, Ind. Eng. Chem. **34**, 1052–6 (1942).
[7] G. J. Dienes, J. Colloid Sci. **2**, 131–61 (1947).
[8] R. S. Spencer, J. Polymer Sci. (to be published).

[9] Glasstone, Laidler, and Eyring, *The Theory of Rate Processes* (McGraw-Hill Book Company, Inc., New York, 1941), p. 500.
[10] G. D. Gilmore and R. S. Spencer, Mod. Plastics (to be published).

TABLE V. Equation of state constants for high polymers.

Polymer	R	ω	π	Viscosity activation energy
Polystyrene	11.6	0.822 cc/g	27,000 p.s.i.	23 kcal./mole
Polymethyl methacrylate	12.05	0.734[a]	31,300	30
Ethyl cellulose	19.95	0.720[a]	34,800	40
Cellulose acetate-butyrate	22.18	0.688[a]	41,300	78
Polyethylene	43.0	0.875[a]	47,600	11

[a] Values uncertain owing to lack of reliable values for equilibrium density.

relatively stable value, which is usually appreciably lower than the ram pressure. Inasmuch as the mold is colder than the polymer, the polymer is being cooled from the time it enters the mold. The mass of the polymer in the mold increases slowly during this time. At the end of this interval the ram is returned to its starting position. The pressure difference between the mold cavity and the channels in the press has now reversed direction and there is certain amount of polymer discharged from the mold cavity. This discharge lowers the pressure in the mold and the discharge rate falls off until there is sufficient cooling at the constricted entrance to the mold cavity (usually called the "gate") to "solidify" the polymer and seal off the mold. Following the discharge period the polymer in the mold cools under conditions of constant mass until the mold is opened and the piece removed.

The cooling characteristics of the mold give us a relationship between polymer temperature and time. The equation of state then gives us the relationship between pressure, mass of polymer in the mold, and temperature. Thus, consideration of any question which involves calculating the pressure or the mass of polymer in the mold must rest on a knowledge of the equation of state. For example, under certain conditions volume defects, such as bubbles or sink marks, appear in the piece. These defects can be rendered unobjectionable by being sure that the mass of polymer sealed in the mold exceeds some minimum value under given sealing conditions. This condition can be set up in terms of controllable quantities by use of the equation of state. As another example, we note that behavior during release of the piece from the mold is determined primarily by the pressure remaining in the mold at the time the mold is opened. The force required to open the mold depends directly upon the residual pressure, as might be expected. If the pressure is too high it will not be possible to open the mold. At lower pressures the piece will stick in the female half of the mold and/or will be objectionably scored in removing from the mold. Finally, if the residual pressure is kept below a certain maximum, the piece releases reasonably easily. If, however, the pressure is allowed to become "negative," there is a tendency to stick on the male half of the mold, and even to crack. The application of the equation of state in considering such questions as the above should be obvious.

A more detailed discussion of these, and other, injection molding problems may be found in reference 10 and in publications to follow.

SUMMARY

The constants in a simplified van der Waal's equation of state have now been determined for the following polymers: polystyrene, polymethyl methacrylate, ethyl cellulose, cellulose acetate-butyrate, and polyethylene. Of these, polystyrene has the lowest internal pressure (or cohesive energy density) and polyethylene has the highest. The unexpectedly high internal pressure exhibited by polyethylene has been associated with the great regularity of the polyethylene molecule and its ability to form closely packed arrangements.

The application of the equation of state in the injection molding field has been illustrated by a very brief discussion of the roles played by pressure, temperature and polymer density in such phenomena as mold release and the formation of bubbles and other defects.

Behavior of Granulated Polymers under Pressure

R. S. Spencer, G. D. Gilmore, and R. M. Wiley
The Dow Chemical Company, Midland, Michigan

In such fabricating processes as extrusion and injection molding it is frequently necessary to force a granular polymer through a channel. Frictional forces between polymer and channel walls lead to a drop in pressure through the granular material. Simultaneously, the applied pressure causes a compaction of the granules.

Assuming that the granular mass has certain fluid-like properties, a simple theoretical expression for pressure transmission is derived. Comparison with data on saran powders and granular polystyrenes shows good agreement between theory and experiment. The effect of lubrication is shown also.

The compaction of granular polystyrene follows the same pattern as that observed in the earth's crust. The porosity decreases exponentially with increasing pressure. The "compressibility coefficient" for the porosity of granular polystyrene is comparable with that given for clays and shales.

INTRODUCTION

THE available literature relating to the behavior of granular solids under pressure is rather scanty. Inasmuch as the handling of some such materials is of considerable technological importance, the reasons for this deficiency are not immediately apparent. It can only be surmised that either an appreciable amount of unreported work has been done or else the practical importance of the problem has not been emphasized sufficiently to those who are in a position to study it adequately.

Most thermoplastics are marketed in granular form. In subsequent fabrication operations, such as extrusion or injection molding, it is usually necessary to force the granular polymer through some sort of channel. In given circumstances, then, one wishes to know what force it is necessary to apply in order to move the granular polymer against a specified resisting force, or, conversely, how much of the applied pressure is transmitted through the granular material. It is probably safe to say that lack of knowledge on this point is not least among the factors which have served to maintain polymer fabrication techniques in the realm of technological arts rather than applied sciences.

The problem to be considered in the present paper is that of the relationship between applied force and resisting force at either end of a plug of granular polymer which is just on the point of motion through a channel of constant, but arbitrary, cross section. That is to say, the conditions at the wall of the channel are those of static friction. The solution of this problem necessitates certain assumptions, which are set up largely by analogy with fluid behavior. This restricts application to those cases in which the particle size is considerably smaller than the dimensions of the channel. Two simple arrangements will be described by which the problem may be studied experimentally, each having certain advantages. Results obtained with saran powders and polystyrene granules will be presented and interpreted with the aid of the simple theory.

At relatively higher pressures, considerable compaction of the granular material may be effected, which is essentially irreversible as long as the plug is confined within the channel. This is taken account of in the assumptions underlying the theory and, experimentally, by always proceeding in the direction of increasing applied pressure. This compaction is of some interest in itself; therefore, a few data are presented and discussed to illustrate the pattern of behavior.

It is doubtless redundant to point out that the treatment throughout is simplified and the investigation undetailed. Our interest in this problem arose because of its place in a larger program of study of polymer fabrication processes. Many points, theoretical and experimental, await clarification. It may be hoped that this will not be too long forthcoming.

EXPERIMENTAL METHODS

The first arrangement, being that used to study saran powders, is shown in Fig. 1. The confining channel was a glass tube of circular cross section. The polymer sample rested upon a rod extending below the tube, and was confined from above by a weight representing the resisting force. Both weight and rod were smaller in diameter than the tube, flaring out to the tube diameter at the end contacting the polymer. This was to minimize binding which would otherwise be occasioned by the trapping of powder granules between the rod and tube. One arrangement utilized a tube of 1.1 cm internal diameter with weights of 17 and 35 g; another, a tube of 2.15 cm internal diameter with weights of 38 and 78 g.

The procedure followed was to assemble the apparatus, using a given amount of saran powder, and set it upright on the platform of a spring scale. Downward force was then exerted upon the glass tube, and the reading of the scale noted at the instant the polymer first began to slip. This was then repeated with different amounts of powder, resisting loads, and tube diameters.

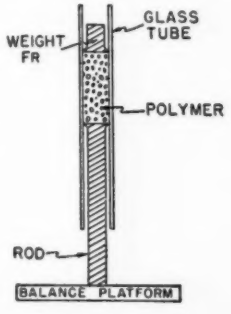

FIG. 1. Experimental arrangement used in the study of saran powders.

TABLE I. Coefficient of friction of saran powders.

Powder No.	D (cm)	μ
1	1.1	0.215
	2.15	0.239
2	1.1	0.144
	2.15	0.144
3	1.1	0.113
	2.15	0.167

It was found that all of the glass tubes examined were not perfectly cylindrical but had varying degrees of taper. It was necessary, then, to select those with the least taper, and to exercise the further precaution of always moving the polymer along the tube in the direction of increasing internal diameter, to avoid jamming. Relatively reproducible results could then be obtained with some care, although experimental errors with this apparatus must be considered to be rather large.

The apparatus used for the study of granular polystyrenes is shown schematically in Fig. 2. It consisted of a heavy-walled steel cylinder of 1.953 in. internal diameter, with two closely fitting pistons. SR-4 strain gauges were mounted on the lower piston and the unit calibrated in terms of force applied to the piston. It was found that any film on the surface of the cylinder wall adversely affected the reproducibility of measurement, therefore, the unit was carefully cleaned with carbon tetrachloride before use. It was then assembled, with the sample in place, and set between the platens of a 30-ton press. Force was applied through a hand-operated hydraulic jack, and the corresponding transmitted force determined from the strain gauge readings.

The saran powders used were commercial materials, denoted as *1*, *2*, and *3*, in order of increasing amount of lubricant in the formulation. The polystyrenes were also commercial materials, very similar to each other. The sarans were in the form of very finely divided powders, whereas the polystyrenes were much coarser, perhaps averaging around 0.15 in. particle diameter. One exception to this was polystyrene No. 2, which was that component of No. 1 which would pass through a U. S. No. 8 screen, and averaged considerably less than that in size, perhaps around 0.04 in.

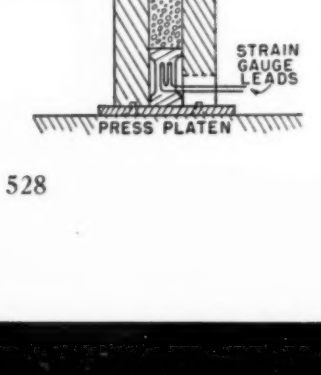

FIG. 2. Experimental arrangement used in the study of pressure transmission through granular polystyrenes.

DISCUSSION

The pressure-transmission problem to be solved has already been stated in the Introduction; it may be made a little clearer, perhaps, by referring to Fig. 3. A plug of granular polymer is confined within a channel of constant cross section. The applied force at one end of the plug is in opposition to the resisting force at the other end. What is desired is the relationship between the forces when the plug is just on the point of moving in the direction of the applied force.

It has been mentioned that increasing the applied force causes compaction of the granules. That is to say, the length of the plug decreases. The state of compaction may be defined by the porosity, or the initial and currently observed lengths of the plug, or by the initial length and the current pair of forces. In general, we must consider that the porosity will vary along the length of the plug; however, we shall be considering in our solution only the equilibrium situation in which the porosity at any point is not changing with time.

We shall define now the following quantities:

x = distance from the forward end of the plug to any plane normal to the axis of the plug.
μ = coefficient of friction of particle on wall.
n = number of particles per unit area contacting the wall at x.
n_0 = number of particles per unit area contacting the piston surfaces at the ends, or in contact over a cross section.
f = contact force between particles at x.
F = total force normal to the cross section at x.
$F_A(P_A)$ = applied force (pressure) necessary to just move the plug.
$F_R(P_R)$ = resisting force (pressure).
L = length of the granular plug in any given state of compaction.
L_0 = original length of the plug when the forces were very small.
C = perimeter of channel cross section.
A = area of channel cross section.
D = diameter of circular cross section.
a, b = sides of rectangular cross section.

The principal assumptions to be made use of are the following:

(1) In a given state of compaction there is no tendency for particles to move with respect to each other, hence the only frictional forces to be considered arise from particle-wall contacts. (2) Contact forces are the same in all directions at a point, and are normal to the walls and ends. (3) The quantity n_0 is constant, independent of F and x. (4) The total number of wall contacts is constant, although, of course, n depends upon F (or upon x in a given state of compaction); further, that $n = n_0$ over the entire wall originally, when the forces are very small.

FIG. 3. Diagram defining quantities in the pressure transmission problem. A = area; C = perimeter.

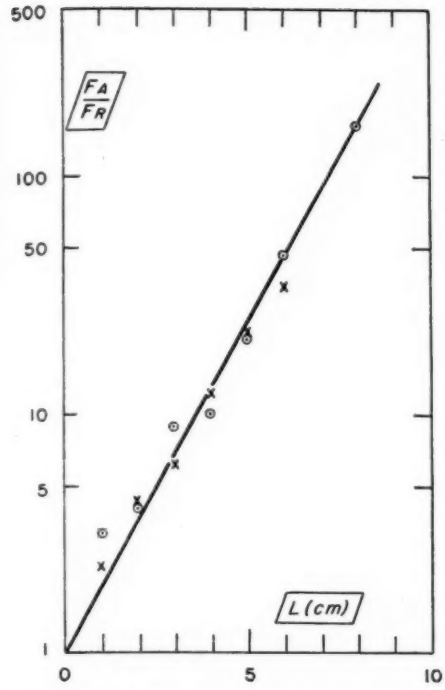

FIG. 4. Dependence of force ratio on length of sample of saran No. 2 in tube of diameter 1.1 cm. Circles represent $F_R=17$ g and crosses represent $F_R=35$ g.

Before proceeding, let us look over the assumptions quickly. There might be some temptation to replace (1) by the more usual assumption that the particles are hard and smooth, i.e., that there is no friction between particles. This is not true, however, as evidenced by the irreversibility of the compaction; thus we prefer the less general assumption (1). The second assumption is arrived at by considering the contact force to be analogous with pressure in a fluid. Actually, assumption (2) is more general than would be required, but it is felt that the analogy is clearer in the form as stated. The origin of assumptions (3) and (4) is more obscure and their plausibility less immediately discernible. It may help to picture the plug as a cylinder of some compressible material, on the surface of which is drawn an evenly spaced network representing the contact points. If this cylinder were compressed axially, while confined radially, the network spacing on the ends would remain unchanged, while the density of network on the sides would increase with the compression strain. Carrying this picture over to our granular material, we need only remember that in calculating the frictional force we are not concerned with the area of contact, but only with the contact force and the number of contacts.

With these preliminaries the solution is now quite straight-forward. Consider an element between x and $x+dx$. The frictional force at the wall is μf per particle, giving a total frictional force of $\mu f n C dx$. The change in F in going from x to $x+dx$ is $dF=An_0df$. By assumption (1) we can equate these two expressions and rearrange to give

$$dF/F=df/f=(\mu Cn/An_0)dx.$$

Integrating from $x=0$ to $x=L$, we obtain

$$\ln F_A/F_R=\frac{\mu C}{An_0}\int_0^L ndx.$$

To evaluate the integral on the right-hand side we utilize assumption (4) and equate the expressions for the number of wall contacts in the uncompacted state L_0 to the number of wall contacts in the compacted state. Thus,

$$n_0CL_0=\int_0^L nCdx$$

or

$$\int_0^L ndx=n_0L_0.$$

Substituting this in our previous equation, we finally arrive at

$$F_A/F_R=P_A/P_R=\exp(\mu CL_0/A).$$

We note that the exponent is merely the coefficient of friction times the ratio of the wall area (uncompacted) to the cross-sectional area. If the cross section is a circle of diameter D, we have

$$F_A/F_R=\exp(4\mu L_0/D).$$

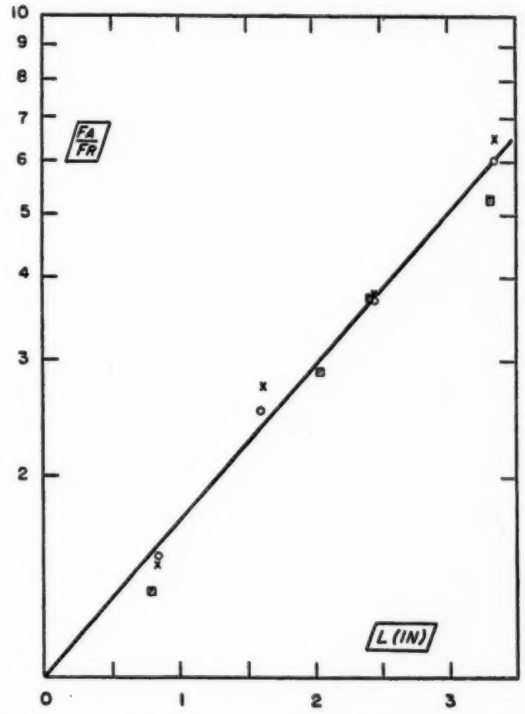

FIG. 5. Dependence of force ratio on length of sample of polystyrene in a steel cylinder of diameter 1.955 in. Circles represent polymer No. 1, crosses, No. 2, and squares, No. 3.

TABLE II. Pressure transmission through granular polystyrene. Force ratio (F_A/F_R).

Polymer No.	L_0(in.)	F_A=7600 lb.	14,700	22,000	29,500	37,000	44,000	51,000	59,000	Average
1	0.834	1.582	1.530	1.469	1.538	1.457	—	—	—	1.515
	1.594	2.71	2.37	2.44	2.57	2.64	2.51	2.45	2.46	2.52
	2.442	3.80	3.86	3.67	3.69	3.63	3.73	3.64	3.74	3.72
	3.354	6.33	5.65	5.79	6.15	6.17	6.29	6.22	5.57	6.02
2	0.829	1.520	1.362	1.448	1.490	1.516	—	—	—	1.467
	1.611	2.92	2.94	2.75	2.78	2.72	2.68	2.58	2.61	2.75
	2.447	3.80	3.34	3.67	3.69	3.85	3.93	3.98	3.74	3.75
	3.349	9.50	7.35	6.46	6.56	6.38	6.47	6.37	6.55	(6.47)
3	0.794	1.226	1.362	1.266	1.461	1.423	—	—	—	1.348
	2.042	3.17	2.83	2.75	2.74	2.72	2.78	2.96	2.98	2.87
	2.417	4.22	3.68	4.07	3.28	3.43	3.60	3.64	3.83	3.72
	3.314	3.46	3.68	3.66	3.99	4.63	4.89	5.31	5.27	(5.27)

TABLE III. Coefficient of friction of polystyrene on tool steel (Roche).

Temperature (°C)	μ
25	0.248
55	0.183
65	0.164
75	0.118
85	0.099

TABLE IV. Effect of surface lubrication of polystyrene granules.

PPM of lubricant	F_A/F_R
0	4.38
150	3.08
300	2.66
500	2.23
750	1.82

If it is a rectangle of sides a and b, we have

$$F_A/F_R=\exp[2\mu(a+b)L_0/ab].$$

If the rectangle approaches a slit, so that $a\gg b$, our expression approaches

$$F_A/F_R=\exp(2\mu L_0/b).$$

With the above results of our semicontinuous-semiparticulate approach to the problem, let us look at the experimental observations. First, we shall consider the data obtained on saran powders with the arrangement of Fig. 1. In Fig. 4 $\log F_A/F_R$ is plotted against L_0, for constant tube diameter and two resisting forces, and it may be noted that a fairly good straight line is obtained, as predicted by the theory. In Table I the data on the saran powders are summarized in the form of values of the coefficient of friction, calculated from the slopes of lines like that of Fig. 4. The constancy of F_A/F_R for different values of F_R is evident in Fig. 4 and the point is not elaborated further in Table I. It must be concluded that the saran data bear out the predicted dependence of F_A upon F_R, L_0 and D. The coefficient of friction of saran on glass is not sufficiently well known to provide a further test, but at least the values in Table I seem reasonable and decrease with increasing lubricant.

In the work with polystyrene, using the apparatus of Fig. 2, data were obtained in somewhat different form. Here it was convenient to use a number of different loadings and thus check in greater detail the predicted constancy of F_A/F_R as the loading increased and compaction proceeded. Quite high loads were possible, so that compaction down to as little as 60 percent of the original volume was achieved, yet F_A/F_R remained relatively constant, as shown in Table II. The effect of original length is shown in Fig. 5, where the average F_A/F_R from Table II is plotted logarithmically against L_0. Not only does a fair straight line result, but it may be seen that all three polystyrenes fall along the same line, which corresponds to a coefficient of friction of $\mu=0.262$. In Table III, we see experimental values for

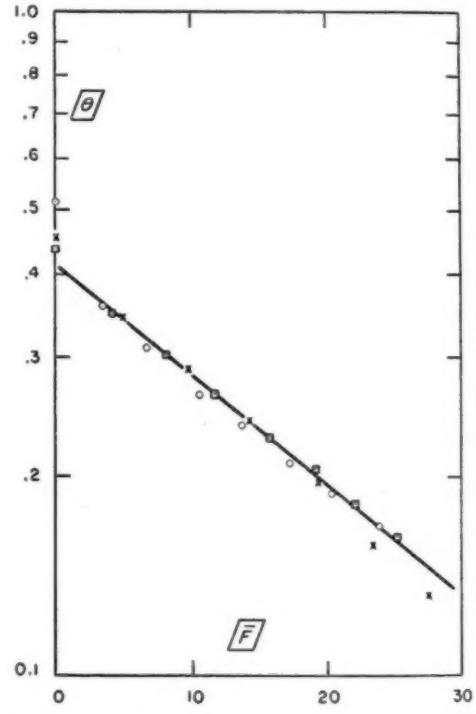

FIG. 6. Dependence of average porosity of polystyrene on average force. Circles represent 140 g of polymer No. 1, 90 g of No. 3, and squares, 140 g of No. 3.

the coefficient of friction of polystyrene on tool steel, as obtained by Roche.[1] Our value of 0.262 compares well with his value of 0.248 at 25°C, providing further evidence that the theoretical expression predicts observed behavior sufficiently well for practical applications.

It has been mentioned that it was necessary to clean the cylinder wall carefully in order to get reproducible results in the work with polystyrene. To see how great the effect of a lubricating film could be, one run was made with polystyrene No. 1 in which the wall was coated generously with Dow Corning No. 200 fluid. This reduced the coefficient of friction to 0.080. The effect of external lubrication on the polystyrene granules is similar. Different amounts of a lubricant in powder form were mixed thoroughly with polystyrene and the pressure transmission through a fixed size of sample determined. The results are shown in Table IV, where it is seen that increasing amount of lubricant reduces the coefficient of friction and thus reduces the ratio F_A/F_R.

Thus far little has been said about the compaction effect, except as incidental to the pressure-transmission problem. For some purposes a more quantitative formulation of the observed behavior may be desirable. The work of Athy[2] on the compaction of the earth's crust with depth suggests that a granular material may behave as if its free volume were characterized by a compressibility coefficient. That is, the porosity, θ, would follow the relationship $\theta=\theta_0 e^{-\beta P}$ where θ_0 is the initial porosity when the pressure, P, is zero, and β is a "compressibility coefficient." (Actually, we shall continue to talk about force, rather than pressure.) In our polystyrene experiments the force varies considerably over the length of the sample, and the porosity will vary accordingly. To correspond to the average porosity calculated from the length of the polymer plug we must calculate an appropriate average force, and this requires that we know the distribution of force along the plug. Assuming this to be of the form $F=F_R e^{kx}$ where k may be a function of L, L_0, etc., we find that the volume-average force is

$$\bar{F}=(F_A-F_R)/\ln(F_A/F_R).$$

Table V summarizes the results on compaction, and in Fig. 6 is plotted $\log\theta$ *vs.* $\bar{F}$. Except for an initial discrepancy, a straight line results which corresponds to a "compressibility coefficient" of $\beta=1.1\times10^{-4}$ in.²/lb. Using Athy's figures for compaction as a function of depth, and taking the mean density of the earth as 5.522 g/cc, we arrive at a value for the earth's crust of $\beta=1.25\times10^{-4}$ in.²/lb. One might surmise from this that the exact behavior in compaction of an aggregate of irregular particles is not very dependent on the nature of the particles.

TABLE V. Compaction of granular polystyrene under pressure.

Sample No.	Weight	$F_A\times10^{-3}$	$F_R\times10^{-3}$	$\bar{F}\times10^{-3}$	θ
1	140 g	0 lb.	0 lb.	0 lb.	0.511
		7.6	1.2	3.47	0.357
		14.7	2.3	6.69	0.309
		22.0	3.9	10.56	0.264
		29.5	4.9	13.70	0.235
		37.0	6.1	17.14	0.207
		44.0	7.2	20.3	0.186
		51.0	8.6	23.8	0.166
2	90	0	0	0	0.453
		7.6	3.0	4.96	0.345
		14.7	6.0	9.71	0.286
		22.0	8.4	14.13	0.240
		29.5	11.6	19.22	0.194
		37.0	13.6	23.4	0.155
		44.0	15.6	27.4	0.130
3	140	0	0	0	0.437
		7.6	1.8	4.03	0.350
		14.7	3.9	8.14	0.303
		22.0	5.3	11.74	0.265
		29.5	7.0	15.64	0.228
		37.0	8.2	19.10	0.203
		44.0	9.0	22.04	0.181
		51.0	10.0	25.15	0.161

SUMMARY

The problem considered was that of the relationship between the forces at the ends of a volume of granular polymer confined in a channel of constant cross section, when the granular mass is just on the point of motion. A solution of this problem was obtained on the basis of assumptions which were drawn, in part, from analogies with fluid behavior. Experiments were carried out with saran powders and granular polystyrenes which served to confirm the details of the theoretical expression within experimental error. The addition of lubricants to either the original polymer or the channel wall, was found to lower the coefficient of friction, as would be expected, and alter the forces correspondingly. As the forces at the ends were increased the length of the sample was observed to decrease. This compaction proceeds as if the average porosity of the sample were characterized by a compressibility coefficient, if an appropriate average force is taken. The magnitude of this coefficient for polystyrene is close to that observed in the compaction of the earth's crust, suggesting that it is the particulate nature of the material which is important, rather than the details of the individual particles.

[1] A. F. Roche, The Dow Chemical Company, Midland, Michigan (unpublished observations).

[2] L. F. Athy, Bull. Am. Assoc. Petroleum Geol. **14**, 1–24 (1930).

Regular Contributed Original Research

Application of the Membrane Analogy to the Solution of Heat-Conduction Problems

L. H. Wilson* and A. J. Miles
Mechanical Engineering Department, Missouri School of Mines, Rolla, Missouri
(Received August 25, 1948)

This paper establishes the feasibility of applying the membrane analogy to the solution of two-dimensional steady-state heat-conduction problems. The membrane analogy is established, and the construction and the use of the apparatus for measuring the film are described. Inexpensive apparatus and simplicity of execution are the predominating features of this type solution.

NOMENCLATURE

t—temperature
x—space coordinate
y—space coordinate
z—vertical deflection of membrane
q—uniform pressure against membrane
S—surface tension of the membrane.

INTRODUCTION

In the solution of heat-conduction problems, the essential consideration is a determination of the temperature field. When irregular geometric configurations are encountered this problem becomes quite difficult and analytical approaches are laborious and at times impossible. As a result of this difficulty, recourse is made, when possible, to graphical or experimental methods, or to methods of analogy. It is the purpose of this paper to call to the attention of the reader a method of determining temperature fields in homogeneous heat-conducting members which has been heretofore neglected.

Consider a homogeneous membrane such as a soap film of any shape supported at the edges, subjected to a uniform tension at the edge, and subjected to a uniform lateral pressure. It may be shown that the mathematical expression for the membrane is as follows:

$$q/S=(\partial^2 z/\partial x^2)+(\partial^2 z/\partial y^2), \qquad \text{(I)}$$

where q is the pressure per unit area of the membrane, S is the uniform tension per unit length of its boundary, and z is the vertical deflection of the membrane. If there is no pressure exerted on either side of the membrane ($q=0$), the equation becomes

$$(\partial^2 z/\partial x^2)+(\partial^2 z/\partial y^2)=0. \qquad \text{(II)}$$

It was pointed out by Prandtl in 1903 that the equation which represents the torsion of an elastic bar of any cross section is identical with Eq. (I) as given above. In 1917, Taylor and Griffith (3)† first used the membrane analogy for the solution of torsion problems. They found that the maximum error encountered under specified conditions was 2 percent. The method was applied to determine the torsional stiffness and strength of cylindrical bars (4), flexure of beams (5), and the torsion and flexure of hollow shafts (6).

Work of a similar nature to that of Taylor and Griffith was performed by Trayer and March (14) with essentially the same equipment and comparable results.

In 1947, Neubauer and Boston (11) applied the membrane analogy to determine the torsional stress analysis of twist-drill sections.

The membrane analogy was used by Miles and Stephenson (9) in 1937 for the solution of a quite different problem. They recognized that the differential equation representing the pressure distribution about an oil or gas well is identical with Laplace's equation. They were able to determine the pressure distribution in oil and gas reservoirs of irregular shape when the reservoir was drained by a number of wells.

It was pointed out by Christopherson and Southwell (1) that every plane-potential problem has a membrane analog and that Prandtl's analog is merely a particular example which was concerned only with Laplace's plane-harmonic equation.

Consider the general equation for steady-state heat conduction in two dimensions.

$$(\partial^2 t/\partial x^2)+(\partial^2 t/\partial y^2)=0. \qquad \text{(III)}$$

From the foregoing discussion it may be seen that the membrane analogy is also applicable to the solution of two-dimensional steady-state heat-conduction problems. By comparing Eq. (II) with Eq. (III) it may be seen that the equations are identical when the temperature, t, in Eq. (III) is replaced by the vertical deflection of the membrane, z, in Eq. (II). Thus it is feasible that the deflection of the membrane represents, to some scale, the temperature distribution throughout the member under consideration, and if the boundary conditions are known (which is generally the case), a model of the heat-conducting member may be constructed accordingly.

* Present address: School of Mechanical Engineering, Purdue University, West Lafayette, Indiana.
† Numbers in parentheses refer to bibliography at the end of the paper.

DISCUSSION OF EXPERIMENTAL PROCEDURE

The apparatus employed was patterned after that used by Miles and Stephenson (9) except that the component parts were cast from aluminum. This change was made in order to reduce contamination of the film caused by oxidation of the metal. The instrument is shown in Fig. 1. The principal parts consisted of an aluminum shell constructed in two sections between which a plate may be inserted; an aluminum model of the member under consideration; a glass plate with a micrometer head projecting through the center of the glass, the plate being large enough to permit the micrometer gauge to be moved to any position in the shell without uncovering any portion of it; and a hinged target (which could always be brought down into the same position relative to the film under investigation), to which was clamped a paper disk on which points on contour lines were plotted. The base of the apparatus was equipped with three leveling screws to facilitate leveling or tilting to any desired angle. The micrometer head was ground to a point on the lower end so that it could be used as a probe to establish contact with the film. The upper end of the micrometer head was fitted with another needle point along the same axis as the lower point in order to mark the position of the probe on the paper target.

The soap solution used was prepared by mixing 2 grams of sodium oleate and 30 cc of glycerin in one liter of distilled water. Care should be taken to keep the soap solution free from impurities as these shorten the life of the membrane.

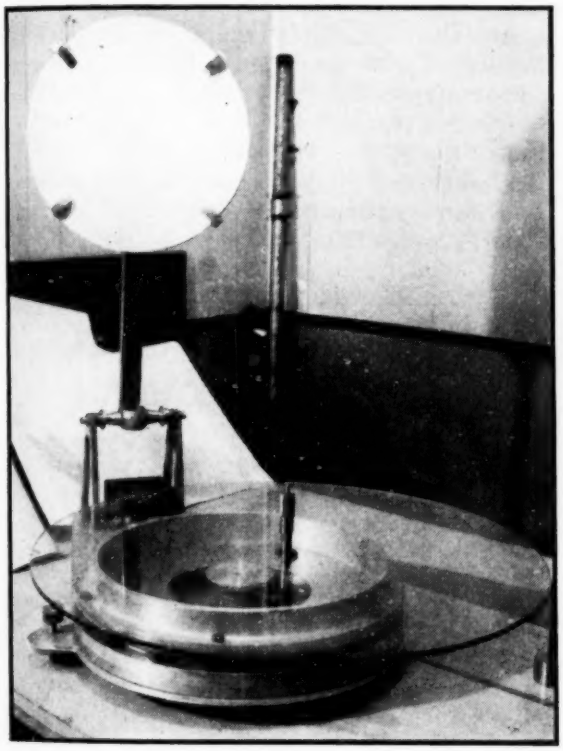

FIG. 1. Membrane apparatus with model of annulus-type heat-conducting member in place.

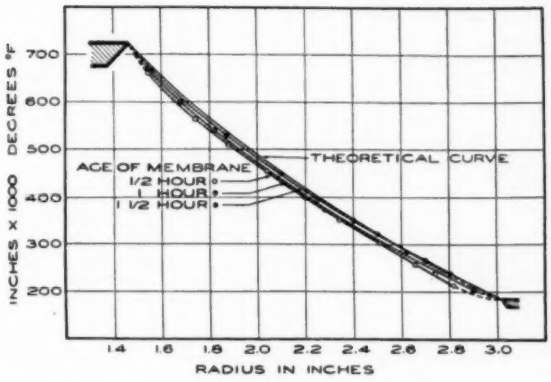

FIG. 2. Temperature distribution through thick-wall cylinder. $r_1 = 1.46$ in., $r_2 = 3.02$ in., $t_1 = 937°F$, $t_2 = 186°F$, slope of membrane = 48.2 percent, plate inclination 0.0°.

The models were constructed to some convenient scale geometrically similar to the heat-conducting member to be studied and in such a fashion that they provided a support for the membrane at the boundaries. These supporting edges were at different elevations such that they reproduced to some scale the temperature profile at the boundaries of the member under investigation. The membrane was then stretched across these boundaries, the elevation of the film at any particular point thereby representing the temperature at that point in the prototype of the member. Figure 1 shows a model of an annular-type heat-conducting member with isothermal boundaries, the inner boundary being at a higher temperature than the outer boundary. The model was made of aluminum to reduce oxidation, and the edges to which the membrane was to be attached were beveled in such a manner that the tangent to the membrane at its point of contact with the edge bisected the angle of bevel. This was necessary in order to reduce the possibility of the membrane's clinging to surfaces other than the beveled edge. When the model was set into the shell, the elevation of all edges representing isothermal conditions was checked with the micrometer head. If they were not level they were adjusted by using small jacks or weights to bring them into place.

With the model in place, a quantity of the soap solution was poured into the shell, care being taken to wet all surfaces of the model. With the aid of a Celluloid strip, a film was drawn over the model. All parts that come into contact with the soap solution were thoroughly cleaned and rinsed with distilled water beforehand. When the film had been drawn over the model, the glass plate was immediately placed over the equipment, since the carbon dioxide from the breath of persons present and also the dust in the air cause damage to the film. Arrangements were made during the manufacture of the model to provide ventilation holes. This was done in order that the pressure changes caused by temperature variation within the closed shell could

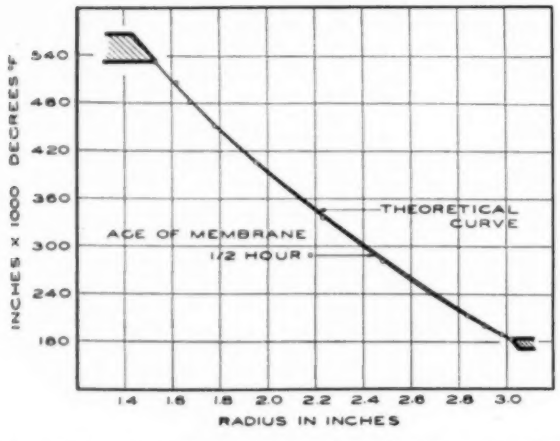

FIG. 3. Temperature distribution through thick-wall cylinder. $r_1=1.53$ in., $r_2=3.02$ in., $t_1=532.5°F$, $t_2=184°F$, slope of membrane = 23.3 percent, plate inclination for drainage 3°, measurements taken on high side.

be equalized on both sides of the membrane. Small bubbles and excess liquid were removed from the membrane by using a saturated pipe cleaner or a soda straw. The membrane should have all such bubbles removed so that the surface is perfectly smooth.

In order to establish contour lines (isotherms) the micrometer was set at some specific height and the glass plate moved around until the lower tip of the micrometer touched the membrane at the desired point. The points of contact were found very accurately by having a light placed in such a position that the reflection of the lower point of the micrometer could be seen in the soap film near the place where the probe was expected to come into contact with the film. A distortion of the image showed that contact had occurred. This position was quite definite, and could be measured within plus or minus 0.001 inch. When contact had been made, the paper disk, which was clamped to the metal target, was brought down and touched lightly to the micrometer head. Contour lines were drawn by connecting all points on the isotherm. Extreme care must be exercised in keeping the lower point of the probe moistened with clean soap solution so that the film will not be destroyed when measurements are made.

Best results will be obtained if the apparatus is housed within a vibration-free building in which the temperature is kept nearly constant.

In order to compare experimental results with theoretical values, a problem for which the solution is known was first investigated.

Consider a hollow, thick-walled cylinder of inside radius, r_1, and outside radius r_2, and an inside temperature of t_1 with a lower outside temperature of t_2. It may be shown that the expression for the temperature, t, at any point, r, in the cylinder is as follows:

$$t=(t_2-t_1)\frac{\ln(r/r_1)}{\ln(r_2/r_1)}+t_1. \qquad \text{(IV)}$$

A model was constructed with an inside radius (r_1) of 1.45 inches and an outside radius (r_2) of 3.01 inches (see Fig. 1). The elevation of the outside shell was fixed at an elevation such that the reading on the micrometer head was 0.185 inch. The temperature at this point was assumed to be 185°F. The inner shell (r_1) was constructed such that the elevation could be varied; that is, the temperature drop through the cylinder could vary. It should be remembered that the difference in elevation of the two plates may represent any temperature difference desired, but in this experiment various elevations of the inside plate were used in order to determine the most appropriate slope of the membrane. Figure 2 shows typical results obtained when observations were made of the elevation of the membrane along a radius of the cylinder at various stages in the life of the membrane. Figure 3 shows the results of this test when the apparatus was tilted about 3° so that the membrane could drain. The maximum deviation from theoretical computations was found to be 2 percent with an average of less than 1 percent.

As an example of the application of the method in solving typical problems, the next problem considered was that of determining the temperature distribution through a rectangular thick-walled cylinder. A model was constructed in the same manner as the one for the circular cylinder, except that in this case the outer boundary was in the form of a 6-inch square at an elevation of 0.179 inch. The temperature here was assumed to be 358°F. The inside plate was 3 inches square at an elevation of 0.521 inch, and the temperature was assumed to be 1042°F. Thus a change of 0.001 inch elevation of the membrane represented a change in the temperature of 2°F. Figure 4 shows a contour map of the isotherms obtained from measurements taken on opposite corners.

The last experiment performed was an investigation of a problem as outlined by McAdams (8). Consider an insulator 4 inches thick, bounded on one side by an

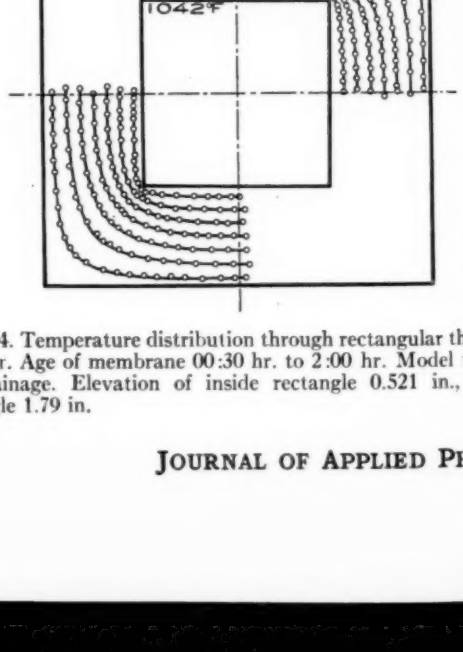

FIG. 4. Temperature distribution through rectangular thick-wall cylinder. Age of membrane 00:30 hr. to 2:00 hr. Model tilted 3° for drainage. Elevation of inside rectangle 0.521 in., outside rectangle 1.79 in.

isothermal metal plate at a temperature of 602°F, and on the lower side by another isothermal metal plate at 200°F. At intervals of 8 inches the lower part of the insulator is penetrated by metal ribs which extend 2 inches into the insulator. The ribs are also at 200°F, and there is no heat flow in the longitudinal direction of the insulator.

A model was constructed to the exact dimensions as those of the problem, except that the longitudinal dimension was made to be 4 inches since each 4-inch section would be symmetrical with the next section. On adiabatic sections of the boundary vertical plates were inserted and the membrane was allowed to seek its own level along the smooth surfaces of these plates. Figure 5 shows a plot of the isotherms obtained.

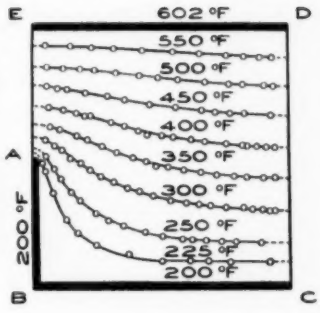

FIG. 5. Temperature distribution through an insulator. Insulator of thickness *CD* bounded by surface *ED* at a temperature of 602°F and by surface *BC* at a temperature of 200°F; at intervals of 2 *BC* the lower part of the insulator is penetrated by ribs *AB* also at a temperature of 200°F. Age of membrane 00:30 hr. to 2:00 hr. Model tilted 3° for drainage.

DISCUSSION OF RESULTS

From the results obtained in the investigation of the problem for which the analytical solution is known, it may be seen that under the proper conditions of test, the accuracy of the membrane analogy is well within the limits required in the solution of most heat-conduction problems. The age of the membrane produces an appreciable effect upon the results obtained, and it is recommended that the membrane be allowed to drain for at least one hour before any measurements are taken. If the measurements extend over a long period of time the membrane becomes fragile, but may be rejuvenated by placing a drop of soap solution on the probe and transferring the drop of solution to the membrane. We conclude from the results of the first tests that the optimum slope of the membrane is about 30 percent. When possible the whole apparatus should be tilted to an angle of about 3° in order that the section on which the measurements are being made may be drained of excess liquid.

In the solution of problems which require plotting of isotherms throughout the member, the greatest error to be encountered is the accuracy with which the model is constructed. Care should be taken to insure proper geometric similarity and a variation in elevation of the isothermal boundaries of less than 0.002 inch. It was found that towards the boundaries the values obtained in determining Q/k vary appreciably, but in the central region where greater accuracy is expected the values are in close agreement.

REMARKS

Although this type of solution is not suggested in competition with alternative methods, its utility lies in the solution of problems in which the geometric considerations produce tedious computations when numerical approaches are attempted. The equipment necessary for the execution of this type solution is quite simple and inexpensive as compared to the apparatus employed with electrical-geometrical analogues.

Further investigation of the membrane analogy is indicated in the realm of unsteady-state heat-conduction.

BIBLIOGRAPHY

(1) B. A. Christopherson and R. V. Southwell, "Relaxations methods applied to engineering problems 111. Problems involving two independent variables," Proc. Roy. Soc. **A168**, 31–350 (1938).

(2) H. W. Emmons, "The numerical solution of heat-conduction problems," Trans. A.S.M.E. **63**, No. 6, 607–615 (August, 1943).

(3) A. A. Griffith and G. I. Taylor, "The use of soap films in solving torsion problems," Adv. Com. Aeronautics, Tech. Report (British) No. 333, **3**, 920–937 (1917–1918).

(4) A. A. Griffith and G. I. Taylor, "The determination of the torsional stiffness and strength of cylindrical bars of any shape," Adv. Com. Aeronautics, Tech. Report (British) No. 334, **3**, 910–920 (1917–1918).

(5) A. A. Griffith and G. I. Taylor, "The application of soap films to the determination of the torsion and flexure of hollow shafts," Adv. Com. Aeronautics, Tech. Report (British) No. 392, **3**, 938–949 (1917–1918).

(6) A. A. Griffith and G. I. Taylor, "The problem of flexure and its solution by the soap-film method," Adv. Com. Aeronautics, Tech. Report (British) No. 399, **3**, 950–969 (1917–1918).

(7) C. F. Kayan, "An electrical geometrical analogue for complex heat flow," Trans. A.S.M.E. **67**, No. 8, 713–718 (November, 1945).

(8) W. H. McAdams, *Heat Transmission* (McGraw-Hill Book Company, Inc., New York, 1942), second edition, p. 1–25.

(9) A. J. Miles and E. A. Stephenson, "Pressure distribution in oil and gas reservoirs by membrane analogy," Trans. A.I.M.E. Tech. Pub., No. 919 (May, 1938).

(10) T. S. Nickerson and G. M. Dusinberre, "Heat transfer through thick insulation on cylindrical enclosures," Trans. A.S.M.E. Paper No. 47-A-63 (December, 1947).

(11) T. P. Neubauer and O. W. Boston, "Torsional stress analysis of twist-drill sections by membrane analogy," Trans. A.S.M.E. **69**, No. 8, 897–902 (November, 1947).

(12) V. Paschkis and H. D. Baker, "A method for determining unsteady-state heat transfer by means of an electrical analogy," Trans. A.S.M.E. **64**, No. 2, 105–112 (February, 1942).

(13) S. Timoshenko, *Theory of Elasticity* (McGraw-Hill Book Company, Inc., New York, 1934), pp. 239–242, 258–263.

(14) G. W. Trayer and H. W. March, "The torsion of members having sections common in aircraft construction," Nat. Ave. Comm. Aeronautics, Tech. Report No. 334, 675–705 (1930).

Work Functions of the Elements

HERBERT B. MICHAELSON
Product Development Laboratories, Sylvania Electric Products, Inc., Kew Gardens, New York
(Received September 6, 1949)

Like the chemical properties of the elements, the work function ϕ is a periodic function of atomic number, as shown clearly by a new compilation of published data for 57 elements. The progressive rise and fall of work function values throughout the table of the elements appears to be sufficiently regular to permit approximations to be made of values for the metallic and semimetallic elements on which no data has yet been published. Since the first ionization potential E_i and electrode potential E^0 exhibit a similar periodic function of atomic number, a striking resemblance exists among the respective plots of ϕ, E_i, and E^0.

I. INTRODUCTION

ALTHOUGH the published data on the work functions of metallic and semiconductor elements is by no means complete, the large number of measurements that have appeared in the literature indicate a well-defined periodicity of the values in the table of the elements. Several attempts have been made in recent years to establish relationships between work function and other periodic physical properties. Empirical equations of this type may provide a criterion for accurate values of work function, provided, of course, that they are derived from reliable data. Since, however, measurements of work function are extremely sensitive to the presence of surface impurities, particularly oxides and gases, there has been a rather large range of published values for each element. In addition, any comparison of published data is further complicated by the anisotropy[1,2] allotropy[3,4] and temperature dependence[5–8] of work function. Regardless of the difficulties in selecting a precise value of the work function for each element, the periodicity in the table of the elements can be shown clearly if *representative* values are cited for a large number of elements. Previously published lists of work functions have given data for less than half of the known elements,[9–16] while the present compilation provides values for 57 elements.

Most of the published methods of calculating work function ϕ have dealt with the relation to physical properties. The empirical formula of Rother and Bomke[17] expresses ϕ in terms of density, atomic weight, and electronic valence. According to Chittum[18] and Gombas,[19] ϕ is a function of the lattice energy in the crystal. Bartelink[20] derived an approximate relationship between work function and the reciprocal of atomic volume for the alkali metals. Another equation was developed by Wigner and Bardeen[21,22] for work functions of the univalent metals in terms of the heats of sublimation.

In addition, there have been a few attempts to correlate ϕ with other electrical measurements. Langmuir[23] observed for nine metals a general parallelism between thermionic work function and electrode potential E^0. This similarity was also noted by Scarpa[24] for 16 metals. More recently an interesting inverse relationship between hydrogen overpotential and ϕ was reported by Bockris.[25] In addition, Bedreag[26] has pointed out that for the alkali metals the first ionization potential E_i is equal to twice the work function. The purpose of this paper is to present a list of the work function data published during the past twenty-five years that have come to the writer's attention and to show graphically an apparent relationship between work function and other electrical data when plotted as a function of atomic number.

II. PERIODICITY OF WORK FUNCTION IN THE TABLE OF THE ELEMENTS

The relationship between work function and atomic number has been widely recognized in the literature.

[1] R. Smoluchowski, Phys. Rev. **60**, 661 (1941).
[2] S. T. Martin, Phys. Rev. **56**, 947 (1939).
[3] H. B. Wahlin, Phys. Rev. **61**, 509 (1942).
[4] A. Goetz, Phys. Rev. **33**, 373 (1929).
[5] S. Seely, Phys. Rev. **59**, 75 (1941).
[6] J. G. Potter, Phys. Rev. **58**, 622 (1940).
[7] A. H. Smith, Phys. Rev. **75**, 953 (1949).
[8] J. J. Markham and P. H. Miller, Jr., Phys. Rev. **75**, 959 (1949).
[9] S. Dushman, "Thermal emission of electrons," *International Critical Tables* (McGraw-Hill Book Company, Inc., New York, 1929), Vol. VI, pp. 53–4, data for 15 elements.
[10] S. Dushman, Rev. Mod. Phys. **2**, 381 (1930), data for 26 elements.
[11] A. L. Reimann, *Thermionic Emission* (John Wiley and Sons, Inc., New York, 1934), pp. 72–102, data for 32 elements.
[12] A. L. Hughes and L. A. DuBridge, *Photoelectric Phenomena* (McGraw-Hill Book Company, Inc., New York, 1932), pp. 65–6, data for 32 elements.
[13] O. Klein and E. Lange, Zeits. f. Elektrochemie **43**, 570 (1937), data for 43 elements.
[14] J. A. Becker, Rev. Mod. Phys. **7**, 123 (1935), data for 40 elements.
[15] Landolf-Boernstein, *Physikalisch-Chemische Tabellen* (1936), data for 37 elements.
[16] C. Herring and M. H. Nichols, Rev. Mod. Phys. **21**, 185 (1949), data for 23 elements (1935–1949).
[17] F. Rother and H. Bomke, Zeits. f. Physik **86**, 231 (1933).
[18] J. F. Chittum, J. Phys. Chem. **38**, 79 (1934).
[19] P. Gombas, Nature **157**, 668 (1946); Muegyetemi Koezlemenyek **1**, 25 (1947); Hung. Acta Phys. **1**, 1 (1947).
[20] E. H. B. Bartelink, Physica **3**, 193 (1936).
[21] E. Wigner and J. Bardeen, Phys. Rev. **48**, 84 (1935).
[22] J. Bardeen, Phys. Rev. **49**, 653 (1936).
[23] I. Langmuir, Trans. Amer. Electrochem. Soc. **29**, 125 (1916).
[24] O. Scarpa, Accad, Naz. d. Lincei, Rend. Cl. Sci. Fis. Nat., Atti **2**, 1062 (1941); Nuovo Cimento **17**, 54 (1940).
[25] J. O'M. Bockris, Nature **159**, 539 (1947); Trans. Faraday Soc. **43**, 417 (1947).
[26] C. G. Bedreag, Comptes Rendus **223**, 354 (1946).

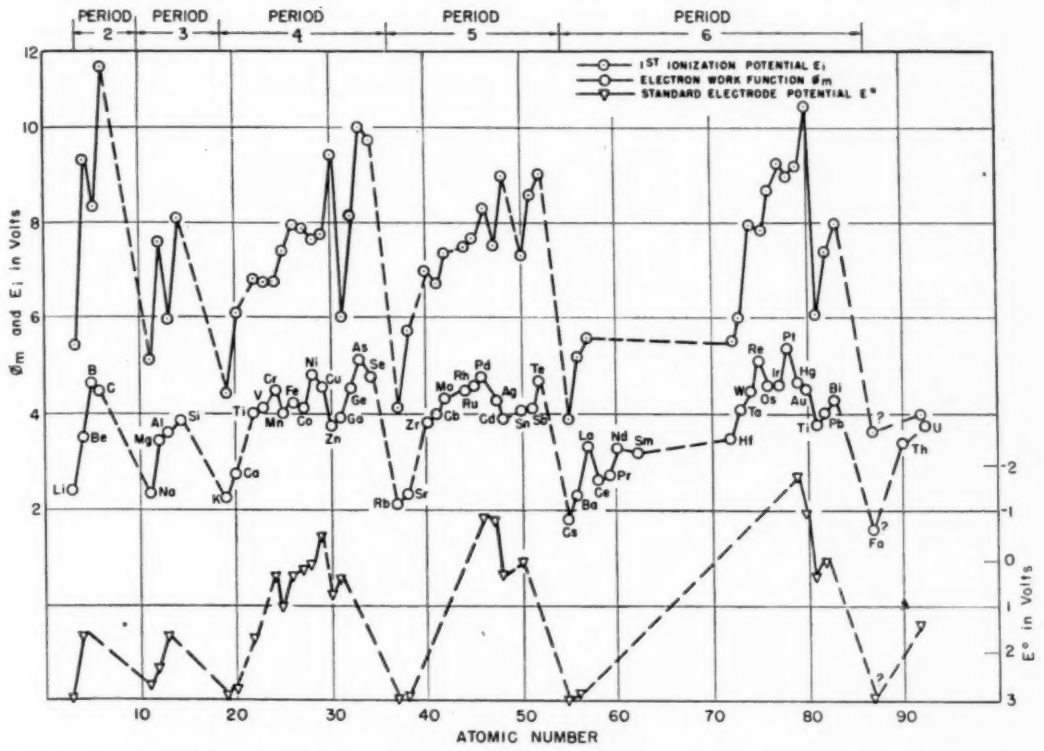

FIG. 1. Plots of work function, first ionization potential, and standard electrode potential *versus* atomic number.

Rother and Bomke,[17] Morecroft,[27] Klein and Lange,[28] and Scarpa[24] have all shown plots of ϕ as a function either of atomic number or atomic weight, the general shape of the curve being the same in either case. In Fig. 1 this previous work has been extended to include published data for a considerably larger number of elements. The data for work functions are taken from the appendix, which lists measurements published during the period 1924–1949. For most of the elements, values obtained by thermionic, photoelectric, or contact potential methods are about the same, and, to obtain *representative* values of work function, the unweighted mean ϕ_m of all data for each element was used for the plot in Fig. 1. For a few of the elements, some definite variance appears to exist among values obtained by different methods of measurement. Examples are the well-known discrepancies between photoelectric thresholds and thermionic work functions for the semiconductor elements.[29,30] These discrepancies, however, are not great enough to invalidate the representative values ϕ_m given here.

Since the temperature variation of ϕ for metals is quite small, the differences in temperature for the various measurements cited in the appendix are also of little consequence in considering the relationship between work function and atomic number. For example, the variation of ϕ with temperature for tungsten is only 3.4×10^{-5} ev/degree, according to Seely.[5]

The curve for ϕ_m in Fig. 1 exhibits a fairly regular rise and fall as it passes through each period in the table of the elements. When viewed from left to right on the periodic chart in Table I, the values in each period show a tendency to rise, except in the second-half of the periods 4, 5, and 6, where the elements in groups of I*B*, II*B*, and III*B* have progressively lower work functions. The peculiar regularities in the various groups and periods are similar to the behavior of chemical and physical properties. A striking resemblance among the curves for ϕ, E_i, and E^0 is in evidence in Fig. 1, where the ionization potentials are from Hubbard and Meggers[31] and the electrode potentials* from Latimer and Hildebrand.[32]

The periodicity of work function in Fig. 1 and Table I appear to be sufficient to provide a basis for the prediction of values for elements on which no data has yet

[27] J. H. Morecroft, *Electron Tubes and Their Applications* (John Wiley and Sons, Inc., New York, 1936), p. 39.
[28] O. Klein and E. Lange, Zeits. f. Elektrochemie **44**, 542 (1938).
[29] Apker, Taft, and Dickey, Phys. Rev. **74**, 1462 (1948).
[30] E. U. Condon, Phys. Rev. **54**, 1089 (1938).

[31] H. D. Hubbard and W. F. Meggers, *Key to Periodic Chart of the Atoms* (W. M. Welch Scientific Company, Chicago, 1947), pp. 22–5.

* The values of E^0 cited in this paper are those of the couple between the zero oxidation state and the next highest known state. For example, the couple for iron is

$$Fe \rightarrow Fe^{++} 2e^-, \quad E^0 = +0.440 \text{ volt.}$$

The scale for E^0 values is based on zero volts for the hydrogen gas—hydrogen ion couple.

[32] W. M. Latimer and J. H. Hildebrand, *Reference Book of Inorganic Chemistry* (The Macmillan Company, New York, 1947), pp. 474–6.

TABLE I. Periodic chart of work functions, mean of published data, 1924–1949.

Group	I A	I B	II A	II B	III A	III B	IV A	IV B	V A	V B	VI A	VI B	VII A	VII B	VIII		
Period 2	Li 2.39			Be 3.37		B 4.5		C 4.39									
3	Na 2.27			Mg 3.46		Al 3.74		Si 4.1		P —		S —					
4	K 2.15		Ca 2.76		Sc —		Ti 4.09		V 4.11		Cr 4.51		Mn 3.95		Fe 4.36	Co 4.18	Ni 4.84
		Cu 4.47		Zn 3.74		Ga 3.96		Ge 4.56		As 5.11		Se 4.72					
5	Rb 2.13		Sr 2.35		Y —		Zr 3.84		Cb 3.99		Mo 4.27		Tc —		Ru 4.52	Rh 4.65	Pd 4.82
		Ag 4.28		Cd 3.92		In —		Sn 4.11		Sb 4.08		Te 4.73					
6	Cs 1.89		Ba 2.29		La 3.3		Hf 3.53		Ta 4.12		W 4.50		Re 5.1		Os 4.55	Ir 4.57	Pt 5.29
		Au 4.58		Hg 4.52		Tl 3.76		Pb 4.02		Bi 4.28		Po —					
7	Fa —		Ra —		Ac —		Th 3.41		Pa —		U 3.74						
Rare earths	Ce 2.7	Pr 2.7	Nd 3.3	Sm 3.2													

appeared in the literature:

Element	Atomic number	ϕ (hypothetical)
Sc	21	3.3 ev
Y	39	3.3
Tc	43	4.4
In	49	4.0
Po	84	4.6
Fa	87	1.5
Pa	91	3.3

If these seven elements follow the periodic electrical properties exhibited by the 57 elements in Fig. 1, the predicted work functions should be correct within a few tenths of a volt.

The writer wishes to express his appreciation to Dr. Harold Jacobs,† George Hees and Henry W. Parker, of the Central Engineering Laboratories, for many enlightening discussions.

APPENDIX.‡ ELECTRON WORK FUNCTIONS OF THE ELEMENTS

(Published Data, 1924-1949)

Element	Mean value ϕ_m	Thermionic work function	Photoelectric work function	Work function by contact potential method	Reference
Ag	4.28	3.09			(1)
		3.56			(2)
		4.08			(3)
			3.67		(4)
			4.1 to 4.75		(5)
			4.56 (600°)		(6)
			4.73 (20°)		(6)
			4.75 (111) face		(7)
			4.81 (100) face		(7)
				4.33	(8)
				4.44	(9)
				4.79 (100) face	(10)
Al	3.74		2.98		(4)
			3.43		(11)
			4.08		(12)
			4.20		(13)
			4.36		(14)
				3.38	(9)
As	5.11		5.11		(15)
Au	4.58	4.0 to 4.58			(2)
		4.32			(3)
			4.73 (740°C)		(16)
			4.82 (20°C)		(16)
			4.86 to 4.92		(5)
				4.46	(9)
B	4.5		4.4 to 4.6*		(17)
Ba	2.29	2.11			(18)
				1.73	(9)
				2.39	(19)
			2.48		(20)
			2.49		(20)
			2.52		(22)
Be	3.37		3.17		(15)
			3.30		(23)
			3.92		(24)
				3.10	(9)
Bi	4.28		4.14		(11)
			4.22 to 4.25		(25)
			4.31		(26)
			4.44		(23)
			4.46		(27)
				4.17	(9)

† Now at Evans Signal Laboratory, Thermionics Branch, Belmar, New Jersey.
‡ Values indicated by an asterisk (*) were not new determinations, but were obtained as a check on experimental conditions.

APPENDIX—*Continued*

Element	Mean value ϕ_m	Thermionic work function	Photoelectric work function	Work function by contact potential method	Reference[a]
C	4.39	4.00			(28)
		4.34			(29)
		4.39			(30)
			4.81		(31)
Ca	2.76	2.24			(32)
			2.42		(15)
			2.706		(22)
			2.76		(33)
			3.20		(34)
			3.21		(35)
Cb	3.99	3.96			(36)
		4.01			(37)
Cd	3.92		3.68		(15)
			3.73		(4)
			3.94		(11)
			4.07		(38)
			4.099		(13)
				4.00	(9)
Ce	2.7	2.6			(39)
				2.84	(34)
Co	4.18	4.40			(40)
			3.90		(33)
			4.12 to 4.25		(41)
				4.21	(9)
Cr	4.51	4.60			(42)
		4.7			(43)
			4.37		(26)
				4.38	(9)
Cs	1.89	1.81			(44)
			1.9		(45)
			1.96		(46)
Cu	4.47	3.85			(1)
		4.26			(2)
		4.38			(3)
		4.55[b]			(47)
			4.07		(4)
			4.18		(33)
			4.86 (111) face		(48)
			5.61 (100) face		(48)
				4.46	(9) (49)
Fe	4.36	4.04			(50)
		γ4.23			(40)
		β4.48			(40)
		4.77			(51)
			3.91		(33)
			3.92		(55)
			4.72		(52)
			4.77		(53)
				4.40	(9)
Ga	3.96		4.12		(15)
				3.80	(9)
Ge	4.56		4.29		(33)
			4.5*		(54)
			4.73		(15)
			4.80		(18)
				4.50	(9)
Hf	3.53	3.53			(56)
Hg	4.52		4.50		(57)
			4.52		(58)
			4.53		(59) (60)
Ir	4.57			4.57	(9)
K	2.15		2.0		(61)
			2.12		(23)
			2.24		(45, 46)
			2.26		(62)
La	3.3	3.3			(39)
Li	2.39		2.28		(45)
			2.42		(15)
				2.49	(63)
Mg	3.46		2.74		(15)
			<3.0		(64)
			3.59		(65)
			3.62		(66)
			3.68		(24)
			3.79		(67)
				3.58	(9)
				3.78	(68)

Element	Mean value ϕ_m	Thermionic work function	Photoelectric work function	Work function by contact potential method	Reference[a]
Mn	3.95		3.76		(15)
				4.14	(9)
Mo	4.27	4.15			(69)
		4.17			(70)
		4.19			(71)
		4.20			(72)
		4.32			(73)
		4.33			(74)
		4.38			(75)
		4.44			(76)
			4.15		(69)
			4.34		(26)
				4.08	(77)
				4.48	(9)
Na	2.27		2.06		(15)
			2.25		(78)
			2.28		(20)
			2.29		(24)
			2.47		(45)
				2.26	(79)
Nd	3.3	3.3			(39)
Ni	4.84	4.61			(40)
		4.63			(50)
		5.03			(80)
		5.1[b]			(47)
		5.24			(116)
			4.06		(32)
			4.87		(26)
			5.01		(53)
			5.05 (625°K)		(116)
			5.20 (1180°K)		(116)
				4.32	(9)
				4.96 (300°K)	(81)
Os	4.55			4.55	(9)
Pb	4.02		3.97		(4)
			4.14		(11)
				3.94	(9)
Pd	4.82	4.99			(82)
			4.97		(82)
				4.49	(9)
Pr	2.7	2.7			(39)
Pt	5.29	5.08			(28)
		5.29			(83)
		5.32			(84)
		6.27			(85)
			4.09		(4)
			6.35		(86)
				4.52	(9)
				5.36	(87)
Rb	2.13		2.09		(46)
			2.16		(45)
Re	5.1	5.1			(88)
			~5.0		(89)
Rh	4.65	4.58			(90)
		4.80			(91)
			4.57		(90)
Ru	4.52			4.52	(9)
Sb	4.08		4.01		(92)
				4.14	(9)
Se	4.72		4.62		(11)
			5.11		(15)
				4.42	(9)
Si	4.1	3.59			(30)
				4.2*	(93)
				4.5 (250°C)*	(54)
Sm	3.2	3.2			(39)
Sn	4.11		3.62		(4)
			3.87		(11)
			(liq.) 4.21		(94)
			γ4.38		(94)
			β4.50		(94)
				4.09	(9)
Sr	2.35		2.06		(95)
			2.24		(15)
			2.74		(68)

APPENDIX—*Continued*

Element	Mean value ϕ_m	Thermionic work function	Photoelectric work function	Work function by contact potential method	Reference[a]
Ta	4.12	4.07			(76)
		4.10			(96)
		4.19			(97)
			4.12		(34)
			4.16		(98)
				3.96	(9)
				4.25	(99)
Te	4.73		4.76*		(17)
				4.70	(9)
Th	3.41	3.35			(75)
			3.38		(34)
			3.47		(100)
			3.57		(11)
				3.46	(9)
Ti	4.09		3.95		(15)
			4.17		(100)
				4.14	(9)
Tl	3.76			3.84	(9)
		3.68			(101)
U	3.74	3.27			(102)
			3.63		(34)
				4.32	(9)
V	4.11		3.77		(15)
				4.44	(9)
W	4.50	4.25			(103)
		4.39 (111) face			(115)
		4.39 (116) face			(115)
		4.45			(117)
		4.46			(104)
		4.52			(28, 105)
		4.53			(106)
		4.56 (001) face			(115)
		4.58			(73, 75)
		4.68 (110) face			(115)
		4.69 (112) face			(115)
			4.35 (310) face		(107)
			4.50 (211) face		(107)
			4.54		(108)
			4.60		(34)
				4.38	(9)
Zn	3.74		3.08		(4)
			3.28		(109)
			3.32 and 3.57		(110)
			3.60		(11)
			3.89		(33)
			4.24		(111)
			4.26 (0001) face		(112)
			4.307		(13)
				3.40	(113)
				3.66	(9)
				4.28	(114)
Zr	3.84	4.12			(56)
			3.73		(34)
			3.91		(102)
				3.60	(9)

[a] Reference numbers:

(1) A. Wehnelt and S. Seliger, Zeits. f. Physik **38**, 443 (1926).
(2) I. Ameiser, Zeits. f. Physik **69**, 111 (1931).
(3) A. Goetz, Zeits. f. Physik **43**, 531 (1927).
(4) P. Lukirsky and S. Prilesaev, Zeits. f. Physik **49**, 236 (1928).
(5) R. H. Fowler, Phys. Rev. **38**, 45 (1931).
(6) R. P. Winch, Phys. Rev. **37**, 1269 (1931).
(7) H. E. Farnsworth and R. P. Winch, Phys. Rev. **58**, 812 (1940).
(8) P. A. Anderson, Phys. Rev. **49**, 320 (1936).
(9) O. Klein and E. Lange, Zeits. f. Elektrochemie **44**, 542 (1938).
(10) P. A. Anderson, Phys. Rev. **59**, 1034 (1941).
(11) R. Hamer, Jour. Opt. Soc. Amer. **9**, 251 (1924).
(12) J. Brady and P. Jakobsmeyer, Phys. Rev. **49**, 670 (1936).
(13) R. Suhrmann and J. Pietrzyk, Zeits. f. Physik **122**, 600 (1944).
(14) E. Gaviola and J. Strong, Phys. Rev. **49**, 441 (1936).
(15) R. Schulze, Zeits. f. Physik **92**, 212 (1934).
(16) L. W. Morris, Phys. Rev. **37**, 1263 (1931).
(17) L. Apker, E. Taft, and J. Dickey, Phys. Rev. **74**, 1462 (1948).
(18) A. L. Reimann, *Thermionic Emission* (Chapman and Hall, London, 1934), p. 37.
(19) P. A. Anderson, Phys. Rev. **47**, 958 (1935).
(20) R. J. Maurer, Phys. Rev. **57**, 653 (1940).
(21) R. J. Cashman and E. Bassoe, Phys. Rev. **55**, 63 (1939).
(22) N. C. Jamison and R. J. Cashman, Phys. Rev. **50**, 624 (1936).
(23) R. Suhrmann and A. Schallamach, Zeits. f. Physik **91**, 775 (1934).
(24) M. M. Mann, Jr. and L. A. DuBridge, Phys. Rev. **51**, 120 (1937).
(25) H. Jupnik, Phys. Rev. **60**, 884 (1941).
(26) H. C. Rentschler and D. E. Henry, J. Opt. Soc. Am. **26**, 30 (1936).
(27) A. H. Weber and C. J. Eisele, Phys. Rev. **59**, 473(A) (1941).
(28) S. Dushman, "Thermal emission of electrons," *International Critical Tables* (McGraw-Hill Book Company, Inc., New York, 1929), Vol. VI, pp. 53–4.
(29) A. L. Reimann, Proc. Phys. Soc. **50**, 496 (1938).
(30) A. Braun and G. Busch, Helv. Phys. Acta **20**, No. 1, 33 (1947).
(31) S. C. Roy, Proc. Roy. Soc. **A112**, 599 (1926).
(32) S. Dushman, Phys. Rev. **21**, 623 (1923).
(33) G. B. Welch, Phys. Rev. **32**, 657 (1928).
(34) Rentschler, Henry, and Smith, Rev. Sci. Inst. **3**, 794 (1932).
(35) I. Liben, Phys. Rev. **51**, 642 (1937).
(36) H. B. Wahlin and L. I. Sordahl, Phys. Rev. **45**, 886 (1934).
(37) A. L. Reimann and C. Kerr Grant, Phil. Mag. **22**, 34 (1936).
(38) H. Bomke, Ann. d. Physik **10**, 579 (1931).
(39) E. E. Schumaker and J. E. Harris, J. Am. Chem. Soc. **48**, 3108 (1926).
(40) H. B. Wahlin, Phys. Rev. **61**, 509 (1942).
(41) A. B. Cardwell, Phys. Rev. **38**, 2033 (1931).
(42) H. B. Wahlin, Phys. Rev. **73**, 1458 (1948).
(43) H. Koesters, Zeits. f. Physik **66**, 807 (1930).
(44) K. H. Kingdon, Phys. Rev. **25**, 892 (1925).
(45) A. R. Olpin, quoted by Hughes and DuBridge, *Photoelectric Phenomena* (1932).
(46) J. J. Brady, Phys. Rev. **41**, 613 (1932).
(47) W. P. Dyke, Thesis, University of Washington (1946).
(48) N. Underwood, Phys. Rev. **47**, 502 (1935).
(49) P. A. Anderson, Phys. Rev. **76**, 388 (1949).
(50) W. Distler and G. Monch, Zeits. f. Physik **84**, 271 (1933).
(51) G. Siljeholm, Ann. d. Physik **10**, 178 (1931).
(52) A. B. Cardwell, Proc. Nat. Acad. Sci. **14**, 439 (1928).
(53) G. N. Glasoe, Phys. Rev. **38**, 1490 (1931).
(54) A. H. Smith, Phys. Rev. **75**, 953 (1949).
(55) G. B. Welch, Phys. Rev. **31**, 709(A) (1928).
(56) C. Zwikker, Physik. Zeits. **30**, 578 (1929).
(57) H. Cassel and A. Schneider, Naturwiss **22**, 464 (1934).
(58) Roller, Jordan, and Woodward, Phys. Rev. **38**, 396 (1931).
(59) C. B. Kazda, Phys. Rev. **26**, 643 (1925).
(60) W. B. Hales, Phys. Rev. **32**, 950 (1928).
(61) H. E. Ives, J. Opt. Soc. Am. **8**, 551 (1924).
(62) H. Mayer, Ann. d. Physik **29**, 129 (1937).
(63) P. A. Anderson, Phys. Rev. **75**, 1205 (1949).
(64) C. Kenty, Phys. Rev. **43**, 776(A) (1933).
(65) J. Cashman and S. Huxford, Phys. Rev. **48**, 734 (1935).
(66) R. J. Cashman and E. Bassoe, Phys. Rev. **53**, 919(A) (1938).
(67) R. J. Cashman, Phys. Rev. **54**, 971 (1938).
(68) P. A. Anderson, Phys. Rev. **54**, 753 (1938).
(69) L. A. DuBridge and W. W. Roehr, Phys. Rev. **42**, 52 (1932).
(70) H. B. Wahlin and J. A. Reynolds, Phys. Rev. **48**, 751 (1935).
(71) H. Grover, Phys. Rev. **52**, 982 (1937).
(72) R. W. Wright, Phys. Rev. **60**, 465 (1941).
(73) A. J. Ahearn, Phys. Rev. **44**, 277 (1933).
(74) E. Freitag and F. Kruger, Ann. d. Physik **21**, 697 (1934).
(75) C. Zwikker, Proc. Roy. Acad. Amsterdam **29**, 792 (1926).
(76) Dushman, Rowe, Ewald, and Kidner, Phys. Rev. **25**, 338 (1925).
(77) C. W. Oatley, Proc. Roy. Soc. **A155**, 218 (1936).
(78) Z. Berkes, Math. Phys. Lapok **41**, 131 (1934).
(79) E. Patai, Zeits. f. Physik **59**, 697 (1930).
(80) G. W. Fox and R. M. Bowie, Phys. Rev. **44**, 345 (1933).
(81) R. C. L. Bosworth, Trans. Faraday Soc. **35**, 397 (1939).
(82) L. A. DuBridge and W. W. Roehr, Phys. Rev. **39**, 99 (1932).
(83) H. L. Van Velzer, Phys. Rev. **44**, 831 (1933).
(84) L. V. Whitney, Phys. Rev. **50**, 1154 (1936).
(85) L. A. DuBridge, Phys. Rev. **32**, 961 (1928).
(86) L. A. DuBridge, Phys. Rev. **31**, 236 (1928).
(87) C. W. Oatley, Proc. Phys. Soc. **51**, 318 (1939).
(88) Agte, Alterthum, Becker, Heyne, and Moers, Naturwiss. **19**, 108 (1931).
(89) A. Eagelmann, Ann. d. Physik **17**, 185 (1933).
(90) E. H. Dixon, Phys. Rev. **37**, 60 (1931).
(91) H. B. Wahlin and L. V. Whitney, J. Chem. Phys. **6**, 594 (1938).
(92) V. Middel, Zeits. f. Physik **105**, 358 (1937).
(93) W. B. Meyerhof, Phys. Rev. **71**, 727 (1947).
(94) A. Goetz, Phys. Rev. **33**, 373 (1929).
(95) R. Doepel, Zeits. f. Physik **33**, 237 (1925).
(96) A. B. Cardwell, Phys. Rev. **47**, 628 (1935).
(97) M. D. Fiske, Phys. Rev. **61**, 513 (1942).
(98) A. B. Cardwell, Phys. Rev. **38**, 2041 (1931).
(99) W. Heinze, Zeits. f. Physik **109**, 459 (1938).
(100) H. C. Rentschler and D. E. Henry, Trans. Electrochem. Soc. **87**, 289 (1945–6).
(101) R. Suhrmann and H. Csesch, Zeits. Chem. **B28**, 215 (1935).
(102) W. L. Hole and R. W. Wright, Phys. Rev. **56**, 785 (1939).
(103) A. H. Warner, Proc. Nat. Acad. Sci. **13**, 56 (1927).
(104) G. M. Fleming and J. E. Henderson, Phys. Rev. **58**, 887 (1940).
(105) W. B. Nottingham, Phys. Rev. **47**, 806(A) (1935).
(106) H. Freitag and F. Krueger, Ann. d. Physik **21**, 697 (1934).
(107) C. E. Mendenhall and C. F. DeVoe, Phys. Rev. **51**, 346 (1937).
(108) A. H. Warner, Phys. Rev. **38**, 1871 (1931).
(109) A. Nitsche, Ann. d. Physik **14**, 463 (1932).
(110) J. H. Dillon, Phys. Rev. **38**, 408 (1931).
(111) C. F. DeVoe, Phys. Rev. **50**, 481 (1936).
(112) W. Klug and H. Steyskal, Zeits. f. Physik **116**, 415 (1940).
(113) C. W. Oatley, Proc. Roy. Soc. **A155**, 218 (1936).
(114) P. A. Anderson, Phys. Rev. **57**, 122 (1940).
(115) C. Herring and M. H. Nichols, Rev. Mod. Phys. **21**, 185 (1949).
(116) A. B. Cardwell, Phys. Rev. **76**, 125 (1949).
(117) M. H. Nichols, Phys. Rev. **59**, 944(A) (1941).

[b] By field current method.

Compilation of Body Wave Velocity Data for Cubic and Hexagonal Metals

LOUIS GOLD
Brown University, Providence, Rhode Island
(Received October 14, 1949)

The directional variation of body wave velocities has been computed for cubic and hexagonal metals where stiffness coefficients are known; the essential data is presented in the form of tables and graphs. The results for aluminum, copper, gold, iron(α), lead and silver are tabulated in terms of the directional indices, and a stereographic coordinate system has been devised for presenting these data in the form of iso-velocity contours for the three wave vectors. The compressional and shear velocities for cadmium, magnesium, and zinc are plotted as a function of the angle formed by the direction of wave propagation and the hexagonal (c) axis from which have been derived the theoretical average velocities which may be compared with measured values for polycrystalline specimens.

1. INTRODUCTION

THE present report makes available for the first time a systematic summary of the velocity of body waves in a number of cubic and hexagonal metals for which the stiffness coefficients have been determined. Recent interest in ultrasonic wave propagation in solids,[1] particularly the question of the scattering of sound waves in polycrystalline metals,[2] has served to stimulate an orderly evaluation and presentation of such velocity data as are offered here. It is not unlikely that the tables and graphs will find application in delay-line design work, quantitative treatment of sound attenuation in polycrystalline aggregates, etc.

Two distinct graphical schemes were devised: a stereographic coordinate system is employed for the cubic metals, whereas a simple plot of velocity *versus* the angle defined by the hexagonal axis and the direction of wave propagation suffices for the hexagonal metals. The crystal symmetry of the hexagonal-close packed metals is such as to effect considerable reduction in the involved relation so that calculation of an average velocity is feasible; this is not true for the cubic metals.

Only those aspects of crystal elasticity theory directly pertinent to the details of the calculations are given. Adequate accounts are available for those who desire further elaboration.[3]

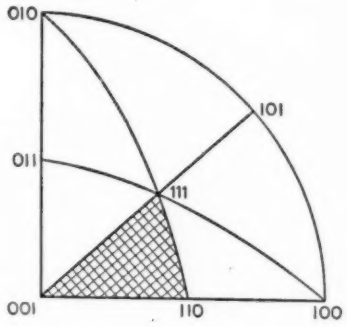

FIG. 1. Quadrant of standard projection for cubic crystal showing the six equivalent triangles of the type indicated by shaded area.

2. TREATMENT OF CUBIC METALS

The three roots of the equation

$$C_n^3 - I_1 C_n^2 + I_2 C_n - I_3 = 0 \tag{1}$$

are related to the wave velocities by the familiar expression $v=(C_n/\rho)^{\frac{1}{2}}$. The coefficients I_1, I_2, and I_3 for crystals of any type of symmetry are defined below

$$\begin{aligned} I_1 &= k_{11}+k_{22}+k_{33} \\ I_2 &= k_{11}k_{22}+k_{22}k_{33}+k_{11}k_{33}-(k_{12}^2+k_{23}^2+k_{13}^2) \\ I_3 &= k_{11}k_{22}k_{33}+2k_{12}k_{13}k_{23}-(k_{12}^2k_{33}+k_{13}^2k_{22}+k_{23}^2k_{11}). \end{aligned} \tag{2}$$

For crystals of cubic symmetry the k's are of the following nature . . .

$$\begin{aligned} k_{11} &= c_{11}\alpha^2+c_{44}(\beta^2+\gamma^2) \\ k_{22} &= c_{11}\beta^2+c_{44}(\alpha^2+\gamma^2) \\ k_{33} &= c_{11}\gamma^2+c_{44}(\alpha^2+\beta^2) \\ k_{12} &= (c_{44}+c_{12})\alpha\beta \\ k_{13} &= (c_{44}+c_{12})\alpha\gamma \\ k_{23} &= (c_{44}+c_{12})\beta\gamma, \end{aligned} \tag{3}$$

where α, β, and γ are direction cosines.

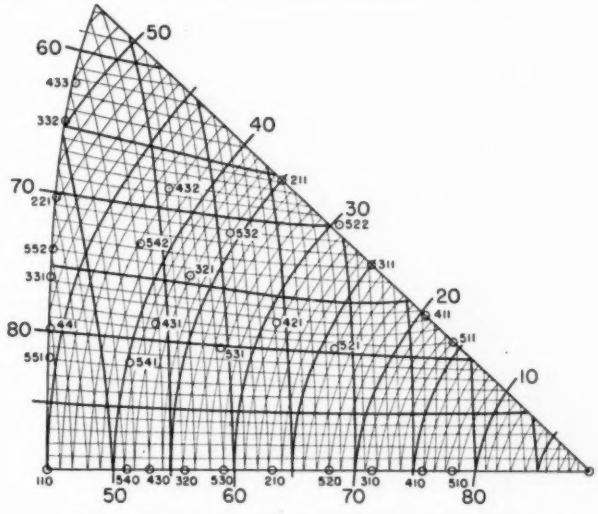

FIG. 2. Stereographic triangle coordinate system.

[1] S. Sokolov, "Absorption of Ultrasonics by Solid Bodies," Akad. Nauk. SSSR Doklady N.S. **59**, 883 (1948); D. Arenberg, "Supersonic Solid Delay Lines," M.I.T. Rad. Lab. Report 932, April 1946.

[2] W. P. Mason and H. J. McSkimin, J. Acous. Soc. Am. **19**, 464 (1947). By the same authors, J. App. Phys. **19**, 940 (1948). W. Roth, J. App. Phys. **19**, 901 (1948).

[3] I. Koga, "Thickness vibrations of piezoelectric oscillating crystals," Physics **3**, 70 (1932).

TABLE I. Cubic metals.*

(Goens) $C_{11}=10.8_2$ $C_{12}=6.2_3$ $C_{44}=2.8_4$

$\times 10^{11}$ dynes/cm²

Aluminum (a)

hkl	C_t $\times 10^{11}$	C_{t_1} $\times 10^{11}$	C_{t_2} $\times 10^{11}$	V_t $\times 10^5$	V_{t_1} $\times 10^5$	V_{t_2} $\times 10^5$
100	10.82	2.84	2.84	6.33	3.24	3.24
110	11.36	2.30	2.30	6.49	2.92	2.92
111	11.54	2.48	2.48	6.54	3.03	3.03
210	11.17	2.49	2.49	6.43	3.03	3.03
211	11.37	2.66	2.47	6.49	3.14	3.03
221	11.46	2.68	2.36	6.52	3.15	2.96
310	11.02	2.64	2.64	6.39	3.13	3.13
311	11.17	2.74	2.59	6.43	3.19	3.10
320	11.28	2.38	2.38	6.46	2.97	2.97
321	11.37	2.73	2.40	6.49	3.18	2.98
331	11.41	2.76	2.33	6.50	3.20	2.94
332	11.50	2.60	2.40	6.53	3.10	2.98
410	10.95	2.71	2.71	6.37	3.17	3.17
411	11.05	2.78	2.67	6.40	3.21	3.14
421	11.24	2.77	2.49	6.45	3.20	3.04
430	11.32	2.34	2.34	6.48	2.94	2.94
431	11.36	2.78	2.36	6.49	3.21	2.95
510	10.90	2.76	2.76	6.36	3.19	3.19
511	10.98	2.80	2.72	6.38	3.22	3.17
520	11.09	2.57	2.57	6.41	3.09	3.09
521	11.14	2.79	2.57	6.42	3.21	3.09
530	11.25	2.41	2.41	6.45	2.99	2.99
540	11.34	2.32	2.32	6.48	2.93	2.93

$C_{11}=17.0$ $C_{12}=12.3$ $C_{44}=7.52$

$\times 10^{11}$ dynes/cm²

Copper (b)

100	17.00	7.52	7.52	4.36	2.90	2.90
110	22.17	2.35	2.35	4.98	1.62	1.62
111	23.89	4.07	4.07	5.17	2.13	2.13
210	20.68	3.84	3.84	4.81	2.07	2.07
211	22.49	5.80	3.75	5.02	2.55	2.05
221	23.20	5.92	2.92	5.09	2.57	1.81
310	19.31	5.21	5.21	4.65	2.41	2.41
311	20.79	6.58	4.67	4.82	2.71	2.29
320	21.59	2.93	2.93	4.91	1.81	1.81
321	22.40	6.45	3.19	5.01	2.69	1.89
331	22.73	6.69	2.62	5.04	2.74	1.71
332	23.58	5.17	3.29	5.14	2.40	1.92
410	18.52	6.00	6.00	4.55	2.59	2.59
411	19.64	6.95	5.45	4.69	2.79	2.47
421	21.36	6.80	3.88	4.89	2.76	2.08
430	21.87	2.65	2.65	4.95	1.72	1.72
431	22.32	6.90	2.82	5.00	2.78	1.78
510	18.06	6.46	6.46	4.49	2.69	2.69
511	18.91	7.14	5.99	4.60	2.83	2.59
520	19.91	4.61	4.61	4.72	2.27	2.27
521	20.47	7.01	4.56	4.79	2.80	2.26
530	21.28	3.24	3.24	4.88	1.90	1.90
540	21.98	2.54	2.54	4.96	1.68	1.68

$C_{11}=19.4$ $C_{12}=16.6$ $C_{44}=4.00$

$\times 10^{11}$ dynes/cm²

Gold (c)

100	19.40	4.00	4.00	3.17	1.44	1.44
110	22.00	1.40	1.40	3.38	0.85	0.85
111	22.87	2.27	2.27	3.44	1.08	1.08
210	21.15	2.25	2.25	3.31	1.08	1.08
211	22.08	3.13	2.19	3.38	1.27	1.07
221	22.50	3.21	1.69	3.41	1.29	0.94
310	20.43	2.97	2.97	3.25	1.24	1.24
311	21.15	3.53	2.72	3.31	1.35	1.19
320	21.66	1.74	1.74	3.35	0.95	0.95
321	22.05	3.48	1.87	3.38	1.34	0.98
331	22.27	3.60	1.54	3.40	1.37	0.89
332	22.70	2.83	1.87	3.43	1.21	0.99
410	20.05	3.35	3.35	3.22	1.32	1.32

TABLE I (*continued*).

(Goens) $C_{11}=19.4$ $C_{12}=16.6$ $C_{44}=4.00$

$\times 10^{11}$ dynes/cm²

Gold (c)

hkl	C_t $\times 10^{11}$	C_{t_1} $\times 10^{11}$	C_{t_2} $\times 10^{11}$	V_t $\times 10^5$	V_{t_1} $\times 10^5$	V_{t_2} $\times 10^5$
411	20.57	3.71	3.12	3.26	1.39	1.27
421	21.48	3.65	2.28	3.34	1.38	1.09
430	21.82	1.58	1.58	3.36	0.90	0.90
431	22.03	3.70	1.66	3.38	1.39	0.93
510	19.84	3.56	3.56	3.21	1.36	1.36
511	20.21	3.81	3.38	3.24	1.40	1.32
520	20.73	2.67	2.67	3.28	1.18	1.18
521	21.00	3.75	2.65	3.30	1.39	1.17
530	21.48	1.92	1.92	3.34	1.00	1.00
540	21.89	1.51	1.51	3.37	0.88	0.88

(Goens+Schmid) $C_{11}=23.7$ $C_{12}=14.1$ $C_{44}=11.6$

$\times 10^{11}$ dynes/cm²

Iron(α) (d)

100	23.70	11.60	11.60	5.49	3.84	3.84
110	30.50	4.80	4.80	6.23	2.47	2.47
111	32.77	7.07	7.07	6.45	3.00	3.00
210	28.55	6.75	6.75	6.02	2.93	2.93
211	30.93	9.33	6.64	6.27	3.44	2.90
221	31.85	9.49	5.56	6.36	3.47	2.66
310	26.75	8.55	8.55	5.83	3.30	3.30
311	28.69	10.36	7.84	6.04	3.63	3.16
320	29.74	5.56	5.56	6.15	2.66	2.66
321	30.81	10.19	5.90	6.26	3.60	2.74
331	31.24	10.50	5.16	6.30	3.65	2.56
332	32.36	8.51	6.04	6.41	3.29	2.77
410	25.72	9.58	9.58	5.72	3.49	3.49
411	27.19	10.84	8.86	5.88	3.71	3.36
421	29.44	10.65	6.81	6.12	3.68	2.94
430	30.10	5.20	5.20	6.18	2.57	2.57
431	30.69	10.78	5.42	6.25	3.70	2.62
510	25.11	10.19	10.19	5.65	3.60	3.60
511	26.23	11.09	9.58	5.77	3.75	3.49
520	27.54	7.76	7.76	5.92	3.14	3.14
521	28.28	10.93	7.69	5.99	3.73	3.13
530	29.34	5.96	5.96	6.11	2.75	2.75
540	30.26	5.04	5.04	6.20	2.53	2.53

(Goens+Weerts) $C_{11}=4.77$ $C_{12}=4.03$ $C_{44}=1.44$

$\times 10^{11}$ dynes/cm²

Lead (e)

100	4.77	1.44	1.44	2.05	1.13	1.13
110	5.84	0.37	0.37	2.27	0.57	0.57
111	6.20	0.73	0.73	2.34	0.80	0.80
210	5.51	0.70	0.70	2.20	0.79	0.79
211	5.89	1.08	0.68	2.28	0.98	0.77
221	6.05	1.11	0.49	2.31	0.99	0.66
310	5.22	0.99	0.99	2.14	0.93	0.93
311	5.52	1.25	0.88	2.21	1.05	0.88
320	5.71	0.50	0.50	2.24	0.66	0.66
321	5.88	1.22	0.55	2.28	1.04	0.70
331	5.95	1.27	0.43	2.29	1.06	0.61
332	6.13	0.96	0.56	2.32	0.92	0.71
410	5.06	1.15	1.15	2.11	1.01	1.01
411	5.28	1.32	1.05	2.16	1.08	0.96
421	5.65	1.29	0.71	2.23	1.07	0.79
430	5.77	0.44	0.44	2.26	0.62	0.62
431	5.86	1.31	0.47	2.27	1.08	0.65
510	4.97	1.24	1.24	2.09	1.05	1.05
511	5.13	1.36	1.16	2.13	1.10	1.01
520	5.34	0.87	0.87	2.17	0.87	0.87
521	5.46	1.34	0.86	2.19	1.09	0.87
530	5.64	0.57	0.57	2.23	0.71	0.71
540	5.80	0.41	0.41	2.26	0.60	0.60

TABLE I (*continued*).

(Röhl)
$C_{11}=12.0$ $C_{12}=8.97$ $C_{44}=4.36$

$\times 10^{11}$ dynes/cm^2

Silver

hkl	C_l $\times 10^{11}$	C_{t_1} $\times 10^{11}$	C_{t_2} $\times 10^{11}$	V_l $\times 10^5$	V_{t_1} $\times 10^5$	(f) V_{t_2} $\times 10^5$
100	12.00	4.36	4.36	3.38	2.04	2.04
110	14.84	1.52	1.52	3.76	1.20	1.20
111	15.79	2.46	2.46	3.88	1.53	1.53
210	13.98	2.38	2.38	3.65	1.50	1.50
211	14.99	3.41	2.32	3.78	1.80	1.49
221	15.40	3.49	1.83	3.83	1.82	1.32
310	13.21	3.15	3.15	3.55	1.73	1.73
311	14.02	3.84	2.86	3.65	1.91	1.65
320	14.51	1.85	1.85	3.72	1.33	1.33
321	14.95	3.78	1.99	3.77	1.90	1.38
331	15.15	3.91	1.66	3.80	1.93	1.26
332	15.62	3.07	2.03	3.86	1.71	1.39
410	12.78	3.58	3.58	3.49	1.85	1.85
411	13.38	4.04	3.29	3.57	1.96	1.77
421	14.35	3.96	2.41	3.70	1.94	1.51
430	14.67	1.69	1.69	3.74	1.27	1.27
431	14.91	4.03	1.79	3.77	1.96	1.30
510	12.54	3.82	3.82	3.46	1.91	1.91
511	12.99	4.15	3.58	3.52	1.99	1.85
520	13.54	2.82	2.82	3.59	1.64	1.64
521	13.85	4.08	2.79	3.63	1.97	1.63
530	14.33	2.03	2.03	3.69	1.39	1.39
540	14.74	1.62	1.62	3.75	1.24	1.24

*Velocities in 10^5 cm/sec.

One can readily appreciate the amount of computational effort required for the evaluation of the data in Table I. By proceeding step-wise with Eqs. (3) and (2), the undertaking reduces primarily to one of routine calculation of the coefficients of Eq. (1). The algebraic solution of the latter equation constitutes a distinct segment of the computing job and the final velocity results follow directly. The three parameters shown in Table I are associated with the longitudinal and two transverse waves, although it is understood that except for the directions 100, 110, and 111, the strict meaning of these terms does not apply.

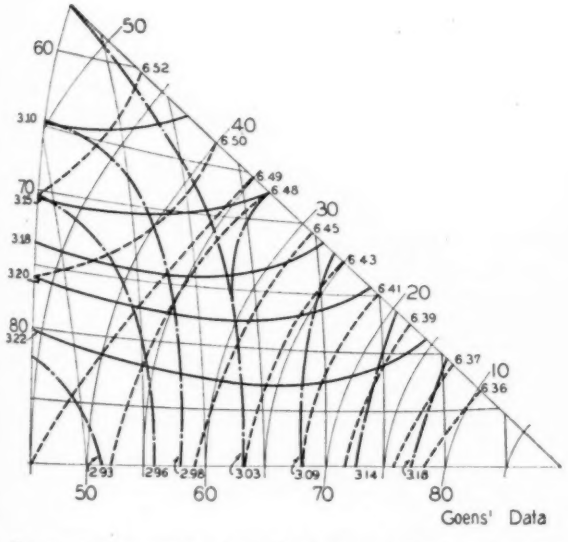

FIG. 3a. Stereographic plot of body wave velocities for aluminum showing iso-velocity contours. Velocities in 10^5 cm/sec. --------- V_l; ———— V_{t_1}; — — — — — V_{t_2}.

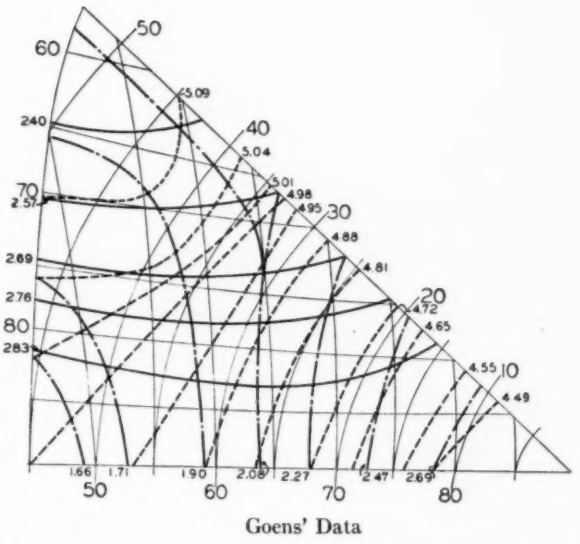

FIG. 3b. Stereographic plot of body wave velocities for copper showing iso-velocity contours. Velocities in 10^5 cm/sec. --------- V_l; ———— V_{t_1}; — — — — — V_{t_2}.

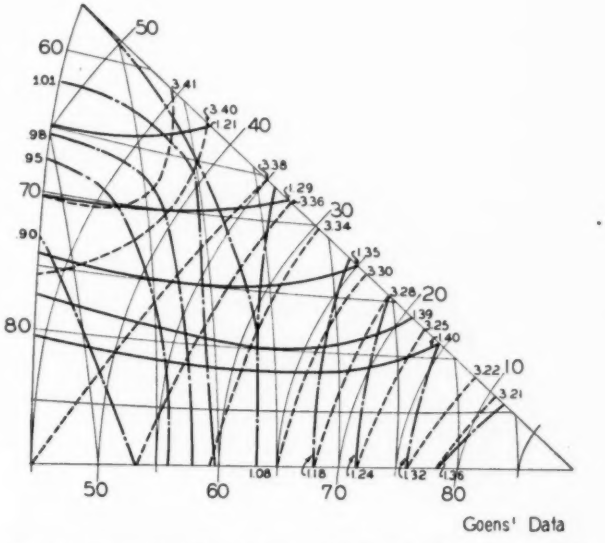

FIG. 3c. Stereographic plot of body wave velocities for gold showing iso-velocity contours. Velocities in 10^5 cm/sec. --------- V_l; ———— V_{t_1}; — — — — — V_{t_2}.

It is difficult to visualize the directional character of the body wave velocities directly from the tables given. The task of representing the data by some graphical scheme was considered. The use of a three-dimensional solid model, so popular for summarizing other directional crystalline properties, could have been invoked; but some thought was given to a two dimensional scheme, with the result that a stereographic coordinate triangle was devised for this purpose.

The underlying basis for this coordinate system may be understood in terms of the following discussion. If one considers a quadrant of a cubic crystal defined by

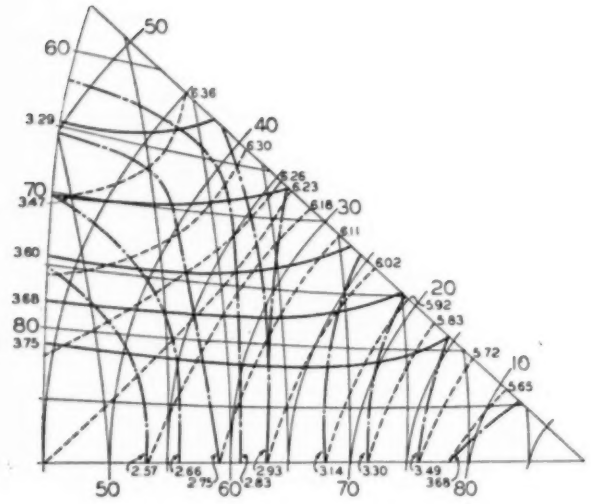

Goens and Schmid's Data

FIG. 3d. Stereographic plot of body wave velocities for iron showing iso-velocity contours. Velocities in 10^5 cm/sec. --------- V_l; ———— Vt_1; — — — — — Vt_2.

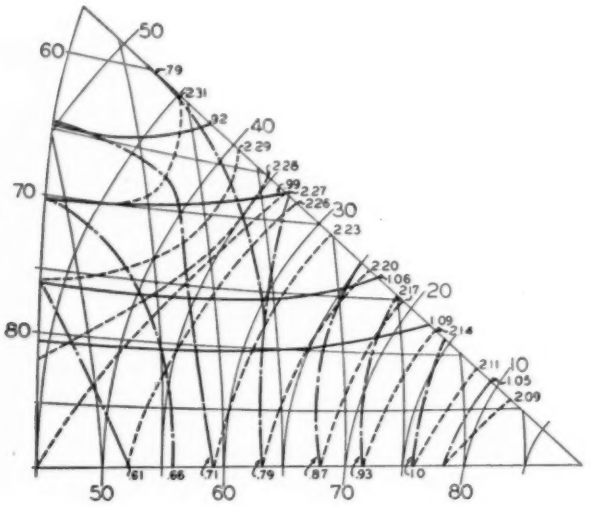

Goens and Weerts' Data

FIG. 3e. Stereographic plot of body wave velocities for lead showing iso-velocity contours. Velocities in 10^5 cm/sec. --------- V_l; ———— Vt_1; — — — — — Vt_2.

the appropriate [001] directions, then the vector along the 111 direction divides the quadrant into six equivalent regions, i.e., the directional properties are sixfold degenerate. In terms of the standard projection scheme, there are six equivalent stereographic triangles whose termini are the poles 001, 110, and 111 as shown in Fig. 1. Directional parameters such as the body wave velocities may all be plotted in one of the six triangles. To facilitate the location of each of the points within the triangle it has been found convenient to employ a coordinate system directly related to the Wulff net.

Figure 2 depicts the character of the coordinates in the stereographic triangle. The angles indicated are all

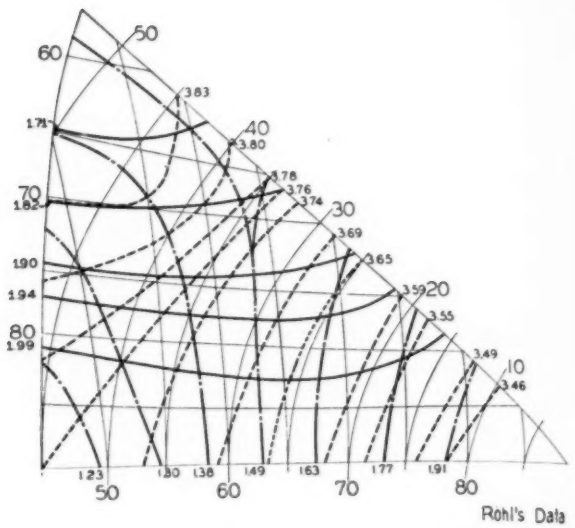

FIG. 3f. Stereographic plot of body wave velocities for silver showing iso-velocity contours. Velocities in 10^5 cm/sec. --------- V_l; ———— Vt_1; — — — — — Vt_2.

referred to the three [001] directions; the coordinate markings for two of the directions are obtained directly from the Wulff net, these being the rulings running essentially parallel to the edges defined by the 111–110 and 110–001 points. The third set of rulings is obtained by rotating the triangle through 90° and again making use of the latitude markings on the Wulff net; these lines also run along the edge 110–111, but have an opposite curvature. It may be readily verified that any point in the triangle fulfills the condition $\cos^2\alpha+\cos^2\beta$

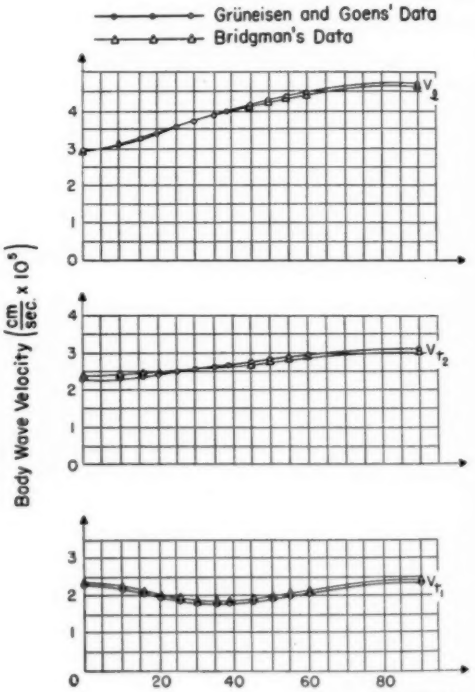

FIG. 4a. Velocities of body wave propagation in zinc.

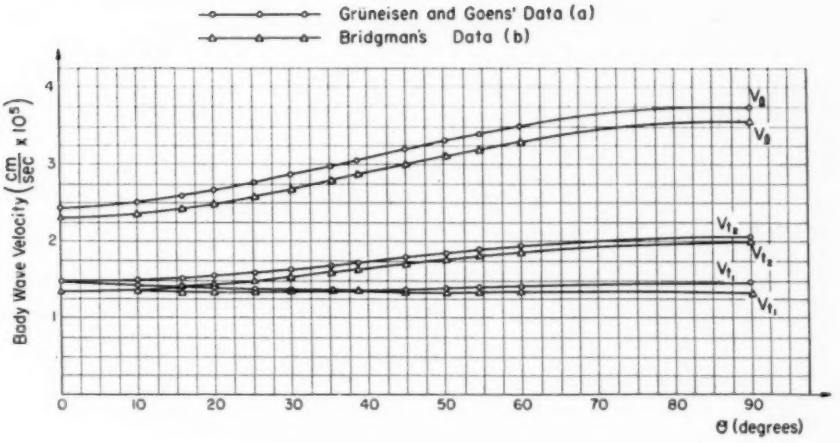

FIG. 4b. Velocities of body wave propagation in cadmium.

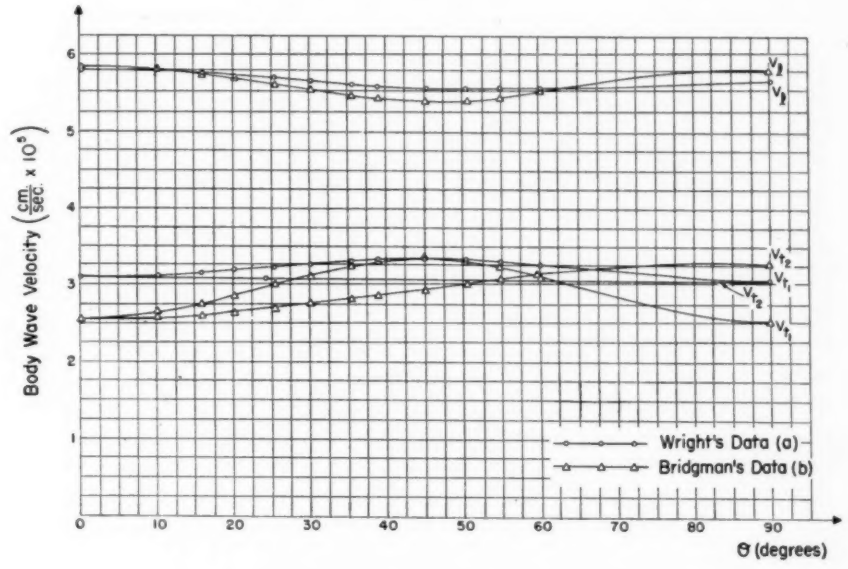

FIG. 4c. Velocities of body wave propagation in magnesium.

$+\cos^2\gamma=1$, so that the triangle is a nomographic chart for this relation.

When the data of Table I are plotted in the stereographic triangle, it is found that lines of constant velocity can be drawn through the various points. Figures 3(a)–(f) show the common features of these iso-velocity contours for the series of metals, aluminum, copper, gold, iron, lead, and silver. One immediate application of these charts is the determination of mode separation along any given direction of propagation. Thus if one is interested in a particular compressional mode, the optimum orientation for minimizing interference from the shear modes may be inferred.

3. TREATMENT OF HEXAGONAL METALS

Hexagonal close-packed metals such as magnesium, zinc, and cadmium have symmetry which restricts the number of independent stiffness coefficients to five. It can be shown that for crystals of this kind the body wave velocities are only dependent upon the angle between the hexagonal axis and the wave propagation direction. By transforming from direction cosines to Eulerian angles the three roots of Eq. (1) become

$$\begin{aligned} C_{n1}&=\tfrac{1}{2}(c_{11}-c_{12})\sin^2\theta+c_{44}\cos^2\theta \\ C_{n21n3}&=\tfrac{1}{2}\{(c_{11}+c_{44})\sin^2\theta+(c_{33}+c_{44})\cos^2\theta \\ &\quad\pm[(c_{11}-c_{44})^2\sin^4\theta+(c_{33}-c_{44})^2\cos^4\theta \\ &\quad+2\sin^2\theta\cos^2\theta\{(c_{11}-c_{44})(c_{44}-c_{33}) \\ &\qquad+2(c_{13}+c_{44})^2\}]^{\frac{1}{2}}. \quad (4) \end{aligned}$$

The computations of the three wave velocities are clearly much simpler for the hexagonal metals than for the cubic metals. Figures 4(a)–(c) contain two sets of body wave curves based upon the independent c_ik

TABLE II.

c_ik data	Metal	θ_l *(a)	θ_l (b)	θ_{t_1} (a)	θ_{t_1} (b)	θ_{t_2} (a)	θ_{t_2} (b)
	Cd	3.13	2.94	1.41	1.34	1.76	1.68
	Mg	5.68	5.63	3.25	2.97	3.10	2.96
	Zn	4.05	4.03	2.03	2.07	2.71	2.68

* These letters refer to c_ik data employed as indicated in Figs. 4.

data of the indicated experimenters. By evaluating the areas under the various curves, one has a means for deriving the theoretical average velocities for the compressional and shear waves. Table II summarizes the findings.

ACKNOWLEDGMENT

The author is indebted to the Staff of the Computing Group of the Graduate Division of Applied Mathematics for assistance in the numerous calculations entailed.

Light Energy and Spectral Distribution for Some Important X-Ray Screens

HOLGER SKÖLDBORN
Department of Physics, Lund University, Sweden

(Received December 12, 1949)

The absolute energy of the light (ergs/cm² per r-unit) and its spectral distribution have been determined for four different types of x-ray fluorescent screens: Patterson E-2, Patterson B-2, Patterson D, and Neossal. The investigation was performed in accordance with an objective spectrophotometric process with the aid of a tungsten ribbon filament lamp as a standard, a light attenuator of reflection type, monochromator, multiplier photo-tube, and galvanometer.

The application of the method employed to the weak light intensities in question is made possible on account of the enormous light sensitivity of the multiplier photo-tube and the possibility of reproducible continuous variation of this sensitivity within very wide limits. The method has proved speedy and accurate and appears to be well suited for investigations of similar character, within the spectral range which may be measured by the commercial types of multiplier photo-tubes.

IN spite of the immense importance and varied applications which the x-ray fluorescent screens have developed in the last decades, one will search in vain for exact information concerning the absolute energy and spectral distribution of the emitted fluorescent light from different types of screens. The present investigation, which was planned early in 1947 after a proposition put forward by medical quarters, is intended to provide these desirable data for some of the most important commercial types of screens. We have chosen three of the firm du Pont's latest makes, Patterson D, Patterson B-2, and Patterson E-2, and the Neossal screen (of German make), which is probably still the most commonly used for fluoroscopy in Sweden. The physical properties of calcium tungstate x-ray screens have been treated in detail by Coltman, Ebbighausen, and Altar in an earlier article in this Journal.[1]

APPARATUS

The main problem of the investigation consisted in the determination of the spectral energy distribution of the fluorescent light from different x-ray fluorescent screens at a given x-ray radiation quality and a given measured r-intensity by comparison with the known spectral energy distribution from a temperature calibrated tungsten ribbon filament lamp. Integration of the spectral curves obtained in this way gives the absolute energy of the fluorescent light per r-unit incident on the screen.

When choosing the method of investigation we were guided by the following points of view. A practicable way for an investigation at these weak light intensities is, of course, the method of comparing in a microphotometer spectrograms recorded from the standard lamp, or the x-ray screen. To give reliable results, however, this method requires among other things an extremely elaborate technique for variable reduction of the filament brightness to a value closely approximating to that of the fluorescent screen at different wavelengths (on account of reciprocity failure of the photographic emulsion). RCA's latest extremely sensitive photo-cells of the multiplier type seemed to suggest the possibility of applying an objective spectrophotometric method, though the light output of the screen under the planned experimental conditions could not be expected to amount to more than 10–100 erg/cm²/sec. After a great number of preliminary experiments, comprising recording of spectrograms of several types of screens, testing of different photo-cells in connection with an appropriate monochromator etc., the final form of the apparatus was such that the method could be regarded as fully satisfactory for the present investigation. The apparatus employed will now be described in greater detail.

A tungsten ribbon filament lamp provided with a quartz window was used as standard source. The ribbon filament is about 10 mm long and 2 mm wide, and is supported in the bulb by heavy nickel leads. The current could easily be kept constant within 0.1 percent.

The lamp was temperature calibrated to the standard of the Physics Laboratory of the University of Lund with the aid of its optical pyrometer. At 13.00 amperes the brightness temperature outside the quartz window was determined at 2244°K for a point midway along the

[1] Coltman, Ebbighausen, and Altar, J. App. Phys. **18**, 530–544 (1947).

filament. This current was used all through the investigation.

When computing the spectral distribution of the radiation emitted by the ribbon filament lamp one must know the true temperature of the filament inside the bulb, the spectral emissivity of tungsten, and the spectral transmission of the quartz window within the intended working range of wave-lengths (4000–7000A). For the spectral emissivity the values determined by Hamaker[2] were used. For the spectral transmission of the quartz window the value 0.92 was used within the whole range of wave-length in question. The error possibly introduced in this way (the lamp was an unused specimen) is, according to Hamaker's results from measurements of absorption in quartz windows of different conditions,[2] not likely to exceed 0.5 percent anywhere. The conversion from the brightness temperature to the true temperature was accomplished by the following formula, derived from Planck's radiation formula:

$$\frac{1}{T_t}=\frac{1}{T_{BO}}+\frac{\lambda}{0.4343C_2}\log_{10}(\epsilon_\lambda\cdot t_\lambda), \tag{1}$$

where T_t = true temperature of the filament, T_{BO} = brightness temperature of the filament outside the window as determined by the optical pyrometer, λ = mean effective wave-length in cm of the red filter used in the optical pyrometer, C_2 = the second constant in Planck's radiation formula, ϵ_λ = the spectral emissivity of tungsten at λ, and t_λ = the spectral transmission of the quartz window at λ.

With $T_{BO}=2244°$K, $\lambda=6650\times10^{-8}$ cm, $C_2=1.435$, $\epsilon_\lambda=0.430$, $t_\lambda=0.920$, the true temperature of the filament is 2483°K.

The spectral energy distribution outside the lamp was obtained by substitution of the above value of the true temperature in Planck's radiation formula, and correcting the result for the spectral emissivities of tungsten and for the spectral transmission of the quartz window:

$$B_\lambda d\lambda=\frac{C_1\lambda^{-5}}{e^{C_2/\lambda T}-1}\epsilon_\lambda t_\lambda d\lambda. \tag{2}$$

In the above formula $B_\lambda d\lambda$ denotes the brightness in ergs/cm²/second per unit solid angle within the wave-length interval $d\lambda$ (λ in cm and C_1 its corresponding value).

An area of 5 mm×0.3 mm of the central portion of the filament was used for projection on the slit of the monochromator. At the pyrometric calibration no temperature differences were observed within this central portion. From Planck's radiation law one derives the percentage change in emitted energy at a given wave-length for a change in true temperature to be

$$\left(\frac{dE_\lambda}{E_\lambda}\right)\text{percent}=100\left(\frac{C_2}{\lambda T^2}\right)dT. \tag{3}$$

For a true temperature of 2483°K the percentage change of E_λ per degree is 0.58 percent at 4000A and 0.36 percent at 6500A. The error in the true, pyrometrically determined temperature is estimated to ±3°K. This means an error in E_λ of 1.7 percent at 4000A and 1.1 percent at 6500A. Considering all sources of error it appears that the combined error in the computed energy varies from about 4 percent at 4000A to about 3 percent at 6500A with an average for the middle of the spectrum of about 3.5 percent.

To make possible a spectrophotometric comparison (in the wave-length range 4000–7000A) between the brightness of the standard lamp filament and the fluorescent screen, the brightness of the former had to be reduced by a factor, which turned out to be of the order of 10^{-5}. The sensitivity of the type of multiplier photo-tube used being variable continuously and reproducibly within very wide limits, this reduction could be obtained by a suitable non-variable light "attenuator" and further reduction arrangements avoided.

A light attenuation of the order of magnitude desired can be accomplished by successive reflections from four air-glass surfaces, and an apparatus designed and constructed according to this principle is described in an article cited above.[1] We constructed such an attenuator with great care of four crown glass prisms, arranged as in Fig. 1, inside a brass box. The principle is immediately clear from the figure; concerning the details we will be as brief as possible, in our reference to the article mentioned. All the prism surfaces, except the ones used for reflection, were covered with a highly absorbent coating of carbon black silted up in zapon lacquer. The non-reflecting and absorbing coating obtained serves to remove to a very high degree the light transmitted into the prism.

According to Fresnel's formula one obtains for the light polarized in the plane of incidence after four successive reflections the following expression for the

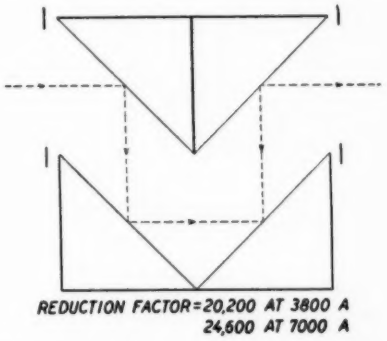

FIG. 1. Schematic arrangement of reflection-type attenuator.

[2] H. C. Hamaker, "Reflectivity and Emissivity of Tungsten," Diss. Utrecht (1934).

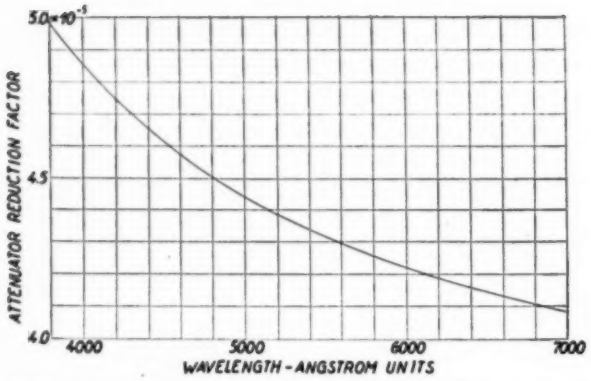

FIG. 2. Reduction factor of attenuator as a function of wave-length

intensity:

$$R(I)=\tfrac{1}{2}\left[\frac{\sin(i-i')}{\sin(i+i')}\right]^8. \tag{4}$$

The polarization being practically complete, the intensity of the light polarized at right angles to the plane of incidence can be neglected (it turns out to be about 9000 times fainter than the other component).

With i fixed at 45° the above formula may be written:

$$R(I)=\tfrac{1}{2}[\tan(45-i')]^8, \tag{5}$$

where i' depends upon n (Snell's law), which in its turn varies with the wave-length. R is thus itself a function of the wave-length, on account of which it was necessary to determine the dispersion curve of the prism material for the range of spectrum to be studied. For this purpose n was determined for one of the prisms for each of the three mercury lines 4046.6, 4358.3, and 5460.7A. The resulting indices were, respectively 1.5302, 1.5367, and 1.5187. This determination was carried out with a Gaertner spectrometer type 568; each value had a standard deviation of 1 unit in the fourth decimal place. With the values of the wave-length and their respective indices, stated above, the constants of the Hartmann interpolation formula were obtained:

$$n=1.4977+\frac{83.969}{\lambda-1462.9}. \tag{6}$$

With intervals of 100A n was determined from (6) for the range 3800–7000A, after which i' from Snell's law and finally the reduction factors from (5) were obtained as a function of the wave-length. The last-mentioned relation is represented by the curve in Fig. 2. The curve in Fig. 3, obtained by applying these reduction factors to the spectral energy distribution curve of the filament outside the lamp, shows the resulting spectral brightness of the standard lamp filament as seen through the attenuator.

As mentioned above the light from the attenuator is practically completely polarized, while the light from the fluorescent screen is unpolarized. To avoid errors which may arise, if the light loss in the monochromator is not the same for both sources, the attenuator was mounted so that the plane of the normals of the reflecting surfaces made an angle of 45° with the slit. In this way the light received by the monochromator may be regarded as isotropic.

The errors in the computed reduction factors are evaluated as follows:

1. An error of 1 unit in the fourth place of $n-1$ results in an error in R of less than 0.1 percent.
2. The error in R to be expected in consequence of the dispersion curve being calculated from only three index determinations is estimated to at most 0.1 percent for the range 4000–7000A.
3. The beam through the attenuator, as defined by a rectangular stop on the collimator lens and the focal distance of this lens, had an angular size of about 5°×3°. Since R was determined for a constant angle of incidence of 45°, it was necessary to obtain an estimate of the error introduced by assuming $i=45°$ for the whole beam. Calculation shows that the error, which is negative, amounts to about 0.5 percent. When this deviation in the reduction factors has been corrected of, any possibly remaining error is unlikely to exceed 0.2 percent.
4. The construction as well as the alignment of the attenuator was performed with great care so that the resulting error in R due to want of accuracy is probably less than 0.5 percent.

From these points we may conclude that the attenuator functions with an accuracy of 1 percent.

The dispersing instrument used was a "Hilger Constant Deviation Wave-Length Spectrometer," type D 187. It has $f=285$ mm for both lenses, and an angular aperture of 1:9. An additional rectangular stop of the size 25 mm×14 mm was fitted close to the collimator lens. Both slits were adjusted to a width of 0.3 mm and a height of 5 mm. The reliability of the wave-length scale was tested with the aid of a line spectrum. After a careful adjustment of the prism it appeared that the wave-length readings for the range of 4000–6500A showed a maximum error of about ±1A. Thus the accuracy is entirely satisfactory for our purpose.

The experimental arrangement is shown in Fig. 4. By means of a mirror and a condensing lens, either the filament or the screen sample could be projected on to the collimator slit at a magnification of 1:1. The mirror (an aluminized plane mirror) could be rotated 90° and mounted in two accurately fixed positions. The alignment was checked by illuminating the emergent slit of the monochromator by a strong light source, the slit then being imaged at the center of the filament.

The photo-cell was a RCA type 1P21 multiplier photo-tube. The light sensitive surface is made up of a cesium-antimony layer on a nickel base and the spectral response curve is of the S-4 type. A number of photocells of the multiplier type often show great, individual differences with respect to sensitivity and dark current. The cell employed was a selected specimen with a high value of the signal-to-noise ratio. We considered a minimizing of the dark current by reducing the temperature,[3] but this was found to be unnecessary for the

[3] R. W. Engstrom, J. Opt. Soc. Am. 37, 420 (1947).

present investigation. The photo-cell was placed in a suitable light-proof brass holder that was screwed on to the site of the eyepiece of the monochromator. The distance from the slit to the photo-cathode was about 28 mm.

The dynode voltage of the photo-cell was provided from a voltage-stabilized mains-connected supply circuit, designed and constructed by Stigmark[4] at the Physics Laboratory. The potential dividers for the dynodes consisted of 9 exactly equal 50,000 ohms wire-wound resistors. The current through these resistors could be continuously varied from 1 to 2 milliamperes and read on a milliammeter, 2 milliamperes corresponding to a voltage drop of 100 volts per stage. When checking the properties of the voltage supply it was found that a change of the mains voltage (220 v) of ± 10 v caused a change of the total dynode voltage (1000 v) of 0.05 percent, corresponding to a variation of the anode output current of about 0.5 percent. This accuracy was considered to be quite satisfactory.

The anode output current was measured by a "Multiflex" mirror galvanometer with a sensitivity of $5 \cdot 10^{-10}$ ampere/mm. The length of the scale being 200 mm, full deflection corresponded to 0.1 microampere.

After the voltage supply had been tested and found to be sufficiently constant, it remained to investigate the fatigue effects of the photo-cell and the linearity of response of the photo-cell-galvanometer combination. Considering what has been written about the fatigue of multiplier photo-tubes,[3,5] we decided from the beginning not to use higher anode current than 0.1 microampere, especially as this could be done without actual inconvenience during the present investigation. From repeated tests made at constant illumination corresponding to an anode current of the order of magnitude mentioned, it appeared that the fatigue effect must be given due attention even at this low light intensity. The galvanometer deflection decreased 3 to 5 percent during the first half-hour; thereafter, however, the fatigue proceeded extremely slowly. At the performance of the investigation we took this fact into account by fatiguing the photo-cell at 0.1 microampere for about one hour before each series of observations. Moreover the series of observations were carried out according to a scheme which ensured that a continued, slight fatigue effect could have practically no influence on the result.

The proportionality between the intensity of the incident light and the deflection of the galvanometer was checked according to a method given by Hamaker,[2] the principle of which will be clear from Fig. 5. By means of the condensing lens L two light sources LS and LS' were focussed on the slit of the monochromator, LS directly and LS' by way of the reflecting glass plate G; S and S' are two shutters. The check simply consisted of observing whether the sum of the deflections caused by the separate intensities was equal to the deflection caused by the sum of the intensities. The advantages of this method are evident; no changes in the experimental arrangements are needed, the stopping down of the light beam remains unaltered and all we have to do is to use the shutters and vary the electric current through the light sources LS and LS'.

By this method the proportionality of deflection and intensity was checked for 10 different positions on the galvanometer scale. Three such series of observations were carried out for three different wave-length settings of the monochromator (4500, 5400, and 6300A). From these checks it was clear that the deflection of the galvanometer varied proportionally with the intensity of the incident light within 0.5 percent for deflections between 20 and 200 mm (full deflection). The small deviations discovered most certainly originate from the galvanometer employed; concerning the photo-multiplier tube there is no reason to doubt a strict proportionality between light intensity and anode current until above 100 microamperes.

At a distance of 35 cm from the focus of the air-cooled x-ray tube there was a lead stop with a hole 5 cm square. Behind this stop an additional filter of 1 mm Al was applied, and in front of the stop, at a distance of 37.5 cm from the focus of the tube, the screen sample was placed in a holder (Fig. 4). The x-ray intensity was measured at the exact place of the screen by means of an ionization chamber (so-called secondary standard), which, for the radiation quality employed, had been specially calibrated to the primary standard of the Radiophysical Institute in Stockholm.

EXPERIMENTAL PROCEDURE

Before the light intensity measurement could suitably commence, there remained the determination of the relative sensitivity of the photo-cell as a function of the applied dynode voltage. Preliminary experiments showed

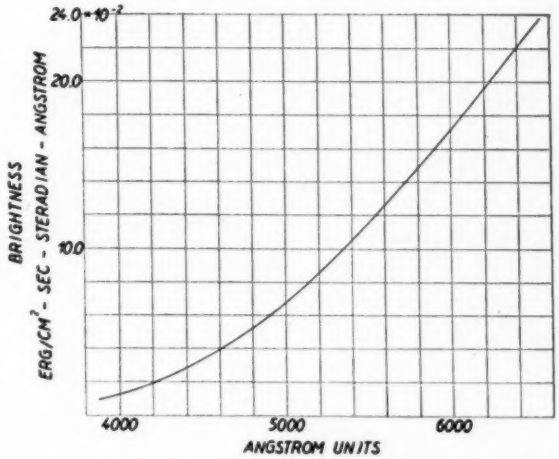

FIG. 3. Spectral brightness of standard lamp as seen through attenuator.

[4] K. Lidén, and L. Stigmark, "Some Experiences from Investigations of the Spectral Intensity Distribution of Weak Light Sources by Means of Multiplier Photo-Tubes," (Manuscript 1948).
[5] K. G. Kessler and R. A. Wolfe, J. Opt. Soc. Am. 37, 133 (1947).

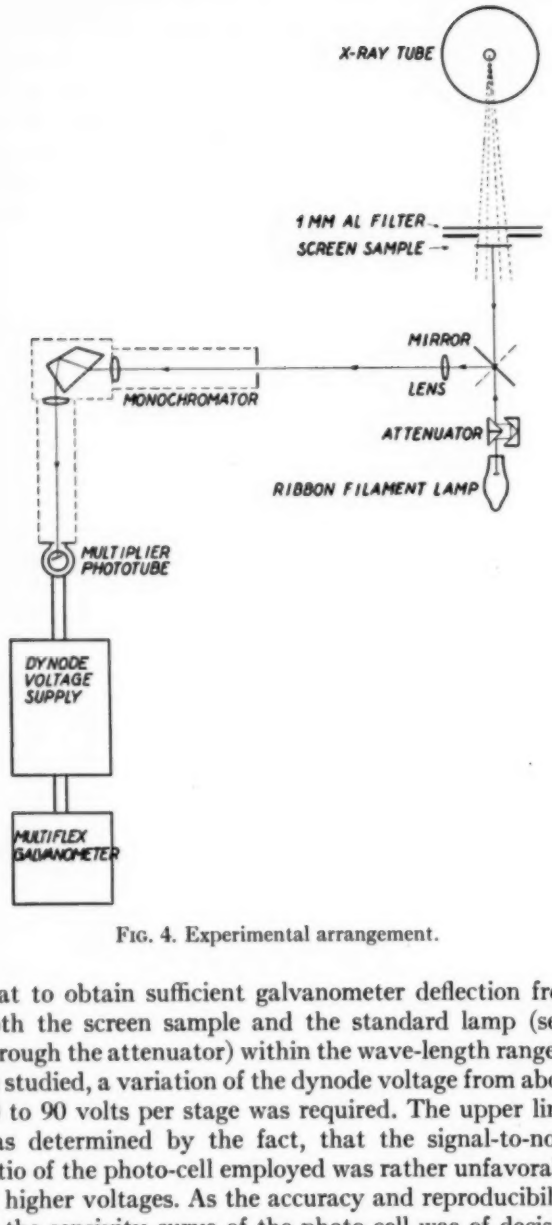

FIG. 4. Experimental arrangement.

that to obtain sufficient galvanometer deflection from both the screen sample and the standard lamp (seen through the attenuator) within the wave-length range to be studied, a variation of the dynode voltage from about 50 to 90 volts per stage was required. The upper limit was determined by the fact, that the signal-to-noise ratio of the photo-cell employed was rather unfavorable at higher voltages. As the accuracy and reproducibility of the sensivity curve of the photo-cell was of decisive importance for our method of measuring, the determination of this curve was given special attention. Sensitivity curves were determined for five different photo-multiplier tubes, and their reproducibility was investigated with respect to the fatigue effects, etc. on several occasions. It was evident from these experiments that the relative sensitivity as a function of the dynode voltage was independent of the fatigue effects and reproducible within limits of error exclusively determined by the accuracy of observation of the instruments.

When determining these sensitivity curves the following method was employed, which, among other things had the advantage of being applicable without change of the experimental arrangements. The electric current through the standard lamp filament was regulated in such a way that the galvanometer showed full deflection at a dynode voltage of 90 volts, after which the deflection was observed for successively lower dynode voltages, as far as the scale of the galvanometer permitted. Then the intensity of the lamp was increased, until full deflection was achieved at a lower dynode voltage, and so forth. Three different light intensities permitted a variation of the dynode voltage from 90 to 50 volts; in this way the curve was joined at two points, the factor of the joint being obtained as the average of two or three double readings. The sensitivity curve of the photo-cell employed (Fig. 6) was computed from the average of four such series of readings. The relative amplification factor varies from 100.0 to 0.910 at a variation of the dynode voltage from 90 to 50 volts. The error in the ratio of two arbitrary values of the curve was calculated to be at most 2 percent.

The determination of the spectral energy distribution of the fluorescent screens was now performed in the following way. After the photo-cell had been fatigued for about an hour and the standard lamp had been allowed to assume temperature equilibrium, the readings for two complete series were performed according to the scheme: $LSL'S'SLS'L'$. The readings were taken with intervals of 100A for the lamp as well as the screen. L and S denote readings of the deflections for the intensities of the standard lamp and the fluorescent screen, respectively, starting at the violet end of the spectrum; L' and S' readings for the same wave-length starting at the red end of the spectrum. This scheme was used in order to eliminate completely the fatigue effect on the average of each determination. To read the deflection for the standard lamp as well as for the screen point by point turned out to be unpractical, as in such a case the dynode voltage had to be readjusted very often. With the above method several readings often could be made in succession before readjusting the dynode voltage to a new value.

In connection with each series of readings three measurements of the x-ray intensity were carried out at the position of the screen according to the scheme $RLSRL'S'R$, where R denotes an r-measurement. The x-ray intensity could be kept constant within 1 percent (temporary fluctuations of the tube current). The accuracy of a separate r-intensity measurement was about 1 percent. The measured x-ray intensity was on an average 0.901 r-unit per second.

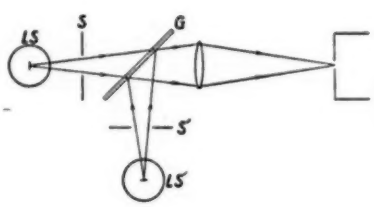

FIG. 5. Arrangement for check of proportionality between light intensity and galvanometer deflection.

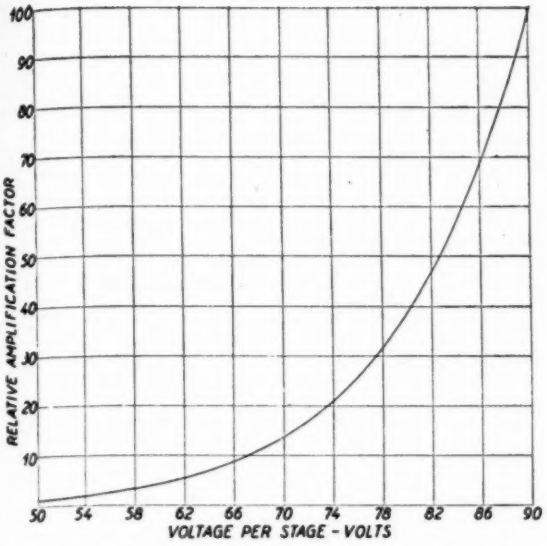

FIG. 6. Variation of relative amplification factor with applied voltage per stage for 1P21 tube used.

EXPERIMENTAL RESULTS

The spectral energy distribution of the screens investigated is plotted in Fig. 7. The spectral curves are given in terms of light energy emerging from the screen per *r*-unit incident on the screen. All results refer to the same x-ray quality, *viz.* 80 kv constant potential x-rays, filtered by one mm Al (tube current 9 mA). The filter equivalent of the wall of the x-ray tube was about 1.0 mm Al. The experimentally determined points succeed each other so smoothly that every point, if plotted, would be found on the drawn lines in Fig. 7.

The values of the absolute energy of the emerging fluorescent light obtained by numerical integration of the curves in Fig. 7 are given in Table I. The second column of this table gives the measured brightness of the screens in ergs/cm²/unit solid angle/*r*-unit incident on the screen. This applies to light emitted in the direction of the normal. The values of the total light emission in the third column have been calculated on the assumption that the departure from Lambert's law is represented by a factor of 0.92. This value was found by Coltman, Ebbighausen, and Altar[1] for a $CaWO_4$ screen excited by 80 kv constant potential x-rays, filtered by 0.5 mm Cu and 1 mm Al. In the present case, however, this value may be inaccurate with an error of one or two percent, owing to variation with radiation quality and material of the screen.

Of the screen samples investigated Patterson *D*, Patterson *B*-2, and Patterson *E*-2, were fresh samples obtained directly from the manufacturer (the Patterson Screen Division of E. I. du Pont de Nemours & Company, at Towanda, Pennsylvania). The Neossal screen, on the other hand, was a several years old sample, which, however, was unused and kept light-proof. All the screens were of the ordinary type with the phosphor layer applied to a white mounting card. The phosphor layer of the Neossal and the Patterson type *E*-2 screens were covered with a protective film of lacquer. On the Patterson type *D* screen, which fairly recently was developed for photo-fluorography, the fluorescent layer is composed of silver-activated zinc sulfide; the other three, which are mostly used for fluoroscopy, may be classed as zinc-cadmium sulfide screens. The Patterson type *B*-2, which was commercially available early last

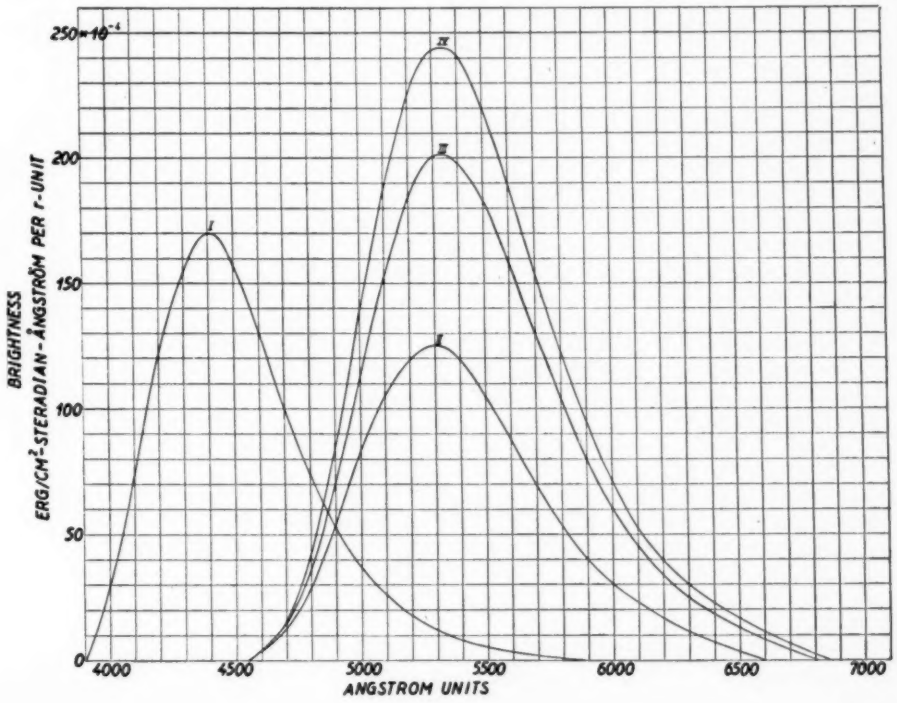

FIG. 7. Fluorescent spectra of four important x-ray screens, excited by 80 kv constant potential x-rays, filtered by 1 mm aluminium. I: Patterson type *D*. II: Neossal. III: Patterson type *B*-2. IV: Patterson type *E*-2.

TABLE I. Brightness and total emission of light of four x-ray fluorescent screens (calculated from Fig. 7).

Screen	Brightness ergs/cm²/steradian/r-unit	Total light emitted from screen ergs/cm²/r-unit
Patterson type *D*	11.8	34.0
Neossal	11.0	31.8
Patterson type *B*-2	18.4	53.2
Patterson type *E*-2	22.1	64.0

year was stated to be 40 percent brighter than the next preceding type Patterson *B*, a statement that we have had the opportunity of verifying. We have also included the results for the Patterson type *E*-2, which is stated to be of the same character as the type *B*-2, but with a protective cleanable surface, owing to the fact that it was found to be not less than 20 percent brighter than the type *B*-2 of the samples received at the same time. The Patterson type *D* with unprotected surface is also manufactured with a protective cleanable surface, and then called type *D-C*. These two variants turned out to be of equal brightness.

The accuracy of an investigation of this kind depends on several factors. If the contributions from all sources of error are summed up according to the calculations and estimates imparted at the description of the corresponding part of the apparatus, and of the experimental procedure, it appears that the results stated above will be correct with a maximum error of about 9 percent.

Unbalanced Terminations on a Shielded-Pair Line*

K. TOMIYASU
Division of the Sperry Corporation, Great Neck, New York
(Received December 7, 1949)

Theoretical calculations indicate that the unbalanced component of current on a two-wire or shielded-pair transmission line can be determined by comparing the different standing-wave distributions on the line conductors. The measurement of reflected components from an unbalanced radiative termination on a slotted shielded-pair line is described. The existence of a condition of minimum unbalanced reflected component from end-coupled antennas is shown experimentally.

INTRODUCTION

SHIELDED-PAIR and two-wire transmission lines differ from coaxial lines in that the former can support simultaneously two transverse electromagnetic (*TEM*) propagating modes. One of the modes called the balanced mode is the conventional transmission line mode where the currents on the two conductors are *opposite* in phase and equal in magnitude at all cross sections. For the other mode called the unbalanced mode, the currents are *in* phase and equal in magnitude and hence the scalar potential difference between the conductors is zero at all cross sections. The unbalanced mode radiates energy from an open two-wire line but does not radiate from a shielded-pair line. Whether the waves are standing or progressive the usual physical effect of the coexistence of the balanced and unbalanced modes is that the currents on the two conductors are unequal in magnitude and of arbitrary phase at all cross sections. This further indicates that the standing-wave distributions will be different on the two inner conductors if a shielded-pair line is excited by a balanced mode and terminated in an unbalanced structure. The reflected balanced and unbalanced modes can be measured from this difference. Measurements have been made on a slotted shielded-pair line which was terminated in unbalanced radiative terminations. Some of the representative measurements are included in this paper.

INCIDENT AND REFLECTED WAVES

The difference between the standing-wave distributions on the two conductors which yields the total characteristics of an unbalanced termination is dependent on the relative phases and amplitudes of four modes or waves: balanced and unbalanced, incident and reflected modes. Since these modes can be added as well as decomposed readily the complex voltage components on the conductors can be written as follows.

$$V_{1BI} = -V_{2B1} = A_0 \exp(-\gamma_B X + j\omega t), \quad (1)$$

$$V_{1BR} = -V_{2BR} = B_0 \exp(\gamma_B X + j\omega t), \quad (2)$$

$$V_{1UR} = V_{2UR} = C_0 \exp(\gamma_U X + j\omega t), \quad (3)$$

$$V_{1UI} = V_{2UI} = D_0 \exp(-\gamma_U X + j\omega t), \quad (4)$$

where B stands for balanced; U stands for unbalanced; I stands for incident; R stands for reflected; A_0, B_0, C_0, D_0 are complex constants; $\gamma = \alpha + j\beta$ is the complex propagation constant; $+X$ is the direction away from generator. γ_B may differ from γ_U for dielectric-filled shielded-pair lines as well as open two-wire lines. The time factor $e^{j\omega t}$ may be omitted for convenience. The

* The research reported in this document was made possible through support extended Cruft Laboratory, Harvard University, jointly by the Navy Department (ONR), the Signal Corps of the U. S. Army, and the U. S. Air Force, under ONR Contract N5-ori-76, T. O. 1.

resultant voltages on each line are

$$V_1 = V_{1BI} + V_{1BR} + V_{1UR} + V_{1UI} = V_{1B} + V_{1U}, \quad (5)$$

$$V_2 = V_{2BI} + V_{2BR} + V_{2UR} + V_{2UI} = V_{2B} + V_{2U}. \quad (6)$$

The addition of these voltage components is illustrated in Fig. 1. Since $V_{1B} = -V_{2B} = 1/2(V_1 - V_2)$ and $V_{1U} = V_{2U} = 1/2(V_1 + V_2)$ as shown in Fig. 1, the balanced and unbalanced components can be determined provided the amplitudes and phase difference of V_1 and V_2 are known.[1] The standing-wave distribution curves which can be obtained from $|V_1|$ and $|V_2|$ of Eqs. (5) and (6) are symmetrical within each half-wave-length for all values of the complex constants.

The desired reflection coefficients which characterize the unbalanced termination can be obtained by considering each line separately. For the general case of four modes, the reflection coefficients can be defined for the terminations as

$$\Gamma_1 = \left|\frac{V_{1BR} + V_{1UR}}{V_{1BI} + V_{1UI}}\right| \underline{/\phi_1'} = \left|\frac{V_{1R}}{V_{1I}}\right| \underline{/\phi_1'}, \quad (7)$$

$$\Gamma_2 = \left|\frac{V_{2BR} + V_{2UR}}{V_{2BI} + V_{2UI}}\right| \underline{/\phi_2'} = \left|\frac{V_{2R}}{V_{2I}}\right| \underline{/\phi_2'}. \quad (8)$$

For this case of balanced and unbalanced, incident and reflected modes on a line where $\gamma_B = \gamma_U$, six unknowns must be determined for the complex constants, A_0, B_0, C_0, and D_0. Since no additional information on an unbalanced termination can be obtained by having an unbalanced *incident* mode, it is mathematically and experimentally convenient to require D_0 to be equal to zero. This reduces the number of unknowns to four, and these can be obtained from the standing-wave ratios and positions of voltage minima of the standing-wave distributions. The other two unknowns necessary for the general case may be the time-phase difference[2] and relative magnitudes of the distribution extremes.

When $D_0 = 0$, the reflection coefficients at the load after arbitrarily assigning a zero phase angle for A_0, are

$$\Gamma_1 \equiv \frac{B_1}{A_0} = \frac{B_0 + C_0}{A_0} = \frac{|B_0 + C_0|}{A_0} \underline{/\phi_1}, \quad (9)$$

$$\Gamma_2 \equiv \frac{B_2}{A_0} = \frac{B_0 - C_0}{A_0} = \frac{|B_0 - C_0|}{A_0} \underline{/\phi_2}, \quad (10)$$

where

$\phi = 2\beta X_{\min} \pm \pi$,
$\beta = 2\pi/\lambda$ = phase constant,
$X_{\min}$ = distance from the load to a voltage minimum

[1] See, for example, R. King, "Coupled antennas and transmission lines," Proc. I.R.E. **31**, 626–640 (November, 1943).

[2] For measurement of time-phase differences, see, for example, T. Morita, Cruft Laboratory Technical Report No. 66, Harvard University, Cambridge, Massachusetts.

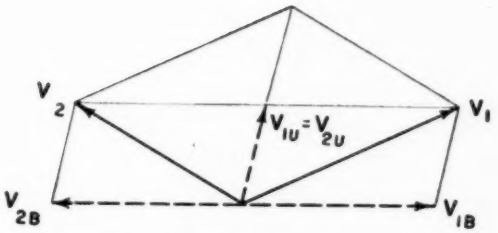

FIG. 1. The components of two unequal voltages.

and the voltage standing-wave ratios are

$$VSWR_1 = \frac{1 + |\Gamma_1|}{1 - |\Gamma_1|}, \quad (11)$$

$$VSWR_2 = \frac{1 + |\Gamma_2|}{1 - |\Gamma_2|}. \quad (12)$$

Defining

$$V_I \equiv A_0, \quad (13)$$

$$V_{BR} \equiv \frac{B_1 + B_2}{2} = B_0, \quad (14)$$

$$V_{UR} \equiv \frac{B_1 - B_2}{2} = C_0 \quad (15)$$

the following equations may be written

$$\frac{V_{BR}}{V_I} = \frac{\Gamma_1}{2} + \frac{\Gamma_2}{2} = \Gamma_1\left(\frac{1}{2} + \frac{1}{2}\frac{\Gamma_2}{\Gamma_1}\right) = \Gamma_1 F \equiv \Gamma_B, \quad (16)$$

$$\frac{V_{UR}}{V_I} = \frac{\Gamma_1}{2} - \frac{\Gamma_2}{2} = \Gamma_1\left(\frac{1}{2} - \frac{1}{2}\frac{\Gamma_2}{\Gamma_1}\right) = \Gamma_1 G \equiv \Gamma_U, \quad (17)$$

where

$$F \equiv \frac{1}{2} + \frac{1}{2}\frac{\Gamma_2}{\Gamma_1}, \quad (18)$$

$$G \equiv \frac{1}{2} - \frac{1}{2}\frac{\Gamma_2}{\Gamma_1}. \quad (19)$$

The quantity Γ_U is actually a "transfer" reflection coefficient since the usual connotation implies that the reflected mode is the same as the incident. The complex parameters F and G can be redefined as:

$$F = \tfrac{1}{2} + \tfrac{1}{2}M\underline{/\alpha} = |F|\underline{/\theta_F}, \quad (20)$$

$$G = \tfrac{1}{2} - \tfrac{1}{2}M\underline{/\alpha} = |G|\underline{/\theta_G}, \quad (21)$$

where

$$M = \frac{|\Gamma_2|}{|\Gamma_1|},$$

$$\alpha = \phi_2 - \phi_1,$$

$$|F| = +\tfrac{1}{2}(1 + M^2 + 2M\cos\alpha)^{\frac{1}{2}}, \quad (22)$$

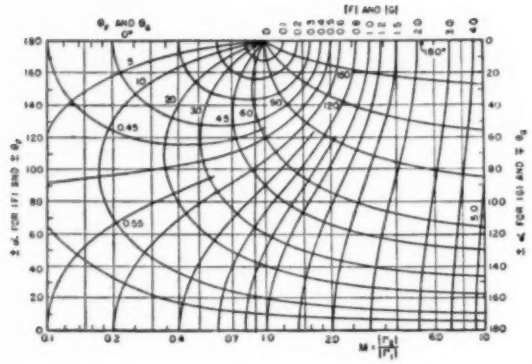

FIG. 2. Parametric plots of $|F|$, $|G|$, θ_F, and θ_G as functions of α and M.

$$|G| = +\tfrac{1}{2}(1+M^2-2M\cos\alpha)^{\frac{1}{2}}, \tag{23}$$

$$\theta_F = \tan^{-1}\frac{M\sin\alpha}{1+M\cos\alpha}, \tag{24}$$

$$\theta_G = \tan^{-1}\frac{-M\sin\alpha}{1-M\cos\alpha}. \tag{25}$$

Orthogonal parametric plots of $|F|$, $|G|$, θ_F and θ_G which are functions of M and α are shown in Fig. 2. Using these plots and Eqs. (16) and (17), the balanced and unbalanced reflected modes can be determined from the measurable quantities $|\Gamma_1|$, $|\Gamma_2|$, ϕ_1, and ϕ_2. It is evident from the plots that there is only one condition for a completely balanced termination: $|\Gamma_1| = |\Gamma_2|$ and $\phi_1 = \phi_2$ simultaneously ($M=1$, $\alpha=0$).

EQUIVALENT TERMINATING IMPEDANCES

From Eqs. (9)–(10) and (16)–(17) it can be seen that the reflections from an unbalanced termination may be represented by either Γ_1 and Γ_2 or Γ_B and Γ_U. Since the termination can be completely represented by two independent impedances related to Γ_1 and Γ_2, a third impedance as required for example in a delta-network is unnecessary. When the generator supplies power in only the balanced mode, Γ_B is a measure of all losses due to both balanced and unbalanced modes. It may be considered incidental if the unbalanced reflected mode propagates along the input line.

COUPLING OF VOLTAGE PROBE TO OPPOSITE LINE

When used on a shielded-pair or two-wire line, a voltage probe will respond to electric fields due to the charges on both conductors. If the coupling to the remote conductor is significant the probe will not yield the true standing-wave distribution on the near conductor. The true reflection coefficients can be determined from the measured reflection coefficients if the "opposite-conductor" coupling is known.

Assuming that the two voltage probes are equally coupled to the shielded-pair line, the effective voltages at the probes are

$$V_1' = A_0(1-K_1)e^{-i\beta X} + B_0(1-K_1)e^{i\beta X} + C_0(1+K_2)e^{i\beta X}, \tag{26}$$

$$V_2' = -A_0(1-K_1)e^{-i\beta X} - B_0(1-K_1)e^{i\beta X} + C_0(1+K_2)e^{i\beta X}, \tag{27}$$

where K_1 = fractional *decrease* caused by coupling of charges of opposite polarity and K_2 = fractional *increase* caused by coupling of charges of same polarity. The modified and measurable reflection coefficients are

$$\Gamma_1' = \frac{B_0(1-K_1)+C_0(1+K_2)}{A_0(1-K_1)} = \Gamma_B + \frac{1}{K_0}\Gamma_U, \tag{28}$$

$$\Gamma_2' = \frac{B_0(1-K_1)-C_0(1+K_2)}{A_0(1-K_1)} = \Gamma_B - \frac{1}{K_0}\Gamma_U, \tag{29}$$

where

$$K_0 \equiv \frac{1-K_1}{1+K_2}. \tag{30}$$

Therefore, the true reflection coefficients are

$$\Gamma_B = \frac{\Gamma_1'+\Gamma_2'}{2} = \Gamma_1'\left(\frac{1}{2}+\frac{1}{2}\frac{\Gamma_2'}{\Gamma_1'}\right), \tag{31}$$

$$\Gamma_U = K_0\frac{\Gamma_1'-\Gamma_2'}{2} = K_0\Gamma_1'\left(\frac{1}{2}-\frac{1}{2}\frac{\Gamma_2'}{\Gamma_1'}\right). \tag{32}$$

Except for the factor K_0 and the primes, the equations are identical to the previous coefficients given in (16)

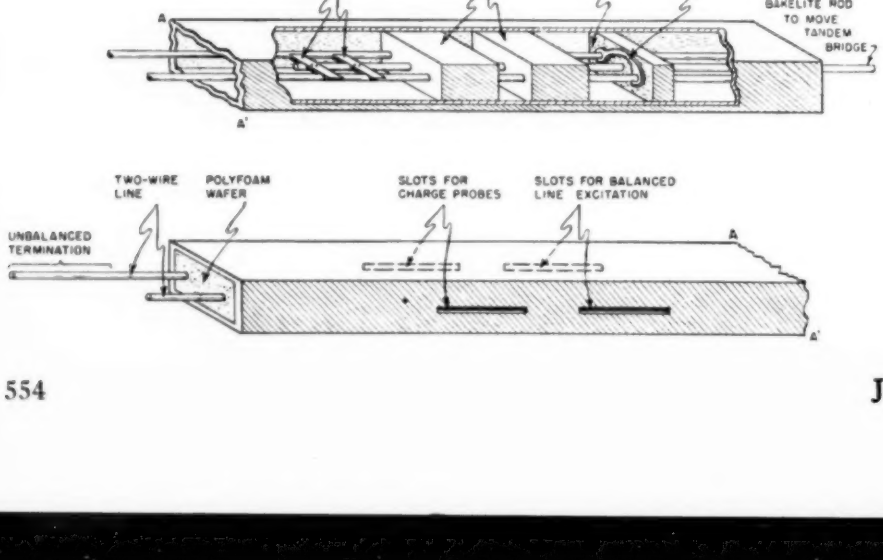

FIG. 3. Slotted shielded-pair transmission line with open end.

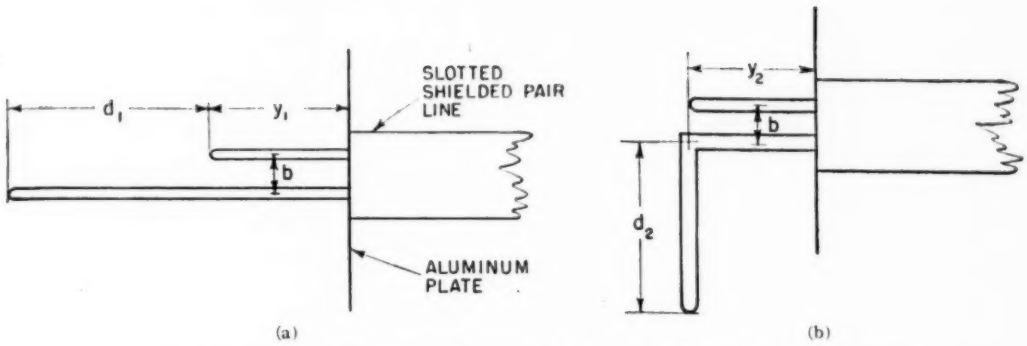

FIG. 4. (a) Collinear end-coupled antenna. (b) Perpendicular end-coupled antenna.

and (17). The quantity K_0 can be determined experimentally. Moreover, in the presence of opposite-conductor coupling, the distribution curves are symmetrical within each half-wave-length.

RATIO OF VOLTAGE MAXIMA

Occasionally the *VSWR* on one conductor may be exceedingly large so that the minimum deflection is masked by the inherent noise of the detector system. For the case of zero incident unbalanced wave, the reflection coefficient on one line is related to both the reflection coefficient of the other line and the ratio of the two voltage maxima. This relationship is written as

$$\frac{|V_{2\,\max}|}{|V_{1\,\max}|}=\frac{|A_0|+|B_2|}{|A_0|+|B_1|}=\frac{1+|\Gamma_2|}{1+|\Gamma_1|}. \tag{33}$$

For a square-law detector, the ratio can be expressed in units of decibel as

$$S_m=40\log_{10}\frac{1+|\Gamma_2|}{1+|\Gamma_1|}\text{db}. \tag{34}$$

For convenience, Eq. (34) can be plotted for parametric values of $|\Gamma_2|$ or $|\Gamma_1|$. The maximum range of S_m is ±12 db. If the measured S_m, $|\Gamma_1|$ and $|\Gamma_2|$ do not satisfy Eq. (34) there exist *both* incident and reflected unbalanced modes.

THE SLOTTED SHIELDED-PAIR LINE

The reflection coefficients of unbalanced terminations were measured on a slotted shielded-pair line. A cutaway view of the measuring line is shown in Fig. 3. The shielded-pair line consists of a standard ½ in.×1 in. *X* band copper wave guide and ⅛ in. O.D. brass inner conductors spaced 0.495 in. between centers. An unbalance squelcher[3] in the generator circuit gave assurance that the balanced mode would be predominantly excited on the line. The 750 mc/sec. r-f signal was amplitude modulated at 1050 c.p.s. With an *SPDT* coaxial switch in the dual charge-probe circuit, standing-wave distributions could be measured on either conductor.[4] From an unbalanced termination the reflected balanced mode does not proceed beyond the tandem bridge, however, the reflected unbalanced mode is completely absorbed at the matched load provided by the Aquadag termination and two quarter-wave-length polystyrene slugs.[5]

With the inner conductors supported only by Polyfoam wafers, the characteristic impedances of the two modes of transmission were determined by measuring capacitances at an audiofrequency.[4] The measured characteristic impedances of the air-dielectric line for the balanced mode was $R_{CB}=165$ ohms and for the unbalanced mode $R_{CU}=39.3$ ohms. The opposite-conductor coupling was also determined under the same conditions in the following way. The line conductor to which the probe is coupled is connected to one output terminal of the audio oscillator. The second line conductor can be connected to either of two potentials: (a) to the other

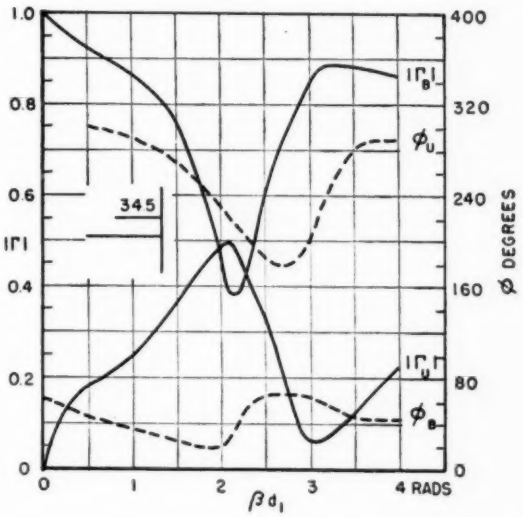

FIG. 5. Γ_B and Γ_U for a collinear end-coupled antenna when $y_1=34.5$ cm.

[3] K. Tomiyasu, Rev. Sci. Inst. **19**, 675–677 (1948).

[4] K. Tomiyasu, Cruft Laboratory Technical Report No. 86, Harvard University (September 6, 1949).

[5] K. Tomiyasu, "Double-slug impedance matching," Cruft Laboratory Technical Memorandum No. 6, Harvard University (August 1, 1949).

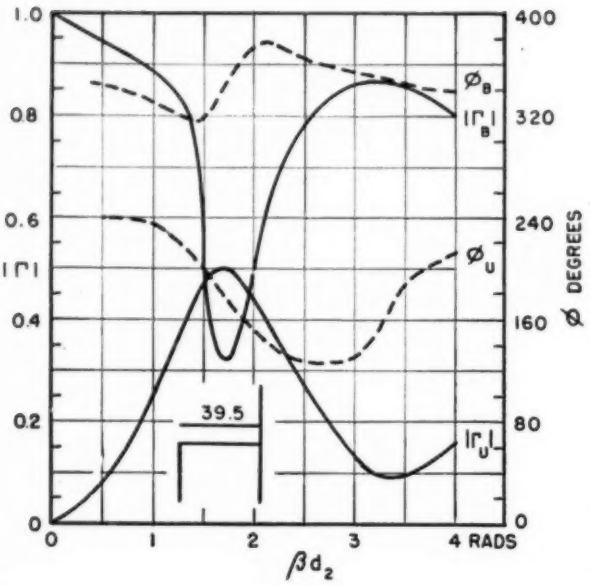

FIG. 6. Γ_B and Γ_U for a perpendicular end-coupled antenna when $y_2 = 39.5$ cm.

output terminal of the oscillator; or (b) to the same terminal. The shield is connected to the center tap of the oscillator output. The quantity K_0 in Eq. (30) is the ratio of the deflections when connections (a) and (b) are made in that order. For the experimental line, K_0 was found to be equal to unity, signifying that each conductor provided a very effective shield from electric fields due to charges on the other line.

This measuring line was rather difficult to operate. The probe couplings for example were not constant for the lengths of the slots. The optimum conditions for line excitation could not be maintained throughout. Due to the several sources of error the experimental data cannot be considered accurate but are included to show representative information.

UNBALANCED RADIATIVE TERMINATIONS

The reflected balanced and unbalanced components of voltages were measured for two types of unbalanced end-coupled antennas, *viz.*, collinear (or extended) antenna, and perpendicular antenna. This is shown in Fig. 4. For various fixed values of y_1 and y_2, "antenna" lengths d_1 and d_2 were varied by inserting threaded sections. The ends of the $\frac{1}{8}$-in. O.D. brass conductors were semispherical in shape. The $\frac{1}{32}$-in. thick 40×42.3-cm aluminum plate minimized the currents on the outside of the slotted line.

In Figs. 5 and 6, Γ_B and Γ_U are plotted for two different structures as a function of "antenna" lengths. These are the *apparent* reflection coefficients of the unbalanced terminations having a reference plane $\lambda/2$ from the aluminum plate. The simultaneous increase in $|\Gamma_U|$ with decrease in $|\Gamma_B|$ implies that additional balanced-mode power is necessary to supply the unbalanced-mode losses. It can be seen that a minimum of $|\Gamma_U|$ occurs when the antenna length is near $\lambda/2$.

Shear Stress in a Turbulent Boundary Layer*

DONALD ROSS AND J. M. ROBERTSON
Ordnance Research Laboratory, The Pennsylvania State College, State College, Pennsylvania
(Received December 9, 1949)

The method initiated by Fediaevsky for evaluating the shear stress distribution in a turbulent boundary layer under the action of an adverse pressure gradient is improved upon. Use is made of a more suitable polynomial and boundary conditions which include the concept that the turbulence which produces the shear at any point has its origin at the surface upstream from its present location. This "history" theory predicts that the transverse shear gradient in the outer portion of the boundary layer remains constant as the boundary layer develops. Comparison with shear distributions measured at the National Bureau of Standards along a simulated airfoil shows good qualitative agreement and appreciable improvement over Fediaevsky's theory.

INTRODUCTION

IN analyzing the flow of a fluid in a diffuser, along the surface of an airfoil, or along the after portion of a streamlined body, the major problem is the evaluation of the effect of the adverse pressure gradient on the flow conditions in the boundary layer. The critical feature of these flows is the occurrence of separation, which results in high losses and other deleterious effects. Despite the common occurrence of this type of incompressible, turbulent boundary-layer flow, the physics of adverse-pressure-gradient effects is still incompletely understood. Undoubtedly, the ultimate solution of this problem will involve a statistical theory of turbulence, but a reasonably useful theory can be developed through the use of the older methods based on the mean motion. The objective of any boundary layer theory is the prediction of the rate of growth of and distribution of the velocity in the boundary layer. As the growth can be found from the von Karman momentum equation if the shapes of the velocity profiles are known, the problem reduces to the prediction of the velocity distributions.

Various researchers have shown that the velocity profiles can be characterized by single form parameters. However, attempts to correlate these parameters with local flow conditions have not been particularly successful. Thus, the methods of analysis developed by Buri[1] and Gruschwitz[2] have only limited application, and they do not appear to be fundamentally sound.[3,4] More recent analyses,[4,5] based on empirical relations for the rate of change of the velocity form parameter, are more successful. In none of these methods, however, is an attempt made to understand the inner mechanics of the flow phenomena.

As the velocity variation in a boundary layer is a result of turbulent shearing motions, a more fundamental understanding of the problem should evolve from a study of shear stress distributions and the origin of the shear. A first attempt at a shear stress theory was made by Fediaevsky[6] in Russia in 1936. He expressed the shear stress as a power series, with the coefficients evaluated in terms of boundary conditions. Comparison of his shear stress profiles with experiment has indicated serious discrepancies; but in spite of this, the method seems so fundamental that the discrepancies may probably be attributed to the boundary assumptions. The shear stress theory presented in this paper, although

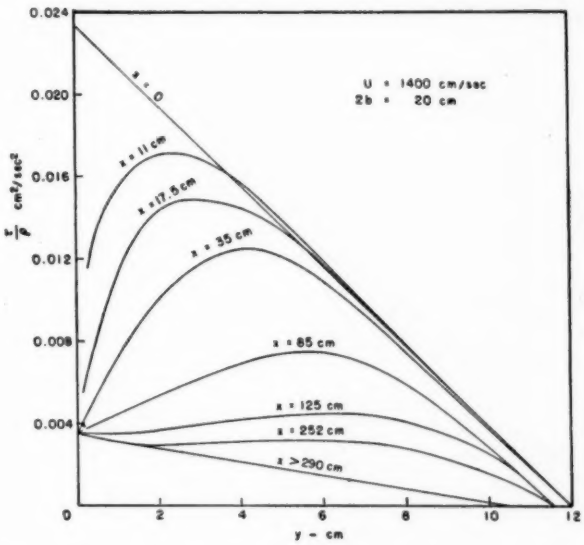

FIG. 1. Shear stress profiles obtained by Jacobs for flow over a smooth surface preceded by a rough surface.

* Work done under Navy Contract NOrd 7958, in connection with the diffuser design for the new water tunnel at The Pennsylvania State College.

[1] A. Buri, "A Method of Calculation for the Turbulent Boundary Layer with Accelerated and Retarded Basic Flow," Thesis No. 652, 1931, Federal Technical College, Zurich Trans. in R.T.P. Translation No. 2073, British Ministry of Aircraft Production.

[2] E. Gruschwitz, Ingenieur-Archiv **2**, 321 (1931). E. Gruschwitz, Zeits. f. Flugtechnik und Motorluftschiffahrt **23** (1932), translated in NACA Tech. Memo 699, 1933.

[3] H. Peters, J. Aero. Sci. **3**, 7 (1935).

[4] A. E. von Doenhoff and N. Tetervin, "Determination of General Relations for the Behavior of Turbulent Boundary Layers," NACA Report No. 772, 1943 (also NACA Wartime Report L382, ACR No. 3G13, July 1943).

[5] H. C. Garner, "The Development of Turbulent Boundary Layers," ARC R & M 2133, 1944.

[6] K. Fediaevsky, "Turbulent Boundary Layer of an Airfoil," Report 282 Central Aero-Hydrodynamical Institute, Moscow, 1936. Trans. in NACA Tech. Memo 822, 1937, also J. Aero. Sci. **4**, 491 (1937).

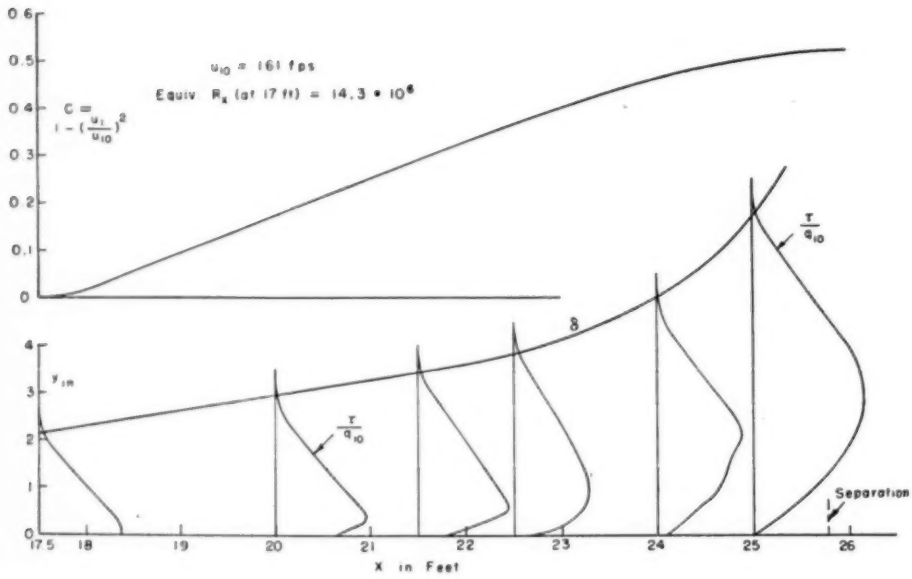

FIG. 2. Shear profiles obtained at the National Bureau of Standards for flow in an adverse pressure gradient. Upper figure shows corresponding pressure regain coefficient. u_1 = velocity just outside boundary layer, u_{10} = initial value of u_1 at start of pressure gradient, $q_{10} = \frac{1}{2}\rho u_{10}^2$.

inspired by Fediaevsky's work, differs from it in several important respects.

FEDIAEVSKY'S THEORY

Fediaevsky[6] used a rational method for determining the form of the velocity distribution for two-dimensional boundary layers from expressions for the shear stress and mixing length distribution. He expressed the transverse form of the shear stress as a power series:

$$\tau/\tau_w = A_0 + A_1(y/\delta) + A_2(y/\delta)^2 + A_3(y/\delta)^3 + \cdots, \quad (1)$$

where τ is the local turbulent shear, τ_w is the wall shear stress, y is the distance from the wall, δ is the disturbance thickness of the boundary layer. He evaluated the coefficients of the first few terms by applying the boundary conditions which must hold at the solid surface and at the outer edge of the boundary layer. At the wall ($y=0$), the function and its first derivative are defined by the following conditions:

(1) $\tau = \tau_w$ by definition of τ_w,
(2) $\partial\tau/\partial y = dp/dx$ from the momentum equation written for the wall streamline.

At the outer edge of the layer ($y=\delta$),

(3) $\tau = 0$ by definition of δ,
(4) $\partial\tau/\partial y = 0$ from the assumption that the derivative with respect to x of the total head is a continuous function.

The derivative of the momentum equation for the wall streamline yields a fifth condition:

(5) $\partial^2\tau/\partial y^2 = 0$ at $y=0$.

By assuming that only the first three conditions are significant, Fediaevsky evaluated the coefficients for a quadratic and obtained

$$\tau/\tau_w = 1+(\delta/\tau_w)(dp/dx)(y/\delta) - [1+(\delta/\tau_w)(dp/dx)](y/\delta)^2, \quad (2)$$

while by assuming all five conditions, he obtained the quartic

$$\tau/\tau_w = 1+(\delta/\tau_w)(dp/dx)(y/\delta) - [4+3(\delta/\tau_w)(dp/dx)](y/\delta)^3 + [3+2(\delta/\tau_w)(dp/dx)](y/\delta)^4. \quad (3)$$

Although Fediaevsky states that he found fair agreement between his theory and the experimental data of Gruschwitz,[2] Dryden[7] found poor correlation with data obtained at the National Bureau of Standards.

ORIGIN OF SHEAR STRESS

One of the shortcomings of Fediaevsky's theory is its failure to consider the origin of the turbulent motions causing the shear and the ensuing mechanism of transfer. For the case of flow with zero or small pressure gradients, the flow conditions and the wall shear stress do not vary significantly in the direction of flow, and one can correlate the entire boundary layer distribution with local conditions. However, when the flow conditions vary, as in a diffuser or along an airfoil surface, this simple correlation does not hold. The motions which cause the shear forces originate at the wall and are diffused into the fluid stream through the action of turbulence. As this diffusion occurs relative to the moving fluid, the shear at any point in the boundary layer has its origin at a point on the surface upstream from its present location. Thus, the shear in the outer boundary layer region is governed by the previous history of the flow, while near the solid surface, local conditions control.

[7] H. L. Dryden, "Some recent contributions to the study of transition and turbulent boundary layers," NACA Technical Note 1168 (April, 1947).

TABLE I. History theory assumed shear stress boundary conditions.

Quantity	at $y=0$		at $y=\delta$	
τ	τ_w	(1)	0	(2)
$\partial\tau/\partial y$	dp/dx	(3)	$-(\tau_{w_0}/\delta_0)^*$	(4)
$\partial^2\tau/\partial y^2$	0	(5)	—	

* Differs from Fediaevsky's Theory (subscript 0 refers to initial conditions).

The concept of the effect of space-history on the flow in the outer region of a boundary layer was proposed by Schultz-Grunow[8] and was suggested by the experiments of Jacobs.[9] Jacobs measured the change in the velocity profile along a smooth surface preceded by a rough surface. An analysis of these profiles yielded the shear stress distributions at several stations. As shown in Fig. 1, Jacobs found that the shear stress gradient in the outer portion of the boundary layer retained the value which it had had over the rough surface for a considerable distance along the smooth surface, while the wall shear fell almost immediately to its smooth-surface value. Jacobs also studied the flow from a smooth to a rough surface, and he again found that the upstream shear stress gradient persisted for a considerable distance, the rough-surface shear gradually being diffused across the boundary layer as the flow proceeded downstream. As noted by Schultz-Grunow, these experiments clearly establish the importance of the history of the flow.

Recent studies on the flow along the surface of a large simulated airfoil were made in the wind tunnel at the National Bureau of Standards and were reported by Dryden.[7] In these experiments, the shear stresses were measured more directly with hot wires. The manner in which the NBS shear stress profiles vary in the adverse pressure gradient is shown in Fig. 2. The slope of the

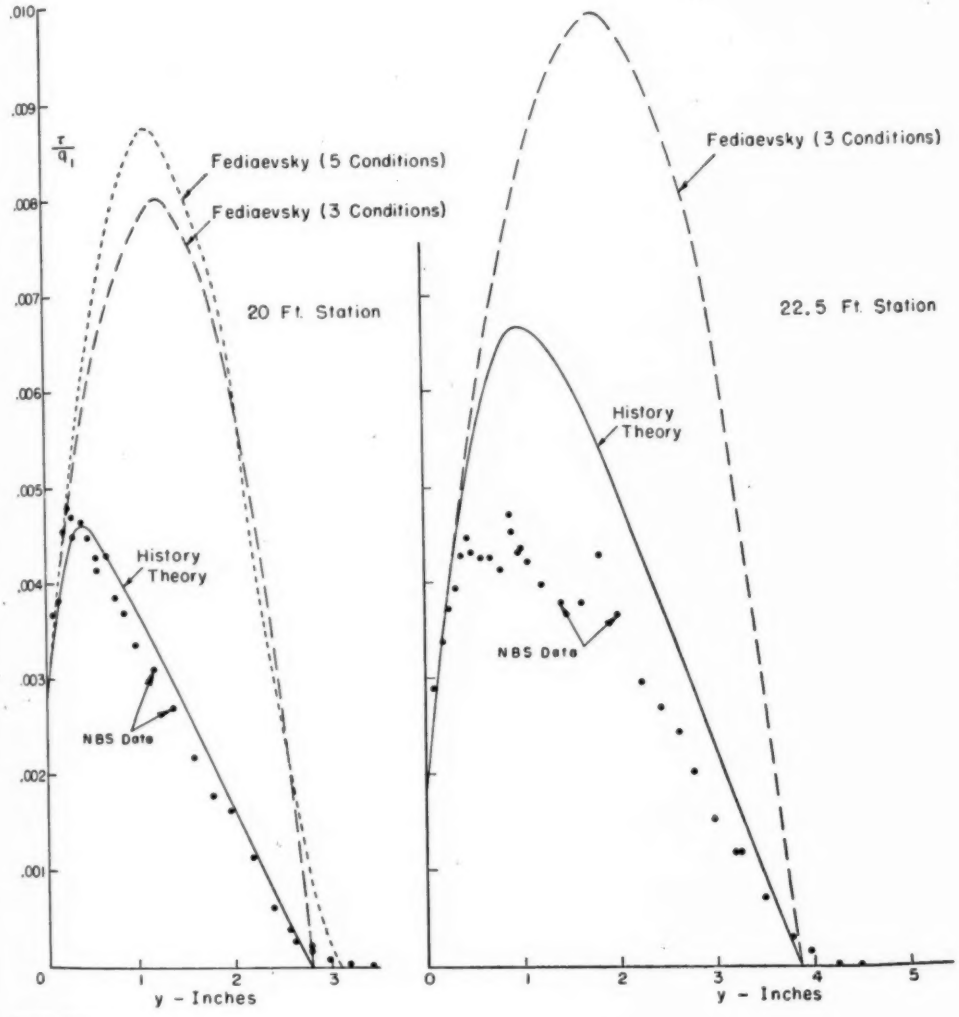

FIG. 3. Comparison of History and Fediaevsky theories with NBS experimental shear measurements for locations near the beginning of the adverse pressure gradient and midway toward separation.

[8] F. Schultz-Grunow, "Über das Nachwirken der Turbulenz bei Örtlich und Zeitlich Verzögerter Grenzschichtströmung," Proc. 5th Int. Cong. Appl. Mech., Cambridge, Massachusetts (1938), pp. 428–435.
[9] W. Jacobs, Zeits. f. angew. Math. u. Mech. **19**, (1939). Translated in NACA Tech. Memo 951 (1940).

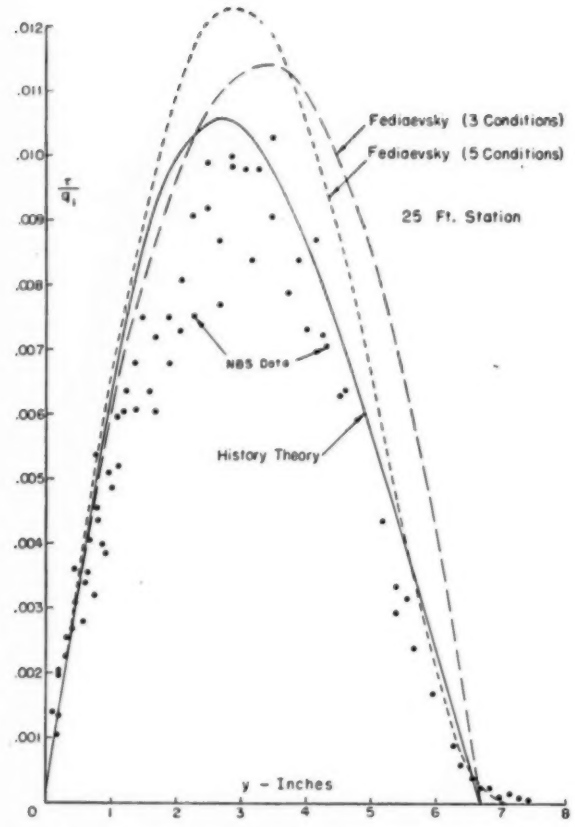

FIG. 4. Comparison of History and Fediaevsky theories with NBS data for station near separation.

shear at the start of the pressure gradient is seen to be carried along in the outer portion of the boundary layer, in qualitative agreement with the history concept.

THE HISTORY THEORY

A theory for the shear stress distribution in a turbulent boundary layer can be derived in a manner similar to that of Fediaevsky but taking into account the space-history effect. Thus, four of the five assumed boundary conditions on the shear stress function presented in Table I agree with those of Fediaevsky. Only the fourth condition, which is for the first derivative of the shear stress function at the outer edge, differs from his assumption. The derivative of the shear stress function is actually zero at the outer limit of the boundary layer, as assumed by Fediaevsky; however, as a polynomial having only a few terms is to be used, the value of the slope over a larger region should be considered. This condition for the slope of the shear stress function at the outer edge of the boundary layer should express the history concept, namely that the slope should have the same value as it had at the beginning of the adverse pressure gradient, where the shear curve is essentially linear.[10] The subscript zeros in condition 4 refer to values at the beginning of the pressure gradient.

As the predominant term in the shear stress function is the linear history term, the shear stress is expressed as a polynomial in terms of the distance from the edge of the boundary layer. To give flexibility to the shape of the curve, while using only a few terms, a function with adjustable exponent has been chosen:

$$\tau = a_0 + a_1[1-(y/\delta)] + a_n[1-(y/\delta)]^n + a_{n+1}[1-(y/\delta)]^{n+1}. \quad (4)$$

Using conditions 1 through 4, the coefficients may be evaluated in terms of the known flow parameters and the exponent n:

$$a_0 = 0,$$
$$a_1 = \tau_{w0}(\delta/\delta_0),$$
$$a_n = (n+1)\tau_w + \delta(dp/dx) - n\tau_{w0}(\delta/\delta_0),$$
$$a_{n+1} = -[n\tau_w + \delta(dp/dx) - (n-1)\tau_{w0}(\delta/\delta_0)].$$

The value of the exponent n may then be fixed from condition 5, yielding

$$n = \frac{2\delta(d\rho/dx) + \tau_{w0}(\delta/\delta_0) + \tau_w}{\tau_{w0}(\delta/\delta_0) - \tau_w}. \quad (5)$$

The resultant expression for the shear stress distribution is

$$\tau = \tau_w(\delta/\delta_0)[1-(y/\delta)] - [\delta(dp/dx) + \tau_{w0}(\delta/\delta_0)] \times [1-(y/\delta)]^n + [\delta(dp/dx) + \tau_w][1-(y/\delta)]^{n+1}, \quad (6)$$

where n is given by (5). At the start of a region of adverse pressure gradient, the exponent n is very large and the equations yield an essentially linear shear profile. As the boundary layer grows, the exponent decreases and the linear term is relegated to the outer portion of the boundary layer. In this manner, the space-history effect governs the essential characteristics of the shear stress distributions.

EXPERIMENTAL CONFIRMATION

A quantitative check of the history theory can be made by comparison with the shear stress data measured at the National Bureau of Standards[7] and introduced in Fig. 2. Detailed comparisons for stations near the beginning of the adverse pressure gradient, near separation, and midway are shown in Figs. 3 and 4. In each case, the results of the Fediaevsky theory are included for comparison. In these figures, the shear stress is expressed in terms of q_1, the dynamic pressure at the edge of the boundary layer, while in Fig. 2, the initial dynamic pressure q_{10} was used. Near the beginning (20-foot station), the agreement is excellent, and the improvement over Fediaevsky's theory is striking. At the second location (22.5 feet), the history theory is not such a good fit, but is a considerable improvement over the older theory. Although both theories agree reasonably well with experiment near separation (Fig. 4), the

[10] This involves a discontinuity in the shear stress and velocity distributions at the outer edge of the boundary layer. As in the case of the turbulent boundary layer along a flat plate, this discontinuity does not introduce any gross discrepancies.

history theory offers only a small improvement. From this limited comparison, it is apparent that the history theory gives reasonable agreement with experiment, especially in the beginning of the adverse pressure gradient where the older theory was most unsatisfactory.

In obtaining the theoretical shear stress distributions shown in Figs. 3 and 4, experimental values of the boundary layer thickness and the wall shear stress had to be used. Near the beginning of the pressure gradient, the wall shear has essentially the flat-plate value, whereas at separation the value is zero. For completeness, a theory is needed which will yield the local wall shear in terms of its initial value and the other flow parameters.

SUMMARY

A satisfactory theory for the shear stress distribution in a turbulent boundary layer has been developed from consideration of the space-history of the turbulence. This theory evolved from Jacobs' observations that the shear stress gradient in the outer portion of the boundary layer is constant, even when the external flow conditions vary in the direction of flow. Following Fediaevsky's method, boundary values are used to determine the coefficients of an arbitrary polynomial. The theory yields a linear shear profile at the beginning of the adverse pressure gradient; and as the boundary layer progresses, this linear characteristic is relegated to the outer part and the shear in the inner region is determined by local conditions. Comparison with shear measurements made at the National Bureau of Standards shows good agreement and appreciable improvement over Fediaevsky's theory. A more complete theory of the shear variation in a boundary layer under an adverse pressure gradient should consider turbulence decay and should also evaluate the wall shear stress.

Propagation of the TM_{01} Mode in a Metal Tube Containing an Imperfect Dielectric*

DAVID L. HETRICK

Department of Physics, Rensselaer Polytechnic Institute, Troy, New York

(Received September 20, 1949)

The TM_{01} mode in a circular dielectric-filled wave guide, where dielectric losses and metal wall losses are considered simultaneously, is analyzed from the viewpoint of the boundary value problem. General expressions for the attenuation and phase constant are obtained, and the percentage errors introduced by (1) neglect of wall losses and (2) assumption that the total attenuation is the sum of dielectric attenuation and approximate wall loss attenuation are computed for a particular case.

INTRODUCTION

THE problem of the propagation of electromagnetic waves in a uniform metal tube has usually been solved for the case where the metal of the tube itself is approximated by a perfect conductor. Even when losses in the enclosed dielectric are considered by retaining the imaginary part of the complex dielectric constant, the analysis does not become difficult.

When losses arising from the penetration of the fields into the metal sheath are to be taken into account, two approaches are available. One may assume that the field configurations are not appreciably altered from those obtained with perfect walls, and, knowing the intrinsic impedance of the bounding medium, compute the power loss and attenuation. The total attenuation is then taken to be the sum of attenuations arising from dielectric losses and wall losses separately.

The more general approach is the boundary value problem wherein the continuity of tangential fields leads to expressions for the attenuation and phase constant. Again, certain approximations are necessary, but these have negligible effect on the accuracy of the results. Insofar as the author is aware, the solution as a boundary value problem has not been carried out previously where dielectric losses and wall losses are considered simultaneously. The object of this investigation is to obtain general expressions for the attenuation and phase constant and to show for a particular case how the results differ from those obtained when (1) the wall losses are neglected and (2) the total attenuation is taken to be the sum of dielectric attenuation and approximate wall loss attenuation. For simplicity, only the circularly symmetric TM mode is considered.

The method followed was first employed by Carson, Mead, and Schelkunoff,[1] and by Barrow.[2] This phase of the problem was investigated in more detail by Linder,[3] though only the wall losses for an air-filled guide were considered in these papers. Recently[4–8] several papers

* Based on a thesis submitted to the Department of Physics of Rensselaer Polytechnic Institute in partial fulfillment of the requirements for the M.S. degree.

[1] Carson, Mead, and Schelkunoff, Bell Sys. Tech. J. **15**, 310–333 (1936).
[2] W. L. Barrow, Proc. I.R.E. **24**, 1298–1329 (1936).
[3] E. G. Linder, Proc. I.R.E. **30**, 554–556 (1942).
[4] W. P. Conner and C. P. Smyth, J. Am. Chem. Soc. **65**, 382–389 (1943).
[5] J. G. Powles, Trans. Faraday Soc. **44**, 537–545 (1948).
[6] W. H. Surber, Jr., J. App. Phys. **19**, 514–523 (1948).
[7] Heston, Hennelly, and Smyth, J. Am. Chem. Soc. **70**, 4093–4096 (1948).
[8] H. L. Laquer and C. P. Smyth, J. Am. Chem. Soc. **70**, 4097–4101 (1948).

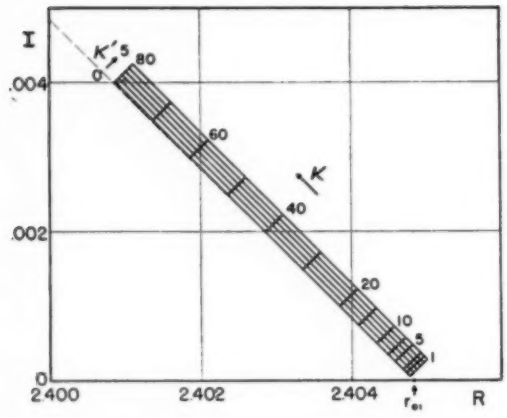

FIG. 1. Curves of constant κ and κ' in the complex ρ_1 plane; $\lambda_0/a=2\pi$, and a free-space wave-length of 1 cm is assumed.

have been published discussing the use of wave guide methods in measuring complex dielectric constants. It is important to know how great an error is introduced into the results when the wall losses are neglected, particularly if these results are to be used in deducing the structures of complex organic molecules.

THE BOUNDARY EQUATION

The fields whose continuity must be preserved at the walls of the wave guide may be expressed as[9] (MKS units)

$$E_{1z}=Ak_1^2J_0(k_1r)\exp(j\omega t-\gamma z), \tag{1}$$

$$E_{2z}=Bk_2^2H_0^{(1)}(k_2r)\exp(j\omega t-\gamma z), \tag{2}$$

$$H_{1\phi}=j\omega\epsilon_{c1}Ak_1J_1(k_1r)\exp(j\omega t-\gamma z), \tag{3}$$

$$H_{2\phi}=j\omega\epsilon_{c2}Bk_2H_1^{(1)}(k_2r)\exp(j\omega t-\gamma z), \tag{4}$$

where

$$k^2=\gamma^2-j\omega\mu(\sigma+j\omega\epsilon), \tag{5}$$

and the propagation constant γ is

$$\gamma=\alpha+j\beta=\alpha+j(2\pi/\lambda).$$

The subscripts 1 and 2 refer to the enclosed dielectric and the metal sheath respectively. These are taken to be regions containing no free charges and having conductivity σ, permittivity ϵ, and permeability μ; α is the attenuation constant, β the phase constant, λ the guide wave-length, ω the angular frequency $2\pi\nu$, A and B arbitrary constants, $J_n(kr)$ and $H_n^{(1)}(kr)$ the Bessel function and Hankel function of the first kind respectively. The complex permittivity ϵ_c is defined as

$$\epsilon_c=\epsilon-j\sigma/\omega. \tag{6}$$

Cylindrical co-ordinates r, ϕ, and z are employed, where z is the direction of the wave guide axis.

Note that $\gamma_1=\gamma_2$ in order to satisfy the boundary conditions for all z and t. The argument kr must be taken as having a positive imaginary part; it can be shown that this leads to no loss of generality.

With the use of Eq. (5), assuming $\mu_1=\mu_0$,

$$k_1=[\gamma^2+(2\pi/\lambda_0)^2(\kappa-j\kappa')]^{\frac{1}{2}} \tag{7}$$

where $\kappa=\epsilon/\epsilon_0$, $\kappa'=\sigma_1/\omega\epsilon_0$, and λ_0 is the free-space wave-length. In the metal, $\omega\mu_2\sigma_2\gg\gamma^2$ and $\omega\mu_2\sigma_2\gg\omega^2\mu_2\epsilon_2$. Assuming $\mu_2=\mu_0$,

$$k_2=2\pi/\lambda_0[-j\sigma_2/\omega\epsilon_0]^{\frac{1}{2}}. \tag{8}$$

Setting $\rho_1=k_1a$ and $\rho_2=k_2a$, where a is the inner radius of the metal sheath, one obtains from the continuity of tangential fields at the boundary

$$\frac{\epsilon_{c1}J_1(\rho_1)}{\rho_1J_0(\rho_1)}=\frac{\epsilon_{c2}H_1^{(1)}(\rho_2)}{\rho_2H_0^{(1)}(\rho_2)}. \tag{9}$$

This condition is sufficient to determine the constants of propagation. In general, a superposition of *TM* and *TE* waves is necessary to satisfy the boundary conditions, but in the circularly symmetric case no new mode is introduced.[9]

The values of ρ_2 justify the use of the asymptotic expansion[10]

$$H_1^{(1)}(\rho_2)/H_0^{(1)}(\rho_2)=e^{-j\pi/2}. \tag{10}$$

Replacing ϵ_{c1}/ϵ_0 by κ_c, and making use of Eqs. (6), (8),

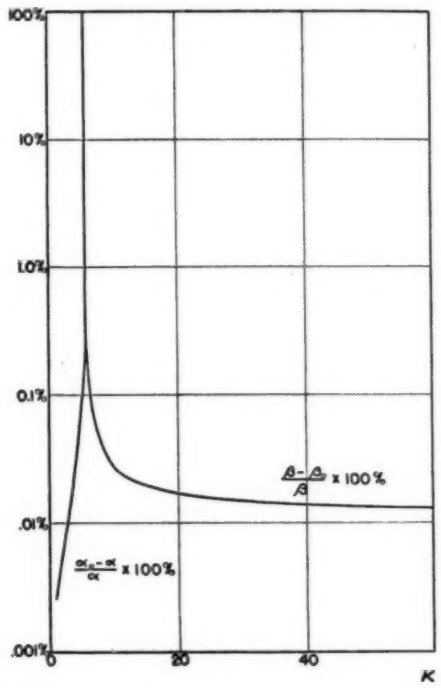

FIG. 2. Percentage errors in attenuation and phase constant introduced when metal wall losses are neglected; $\lambda_0/a=2\pi$ and $\kappa'=0$.

[9] J. A. Stratton, *Electromagnetic Theory* (McGraw-Hill Book Company, Inc., New York, 1941), p. 521 *et seq.*

[10] R. I. Sarbacher and W. A. Edson, *Hyper and Ultrahigh Frequency Engineering* (John Wiley & Sons, Inc., New York, 1943), p. 231 *et seq.*

and (10), Eq. (9) becomes

$$\frac{\kappa_c J_1(\rho_1)}{\rho_1 J_0(\rho_1)}=\frac{\lambda_0}{2\pi a}\left[\frac{\sigma_2}{2\omega\epsilon_0}\right]^{\frac{1}{2}}(1+j). \tag{11}$$

Since $\kappa_c=\kappa-j\kappa'$, divide by κ_c to obtain

$$J_1(\rho_1)/\rho_1 J_0(\rho_1)=c+jd \tag{12}$$

where

$$c=\frac{\lambda_0}{2\pi a}\left[\frac{\sigma_2}{2\omega\epsilon_0}\right]^{\frac{1}{2}}\frac{\kappa-\kappa'}{\kappa^2+\kappa'^2} \tag{13}$$

and

$$d=\frac{\lambda_0}{2\pi a}\left[\frac{\sigma_2}{2\omega\epsilon_0}\right]^{\frac{1}{2}}\frac{\kappa+\kappa'}{\kappa^2+\kappa'^2}. \tag{14}$$

In order to solve Eq. (12) for ρ_1, replace the Bessel functions by the first two terms of their complex Taylor series expansions

$$J_1(\rho_1)=J_1(r_{01})+(\rho_1-r_{01})J_1'(r_{01})+\cdots,$$
$$J_0(\rho_1)=J_0(r_{01})+(\rho_1-r_{01})J_0'(r_{01})+\cdots,$$

where $r_{01}=2.404,825,558$, the root[11] of rank one of $J_0(k_1 a)=0$, and the limiting value of ρ_1 as σ_2 becomes infinite.[10] This yields expressions for the TM_{01} mode.

One obtains a quadratic

$$[c+jd]\rho_1^2-[(r_{01}c+1/r_{01})+jr_{01}d]\rho_1+2=0 \tag{15}$$

having the solution

$$\rho_1=R+jI, \tag{16}$$

where

$$R=\frac{r_{01}}{2}+\frac{c}{2r_{01}(c^2+d^2)}+\left[\frac{L}{2}+\frac{1}{2}(L^2+M^2)^{\frac{1}{2}}\right]^{\frac{1}{2}}, \tag{17}$$

$$I=-\frac{d}{2r_{01}(c^2+d^2)}+\left[-\frac{L}{2}+\frac{1}{2}(L^2+M^2)^{\frac{1}{2}}\right]^{\frac{1}{2}}, \tag{18}$$

$$L=\frac{r_{01}^2}{4}+\frac{c^2-d^2-6cr_{01}^2(c^2+d^2)}{4r_{01}^2(c^2+d^2)^2}, \tag{19}$$

$$M=\frac{3dr_{01}^2(c^2+d^2)-dc}{2r_{01}^2(c^2+d^2)^2}, \tag{20}$$

and c and d are defined by Eqs. (13) and (14).

The ambiguity in sign arising in the solution of the quadratic is removed by observing the effect of allowing σ_2 to increase without limit. The sign has been chosen so that $\rho_1\to r_{01}$; the alternative leads to the impossibility $\rho_1\to 0$.

Figure 1 is a typical set of curves of constant κ and κ' in the complex ρ_1 plane showing the departure from the case of perfect walls. The curves are for a copper tube, assuming a free-space wave-length of 1 cm and a ratio $\lambda_0/a=2\pi$. Note that the curve for $\kappa'=0$, when extended, passes through the point $R=r_{01}$, $I=0$. For $I<0.002$, the curves of constant κ' approach straight lines.

[11] Gray, Mathews, and MacRobert, *A Treatise on Bessel Functions* (MacMillan & Company, London, 1922), p. 244.

ATTENUATION AND PHASE CONSTANT

From Eq. (7),

$$\rho_1^2=(R+jI)^2=a^2[(\alpha+j\beta)^2+(2\pi/\lambda_0)^2(\kappa-j\kappa')].$$

Equating real and imaginary parts, a quadratic in $(a\alpha)^2$ is obtained. Choosing only positive real values for α, one obtains

$$a\alpha=2^{-\frac{1}{2}}[q_1+(q_1^2+q_2^2)^{\frac{1}{2}}]^{\frac{1}{2}}, \tag{21}$$

where

$$q_1=R^2-I^2-(2\pi a/\lambda_0)^2\kappa,$$
$$q_2=2RI+(2\pi a/\lambda_0)^2\kappa'.$$

The phase constant is given by

$$a\beta=q_2/2a\alpha. \tag{22}$$

Equations (21) and (22) will be convenient for numerical computations only in the "region of attenuation" where $(\lambda_0/a)\kappa^{-\frac{1}{2}}>2\pi/r_{01}$. In the "region of propagation" a quadratic in $(a\beta)^2$ yields

$$a\beta=2^{-\frac{1}{2}}[-q_1+(q_1^2+q_2^2)^{\frac{1}{2}}]^{\frac{1}{2}}. \tag{23}$$

Once the phase constant is known from Eq. (23), Eq. (22) may be employed to obtain the attenuation.

In the limiting case of perfectly conducting walls where $R\to r_{01}$ and $I\to 0$, these general expressions yield the attenuation and phase constant for the case of dielectric loss only. If, in addition, $\kappa'\to 0$, one obtains the expressions for the completely lossless case.[10]

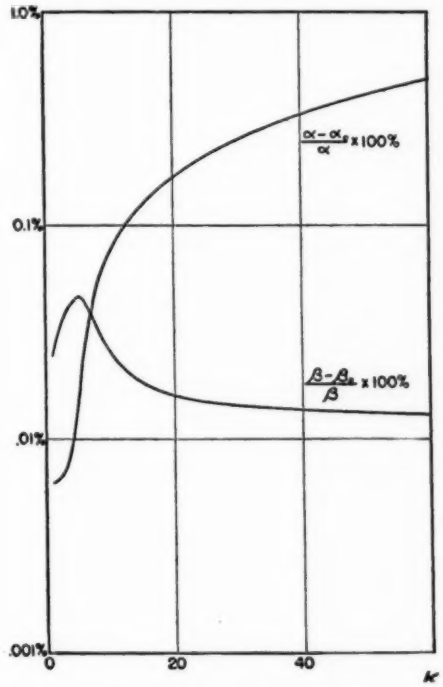

FIG. 3. Percentage errors in attenuation and phase constant introduced when metal wall losses are neglected; $\lambda_0/a=2\pi$ and $\kappa'=3$.

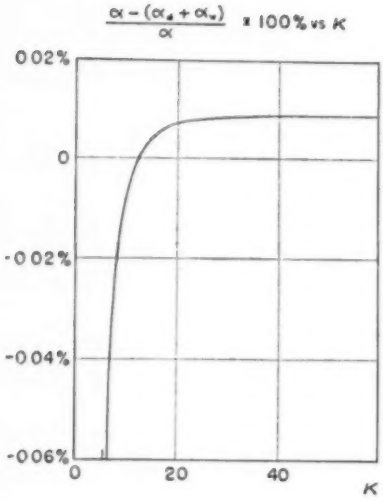

FIG. 4. Percentage error in attenuation introduced by assuming $\alpha=\alpha_d+\alpha_w$; $\lambda_0/a=2\pi$ and $\kappa'=3$.

NUMERICAL RESULTS

The percentage errors in attenuation and phase constant introduced by neglecting wall losses are shown in Figs. 2 and 3, where $\kappa'=0$ and 3 respectively. The subscript 0 on α and β denotes the completely lossless case, and the subscript d denotes values obtained from Eqs. (21) through (23) for dielectric loss only. Values obtained from these equations when wall losses are included are indicated without subscripts. The critical point, or transition from attenuation to propagation for the lossless guide, is found at $\kappa=5.78$ for the case chosen.

The errors arising from the assumption that the total attenuation is $\alpha_d+\alpha_w$, where α_w represents the approximate wall loss attenuation as computed from power flow considerations,[10] are shown in Fig. 4.

Two remarkable effects will be noted. In Fig. 2, where no dielectric loss is present, the attenuation decreases when wall losses are added; $\alpha_0>\alpha$. This seems contrary to expectation at first glance. A qualitative explanation may be offered as follows: α_0 is a purely reactive attenuation. When wall losses are added, the penetration of the fields into the metal causes an effective change in the field configuration which reduces the reactive attenuation. This is evidently more than enough to compensate for the resistive attenuation caused by the metal walls.

The second interesting effect is that the error curve in Fig. 4 changes sign; there is one value of κ for which $\alpha=\alpha_d+\alpha_w$ exactly.

While these curves apply to a specific set of parameters, one may conclude in general that the assumption $\alpha=\alpha_d+\alpha_w$ is an excellent approximation anywhere in the "region of propagation" except in the immediate neighborhood of the critical point; the relative error in attenuation remains of the order of magnitude of 10^{-4} for most of the range of operation. On the other hand, the wall losses cannot be entirely neglected in this range of operation where relative errors less than 10^{-3} are desired. The order of magnitude of the errors involved will not vary greatly as the cross-sectional configuration of the wave guide is altered.

DIELECTRIC CONSTANT AND POLAR MOLECULES

It can be shown[12] that if the real and imaginary parts of the dielectric constant of a polar liquid are known, much information may be gained about the molecular structure of the liquid. For example, the polarizability, dipole moment, and relaxation time of the dipoles may be calculated if κ and κ' are known with sufficient accuracy.

The κ' referred to here arises from polarization losses only. If ionic conduction is present, its effect must be subtracted.

The values of κ and κ' may be obtained from wave guide measurements of attenuation and phase constant in the following way: Suppose that curves of $a\alpha$ and $a\beta$ *vs.* κ for various κ' are available.** If horizontal lines are drawn on each set of curves corresponding to measured values of $a\alpha$ and $a\beta$ respectively, data for curves of constant $a\alpha$ and $a\beta$ in the complex κ_c plane are obtained. The intersection determines κ and κ'.

ACKNOWLEDGMENT

The author wishes to express his appreciation to Professor Philip Rosen of the Department of Physics of Rensselaer Polytechnic Institute for his suggestion of this investigation and for his assistance in its completion. Particular thanks are due to Professor Alfred W. Jones of the Department of Mathematics and to Professor Robert M. Whitmer of the Department of Physics for their invaluable aid.

[12] Glasstone, Laidler, and Eyring, *The Theory of Rate Processes* (McGraw-Hill Book Company, Inc., New York, 1941), pp. 544–546.

** It is not necessary that the only term in κ', as used in preceding sections, be the term $\sigma_1/\omega\epsilon_0$. The introduction of a polarization loss in the dielectric does not alter the wave guide equations.

Ultra Speed Tensile of Rubber and Synthetic Elastomers*

D. S. VILLARS†
General Laboratories, United States Rubber Company, Passaic, New Jersey
(Received October 6, 1949)

A high speed stress-strain machine has been developed which is capable of recording the stress-strain curve of elastomers at elongation rates up to 270 percent/msec. Data are reported on two series of gum and tread stocks of hevea and of the synthetic elastomers, GR-S, Hycar OR, butyl, Perbunan, and Neoprene GN. The second (elastomer) series was also run at 150°C. In general, stress-strain curves fall into two classes. Stocks of elastomers which are known to crystallize on stretching tend to show tensiles which decrease with increasing speed up to about 10 percent/msec., pass through a minimum and rise more or less drastically to values 100 percent (or more) greater than the Scott tensile. Elastomers which do not crystallize on stretching tend to show a steady rise in tensile with increasing speed. Elongation at break curves show a maximum with crystallizing stocks and no maximum with non-crystallizing stocks. The shape of the modulus *versus* speed curves is accounted for on the hypothesis of different types of slipping bonds with different characteristic relaxation times. The shift of curves for tread stocks with temperature allows the estimation of a heat of activation of slippage. This comes out to be of the order of 3 kg cal.

INTRODUCTION

A MACHINE has been developed which is capable of recording the stress-strain curve of rubber at rates of elongation up to 9000 times that used in the Scott tensile test. This is over 100 times faster than any rate previously attained in any rubber tests. Availability of such high speed, which shall hereinafter be designated as "ultra speed," enables one now, for the first time, to study the relationship to service behavior of fundamental physical properties of commercial rubber stocks. The present paper presents a brief description of the machine and surveys the speed dependence of tensile strength, elongation at break, modulus and breaking energy of rubber and synthetic elastomers.

Other investigators have attempted to measure short time stress strain and tensile of rubber. Albertoni[1] described a pendulum impact tester which measured energy expended to stretch individual samples to definite predetermined elongations and to break. Roth and Holt[2] built a clever guillotine type of machine which stretched samples by means of a vertically falling weight. Dart, Anthony, and Wack[3] devised a fast stress-strain machine working on "the principle of a mechanical balance."

Objections to the foregoing types of machine are: (1) Time of break is not short enough. (2) Too much calculation is required to obtain the stress-strain curve (excessive calculation precludes large volume of investigation). (3) Rate of elongation in Roth-Holt machine is not uniform. (4) A different sample is tested for each point on the stress-strain curve when using the Albertoni machine.

Our present new machine overcomes each of these objections. It gives times of break down to $\frac{1}{2}$ msec. with constant rates of elongation almost 100 times that of the Albertoni machine, 200 times the mean rate of the Roth and Holt apparatus, 1000 times that obtained with the highest frequency dynamic hysteresis apparatus (Naunton and Waring,[4] *ca.* 1000 cycles/sec.) and 9000 times that of the Scott tensile machine. It gives direct photographs of the complete stress-strain curve of a particular sample, without any reduction by integration or differentiation.

Description of Ultra Speed Machine

The machine (cf. Fig. 1) consists of a rotating wheel, on the circumference of which a pin strikes the middle enlarged part of a double dumbbell test piece hanging in the form of a loop. This dumbbell was designed especially for this machine. The two narrow parts are 0.1 in. wide and 17/64 in. long. The total length of test piece is $5\frac{7}{32}$ in. The stress produced is communicated mechanically to a piezoelectric crystal which generates an electrical potential directly proportional to the stress. This potential is amplified and recorded on an oscillograph screen. The oscillograph trace, which is the

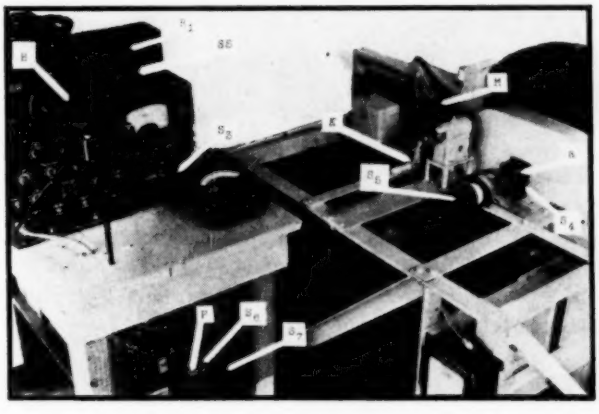

FIG. 1. Ultra speed machine.

* Presented before the Division of Rubber Chemistry at the Atlantic City meeting of the American Chemical Society, September, 1949.

† Present address: U. S. Naval Ordnance Test Station, China Lake, California.

[1] G. J. Albertoni, Ind. Eng. Chem. Anal. **9**, 30–4 (1937); R.C. T. **10**, 317 (1937).

[2] F. L. Roth and W. L. Holt, J. Research Nat. Bur. Stand. **23**, 603–16 (1939); R.C.T. **13**, 348–60 (1940).

[3] Dart, Anthony, and Wack, Phys. Rev. **69**, 52(A) (1946).

[4] Naunton and Waring, Proc. Rubber Tech. Conf. London, 805–20 (1938).

TABLE I.

	ADJ	ADK	ADL	ADM
Pale crepe	100	100		
GR-S			102	102
Blended black		47		46
Stearic acid	2	5	1.5	1.5
XX zinc oxide	5	8	5	5
Antioxidant[a]	1	1		
Captax[b]	1	1	1.5	1.5
Sulfur	2.5	2.5	1.5	1.5
Cure	35 min. @ 30 lb.	30 min. @ 40 lb.	30 min. @ 50 lb.	45 min. @ 50 lb.
	ADN	ADO	ADP	ADQ
Hycar OR	100	100		
GR-I			101.5	101.5
Blended black		44		46
Stearic acid	1	1	3	3
Zinc oxide	5	5	5	10
Age rite powder	1	1		
Altax[e]	1	1		
Tuex[d]			1	1
Sulfur	1	1	0.5	1.5
Cure	30 min. @ 50 lb.	30 min. @ 50 lb.	30 min. @ 50 lb.	45 min. @ 55 lb.
	ADR	ADS	ADT	ADU
Perbunan	100	100		
Neoprene GN			100	100
Blended black		44		35
Stearic acid	1.5		0.5	0.5
Lauric acid		1.5		
Zinc oxide	5	5	1	1
Extra lt. cal. mag.			4	4
552 acc.[e]			0.5	1.5
Neozone A[f]			2	2
Altax[e]	1	1.25		
Sulfur	1.2	1.25		
Cure	15 min. @ 50 lb.	45 min. @ 50 lb.	15 min. @ 50 lb.	30 min. @ 45 lb.

[a] Reaction product of acetone and diarylamine.
[b] 2-mercapto benzothiazole.
[c] Bis-2-thiobenzothiazole.
[d] Tetramethyl thiuram disulfide.
[e] Piperidine salt of *N,N*-pentamethylene dithiocarbamic acid.
[f] Phenyl-β-naphthylamine.

stress-strain curve, is photographed on 35-mm film. Calibration is carried out by suddenly applying a steady force upon the crystal by means of an electromagnet. The strength of the latter is in turn determined by weighing the force necessary to break the armature away from the magnet. By means of a variable speed transmission, and speed reducing pulleys, all wheel speeds between 60 and 1700 r.p.m. can be obtained. The corresponding elongation rates in rubber samples vary from 9.3 to 270 percent/msec. The output of the machine is 13 to 16 stress-strain curves per day.

It is planned to submit a detailed technical description of the machine to *The Review of Scientific Instruments*.

Stocks

Two series of stocks are considered in this paper. In the first, called the "Replication series," standard tread stocks, containing 50 parts carbon black (per hundred of elastomer), and standard gum stocks, omitting all carbon black, were compounded and cured. The second series is of six different elastomers, without and with 21 volumes channel black per 100 volumes matrix (rubber plus soluble components). Table I gives formulas of the second series.

RESULTS

Shape of Stress-Strain Curve

A typical ultra speed stress-strain curve taken at 57 percent/msec. is reproduced in the upper half of Fig. 2. It is approximately linear. Figure 3 plots the average of three stress-strain curves of a rubber gum stock taken at 36 percent/msec. At highest ultra speeds, the stress-strain curves assume a wave form (lower half of Fig. 2), sometimes multiple in character. The reason for this multiplicity is not known. It may have something to do with slippage of the samples in the holders. It may be associated with resonance chattering oscillations in the crystal holder or crystal itself. That it is not due to each wave representing individual non-simultaneous breaks of the two sample sides was shown by the fact that samples with one side cut beforehand also showed double loops.

Velocity of Sound

At the greatest ultra speeds the possibility has been taken into consideration of perturbing effects which might be introduced by the wave character of stress response whenever the rate of elongation approaches too closely the velocity of sound in the sample. For zero hysteresis the stress recorded at the held end of a uniform sample elongated at a constant rate should increase with time by finite perpendicular steps.[5] Al-

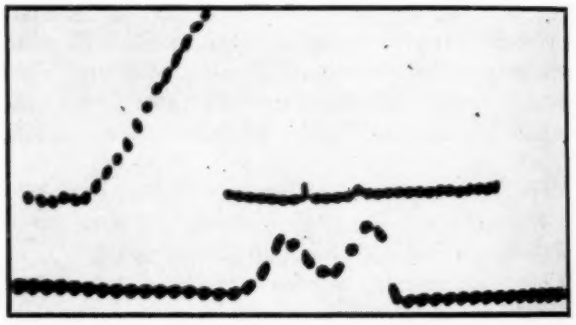

FIG. 2. Ultra speed stress strain curves. Upper curve: rubber tread; elongation rate: 57 percent/msec.; timing frequency: 2000 c.p.s.; tensile: 3530 lb./in².; elongation at break: 325 percent; time of break: 5.7 msec. Lower curve: special rubber tread; elongation rate: 238 percent/msec.; timing frequency: 5000 c.p.s.; tensile: 6600 lb./in².; elongation at break: 143 percent; time of break: 0.6 msec.

[5] Fourier analysis of the equation

$$(\partial^2 y/\partial \tau^2) = (\partial^2 y/\partial \xi^2)$$

for the boundary conditions,

$$\begin{aligned} y &= 0 \quad \text{at } \tau = 0, \\ (\partial y/\partial \tau) &= 0 \quad \text{at } \tau = 0, \\ y &= 0 \quad \text{at } \xi = 0, \\ y &= \alpha\tau \quad \text{at } \xi = 1, \ \tau > 0 \end{aligned}$$

though we know that we are dangerously near the velocity of sound at highest speeds, no elastomer curves have yet been observed which have the step shape predicted by wave theory. This fact indicates that none of our conclusions are subject to modification because of wave phenomena. However, it is still possible that large specific acoustic absorption effects at the frequencies concerned might reduce the steepness of the "steps." This could result in the steps being overlooked.

Preworking

Possibility of an effect of preworking was checked by running a series of rubber tread stocks, half of the samples of which were preworked by (hand) stretching ten times out to the "hardening" point and back. The order of testing these and unworked controls was random. Results (Table II) indicate no great effect on either tensile or elongation.

Comparison of High and Low Speed Stress-Strain Curves

Figure 3 compares the average of three ultra speed curves (elongation rate 36 percent/msec.) of rubber gum stock with a slow speed stress (single pull—no preworking) strain curve of a sample from the same slab of rubber, as recorded by an autographic stress strain machine designed by H. M. Smallwood, H. T. Battin, and W. Moorman. This machine uses ring-shaped test pieces, 1.373 in. o.d. and 1.173 in. i.d. Such test pieces never give the full value of the tensile strength, probably "because of uneven distribution of stress over the cross section caused by the fact that the inside of the ring is stretched more than the outside during elongation and because of the effect of the clamp pulleys on the portions of the ring passing over them."[6] However, the autographic curve, Fig. 3, is seen to head for the Scott tensile value, also determined on pieces from the same slab. It breaks away from the ultra speed curve at about 400 percent elongation.

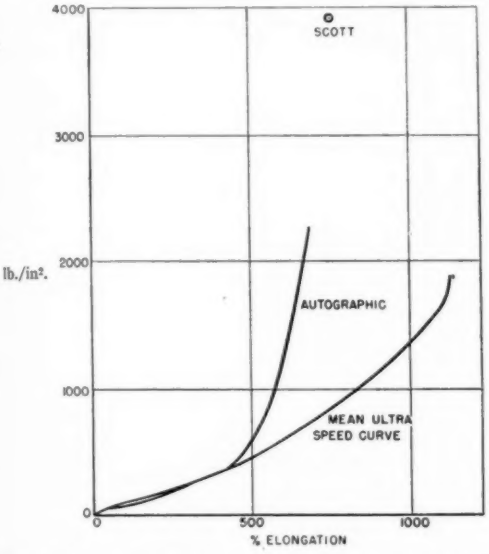

FIG. 3. Comparison of ultra speed with autographic stress-strain curve—rubber gum. Times of break—ultra speed: 28 msec.; Scott: 30 sec.; autographic: 88 sec.

gives:

$$y=\alpha\xi\tau+\frac{2\alpha}{\pi^2}\sum_{m=1}^{\infty}\frac{(-1)^m}{m^2}\sin m\pi\xi\,\sin m\pi\tau.$$

In these equations the dimensionless quantities are defined as:

$$y=u/L;\quad \xi=x/L;\quad \tau=t/(L/v);\quad \alpha=a/v,$$

where u is the displacement of a point in the sample of total length L, originally at a distance x from the fixed end, t is time, a is the uniform velocity of displacement of the other end of the sample and v is the velocity of sound in the rubber (taken as constant). The local elongation $\partial y/\partial\xi$ at $\xi=0$ (and hence stress) may be shown to represent a series of perpendicular steps, each of height 2 dimensionless units and of length 2 units of τ.

TABLE II. Effect of preworking rubber tread. Mean time of break, 8 msec.

Tensiles		Elongations	
Unworked	Preworked	Unworked	Preworked
2910	3180	442	540
2790	2610	442	388
	2010		334
Mean 2850	2600	442	421

TABLE III. Testing error of ultra speed tensile—quartz crystal. Tread stocks—AKE-I.

Elongation rate percent/msec.	Standard deviation, lb./in.² mean of five
11	80
24	120
55	170
120	305
260	370

Reproducibility of Measurement

To obtain an accurate estimate of the variability of measurement, triplicate mixes of Hevea and GR-S gum and tread stocks were mixed in random order and cured. Each test slab was $6\frac{1}{2}\times6\frac{1}{2}\times0.1$ in. and can supply five ultra speed stress-strain, four Scott, and one autographic stress-strain test pieces. In this test, five speeds were investigated and each mix-speed combination was run in random order until each combination was represented. Such a "block" was then repeated in a new random order until five blocks were completed.

In carrying out such a program plan, stress-strain curves are occasionally missed. This is sometimes caused by faulty synchronization, sometimes by failure of the sweep trigger mechanism, not to speak of human failures to open the camera shutter or turn the film on to the next frame. Such missing values were filled in by the method of Yates.[7]

[6] Arthur W. Carpenter in Davis and Blake, *The Chemistry and Technology of Rubber* (Reinhold Publishing Corporation, New York, 1937), p. 791.

[7] F. Yates, "Analysis of replicated experiments where . . . results are incomplete," Empire J. Exper. Agric. **1**, 129–42 (1933).

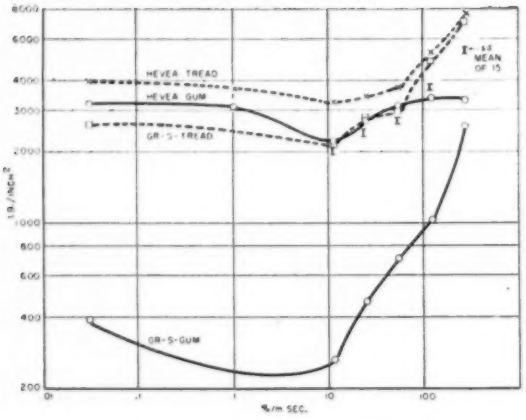

FIG. 4(a). Tensile—Replication series AEG-J.

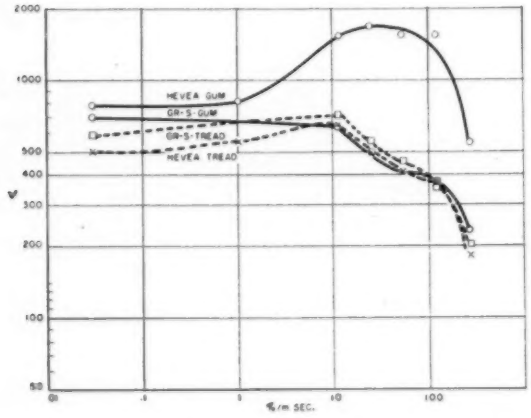

FIG. 4(b). Elongation at break—Replication series AEG-J.

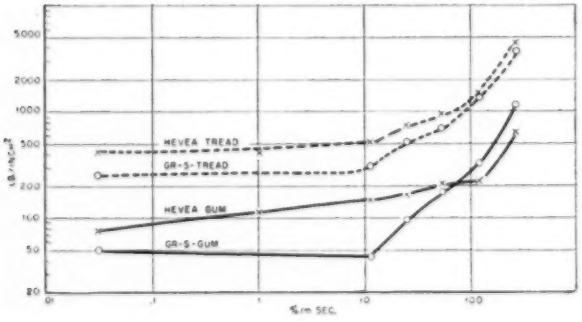

FIG. 4(c). Modulus—Replication series AEG-J.

The standard deviations of testing error were determined separately for each individual rate of elongation. See Table III. It may be seen from the I-shaped marks on Fig. 4(a) that the standard deviation of tensile strength tends to vary in direct proportion with the value of the tensile (coefficient of variation is more constant than the standard deviation).

No mixing error (significantly greater than testing error) was found except at speed 120 percent/msec. This means that testing error is the predominant source of variability.

TENSILE STRENGTH

Dependence on Speed

Figure 4(a) plots the results of ultra speed tensile measurements on the first (replication) series of Hevea gum and tread and GR-S gum and tread. The abscissae are logarithms of elongation rates. At the left of the graph is the Scott tensile value, plotted at 0.03 percent/msec. Each of the ultra speed values (in this series only) is the mean of five samples each of three independent mixes of the same stock and the standard deviations, listed in Table III as for means of 5, are indicated by the limits of the I-shaped figures on the graphs (after converting to means of 15). From these limits one may judge visually the significance of the trends exhibited.

Roth and Holt[2] values for Hevea are inserted at 1 percent/msec. Their tread compound contained 40 parts channel black, while ours contained 50 parts. That particular point falls reasonably on our curve, as if variation in carbon black loading in that range makes little difference at that low a speed.

It may be seen that for our stocks there is a significant drop in tensile with increasing speed up to about 10 percent/msec. Somewhere near this speed (before it if not at it) the tensile goes through a minimum and rises more or less drastically until at the highest speeds observed it is, for the tread stocks, 100 percent (or more) greater than the Scott tensile. The Hevea gum tensile at highest speed is about the same as the Scott tensile, but the tensile of the GR-S gum is multiplied sevenfold.

Effect of Curing

Figure 5(a) shows ultra speed tensiles obtained on raw Hevea gum and tread stocks. The samples for these runs were interspersed in random order among those of the replication series. It may be seen that raw smoked sheet, which has zero Scott tensile, attains a tensile of 900 lb./in.^{2} at highest speed. Compounded (but uncured) tread stock has a Scott tensile of 530 lb./in.^{2}. This increases to 4200 lb./in.^{2} at highest ultra speed.

Dependence on Elastomer

Tensile data on the elastomers of the second series are to be found plotted in Figs. 6(a)–11(a). In this series GR-S does not show a minimum in tensile (it shows a slight minimum in the Replication series), but a steady rise as speed is increased. Hycar OR and Perbunan also show a steady rise. The other synthetics show the minimum as Hevea does.

It is to be noted that the stocks which exhibit the minimum (except for GR-S) are ones which are known to crystallize at ordinary slow rates of stretch. The other stocks do not crystallize. The minimum in the first GR-S series may be related to an orientation, of lower order than crystallization.

Dependence on Temperature

Figures 6–11(a) also show the results of a study of effect of temperature on ultra speed tensile. In general,

ultra speed tensile of gum stocks at 240 percent/msec. is reduced by 67 to 75 percent by heating to 150°C; of tread stocks, it is reduced only by 20 to 50 percent (exception: possibly Perbunan). At 150°C, gum GR-S has such a poor ultra speed tensile that the pin on the wheel knocks out from the sample by a clean cut an exact replica of the pin.

ELONGATION AT BREAK

Dependence on Speed

Figure 4(b) gives the elongation at break obtained from measurement of the replication series. It shows at 1 percent/msec. elongation values of Roth and Holt. The Hevea stocks, especially the gum, show a maximum in elongation at break twice that at Scott speed, between 10 and 30 percent/msec. The GR-S stocks do not exhibit this phenomenon to as marked an extent, if at all. At highest ultra speed all stocks become drastically shortened.

Effect of Curing

See Fig. 5(b). Elongation at break of the uncured smoked sheet and tread compound shows curves similar to those of the cured stocks, except for an upward displacement of the tread stock. The ultra speed values of the uncured smoked sheet agree fairly closely with those at the same speeds for the cured gum stocks.

Dependence on Elastomer

See Figs. 6(b)–11(b). The different elastomers, in general, are classifiable into two groups; one in which the elongation at break passes through a maximum at an intermediate ultra speed (such as Hevea, and Butyl) and one for which it steadily decreases with increasing speed of break. Except for Neoprene GN, this classification is the same as that of elastomers which do or do not crystallize on stretching.

Dependence on Temperature

Ultra speed elongation at break at 150° seems, in general, to be greater for tread stocks than for gum stocks at all speeds except the highest. Heating to 150° *reduced* elongation of all stocks except butyl tread.

Modulus

The ultra speed modulus was computed from the tensile and elongation at break on the approximation that the ultra speed stress-strain curve is linear. For Scott speed the modulus was arbitrarily taken as the slope of the line between the origin of the (single-pull) autographic stress-strain curve and the point of inflection. This value thus does not include the subsequent increase in modulus which many elastomer stocks undergo at higher elongations (usually ascribed to orientation). It lies between the Wall-Young's modulus and the shearing modulus as computed from Young's modulus by dividing the latter by three. Within this range, the comparability of the low speed values with the ultra speed values is somewhat uncertain.

Dependence on Speed

Figure 4(c) gives modulus measurements obtained from the Replication series. It contains at 1 percent/msec. modulus values of Roth and Holt. Modulus is almost independent of elongation rate up to 10 percent/msec., above which speed it rises rapidly.

Effect of Curing

Modulus of uncured smoked sheet and of uncured tread compound shows curves similar to those of the

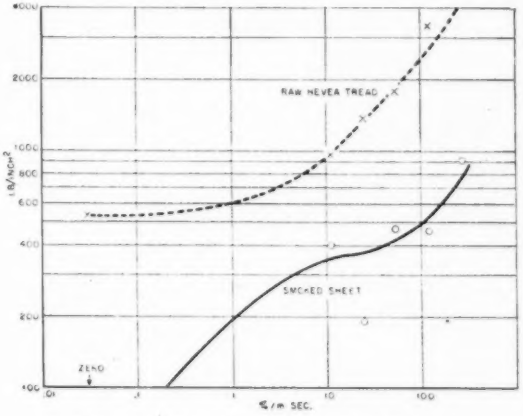

FIG. 5(a). Tensile—unvulcanized Hevea.

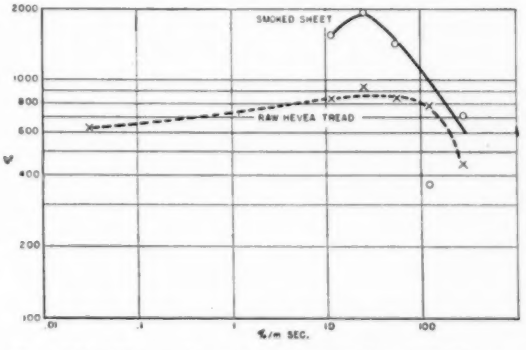

FIG. 5(b). Elongation at break—unvulcanized Hevea.

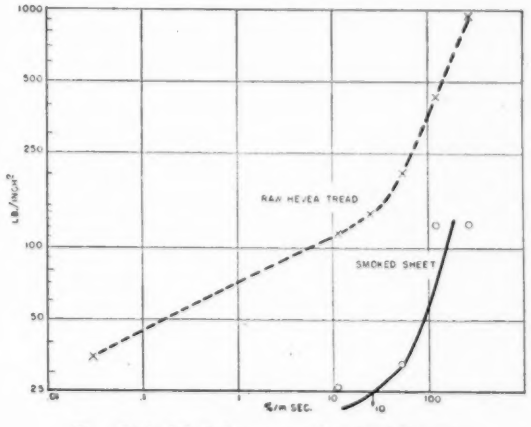

FIG. 5(c). Modulus—unvulcanized Hevea.

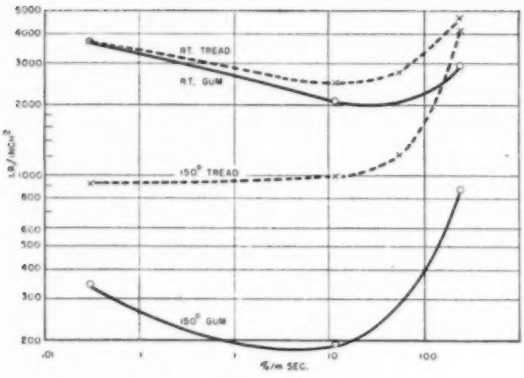

FIG. 6(a). Tensile—Hevea ADJ, K.

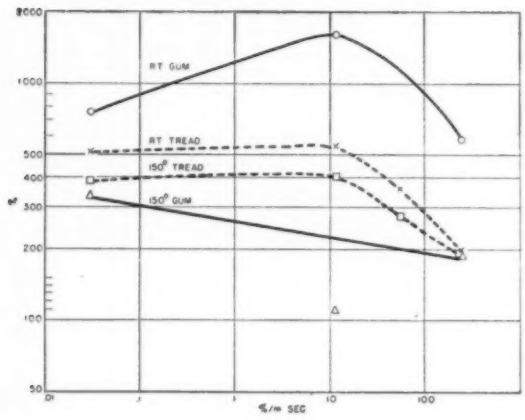

FIG. 6(b). Elongation at break—Hevea ADJ, K.

cured stocks, except for a downward displacement in value. See Fig. 5(c).

Dependence on Elastomer

Plots of moduli of the elastomer series, in general, show that modulus is more or less constant until the ultra speeds are reached, when it starts to increase with an accelerated pace.

Dependence on Temperature

Modulus of gum stocks is little affected by increasing temperature to 150°; that for tread stock is shifted to the side of higher elongation rate. Exceptions to this last generalization are Hevea and Neoprene, where the curves for tread stocks rise to the same modulus at highest speed.

Energy of Break

Ultra speed energy of break was computed from the tensile and elongation at break on the approximation that the ultra speed stress-strain curve is linear. For Scott speed, energy of break was obtained by integrating (by planimeter) the complete single-pull autographic stress-strain curve after extending it to the Scott tensile and elongation at break. The slow speed energy thus includes the contribution of all orientation effects. Energy of break values appear to be subject to an excessively large error. They fluctuate so greatly that no trends with speed appeared significant.

Independent Determination of Energy of Break

Energy of break was checked independently by measuring the instantaneous drop in wheel speed occurring when the sample is broken. This was measured by connecting the oscillograph to give a changing pattern, the frequency of which was the difference between the wheel frequency and an adjustable reference frequency. The difference between this difference frequency before and immediately after breaking a sample was combined with the moment of inertia of the wheel to compute the energy of break.

Two values obtained are 18.5 and 15.6 ft. lb. for rubber tread. These values, determined at 25 cycles/sec. wheel speed, are to be compared with the total energy of break, 10.12 ft. lb., given by a stress-strain curve at 23 cycles, of a similar sample. The latter figures include 1.69 ft. lb. kinetic energy of the end thrown off. The high tensiles indicated by our measurements of the stress-strain curves are thus independently confirmed.

DISCUSSION

Crystallization and Relaxation

In explaining the observed effects of elongation rate on the stress-strain properties of elastomers, it is necessary to consider two phenomena which can be induced in an elastomer by stretching, but which require finite

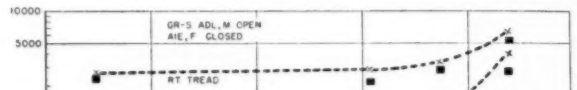

FIG. 7(a). Tensile—GRS. ADL, M; AIE, F.

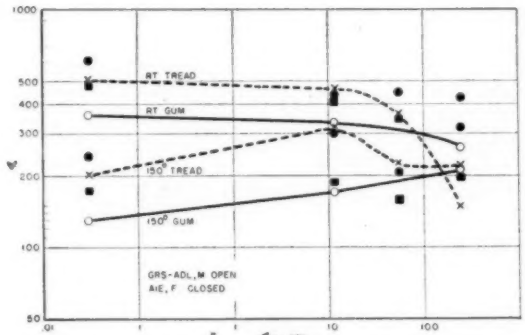

FIG. 7(b). Elongation at break—GRS. ADL, M; AIE, F.

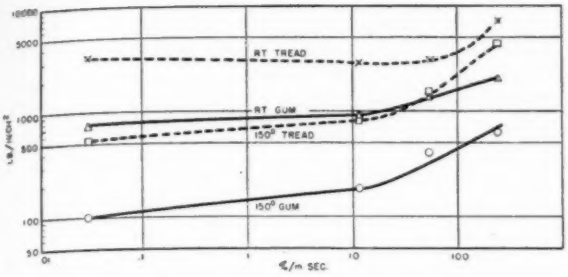

FIG. 8(a). Tensile—Hycar OR. ADN, O.

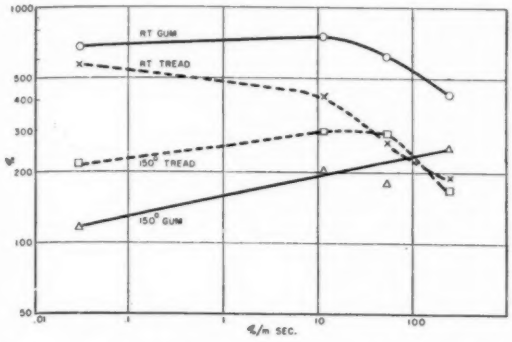

FIG. 8(b). Elongation at break—Hycar OR, ADN, O.

time for completion. These phenomena are, first, crystallization and, second, relaxation.

The fact that rubber crystallizes on stretching is familiar to all rubber chemists. Many, if not most, attribute the upbend in the ordinary stress-strain curve to onset of crystallization. According to Acken, Singer, and Davey,[8] a minimum time of the order of 1.2 sec. is required after stretching before enough crystallization develops to show up in a x-ray picture. As our ultra speed curves are produced in times of lower order of magnitude than this, it is plausible to attribute differences between those obtained at the lesser ultra speeds and those obtained at slow speed to lack of time for crystallization to develop. This lack of time would account for the approximate linearity of the ultra speed stress-strain curves.

This theory may be used to account for the differences in tensile and elongation at break between the slow autographic stress-strain and the mean ultra speed curve of Fig. 3. Since the latter was produced in an average time of 28 msec., presumably much too short for crystallization, we may conclude that crystallization increases tensile strength but shortens the elongation at break.

A corollary of the hypothesis of a finite time requirement for completion of crystallization is of interest to problems of abrasion resistance. Inasmuch as abrasion processes generally occur in cycles shorter than 20 msec., it appears questionable whether the crystallization characteristics of a tread stock can have any direct effect on its abrasion resistance.

Relaxation, the second phenomenon invoked to explain the ultra speed results, is the loss of stress with time in a sample held at a constant deformation. It is thought to be due to a slow intermolecular slippage within the rubber, accompanied sometimes by a reversible, sometimes irreversible, breaking of bonds. Kuhn[9] and others have suggested that many properties of rubber may be explained by postulating more than one type of slippage bonds, the different types being distinguished by different relaxation rate constants.

Now, if the time of test is made shorter than the relaxation time of the rapidly relaxing components they contribute more and more toward the total modulus. This is how we account for the increase in modulus as rate of elongation increases to 200 percent/msec. and greater. The increase in tensile with increasing speed implies that the slipping bonds also add to strength when not given time to slip.

The minima in tensile and maxima in elongation observed with crystallizing stocks now may be interpreted as the point of balance between decreasing importance of crystallization and increasing importance of slipping bonds that fail to slip as speed is increased. If the 90 percent drop in tensile of gum Hevea which is observed at Scott speed on heating from room temperature to 150° is a measure of the contribution of crystallinity, the formation of only about one-third of the total crystallinity is prevented by stretching at the lower ultra speeds.

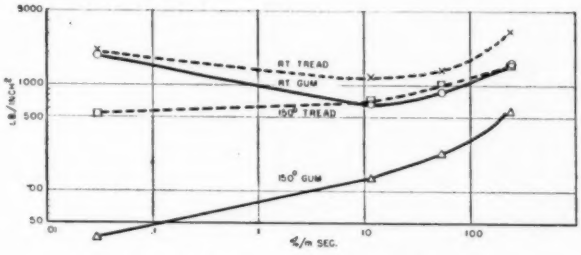

FIG. 9(a). Tensile—butyl. ADP, Q.

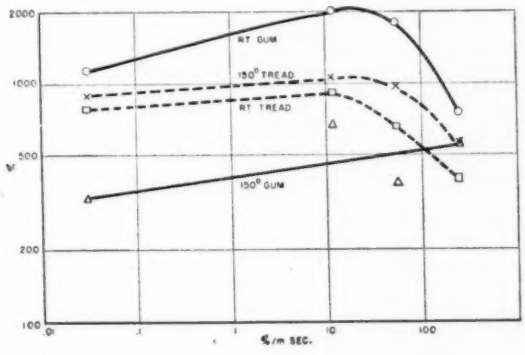

FIG. 9(b). Elongation at break—Butyl. ADP, Q.

[8] Acken, Singer, and Davey, Ind. Eng. Chem. **24**, 54–7 (1932), R.C.T. **5**, 30–8 (1932).

[9] W. Kuhn, Zeits. f. physik Chemie **42B**, 1–38 (1939).

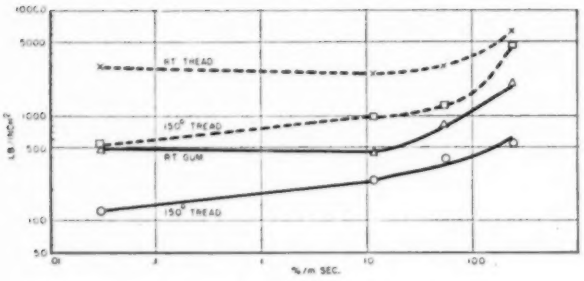

FIG. 10(a). Tensile—Perbunan, ADR, S.

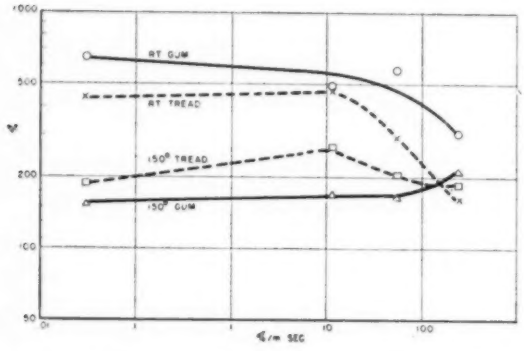

FIG. 10(b). Elongation at break—Perbunan, ADR, S.

On the slipping bond hypothesis the elongation rate at which the sharp rise occurs, 200 percent/msec., qualitatively gives the order of magnitude of the relaxation time as 0.5 msec. It is believed that many service processes may occur within times of this order of magnitude. For example, Markwick and Starks[10] report high frequency oscillations of 1400 cycles/sec. in tread rubber retracting from a dry road. As far as we know, no one has reported confirmation of this observation and it may possibly be a spurious mechanical effect. However, if an important part of the strength of a stock originates from rapidly relaxing elements, it is clear that a completely successful correlation between laboratory and service can never be expected until the time of test is reduced to that characteristic of the service condition.

Heat of Activation of Slippage

If the above hypothesis be true that the rise in modulus and tensile may be attributed to bonds, which ordinarily completely relax within the time of stretching, not having time to relax completely at the higher ultra speeds, then it would be reasonable to expect to find a particular curve to shift bodily to the side of higher elongation rate on going to higher temperature. For, if one used as abscissae the parameter, speed/relaxation rate (or speed×relaxation time), increase of temperature increases relaxation rate, so to find the same modulus one should look for it at a greater speed. A complete shift of the curve without change in shape is too much to expect, inasmuch as it could occur only in the unlikely event of only one relaxation type. With more than one type, the modulus contribution of each would be shifted by a different amount corresponding to its different change in relaxation rate. This would bring about a change in shape of the composite curve which is the sum of the individual components.

We have noted the above shift for the case of carbon black stocks. A heat of activation may therefore be roughly computed from the ratio of rates at 150° and at room temperature. A list of such values is given in Table IV.

It may be seen that the heat of activation is of the order of magnitude of 3 kg cal. This may be compared with 10.3 kg cal. heat of adsorption of benzene on graphite[11] (the nearest similar process to adsorption of rubber on carbon black on which there are published data), 10 kg cal. heat of activation of shear in raw rubber,[12] 15 kg cal. for shear in raw GR-S,[13] 15 kg cal. for transient relaxation in cured rubber, and 15 kg cal. for steady relaxation in cured rubber.[14] The considerably lower value of 3 kg cal. is in accord with a "slide-fastener" mechanism of slippage of rubber molecules along a carbon black surface proposed by the present author. In this mechanism the attached segments of rubber are supposed to slip with moderate resistance along the surface of the black from one end to the other

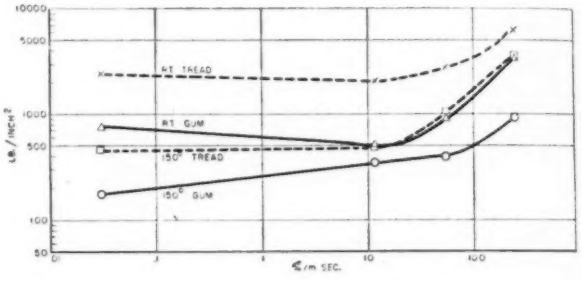

FIG. 11(a). Tensile—Neoprene GN. ADT, U.

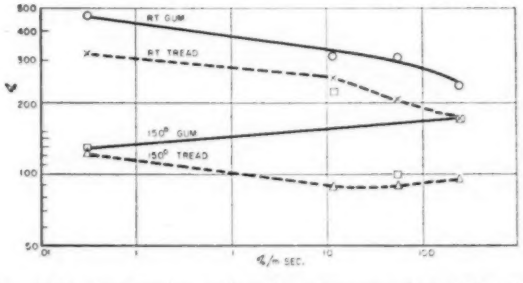

FIG. 11(b). Elongation at break—Neoprene GN. ADT, U.

[10] (a) Report of Road Research Board for the year ending March 31, 1939, pp. 150–6, Great Britain Department of Science and Industry Research. (b) A. D. H. Markwick and H. J. H. Starks, J. Inst. Civil Eng. (London) **16**, 309–25 (1941).

[11] W. D. Harkins and G. E. Boyd, J. Am. Chem. Soc. **64**, 1195-1204 (1942), Table III.

[12] H. M. Smallwood, J. App. Phys. **8**, 505 (1937).

[13] M. Mooney (private communication).

[14] Mooney, Wolstenholme, and Villars, J. App. Phys. **15**, 324-337 (1944).

without pulling away free from it. When the rubber-black bond reaches the end of the "zipper" it is fairly permanently resistant to complete separation.

The failure to find a shift in the gum stock curves means, on the above hypothesis, that the heat of activation of slippage for the other types of slippage is very low; i.e., the relaxation rates involved have too low a temperature coefficient to be measurable within the accuracy of the experiment.

TABLE IV. Heat of activation of relaxation rate in tread stocks.

Elastomer	ΔH, kg cal.
Hevea	3.08
GR-S	3.67
Hycar OR	3.75
Butyl	3.77
Perbunan	2.78
GR-M	1.57

ACKNOWLEDGMENT

Appreciation is herewith expressed to the various members of the staff who have been consulted in the development of the machine; in particular to Drs. E. M. Grabbe, M. Mooney, and S. A. Black. Mr. R. B. Frost designed and supervised the original construction of the machine and Mr. T. J. Rhodes designed several of the later modifications. The experimental work of operating the machine was carried out by Mr. O. K. Laible.

Relations Concerning Wave Fronts and Reflectors

K. S. KELLEHER

Naval Research Laboratory, Washington, D. C.

(Received October 20, 1949)

By means of a vector notation for surfaces, relations are derived among an incident wave front, reflector and reflected wave front. A method is introduced for evaluating the deviation of a wave front surface from a plane. Problems are included in order to indicate the simplicity and utility of the analysis.

INTRODUCTION

IN working with microwave antennas, it is desirable to know the characteristics of their wave fronts. Some knowledge can be obtained by employing geometrical optics principles to trace a few selected rays. It is the intention of the present paper to consider the reflection of a normal congruence of rays, defined by a wave front surface.[1] The problem presented and solved is: Given any two of the three surfaces, incident wave front, reflector and reflected wave front, find the third.

THE REFLECTED WAVE FRONT

The incident wave front surface $X(u, v)$[2] and the reflector $R(s, t)$ are indicated in Fig. 1. The reflected wave front $Y(u, v)$ can be obtained by using the definition that all points of $Y(u, v)$ lie at equal ray path length from $X(u, v)$ together with the fact that rays are orthogonal to the wave front surfaces. From the figure, two values of the general reflected ray can be obtained and equated.

$$Y-R=(C-|R-X|)\xi, \tag{1}$$

where C is the total ray path length from X to Y; $|R-X|$ is the length of the incident ray; and ξ is a unit normal to the reflected wave front, Y.

The vector, ξ, is determined[3] from the fact that incident and reflected angles at the reflector surface are equal.

$$\xi=r-2\eta(\eta\cdot r) \tag{2}$$

where $r=(R-X)/|R-X|$ and η is the unit normal to the reflector at the point of incidence.

Placing (2) in (1) and reducing, there results

$$Y=C\xi+X+2\eta[\eta\cdot(R-X)]. \tag{3}$$

For most practical purposes, it is convenient to consider the reflected wave front surface at zero path length ($C=0$) from the incident wave front. This fictitious wave front is a parallel surface[4] to any actual reflected wave front and therefore can be used to define the reflected congruence of rays. Such a wave front could be subjected to further reflections in the same way that X was reflected from R.

Substituting $C=0$ in (3), the reflected wave front is

$$Y(u, v, s, t)=X(u, v)+2\eta(s, t)[\eta(s, t)\cdot\{R(s, t)-X(u, v)\}]. \tag{3a}$$

The parentheses are used to indicate the dependence of the functions on the various parameters involved. A relation between u, v and s, t is required in order that Y should be a function of only two parameters. This is obtained from the condition that the incident rays are normal to the incident wave front. Using tangent vectors to the surface, this condition is written

$$(R-X)\cdot X_u=0 \quad \text{and} \quad (R-X)\cdot X_v=0, \tag{4}$$

[1] W. Blaschke, *Differential Geometric I* (Dover Publications, New York, 1945), p. 104.

[2] This vector notation is discussed in Blaschke.

[3] L. Silberstein, *Simplified Method of Tracing Rays Through Any Optical System* (Longmans, Green and Company, London, 1918), p. 1.

[4] L. P. Eisenhart, *An Introduction to Differential Geometry* (Princeton University Press, Princeton, 1940), p. 272.

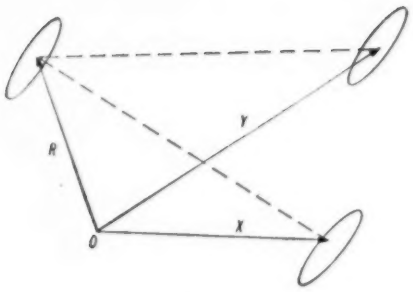

FIG. 1.

where the subscripts denote partial differentiation. From these expressions $s=s(u, v)$ and $t=t(u, v)$ can be obtained and when they are substituted in (3a) yield the desired reflected wave front surface $Y(u, v)$.

Since the incident and reflected wave fronts could be interchanged without altering the above treatment, there remains only the problem of determining the reflector which transforms a given incident wave front into a given reflected wave front.

THE REFLECTOR

In order to find this reflector, use (1) with the sign of the unit normal reversed, so that ξ points toward the reflector.

$$R=Y+(C-|R-X|)\xi. \tag{5}$$

As before, ξ is the normal to the wave front $Y(p, q)$, and $X=X(u, v)$ is the second wave front surface. In this expression, $|R-X|$ can be evaluated by subtracting X from both sides and taking the scalar product of each side with itself. The result reduces to

$$|R-X|=\frac{C^2+(Y-X)^2+2C(Y-X)\cdot\xi}{2[C+(Y-X)\cdot\xi]}.$$

Using this, (5) becomes

$$R(u, v, p, q)=Y+\xi\frac{[C^2-(Y-X)^2]}{2[C+(Y-X)\cdot\xi]}=Y+\xi G. \tag{5a}$$

R is obtained as a function of u and v alone through use of the condition that $(R-X)$ is normal to the surface X.

$$(R-X)\cdot X_u=0 \quad \text{and} \quad (R-X)\cdot X_v=0,$$

or

$$(Y-X+\xi G)\cdot X_u=0 \quad \text{and} \quad (Y-X+\xi G)\cdot X_v=0. \tag{6}$$

These two equations are solved for $p(u, v)$ and $q(u, v)$ which when substituted in (5a) gives R as a function of u and v alone.

DEVIATION FROM A PLANE WAVE

Given a wave front surface, it is normally desirable to know its deviation from a plane, since such knowledge gives an indication of the far field radiation pattern. Referring to Fig. 2, let the wave front be represented as $Y(u, v)$ and designate a unit normal to the plane as N. Introduce a constant vector Y_0 from the origin to a point of tangency of the plane with the surface. From the figure, it is evident that the deviation, Δ, is the projection of the vector $(Y-Y_0)$ on N. Analytically stated,

$$\Delta(u, v)=|Y-Y_0|\cos\beta=(Y-Y_0)\cdot N. \tag{7}$$

Therefore, for any point (u, v) of the surface, the deviation can be determined.

CONICAL WAVE FRONT AND PARABOLIC CYLINDER

A line source with linear phase distribution produces a conical wave front.[5] If the source is positioned along the

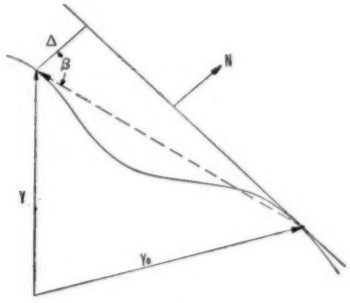

FIG. 2.

focal line of the reflector (Fig. 3), the incident wave front may be written

$$X=Fi+uj+vk$$

where

$$F=[(h-v)^2\tan^2\alpha-(u-f)^2]^{\frac{1}{2}}.$$

The reflector is

$$R=si+(s^2/4f)j+tk.$$

The normal to the surface R can be obtained from the vector product of two tangent vectors.

$$R_s\times R_t=[i+(s/2f)j]\times k.$$

The unit normal then is

$$\eta=[si-2fj][s^2+4f^2]^{-\frac{1}{2}}.$$

Upon substitution of these values in (3a), the reflected wave front becomes

$$Y=i\frac{[s(s^2+4uf)-(s^2-4f^2)F]}{s^2+4f^2}+j\frac{[s^2(u-2f)-4uf^2+4fsF]}{s^2+4f^2}+kv.$$

This expression for Y involves three parameters, so that a given point on the incident wave front $X(u, v)$ does not yield a single value of Y, but rather a value which depends on s. It is therefore necessary to find an auxiliary

[5] K. S. Kelleher, "Antenna Wavefront Problems," Naval Research Laboratory Report R-3530.

relation between s, u and v. This relation, obtained from the condition $(R-X)\cdot X_u=0$ is $(s^2-4f)F=4fs(u-f)$. Substituting this and reducing, Y becomes

$$Y=si+[(f-u)\sec\theta-f]j+vk$$

where

$$\sec\theta=(f+s^2/4f)/(f-s^2/4f).$$

From Fig. 4, the angle θ can be related to the cone angle α.

$$(f-u)\sec\theta=(h-v)\tan\alpha.$$

Thus the reflected wave front can also be written

$$Y=si-[(f-h\tan\alpha)+v\tan\alpha]j+vk.$$

This surface is a plane, intersecting the $x-y$ plane in the line $y=-(f-h\tan\alpha)$ and at an angle $\pi-\alpha$. (This can be verified by using (7) to show that the deviation of this Y surface from such a plane is zero.)

POINT SOURCE AND SPHERICAL REFLECTOR

When a point source is used to feed a spherical reflector, it is possible to obtain a nearly plane wave front characteristic by placing the feed near the half-radius point of the reflector.[6] The positioning of the feed as well as the deviation of the wave front from a plane can be found using (3a). Choose a spherical reflector with center at the origin. For convenience, normalize all points to the radius of the sphere. Then the reflector, unit normal and feed vectors may be written:

$$R=xi+(1-r^2)^{\frac{1}{2}}j+zk,$$
$$\eta=R,$$
$$X=jd,$$

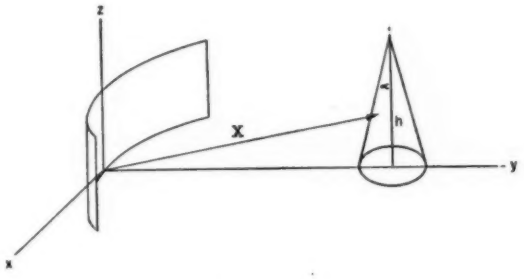

FIG. 3.

where

$$r^2=x^2+z^2.$$

The wave front, Y, is found by substituting these vectors in (3a)

$$Y=Dxi+[D(1-r^2)^{\frac{1}{2}}+d]j+Dzk,$$

where

$$D=2-2d(1-r^2)^{\frac{1}{2}}.$$

The deviation of this wave front from a plane is found by using (7) with $N=j$ and $Y_0=(2-d)j$

$$\Delta=2(1-r^2)^{\frac{1}{2}}+2(dr^2-1).$$

It is evident that $\Delta(0)=0$, but this deviation will also vanish at another value of r if d, the feed position, is properly chosen. Setting $\Delta=0$ and solving for d, there results,

$$d=[1-(1-r^2)^{\frac{1}{2}}]/r^2.$$

Therefore, given a value of r for which the deviation, Δ, should vanish, the required feed position, d, can be immediately determined.

Once the value of d has been established, it is possible to find the maximum value of $\Delta(r)$ in the usual manner. The result is

$$\Delta_{\max}=2(d-0.5)^2/d$$

for a reflector of unit radius.

REFLECTORS WHICH YIELD VIRTUAL POINT SOURCE

Occasionally in microwave antenna design it is advisable to use a virtual point source feed.[7] A catalog of the reflectors which will produce a spherical wave front from a point source feed, can be obtained from Eq. (5a). From the analysis, the reflector desired is

$$R=Y+\frac{C^2-(Y-X)^2}{2[C+(Y-X)\cdot\xi]}\xi \qquad (5a)$$

where Y and X in this case are points. Let $X=0$ and $Y=ai$; the unit normal to the Y wave front is

$$\xi=(x-a)i+yj+zk$$

where

$$y=[1-z^2-(x-a)^2]^{\frac{1}{2}}.$$

Substituting these values, the reflector becomes

$$R=\frac{[(x-a)(C^2+a^2)+2aC]i+y(C^2-a^2)j+z(C^2-a^2)k}{2[C+a(x-a)]}.$$

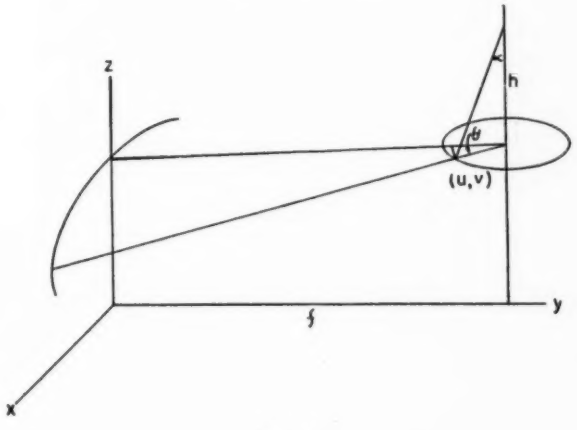

FIG. 4.

[6] J. Ashmead and A. B. Pippard, "The Use of Spherical Reflectors as Microwave Scanning Aerials," J. Inst. Elec. Eng. **93**, 627 (1946).

[7] R. F. Rinehart, J. App. Phys. **19**, 862 (1948).

In terms of components, r, s and t along the x, y and z axes,

$$R=ri+sj+tk.$$

It is possible to eliminate the parameters x, y and z and obtain

$$\frac{(r-a/2)^2}{C^2/4}+\frac{s^2+t^2}{(C^2-a^2)/4}=1.$$

From inspection of this equation, the following tabulation may be made:

For $C>|a|$, the reflector is an ellipsoid, unless $a=0$ in which case it is a sphere of radius $C/2$. For $C<|a|$, the reflector is a hyperboloid of revolution, unless $C=0$ in which case it is the plane, $x=a/2$. For $C=a$, the result is $r=0$ or $r=a$, and so has no practical meaning.

REFLECTOR WHICH WILL PRODUCE A PLANE WAVE

A less trivial application of (5a) is had when it is desired to find the reflector which will transform an arbitrary incident wave front $X(u, v)$ into a plane wave front $Y(p, q)$.

If the general wave front surface is given by $y=y(x, z)$, in vector notation it can be written

$$X=ui+F(u, v)j+vk.$$

Let the plane wave front be the $x-z$ plane so that

$$Y=pi+qk$$

and the unit normal to this wave front, $\xi=j$. When these values are substituted into (5a), there results

$$R=Y+G\xi=pi+Gj+qk. \tag{8}$$

Here

$$G=\frac{C^2-(Y-X)^2}{2[C+(Y-X)\cdot\xi]}=\frac{C^2-(p-u)^2-F^2-(q-v)^2}{2[C-F]} \tag{9}$$

where C is the constant path length from wave front X to wave front Y.

In order to obtain R as a function of only two parameters, use (6) which relates the four parameters u, v, p, q.

$$\begin{aligned}(R-X)\cdot X_u&=(p-u)+(G-F)F_u=0,\\ \text{and}\qquad (R-X)\cdot X_v&=(q-v)+(G-F)F_v=0.\end{aligned} \tag{10}$$

The substitution of values from (10) into (9) yields

$$2G(C-F)=C^2-F^2-(G-F)^2(F_u^2+F_v^2).$$

Subtract $2F(C-F)$ from both sides and the equation becomes a quadratic in $(G-F)$,

$$2(G-F)(C-F)=(C-F)^2-(G-F)^2(F_u^2+F_v^2)$$

which has the solution

$$G-F=(F-C)[1\pm(1+F_u^2+F_v^2)^{\frac{1}{2}}][F_u^2+F_v^2]^{-1}. \tag{11}$$

The ambiguity of sign can be resolved in a particular case.

Since $G=G(u, v)$ can be obtained from this equation, (10) and (11) yield $p=p(u, v)$ and $q=q(u, v)$. Therefore the reflector R in (8) is given as a function of u and v alone. In some simple problems, it is possible to eliminate the parameters u and v to obtain the reflector surface as $G=G(p, q)$.

As an example of the preceding analysis, let the wave front $X(u, v)$ be that produced by a source along the z axis whose phase variation is such as to yield the wave front surface $y^2=[(r^2-z^2)^{\frac{1}{2}}-a]^2-x^2$. In this case $y=F$, $x=u$, $z=v$.

In order to use (11), it is first determined that

$$y_z^2+y_z^2=(x^2+z^2T^2)/y^2$$

where

$$T^2=(x^2+y^2)/(r^2-z^2).$$

Then, from (11) one component of R is

$$G=y+\frac{y(y-C)[y\pm rT]}{x^2+z^2T^2}=y(1+D).$$

When this value is substituted into (10) the other two components of R become

$$\begin{aligned}p&=x(1+D),\\ q&=z(1+DT).\end{aligned}$$

Points on the reflector surface are obtained by computing G, p, and q for appropriate values of x, y, z. If z is set equal to zero, the reflecting curve is one of two parabolas, due to the ambiguity of sign. The correct reflector corresponds to the negative sign of the radical in (11).

As a check of the method, it might be noted that setting $a=0$ yields a spherical wave front, such that $T=1$ and $D=(C-y)/(r+y)$. Upon elimination of y from the components of R, there results

$$p^2+q^2=-(C+r)[2G-(C+r)]$$

which is the expected paraboloid surface.

The Effect of an Obstacle in the Fresnel Field on the Distant Field of a Linear Radiator

G. A. WOONTON
Department of Physics, McGill University, Montreal, Quebec, Canada
(Received October 19, 1949)

At radio wave-lengths the use of mirrors and lenses in the measurement of radiators, by methods which are customary in physical optics, is possible only if errors, due to incidental diffraction from the relatively small apertures of such apparatus, can be corrected by calculation. Theory is developed in this paper from which these calculations can be derived for linear radiators. A new relation which expresses the Fresnel field in terms of the distant field is fundamental to the method. Satisfactory agreement has been obtained between the predicted and measured distant fields of several electromagnetic horns whose near fields were obstructed; the dispersion between measured and predicted values is given as under one-half decibel but the details of the experiment are not reported.

INTRODUCTION

AT radio wave-lengths, the information from optical measurements often is obscured by incidental diffraction from the apertures of the component lenses, mirrors, and slits of the optical system. Incidental diffraction, although present in optical systems for visible light, can usually be neglected, but in the radio case, even for the shortest microwaves, the ratio of aperture dimension to wave-lengths is such that these effects, always, must be considered; practical limitations on physical dimensions and weight make it impossible to scale radio-optical devices in proportion to wave-length so that the ratio of aperture diameter to wave-length in the radio case is different by a factor of at least 10^{-5} from the ratio used in apparatus for measurements with visible light. It is for this reason that the application of optical techniques to radio measurements depends on the ability of the experimenter to calculate instrument errors and to use the calculations to plan the location of apertures so as to minimize the disturbance that they cause.

A problem of this nature, which is fundamental to many radio measurements, can be stated in specific terms; the radiation field from a linear radiator, for example a sectoral electromagnetic horn, is obstructed by a second aperture placed a short distance in front of it and at an arbitrary angle to its normal;[1] find the distant field produced by the combination. The analysis which follows is a general solution of this problem, and is capable of quantitative application to particular systems.

OPTICAL THEORY

An experimental investigation reported by Woonton, Hay, and Vogan[2] has shown that Kirchhoff's scalar formulation of Huygen's principle[3] is adequate to describe the distant diffraction field of a rectangular aperture whose dimensions are as small as 10 wave-lengths to a side and to describe the near field of the same aperture at a distance no greater than 10 or 20 wave-lengths from its opening. In the same investigation it was verified, also, that as in the optics of visible light, the complete fields can be calculated as the product of two independent, one-dimensional fields due separately to the electric distribution along the X axis of the aperture and along the Y axis. For these reasons, the solution which follows is based on the Kirchhoff formula and assumptions, and expresses the fields in terms of one coordinate only.

A system of Cartesian coordinates is chosen so that the origin lies at the intersection of the diagonals of a plane, rectangular, radiating aperture which will be called S_1; for first consideration S_1 is not rotated and lies wholly in the XY plane. The distribution of electric intensity along its X axis is given in both phase and amplitude by $F_1(x)$. At a distant point in the XZ plane, $P_1(R_1\theta_1)$ (where R_1 is the radius vector from the origin to P_1 and θ_1 is the angle between R_1 and the Z axis), the distant field (subject to the usual approximations, which include the requirements that θ_1 is not too great) is:

$$\varphi_1\left(R_1, \frac{\sin\theta_1}{\lambda}\right) = Re\frac{(\cos\theta_1+1)}{R_1}\exp(j[\omega t - kR_1]) \times Y\left(\frac{j}{2\lambda}\right)^{\frac{1}{2}}\int_{-\infty}^{\infty} F_1(x)\exp(-j2\pi x\gamma_1)dx, \quad (1)$$

in which λ = wave-length of the radiation, $k=2\pi/\lambda$, ω = angular velocity of the field, $j=(-1)^{\frac{1}{2}}$, Y = a factor which remains constant as long as P is confined to the XZ plane and which is an integral of the same form as that which appears in (1) but is related to aperture distribution in the Y direction, $\gamma_1=-(\sin\theta_1)/\lambda$.

Equation (1) represents a circular wave, expanding from the origin, whose front at radius R_1, in the XZ plane, is modified in phase and amplitude by the integral factor:

$$G_2(\gamma_1)=\int_{-\infty}^{\infty} F_1(x)\exp(-j2\pi x\gamma_1)dx. \quad (2)$$

[1] Woonton, Borts, and Carruthers, J. App. Phys. **21**, 428 (1950).
[2] Woonton, Hay, and Vogan, J. App. Phys. **20**, 71 (1949).
[3] J. S. Slater and N. H. Frank, *Electromagnetism* (McGraw-Hill Book Company, Inc., New York, 1947), p. 167.

(The use of the negative sign in the definition will be clear later.)

The distribution $F_1(x)$ produces a Fresnel distribution of electric intensity in front of the radiator, as well as the field at a great distance. At $z=b$ define an auxiliary set of $(\xi;\eta)$ coordinates in which the ξ- and η-axes are parallel to those of X and Y and take the new origin at $(0, 0, b)$. The distribution produced along the ξ-axis by $F_1(x)$ is $F_2(b, \xi)$, which for convenience will be described as $F_2(\xi)$. At a distant point $P_2(R_2\theta_2)$ (where R_2 is the radius vector from $z=b$ to P_2, and θ_2 is measured at $(0, 0, b)$ the distribution $F_2(\xi)$ may be thought of as producing the field instead of $F_1(x)$. This field is given by:

$$\varphi_2\left(b, R_2, \frac{\sin\theta_2}{\lambda}\right)=Re\frac{(\cos\theta_2+1)}{R_2}\exp(j[\omega t-kR_2])$$

$$\times Y'\left(\frac{j}{2\lambda}\right)^{\frac{1}{2}}\int_{-\infty}^{\infty}F_2(\xi)\exp(-j2\pi\xi\gamma_2)d\xi \quad (3)$$

where

$$\gamma_2=-(\sin\theta_2)/\lambda.$$

Equation (3) describes a circular wave expanding from $(0, 0, b)$ whose front at radius R_2 (measured from $z=b$) is modified in amplitude and phase by the integral factor

$$G_2(\gamma_2)=\int_{-\infty}^{\infty}F_2(\xi)\exp(-j2\pi\xi\gamma_2)d\xi. \quad (4)$$

The relation between the integral factors (2) and (4) which appear in Eqs. (1) and (3) can be found by comparison of (1) and (3) after (1) has been modified to express the field along the circular wave front marked out by P_2 as θ_2 varies. Let $R_1=(R_2+b)$ so that Eqs. (1) and (3) express the same field at $\theta_1=\theta_2=0$. Choose R_1 and R_2 both very large compared to b, so that in the amplitude factors of the two equations R_1 can be interchanged with R_2 and so that a single angle θ can be used to represent the θ-coordinate of corresponding points on the two circular wave fronts instead of separate angles θ_1 and θ_2. Because Eqs. (1) and (3) both express distant fields, one can reason that at any angle θ the two equations differ only in phase and this difference can be traced to two causes: the translation of the origin directly and the separation of the perimeters of the two circles which the translation of the origin causes. The first phase difference is constant and can be written by substitution:

$$\exp(-jkR_1)=\exp(-jk[R_2+b])$$
$$=\exp(-jkR_2)\exp(-jkb). \quad (5)$$

The second phase difference arises because Eq. (1) describes the field along a circle of radius (R_2+b) with center at the origin while Eq. (3) describes the field along a circle of radius R_2 with center at $(0, 0, b)$. At any angle, θ, the perimeters of the two circles are separated by a distance, δ, which can be written to an approximation that improves with the magnitude of R_1 and R_2 as:

$$\delta\doteqdot b(1-\cos\theta)\doteqdot b(\sin^2\theta)/2. \quad (6)$$

Equation (1) will describe the field along the circle marked out by R_2 only if its phase is corrected by the constant factor (5) and advanced by a variable factor proportional to the distance, δ, namely:

$$\exp(jkb\sin^2\theta/2)=\exp(j\pi b\lambda[\sin\theta/\lambda]^2). \quad (7)$$

Equate the modified Eq. (1) to Eq. (3) and cancel the common factors:

$$Y\exp(-jkb)\exp\left(j\pi b\lambda\left[\frac{\sin\theta}{\lambda}\right]^2\right)$$

$$\times\int_{-\infty}^{\infty}F_1(x)\exp(-j2\pi x\gamma)dx$$

$$=Y'\int_{-\infty}^{\infty}F_2(\xi)\exp(-j2\pi\xi\gamma)d\xi. \quad (8)$$

Define

$$G_3(\gamma)=\exp\left(j\pi b\lambda\left[\frac{(\sin\theta)}{\lambda}\right]^2\right);$$

then in the abbreviated notation:

$$Y\exp(-jkb)G_3(\gamma)G_1(\gamma)=Y'G_2(\gamma). \quad (9)$$

Because relative, rather than absolute amplitudes and phases are important in experimental work, in the discussion of the next section the constant factors in Eq. (9) will be dropped, for convenience, and the relation taken to be:

$$G_3(\gamma)G_1(\gamma)=G_2(\gamma). \quad (9a)$$

Figure 1 illustrates the relations between the aperture field, the Fresnel field, and the distant fields.

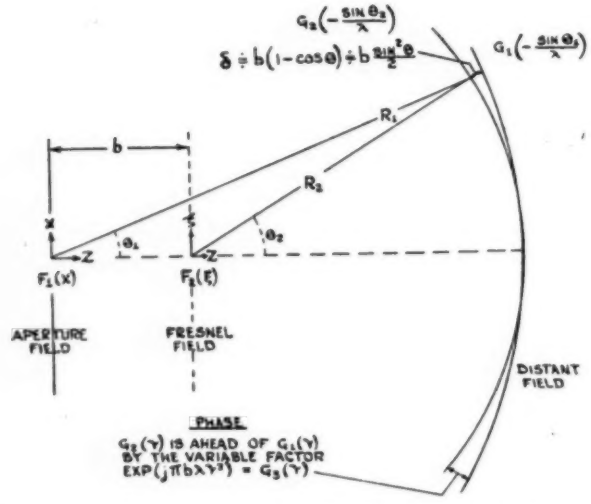

FIG. 1. Relations between the aperture field, Fresnel field and the distant field.

FOURIER TRANSFORM THEORY AND THE SOLUTION

For convenience in using tables[4] and to agree with Ramsay,[5] the definition has been made:

$$\gamma = -(\sin\theta)/\lambda$$

so that Eq. (2) has been written

$$G_1(\gamma) = \int_{-\infty}^{\infty} F_1(x) \exp(-j2\pi\gamma x)dx.$$

Michelson[6] in the field of optics of visible light and Spencer[7,8] and Ramsay[5] in connection with radiators have discussed the reciprocal relation of the Fourier transform pair that holds between an intensity distribution and the diffraction, or antenna pattern that it causes. These authors justify the use of the process inverse to that described in (2):

$$F_1(x) = \int_{-\infty}^{\infty} G_1(\gamma) \exp(j2\pi\gamma x)d\gamma. \tag{2a}$$

To abbreviate the analysis, transformation symbols are now introduced as has been done in the work of the writers,[5,7,8] who have been mentioned. Equations (2) and (2a) are written:

$$F_1(x) \leftrightarrow G_1(\gamma), \tag{10}$$

and in the same way:

$$F_2(\xi) \leftrightarrow G_2(\gamma), \tag{11}$$

$$F_3(\xi) \leftrightarrow G_3(\gamma) = \exp(j\pi b\lambda\gamma^2). \tag{12}$$

Since $G_2(\gamma) = G_1(\gamma)G_3(\gamma)$ it appears that on making use of the convolution theorem:

$$F_2(\xi) = \int_{-\infty}^{\infty} F_1(t)F_3(\xi - t)dt \leftrightarrow G_1(\gamma) \times G_3(\gamma). \tag{13}$$

$F_2(\xi)$ is the variable factor in the expression for the Fresnel field at $z=b$; Eq. (13) can be put into explicit form by first finding the transform of $F_3(\xi - t)$ from that of $F_3(\xi)$:

$$F_3(\xi - t) \leftrightarrow \exp(-j2\pi\gamma t)G_3(\gamma) = \exp(-j2\pi\gamma t) \exp(j\pi b\lambda\gamma^2) \tag{14}$$

and, by then writing out the integral implied by the transformation symbol:

$$F_3(\xi - t) = \int_{-\infty}^{\infty} \exp(j\pi b\lambda\beta^2) \times \exp(-j2\pi\beta t) \exp(j2\pi\beta\xi)d\beta \tag{15}$$

where the dummy label, β, has been introduced in place of, γ, to avoid confusion. Substitute (15) in (13):

$$F_2(\xi) = \int_{-\infty}^{\infty} F_1(t) \int_{-\infty}^{\infty} \exp(j\pi b\lambda\beta^2) \times \exp(-j2\pi\beta t) \exp(j2\pi\beta\xi)d\beta dt. \tag{16}$$

Equation (13) expresses the Fresnel field as a Fourier transform of the distant field and Eq. (16) expresses the Fresnel field in terms of the aperture field. Equation (9) and the reasoning that leads to it can be verified by evaluating the inner integral of Eq. (16) which then becomes:

$$F_2(\xi) = \left(\frac{j}{b\lambda}\right)^{\frac{1}{2}} \int_{-\infty}^{\infty} F_1(t) \exp\left(-j\frac{\pi}{b\lambda}[\xi - t]^2\right)dt. \tag{16a}$$

Equation (16a) will be recognized as the variable part of the Fresnel field expressed in the conventional manner by a Fresnel's integral and, in fact, (16a) can be made to agree completely with the conventional expression if the constant factors, which were dropped between Eqs. (9) and (9a), are reintroduced.

Up to this point there has been no suggestion of an obstruction in front of the aperture. Let a large screen be erected in the (ξ, η) plane at a distance, b, in front of S_1 and cut in it a rectangular opening, S_2, which extends along the ξ-axis from $-c/2$ to $+c/2$. Follow Kirchhoff in the assumption that in the opening S_2, $F_2(\xi)$ has its uninterrupted value, and that the intensity on the front surface of S_2 is zero everywhere else. $F_2(\xi)$ then must be given the mutilated form expressed by:

$$\begin{aligned} &F_2(\xi) = 0, && c/2 \leq |\xi| \leq \infty, \\ &F_2(\xi) \text{ is unchanged}, && -c/2 \leq \xi \leq c/2. \end{aligned} \tag{17}$$

The distant pattern will be modified from $G_2(\gamma)$ to a new function $G_{2m}(\gamma)$ by the mutilation of $F_2(\xi)$ which is caused by the screen. This can be written as the transform of $F_2(\xi)$ when expressed as in Eq. (16).

$$G_{2m}(\gamma) = \int_{-c/2}^{c/2} F_2(\xi) \exp(-j2\pi\xi\gamma)d\xi. \tag{18}$$

Reverse the order of integration so as to integrate first with respect to ξ, then with respect to t.

$G_{2m}(\gamma)$ is then found to be given by:

$$G_{2m}(\gamma) = c\int_{-\infty}^{\infty} G_1(\beta)\frac{\sin[\pi c(\beta - \gamma)]}{\pi c(\beta - \gamma)} \times \exp(j\pi b\lambda\beta^2)d\beta. \tag{19}$$

To convert $G_{2m}(\gamma)$ to $G_{1m}(\gamma)$, which is expressed as a wave diverging from S_1 (the original aperture), divide

[4] G. A. Campbell and R. M. Foster, "Fourier integrals for practical application," Bell Telephone System Monograph, B-584 (1931).
[5] J. F. Ramsay, Marconi Rev. **IX**, 139 (1946) ff.
[6] A. A. Michelson, Phil. Mag. **9**, 506 (1906).
[7] R. C. Spencer, Radiation Lab. Report 762-1 (December, 1945).
[8] R. C. Spencer, Radiation Lab. Report 762-2 (March, 1946).

by $G_3(\gamma)$ as indicated by Eq. (9a):

$$G_{1m}(\gamma)=c\int_{-\infty}^{\infty}G_1(\beta)\frac{\sin[\pi c(\beta-\gamma)]}{\pi c(\beta-\gamma)}\times\exp(j\pi b\lambda[\beta^2-\gamma^2])d\beta. \quad (20)$$

Equation (20) when substituted in Eq. (1) gives the distant field of S_1 as modified by S_2 at $z=b$ when S_1 is not rotated and lies in the XY plane; the solution is in terms of the unmutilated pattern $G_1(\beta)$, the width, c, of S_2, the distance, b, between the two screens, and the wave-length, λ, of the radiation.

The effect of rotating S_1 out of the XY plane by an angle, α, measured between the normal to S_1 and the Z axis can be found as follows: If α is not too great, and b not too small, the effect of rotation is to introduce a linear phase shift into the original $F_1(x)$ distribution. This is expressed by:

$$F_{1a}(x)=F_1(x)\exp[-j2\pi x(\sin\alpha)/\lambda] \quad (21)$$

which leads to the transformation:

$$F_1(x)\exp[-j2\pi x(\sin\alpha)/\lambda]\leftrightarrow G_1[\beta+(\sin\alpha)/\lambda]. \quad (22)$$

On substituting $G_1[\beta+(\sin\alpha)/\lambda]$ for $G_1(\beta)$ in Eq. (20) the complete solution of the problem is obtained:

$$G_{1am}(\gamma)=c\int_{-\infty}^{\infty}G_1\left[\beta+\frac{(\sin\alpha)}{\lambda}\right]\times\frac{\sin[\pi c(\beta-\gamma)]}{\pi c(\beta-\gamma)}\exp(j\pi b\lambda[\beta^2-\gamma^2])d\beta. \quad (23)$$

Equation (23) can be verified by reducing it to known forms. Put $\alpha=0$ and $b=0$ so that the second aperture S_2 lies on S_1 and limits $F_1(x)$ to the range $|x|\leq c/2$. Equation (23) becomes:

$$G_{1am}(\gamma)=c\int_{-\infty}^{\infty}G_1(\beta)\frac{\sin[\pi c(\beta-\gamma)]}{\pi c(\beta-\gamma)}d\beta, \quad (24)$$

which is a result obtained by Ramsay.[9]

If in Eq. (23) $c\to\infty$, then the screen S_2 no longer obstructs the near field. Since:

$$Lt_{c\to\infty}\frac{\sin[\pi c(\beta-\gamma)]}{\pi c(\beta-\gamma)}=\frac{1}{c}S_0(\beta-\gamma), \quad (25)$$

where $S_0(\beta-\gamma)$ is a unit impulse at $\beta=\gamma$, Eq. (23) reduces to the unmutilated distant field, $G_1[\beta+(\sin\alpha)/\lambda]$, when S_2 is removed from the near field.

[9] J. F. Ramsay, Marconi Rev. X, 90 (1947).

EXPERIMENTAL METHODS AND RESULTS

The amplitude of the electric field, in the aperture of an electromagnetic horn, in the E-plane, can be expressed to a good approximation by:

$$F_1(x)=F_A\exp[-j(\pi x^2/\lambda l)]$$

where

$$F_A=0 \text{ if } (a/2)<|x|, \qquad F_A=A \text{ if } |x|<a/2 \quad (26)$$

in which l = distance from the vertex to the aperture plane of the horn, a = width of the horn aperture in the E-plane. The E-plane aperture distribution function, for an electromagnetic horn, which may be rotated out of the XY plane as in Eq. (21) is therefore:

$$F_1(x)=F_A\exp\left(-j\left[\frac{\pi x^2}{\lambda l}+\frac{2\pi x\sin\alpha}{\lambda}\right]\right) \quad (27)$$

with F_A restricted as in (26).

Elliot and Rigby* have shown that on substitution of Eq. (27) in Eq. (18) it is possible to integrate Eq. (18) twice, then expand the resulting integral into an asymptotic series. They have estimated that when the constants of the expansion have the values $c=110$ cm, $b=100$ cm, $a=32$ cm, $\lambda=3.2$ cm, the first two terms of the series give the relative amplitudes of $G_{2am}(\gamma)$ to a precision of not worse than 1 db in the angular interval $-20°\leq\alpha\leq 20°$.

The E-plane amplitudes of $G_{2am}(\gamma)$ have been calculated at $\alpha=0$, 5, 10, 15, and 20 degrees for two horns, radiating 3.2-cm waves, through a mutilating aperture, 110 cm wide in the E-plane by 22 cm high in the H-plane, placed 100 cm in front of the horn aperture. The aperture of both horns was taken to be square, 32 cm to the side, and the lengths of the horns were taken as 100 and 50 cm, respectively. Patterns measured at a wave-length of 3.2 cm both with and without the mutilating aperture, for two horns of these dimensions are reported in Figs. 4 and 5 of a companion paper.[1] Comparison of the measured and calculated points, between $\pm 20°$ indicate that the probable error in the calculation, for the horn of length 100 cm is ± 0.25 db, and for the 50-cm horn, is ± 0.34 db.

ACKNOWLEDGMENT

The experimental work associated with this research was made possible by a grant for equipment from the Defence Research Board of the Department of National Defence, Ottawa, Canada. The writer wishes to thank Dr. H. A. Elliot and Miss E. C. Rigby, both of McGill University, for permission to refer to their unpublished expansion of Eq. (18).

* H. A. Elliot and E. C. Rigby (unpublished).

Second-Order Transition Temperatures and Related Properties of Polystyrene. I. Influence of Molecular Weight*

THOMAS G. FOX, JR., AND PAUL J. FLORY
Department of Chemistry, Cornell University, Ithaca, New York
(Received November 17, 1949)

Dilatometric and viscometric data on fractionated polystyrenes containing diethylbenzene end groups are presented over wide temperature ranges. The second-order transition temperature, viscosity-temperature coefficient, and specific volume all change rapidly with increasing molecular weight toward asymptotic limits which are practically reached at $M \cong 30{,}000$. Empirical expressions are presented relating these properties to molecular weight and temperature. In each case the dependence on molecular weight is expressed as a simple function of $\bar{M}_n^{-1}$. These observations are interpreted and correlated on the basis of the hypothesis that the local configurational order in a liquid polymer is disturbed by the introduction of end groups to a degree that is proportional to their number. The second-order transition does not represent an isoviscous state. The internal local configurational structure appears to be equivalent, and independent of temperature, in all polystyrenes below their second-order transition temperatures.

INTRODUCTION

A LIQUID which may be cooled without incidence of crystallization solidifies to a glass over a fairly narrow temperature range which is characteristic of the substance.[1,2] This is true not only of hydrocarbons, polar and hydrogen-bonding liquids, inorganic glasses, etc., but also of amorphous polymers (including semi-crystalline, or semi-amorphous polymers) regardless of their composition or structural pattern (i.e., non-linear network polymers as well as linear ones). The temperature about which this transformation takes place is usually referred to as the "glass" temperature T_g, or the "second-order transition temperature"; for polymers it is often designated as the "brittle temperature," inasmuch as the polymer changes from a highly viscous liquid, or rubbery solid, to a brittle substance which will not tolerate appreciable deformation without fracture at all lower temperatures.

It is well established that this so-called "second-order transition" is not an equilibrium transition in the thermodynamic sense, but that it originates from kinetic limitations on the rates of the internal adjustments occasioned by changes in temperature (or by mechanical stress). At temperatures below T_g, the internal mobility is insufficient for maintenance of the equilibrium internal configuration and, hence, of the equilibrium volume. No discontinuity is observed in the first-order properties, volume and internal energy, but the second-order properties, thermal expansion coefficient and heat capacity, exhibit abrupt changes by means of which the "transition" is easily located.

The macroscopic viscosity often is employed as an inverse measure of internal mobility in monomeric substances, and it has been pointed out that the second-order transition generally occurs at a viscosity of about 10^{12} poises. The macroscopic viscosity of a polymer, however, depends not only on the mobility of each segment but also on an intersegment cooperation factor which increases rapidly with molecular weight.[3,4] If the second-order transition in polymers depends only on the local segment mobility and not on the interactions between all of the segments of a given molecule, then the magnitude of the macroscopic viscosity should not afford a universal measure of the approach to the second order transition; viscosities well above 10^{12} poises at T_g should be expected if the molecular weight is large. On the basis of the same postulate, the second-order transition might be expected to be independent of the molecular weight of the polymer except insofar as it affects the liquid configuration of the polymer.

Considerations such as these point to the desirability of securing reliable information on the dependence of the volume (as an index of liquid configuration) and of the viscosity of polymers on their molecular weights and temperatures, and on the dependence of T_g on molecular weight. Asymptotic increases of T_g's for polystyrenes,[5] polyisobutylenes,[6] and poly-(ethylacrylates)[7] with their "molecular weights" have been indicated by previous work on polymers of unknown degrees of heterogeneity. In a recent paper we have reported a qualitatively similar asymptotic increase in the viscosity-temperature coefficient with the molecular weights M of polystyrene fractions.[4] The rapid increase of both T_g and the viscosity-temperature coefficient toward their limiting values with increase in M contrasts sharply with the sustained increase in viscosity with increasing M even to the highest values investigated.[4]

* The work presented in this paper was carried out at Cornell University in connection with the Government Research Program on Synthetic Rubber under contract with the Office of Rubber Reserve, Reconstruction Finance Corporation.

[1] W. Kauzmann, Chem. Rev. **43**, 219 (1948).

[2] R. F. Boyer and R. S. Spencer, *Advances in Colloid Science* (Interscience Publishers, Inc., New York, 1946), Vol. II, p. 1.

[3] P. J. Flory, J. Am. Chem. Soc. **62**, 1057 (1940).

[4] T. G. Fox, Jr. and P. J. Flory, J. Am. Chem. Soc. **70**, 2384 (1948).

[5] E. Jenckel and K. Ueberreiter, Zeits. f. physik. Chemie **A182**, 361 (1938).

[6] K. Ueberreiter, Zeits. f. physik. Chemie **B45**, 25 (1940).

[7] R. H. Wiley and G. M. Brauer, J. Polymer Sci. **3**, 647 (1948).

TABLE I. The polystyrenes used for fractionation.

Polymer	Molar ratio styrene/diethylbenzene	Reaction temperature	Reaction time, hours	Extent of reaction (percent)	$\bar{M}_v$	Initial conc. for fractionation g/100 ml
A	1	150°	2	27	120,000	2.0
B	0.093	150°	9	72	9560	2.0
C	0.051	150°	17	90	4870	1.5

In the present investigation the specific volumes of polystyrene fractions have been investigated as functions of temperature and molecular weight. Second-order transition temperatures have been secured in the customary fashion from the discontinuity in the thermal expansion coefficient. The results have been correlated with the viscosity-temperature coefficient and its observed dependence on M. Polystyrene has been chosen as a model non-polar polymer for this investigation on account of the convenient location of its second-order transition temperature, the simplicity of its structure, and the comparative abundance of information concerning its various properties.

EXPERIMENTAL

Preparation and Fractionation

Three polymers of styrene of varying molecular weights (Table I) were prepared by thermal polymerization in diethylbenzene *in the absence of added catalyst*. The concentrations of styrene employed and other details pertinent to these polymerizations are summarized in Table I. The polymers were separated by precipitation in an excess of vigorously stirred methanol and were dried in vacuum at 60°.

These polymers were fractionated by the single precipitation technique described in a previous paper.[4] The initial concentrations of the solutions employed are shown in the last column of Table I. Each of the two polymers of lower molecular weight was separated into nine fractions by fractionating from acetone solution at 30° using as the precipitant a mixture consisting of equal volumes of water and methanol. Each individual fraction employed here represented from 5 to 17 percent of the whole polymer (Table II). The polystyrene of higher molecular weight (120,000) was separated into three fractions employing methyl ethyl ketone-methyl alcohol as the solvent-precipitant combination. Only the middle fraction, $M=85{,}000$, representing 38 percent of the whole polymer was retained for subsequent experiments.

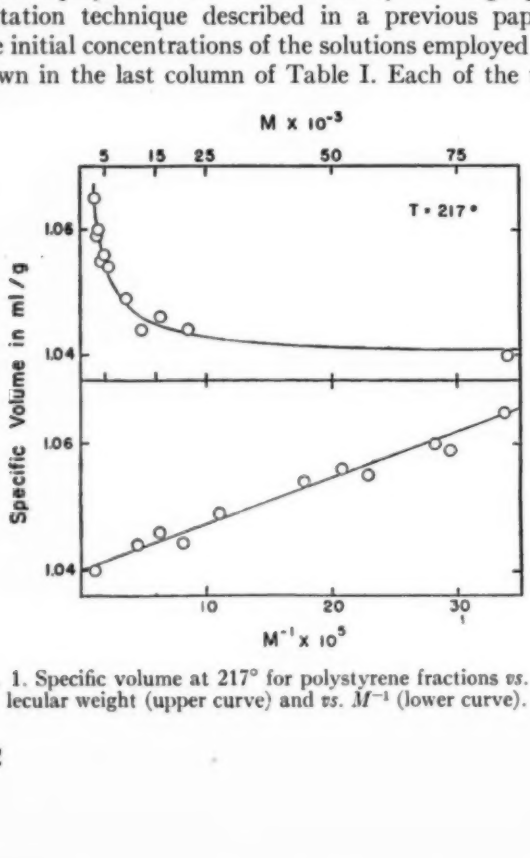

FIG. 1. Specific volume at 217° for polystyrene fractions *vs.* molecular weight (upper curve) and *vs.* M^{-1} (lower curve).

Molecular Weight Determination

Molecular weights of the polystyrene fractions have been calculated from their intrinsic viscosities, $[\eta]$, in freshly distilled benzene, using the relationship of Ewart[8]

$$\log\bar{M}_v=(\log[\eta]+4.013)/0.74,$$

where $\bar{M}_v$ is the viscosity average molecular weight. The solution viscosities were measured at 30.00±0.01° using a Ubbelohde No. 1 viscometer the calibration of which included the kinetic energy term.[9] In each case the intrinsic viscosity has been calculated from the relative viscosity, η_r, of a single solution by means of the viscosity-concentration relationship reported by Tingey.[10]

$$\ln\eta_r/c=[\eta]-0.125[\eta]^2c,$$

where c is expressed in g/100 ml.

Molecular weights determined in this way are generally reproducible to ±2 percent.

Determination of Specific Volumes

The pycnometers and the technique employed were similar to those described in a previous publication.[3] Densities were determined at 217° by filling a weighed pipette of known volume (from 1 to 2 ml) with the liquid polymer at this temperature, and subsequently weighing at room temperature. The reproducibility of the data was generally within ±0.1 percent.

Dilatometric Measurements

The dilatometers and techniques employed resemble those described by Bekkedahl.[11] A weighed quantity (generally about two grams) of bubble-free polymer, previously dried under vacuum at 217°, was placed in the bulb of a glass dilatometer and the bulb was sealed, with precautions to avoid heating the polymer. Mercury was introduced under vacuum (0.005 mm Hg).

[8] R. H. Ewart, paper presented at the Atlantic City Meeting of the American Chemical Society (April 14, 1947).

[9] The calibration method outlined in ASTM Designation D445-39T was employed.

[10] H. C. Tingey, unpublished data referred to by R. H. Ewart, *Advances in Colloid Science* (Interscience Publishers, Inc., New York, 1946), Vol. II, p. 210.

[11] N. Bekkedahl, J. Research Nat. Bur. Stand. **43**, 145 (1949).

TABLE II. Dilatometric data on polystyrene fractions.

Polymer fraction	Percent of unfractionated polymer	M	T_g	v_{140} ml/g	v_g ml/g Obs.	v_g ml/g Calc. by Eq. (4)	(dv/dT), ml/g/° $\times 10^4$ $(dv/dT)_1$	$(dv/dT)_2$	$(dv/dT)_3$
A2	38	85000	100°	0.989	0.969	0.968	—	4.9	2.3
A2	38	85000	100	0.990	0.969	0.968	7.2	5.1	2.0
A2	38	85000	98	0.989	0.970	0.968	—	4.6	2.2
A2	38	85000	99	0.991	0.970	0.968	7.1	5.0	2.4
B1	10.0	22000	89	0.992	0.963	0.965	—	5.7	2.7
B2	15.0	16000	86	0.993	0.962	0.964	—	5.7	2.3
B4	16.7	9150	77	0.996	0.960	0.962	—	5.6	2.4
B5	12.5	7200	78	0.998	0.964	0.962	7.0	5.5	—
B6	10.0	5600	73	1.003	0.963	0.960	—	6.1	2.6
B6	10.0	5600	75	1.000	0.967	0.960	—	5.1	2.7
B6	10.0	5600	76	1.002	0.966	0.960	7.3	5.6	—
C6	16.7	4810	64	1.003	0.962	0.959	—	5.3	2.6
C6	16.7	4810	66	1.003	0.962	0.959	7.6	5.5	—
B7	5.4	4300	62	1.003	0.956	0.958	—	6.0	2.4
B7	5.4	4300	63	1.003	0.957	0.958	—	5.8	2.5
B7	5.4	4300	62	1.002	0.956	0.958	7.6	6.0	—
B7	5.4	4300	63	1.003	0.957	0.958	—	5.9	2.8
C7	12.3	3540	53	1.005	0.957	0.956	—	5.5	2.6
C8	10.5	2970	40	1.007	0.955	0.953	—	5.3	2.1
C8	10.5	2970	—	1.005	0.953	0.953	8.4	5.3	—
C8	10.5	2970	—	1.006	0.953	0.953	8.0	5.3	—
C8	10.5	2970	—	1.007	0.952	0.953	—	5.5	—

The amount of mercury in the dilatometer was determined by weighing. The volume of polymer plus mercury was calculated at the calibration temperature, 217°, where the density of the polymer was known from the absolute specific volume measurements. The position of the mercury in the capillary tube was noted at 217° and then at lower temperatures usually at intervals of 10°. The measurements were made in a constant temperature bath regulated within ±0.1° and the relative densities generally were accurate to ±0.03 percent. At all temperatures except those in the vicinity of T_g, volume equilibrium was quickly established and in trial experiments no further change could be observed over a period of 24 hr. Hence before recording the volume the sample was held for a period of 10 to 60 min. at each temperature 10° or more above T_g and from 6 to 12 hr. at all lower temperatures.

Melt Viscosities

Melt viscosities in the range of 10 to 10^6 poises were determined by observing the rate of flow into uniform bore capillary viscometers under a measured pressure differential. The calibration and use of these viscometers have been described.[4] For measurement of viscosities from 0.1 to 10 poises, pipette type viscometers were employed. These consisted in each case of a Pyrex capillary tube of 1-mm bore with a small bulb (capacity 0.2 to 1.0 ml) about 12 to 15 cm from the lower end of the capillary. Absolute viscosities in poises were calculated in this case from $\eta = klp$, where l is the measured time required to fill the viscometer bulb under a predetermined pressure differential p, and k is a constant determined from the lp product for an oil the viscosity of which was accurately determined with the capillary viscometers mentioned above. Temperature control was provided by means of vapor baths (±0.3°) above 100° and by thermostated oil baths (±0.1°) at lower temperatures. The viscosity values usually were reproducible to ±3 percent.

High Temperature Stability

It was reported previously[4] that phenyl β-naphthylamine greatly retards the degradation of polystyrene at high temperatures, and that 0.5 percent of this substance assures adequate stability to permit measurement of viscosities up to 217°. The experiments on which this conclusion was based were conducted on polymers of high molecular weight, the assumption being made that the lower polymers would be at least

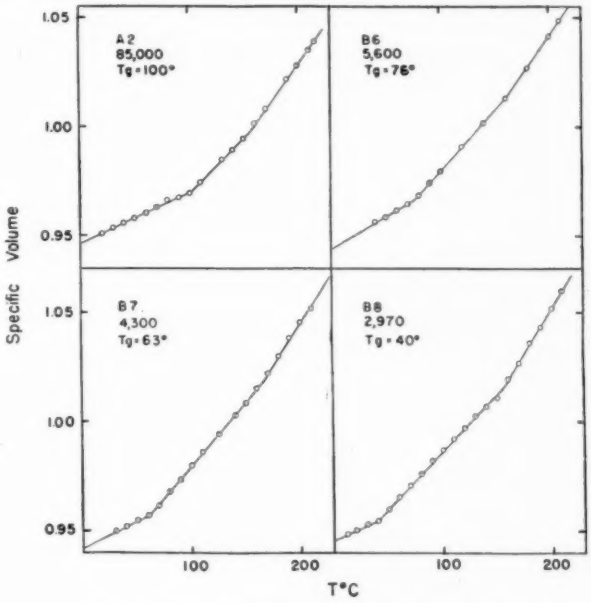

FIG. 2. Specific volume-temperature curves for polystyrene fractions.

TABLE III. Viscosity-temperature data for polystyrene fractions.

Polymer fraction	M	η_{217}, poises	log(η_T/η_{217}) at the indicated temperature (°C) 190	160	140	130	120	110	100	95	90	85	80	75
*A*2	85000	2000		2.0										
*B*1	21500	51.3	0.70	1.94	3.36	4.10								
*B*2	16000	26.7	0.74	1.85	3.21	3.89								
*B*3	12300	15.7												
*B*4	9100	9.13	0.54	1.61	2.80[a]	3.45	4.31							
*B*5	7230	5.29												
*B*6	5600	2.60	0.50	1.44		2.99		4.58	5.72					
*C*6	4810	1.36	0.45	1.25	2.17			4.03	4.95	5.52				
*B*7	4300	1.55	0.38	1.26		2.53		4.06	4.96					
*C*7	3540	0.59	0.47	1.11	1.89			3.54	4.29		5.24	5.83		
*B*8	3400	0.80	0.42	1.01		2.16			4.19		5.25			
*C*8	2970	0.32	0.41	0.93	1.58			3.07	3.58		4.38		5.33	5.92

[a] Interpolated.

as stable. Subsequent experiments revealed, however, that phenyl β-naphthylamine fails to inhibit degradative reactions in the lower polystyrenes included in the previous investigation. These low polymers were prepared with the aid of benzoyl peroxide initiation, and a connection between the observed instability and the presence of benzoate end groups in the polystyrene molecules[12] was indicated by the sublimation of a quantity of pure benzoic acid when these polymers were heated at 217° under reduced pressure. The low molecular weight polystyrenes prepared as described above *without the use of catalyst* (Table I) were relatively stable. When heated for an hour at 217° in an inert atmosphere (pure nitrogen) they discolored only slightly and exhibited no change in intrinsic viscosity even in the absence of inhibitor.

RESULTS

Specific Volumes at 217° *vs.* Molecular Weight for Polystyrene Fractions

The specific volumes of eleven polystyrene fractions ranging in molecular weight from 2970 to 85,000 were determined at 217° by the constant volume pipette method. The specific volume at 217°, v_{217}, decreases with increasing molecular weight in the lower range and is relatively constant for molecular weights above 25,000 (upper curve of Fig. 1). When the specific volume is plotted against $1/M$ as in the lower portion of Fig. 1, the data are well represented by the straight line, the equation of which is

$$v_{217}=1.040+72/M. \tag{1}$$

The units employed for the specific volume throughout this paper are ml/g.

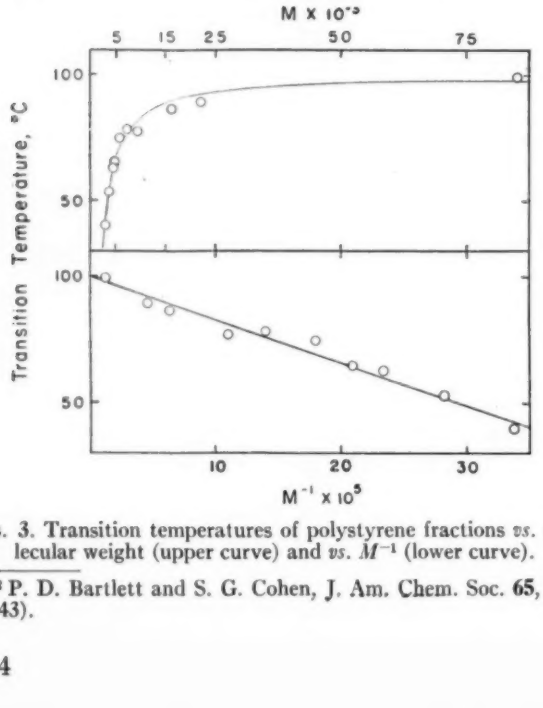

FIG. 3. Transition temperatures of polystyrene fractions *vs.* molecular weight (upper curve) and *vs.* M^{-1} (lower curve).

[12] P. D. Bartlett and S. G. Cohen, J. Am. Chem. Soc. **65**, 543 (1943).

Dilatometric Data on Polystyrene Fractions

Specific volumes were measured by the dilatometric method as a function of temperature on ten polystyrene fractions ranging from 2970 to 85,000 in molecular weight. As illustrated in Fig. 2, the volume-temperature curve up to 160° for each polymer may be represented by two intersecting straight lines. The temperature at which these lines intersect is taken as the second-order transition temperature, T_g. In the vicinity of 160°, the volume-temperature coefficient (i.e., the slope) exhibits a further increase with increasing temperature. The results in this range may again be approximated, for simplicity, by two intersecting straight lines, the temperature at the intersection being about 160°. Hence, each polymer may be characterized by five quantities: T_g, the volume v_g at T_g, and three volume-temperature coefficients, $(dv/dT)_1$ above 160°, $(dv/dT)_2$ between 160° and T_g, and $(dv/dT)_3$ below T_g. The values of these parameters, as obtained from a series of experiments, details for which are not included here, are presented in Table II.

The transition temperature T_g becomes almost independent of molecular weight above 25,000 but decreases rapidly with decreasing molecular weight below this value (upper curve of Fig. 3). In analogy with the dependence of specific volume on M^{-1}, T_g is likewise a linear function of M^{-1}, as is shown in the lower curve of Fig. 3. The equation of the straight line is

$$T_g=100-1.7\times10^5/M \tag{2}$$

from which the upper curve of Fig. 3 has been calculated.

Although at T_g the abrupt change in slope and the accompanying increase in the time needed for equilibration justify the use of a function with a discontinuity in its slope at this temperature, the use of two straight lines intersecting at 160° to represent the data above T_g is arbitrary. The change of slope at 160° is much smaller than that observed at T_g, and a line with curvature over a wide range about 160° would represent the data equally well.

The specific volume-temperature coefficients $(dv/dT)_2$ and $(dv/dT)_3$ (Table II) appear to be independent of molecular weight within the admittedly large experimental error involved in their evaluation over limited temperature ranges. Average values are 5.5 and 2.5 $\times 10^{-4}$, respectively. The value of $(dv/dT)_1$ is about 7×10^{-4} with an indication of an increase at very low molecular weight.

The portion of the volume-temperature curve between T_g and 160° may be represented by the equation

$$v = A + 5.5\times 10^{-4}T + 53/M, \quad 160 \geq T \geq T_g, \qquad (3)$$

where A is a constant equal to 0.913 and T is in degrees centigrade. Combining this with Eq. (2), we obtain

$$v_g = 0.943 + 2.4\times 10^{-4}T_g. \qquad (4)$$

Values of v_g calculated by this equation agree within experimental error with the observed values, as shown in Table II. In view of the non-dependence of $(dv/dT)_3$ on molecular weight, the specific volume below T_g is given by

$$v = v_g - 2.5\times 10^{-4}(T_g - T), \quad T \leq T_g$$

and combining this with Eq. (4), ignoring the slight difference between the two temperature coefficients, we obtain

$$v = 0.943 + 2.5\times 10^{-4}T, \quad T \leq T_g. \qquad (5)$$

This equation illustrates the important observation that the specific volume below the transition temperature is substantially independent of the molecular weight.

Volume-Time Relationships

The effect of temperature on the rate of volume relaxation was determined for several polystyrene fractions exhibiting values of T_g from 60 to 100°. In each case a dilatometer containing the polymer (and mercury) was quickly transferred from a bath at temperature T_1, generally about 30° above T_g, to a second constant temperature bath at a lower temperature T_2. The volume was then observed as a function of time. Subsequently the polymer was again heated to T_1 and the procedure repeated at a different temperature T_2. At temperatures T_2 exceeding T_g by about 10°, temperature and volume equilibria appeared to be attained simultaneously. At lower temperatures the volume was observed to decrease approximately linearly with the logarithm of time, at least for periods up to 24 hr. The magnitude of the rate of volume relaxation, which was too high to measure about 10° above T_g, had a value of about 30 to 50×10^{-4} at T_g, as measured by the slope of the v *vs.* log$t$ curve (t in min.), and decreased rapidly with decreasing temperature, becoming practically constant at a temperature generally about 10° below T_g. This limiting value of $-dv/d\log t$ was about 8×10^{-4} for all polystyrenes studied.

These results emphasize the fact that although the value of T_g depends on the observation time employed, the marked temperature dependence of the rate of volume relaxation in the vicinity of T_g makes it impossible, using reasonable periods of time, to appreciably alter the value of T_g; it would, for example, be increased by only 5 or 10° on decreasing the time scale of the experiment from 24 hr. to 5 min.

It has been reported[13] that high molecular weight polystyrene previously kept at 20° for two years can be heated from 20 to 140° without undergoing a second-order transition and, further, that the annealing times for this polymer at 20 to 30° below the usual value of T_g are measured in hours or at most in a few days. This reported observation cannot be reconciled with the present results which indicate that the annealing time in this range would consist of many centuries at the least. It is therefore doubtful whether an equilibrium volume-temperature curve for polystyrene has been obtained in the indicated range.[14]

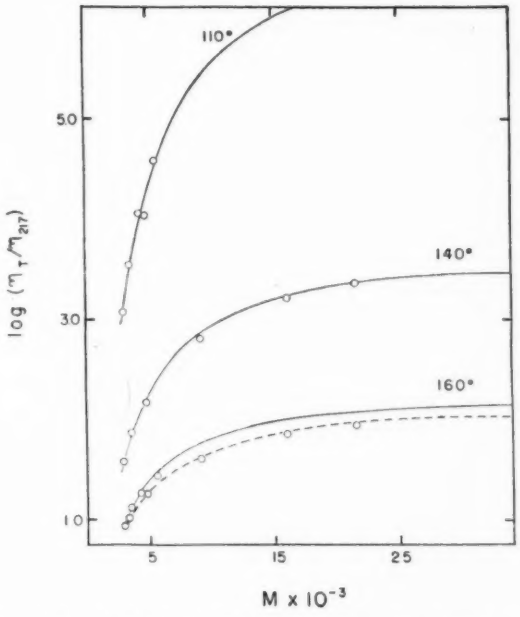

FIG. 4. Log(η_T/η_{217}) *vs.* M for polystyrene fractions at several temperatures. The solid curves are calculated by Eq. (7). The dotted line is calculated by Eq. (6) using the value of $F(T)$ at 160° obtained from Fig. 5.

[13] R. S. Spencer and R. F. Boyer, J. App. Phys. **17**, 398 (1946).

[14] Close scrutiny indicates that the reproducibility of the data of reference 13 is poor. In at least one of the two experiments the

Viscosity-Temperature-Molecular Weight Relationships for Polystyrene Fractions

Viscosities were measured at 217° and at lower temperatures for twelve polystyrene fractions of molecular weight from 2970 to 85,000 (Table III). The viscosities at 217° (η_{217}) for the fractions of higher molecular weight are in good agreement with the viscosities previously reported,[4] while those for the fractions of lower molecular weight are generally about 10 percent higher. This discrepancy almost certainly arises from the susceptibility to decomposition of the lower polystyrenes previously used as pointed out in the Experimental section. The relation between $\log(\eta_T/\eta_{217})$ and $1/T$ (in °K) is non-linear and its dependence on molecular weight is qualitatively similar to that previously reported.[4,15]

The dependence of the viscosity-temperature coefficient on molecular weight is illustrated in Fig. 4 where values of $\log(\eta_T/\eta_{217})$ at 160, 140, and 110° are plotted *vs.* the molecular weight. At a given temperature T the quantity $\log(\eta_T/\eta_{217})$ increases with increasing molecular weight up to about 25,000 beyond which it is relatively constant. Its dependence on M is similar for different temperatures, which suggests that $\log(\eta_T/\eta_{217})$ may be expressed as the product of two factors, one of which depends only on T and the other only on M. In further support of this supposition, and in analogy with the dependence of the specific volume and the second-order transition temperature on M, plots (Fig. 5) of $\log\log(\eta_T/\eta_{217})$ *vs.* $1/M$ from 90 to 190° are represented by a set of parallel straight lines. The indicated relationship may be written

$$\log(\eta_T/\eta_{217}) = F(T)e^{-2530/M} \tag{6}$$

where $F(T)$ is a function of the absolute temperature only. This equation offers a satisfactory limiting form at both very low and very high molecular weights.[16]

In the quest for a suitable empirical expression for $F(T)$, the viscosity-temperature function at $M=\infty$, it has been found (Fig. 6) that the values of $F(T)$ obtained from the intercepts at $1/M=0$ in Fig. 5 are linear functions of $1/T^6$, where T is in °K.[17] Hence the empirical relationship

$$\log(\eta_T/\eta_{217}) = 2.92\times10^{15}(1/T^6 - 1/\langle 490\rangle^6)e^{-2530/M} \tag{7}$$

expresses the dependence of the temperature coefficient of viscosity on both temperature and molecular weight. Differentiating we obtain the expression for E_T, a quantity which we have called the "apparent energy of activation for viscous flow."[4]

$$R\,d\ln(\eta_T/\eta_{217})/d(1/T) = E_T = (8.1\times10^{17}/T^5)e^{-2530/M} \tag{8}$$

where the units for E_T are cal./mole.

The extent to which the data of Table III conform to Eq. (7) is illustrated in Fig. 4. The solid curves are calculated by Eq. (7) and the circles represent the experimental points. At 110 and 140° the agreement is good, while at 160° the calculated ratio (solid line) is too high. This failure is due to the inadequacy of the form of the temperature dependence rather than to the exponential dependence on the molecular weight, as is indicated by the agreement between the dotted line of Fig. 6 and the experimental points at 160°. The latter line was calculated using the value of $F(T)$ obtained from the extrapolation of the data at 160° to $M=\infty$ (Fig. 5) rather than from Eq. (7). [The values of $F(T)$ at 140 and 100° obtained from the intercepts of Fig. 5 are in agreement with the respective values calculated for $M=\infty$ by Eq. (7).]

In general the discrepancy between viscosities calculated by Eq. (7) and the observed values is less than 20 percent. It is possible that the higher discrepancies which occur are due to a slight degradation of the polymer during the viscosity determinations. On the other hand, Eqs. (7) and (8) are presented merely as approximate empirical representations of the data, which may not necessarily be significant theoretically. They are included primarily for their value in interpolating and extrapolating the experimental measurements.

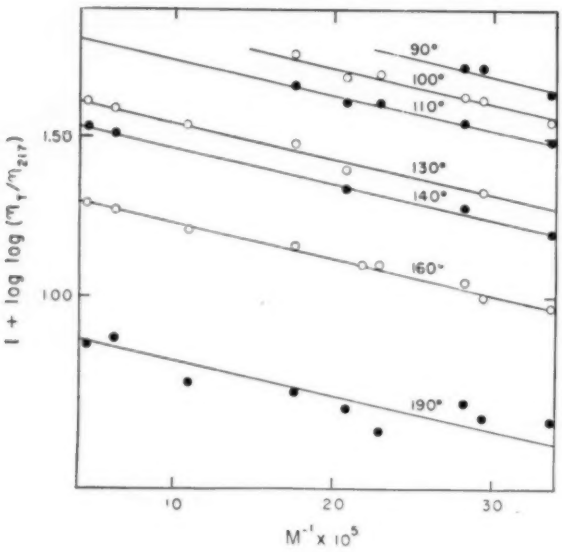

FIG. 5. Log $\log(\eta_T/\eta_{217})$ *vs.* $1/M$ for polystyrene fractions at various temperatures.

data could be represented as having a second-order transition at 90°. It may be significant that the values of the "equilibrium" expansion coefficients were about 25 to 30 percent lower than that corresponding to the value of $(dv/dT)_2$ reported here.

[15] The viscosity-temperature coefficients for the high molecular weight polystyrene fractions are identical with those reported in reference 4, but they decrease less rapidly with decreasing molecular weight. These differences probably are due to the occurrence of decomposition in the previous unstable fractions.

[16] Over the molecular weight range investigated, $\log(\eta_T/\eta_{217})$ may alternately be represented as decreasing linearly with $1/M$. However, this relationship must fail at low molecular weights when the quantity $(1-\text{const.}/M)$ becomes small or negative (const.$\cong$1600).

[17] The use of the sixth power of the temperature affords a better approximation to the data than either the fifth or the seventh powers. No attempt was made to employ a fractional power of T.

The use of these equations is illustrated in Table IV where values of $\log\eta$ and E_T have been calculated for polystyrenes of various molecular weights at their transition temperatures. Here T_g has been calculated in each case from the molecular weight by Eq. (2); $\log\eta_T$ at T_g has been calculated from Eq. (7) together with the viscosity-molecular weight relationship at 217°,[4] and E_T has been calculated by Eq. (8). The viscosities of polystyrene fractions at their transition temperatures are not identical but on the contrary vary considerably with molecular weight. The calculated values of E_T at T_g for the various polystyrene fractions, however, are all within 2 kcal. of 110 kcal. per mole. The second-order transition temperatures for a series of polystyrenes do *not* occur at an isoviscous state but *the viscosity-temperature coefficient at the transition temperature is independent of molecular weight.*

The approximate constancy of E_T at T_g may be deduced alternately from Eq. (8). If we require the temperature T at which a polystyrene of molecular weight M has the same value of E_T as that for polystyrene of $M=\infty$ at the transition temperature of the latter ($T_{g,\infty}$), then from Eq. (8)

$$\frac{8.1\times10^{17}}{T^5_{g,\infty}}=\frac{8.1\times10^{17}}{T^5}e^{-2530/M}$$

or solving for T and using the first two terms of the series expansion of the exponential term

$$T=T_{g,\infty}(1-506/M). \tag{9}$$

Inserting the value of 373°K for $T_{g,\infty}$, and converting to °C

$$T=100-1.9\times10^5/M \tag{10}$$

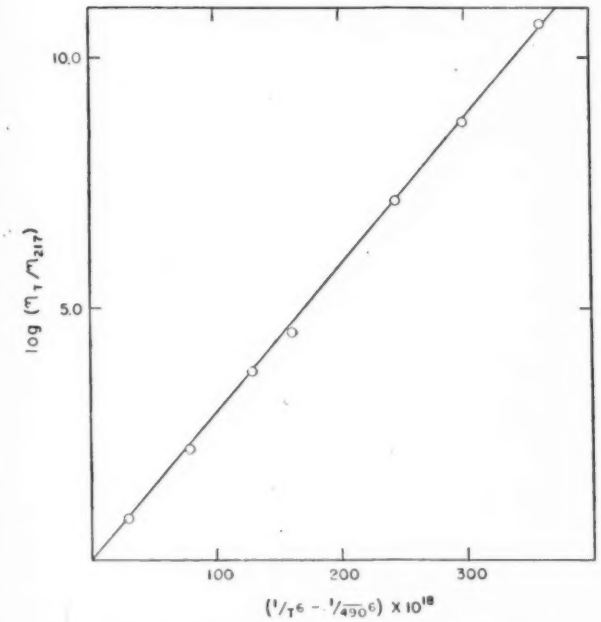

FIG. 6. Log (η_T/η_{217}) for polystyrene of infinite molecular weight *vs.* $(1/T^6-1/\langle490\rangle^6)$.

TABLE IV. Viscosities and viscosity-temperature coefficients of polystyrene fractions at their transition temperatures.

M	T_g	$\log\eta$ at T_g	E_T at T_g kcal./mole
300,000	99°	14.19	112
100,000	98	12.40	112
50,000	97	11.40	111
25,000	93	10.93	111
15,000	89	10.57	110
10,000	83	10.58	110
5000	66	10.66	109
4000	58	10.69	108
3000	43	11.31	111

which is identical with Eq. (2) within the limits of experimental accuracy and the approximations involved.

Mixtures of Polystyrene Fractions

Equations (1), (3), (2), and (7) relating the specific volume, the transition temperature, and the viscosity-temperature coefficient to the molecular weight M have been established from measurements on polystyrene fractions which, for the purpose of the experiments described, may be considered to be essentially homogeneous in molecular weight. In order to establish the particular average (if any) on which these properties depend, three mixtures of polystyrene fractions were prepared having the compositions given in Table V. The values of $\bar{M}_n$ and $\bar{M}_w$ calculated by the usual equations

$$\bar{M}_n=\sum_i w_i/\sum_i(w_i/M_i) \tag{11}$$

$$\bar{M}_w=\sum_i w_i M_i/\sum_i w_i \tag{12}$$

where w_i is the weight fraction of the species of molecular weight M_i are also listed in Table V. In each case a benzene solution containing the indicated proportions of the two fractions of widely separated molecular weights was evaporated to dryness in order to assure intimate mixing of the constituents. Measured specific volumes, transition temperatures, and viscosity-temperature coefficients are compared in Table V with the values computed from Eqs. (1), (2) and (7), using the number and the weight average molecular weights of each mixture. In every case the observed value of the given property agrees more nearly with that calculated for a fraction possessing a molecular weight which matches the number rather than the weight average molecular weight of the mixture. Agreement with the calculations based on the number average molecular weight is in all cases within the experimental error. Hence, for a heterogeneous polystyrene the specific volume, transition temperature, and the viscosity-temperature coefficient[18] depend explicitly on the number average molecular weight of the polymer, in accordance with Eqs. (1), (2), (3), (7), and (8).

The volume-temperature coefficients observed for the

[18] The dependence of the viscosity-temperature coefficient for a heterogeneous polystyrene on $\bar{M}_n$ was reported in reference 4.

TABLE V. Mixtures of polystyrene fractions.

A. Molecular weights and specific volumes

Designation	Components	$\bar{M}_w$, calc.	$\bar{M}_n$, calc.	v_{217} ml per g: For fraction of same $\bar{M}_w$	v_{217} ml per g: For fraction of same $\bar{M}_n$	Obs.
1	85,000(0.5) 4810(0.5)	45,000	9110	1.042	1.048	1.046
2	85,000(0.5) 3540(0.5)	44,300	6800	1.042	1.051	1.048
3	85,000(0.25) 3540(0.75)	23,900	4650	1.043	1.055	—

B. Second-order transition temperature and volume temperature coefficients

Designation	T_g: For fraction of same $\bar{M}_w$	T_g: For fraction of same $\bar{M}_n$	Obs.	(dv/dT) in ml/g/°$\times 10^4$: $(dv/dT)_1$	$(dv/dT)_2$	$(dv/dT)_3$
1	96	81	80	6.8	5.3	2.4
2	96	75	70	6.8	5.5	2.3
3	93	63	60	6.8	5.5	2.6

C. Viscosity-temperature coefficients

Designation	η_{217}, poises	$\log(\eta_{140}/\eta_{217})$: For fraction of same $\bar{M}_w$	$\log(\eta_{140}/\eta_{217})$: For fraction of same $\bar{M}_n$	Obs.	$\log(\eta_{140}/\eta_{217})$: For fraction of same M_w	$\log(\eta_{140}/\eta_{217})$: For fraction of same M_n	Obs.
1	128	2.19	1.76	1.64	3.57	2.85	2.83
2	88	2.19	1.60	1.54	3.57	2.60	2.63

mixtures (Table V) are similar to those found for the fractions.

DISCUSSION

According to current concepts,[19] the equilibrium configuration of a liquid changes continuously with temperature in a manner such that the density of packing of the molecules, or of the chain segments in the case of a polymer, increases with decreasing temperature. The degree of order also increases as the temperature is lowered, and the character of the spatial arrangement, as expressed for spherical molecules by the average coordination number, may change as well.

The linear increases in the specific volume v of polystyrene with $1/\bar{M}_n$ may be interpreted as an influence of the end groups which is proportional to their concentration. Since the end groups, i.e., the $C_2H_5—C_6H_4—\overset{CH_3}{\underset{|}{C}}H—$ groups, occurring in the polystyrenes used here and the styrene structural unit should possess similar net densities, we are led to suggest that the observed dependence of specific volume on molecular weight reflects changes in average density of packing with the concentration of end groups. Thus, the end groups act like a foreign substance in disrupting the local configurational order of the styrene units, and this is manifested by an increase in the specific volume v which is proportional to the concentration of end groups, or to $1/\bar{M}_n$. It follows also that the specific volume affords a convenient index of the average internal configuration or of the average density of packing irrespective of M.

The specific volume-temperature relationships for polystyrene are summarized in Fig. 7. Three parallel straight lines represent the equilibrium v-T relationships for polystyrenes of different molecular weights. The broken line intersecting these v-T lines represents the barrier imposed by the second-order transition. The dotted extensions of the v-T lines into the region below the second-order transition are essentially unrealizable experimentally. All polystyrenes whose *equilibrium* v-T lines would place them in this forbidden region exhibit the *same specific volume-temperature relationship*, as given by the broken line, *independent of molecular weight*. The position of the broken line representing the glassy state depends somewhat on the rate at which observations are made, but, as has been pointed out above, this rate must be altered by several orders of magnitude before it is shifted appreciably.

The internal changes in liquid configuration which must occur on lowering of the temperature obviously involve the motion of segments relative to their nearest neighbors from one configurational arrangement to another. When the temperature is altered well above T_g this motion of the segments relative to their neighbors in the relatively "loose" or "open" structure is rapid and volume equilibration is practically instantaneous. As the temperature approaches T_g however, the configurational structure becomes more and more compact and hence the rate of volume equilibration diminishes rapidly. Finally, at T_g the segments are so densely packed that the internal mobility is negligibly small and consequently, the liquid structure is "frozen-in," and therefore *remains the same for all temperatures below* T_g. The identity of the specific volumes for polystyrenes of different molecular weight at all temperatures below this second-order transition leads at once to the conclusion that *below* T_g *the local configurational arrangement of the polymer segments is independent of both* M *and* T. Furthermore, it is clear that since the presence of end groups in the liquid polymer at a given temperature decreases the density of the configurational structure in proportion to $1/\bar{M}_n$ and since lowering the temperature increases this density of packing in proportion to T, the temperature at which this critical

[19] J. D. Bernal, Trans. Faraday Soc. **33**, 27 (1937).

structure of low mobility is reached (T_g) must decrease in a linear fashion with $1/\bar{M}_n$.

Although the configurational structure remains unchanged as T is lowered below T_g, there remains a small linear decrease in volume with temperature associated with the crystal-like "contraction of the lattice" due to decreased amplitudes of oscillation of the segments about mean fixed positions. Obviously the equilibration rate for this process should be very rapid and should be essentially independent of the structural details mentioned above.

If a model for the liquid is chosen in which the chain segments are represented as hard, inelastic bodies, in accordance with certain approximate theories of the liquid state,[20,21] the above conclusions translate to the statement that the "free volume" (or volume of "holes" between the segments) in polystyrene below its transition temperature is a constant independent of both molecular weight and temperature. This follows from the separation of the specific volume into the sum of the free volume v_f and the occupied volume v_0, the latter being given by

$$v_0 = A_0 + (dv/dT)_3 T, \tag{13}$$

where A_0 is the hypothetical volume of the solid (glass) at $T=0$°C. Subtracting this expression from Eq. (3) for the temperature range from T_g to 160° we obtain

$$v_f = A_f + [(dv/dT)_2 - (dv/dT)_3]T + 53/M, \tag{14}$$

where $A_f = A - A_0$. Imposing the requirement that the equilibrium free volume of a polystyrene of molecular weight M at its transition temperature T_g be equal to that of one for which $M=\infty$ at its transition temperature $T_{g,\infty}$, then

$$T_g = T_{g,\infty} - 53/[(dv/dT)_2 - (dv/dT)_3]M. \tag{15}$$

Substituting the values of the parameters given above,

$$T_g = 100 - 1.8\times 10^5/M, \tag{16}$$

which is identical within the limits of experimental accuracy with Eq. (2). Hence, the second-order transition for polystyrene represents a state of "*iso-free volume*," and this same free volume is retained at all temperatures below T_g.

The above considerations suggest that the internal relaxation rate (mobility) is determined almost entirely by the configurational arrangement of the segments (or by the free volume associated with the given configuration) and that it is otherwise very nearly independent of both temperature and molecular weight. A corresponding dominant role of the volume in determining the internal mobility of simple non-polar liquids is illustrated by the fact that their fluidities depend primarily on the specific volume, i.e., the viscosity-temperature coefficient at constant volume is nearly zero.[22] As the temperature is lowered (for any liquid substance) toward T_g, the free volume shrinks to a small value and below T_g remains constant for all lower temperatures. Inasmuch as the volume decreases about linearly with temperature, the *percentage* change in free volume per degree increases rapidly as the temperature is lowered near T_g. Both the observed precipitous decrease of $-dv/d\log t$ for polystyrene near T_g and the approximate constancy of this coefficient below T_g follow as consequences of these considerations.

These concepts may be re-stated in mathematical form. The observations cited[22] on the fluidities of simple liquids suggest that the viscosity of such a substance may be expressed as the product of two functions as follows:

$$\eta = f(v_f)g(T) \tag{17}$$

where $f(v_f)$ is a function only of the free volume (and hence implicitly of the specific volume), or of the liquid configuration, and $g(T)$ is a function of temperature only. For non-polar liquids at least, the value of the latter function changes relatively slowly with T, hence the viscosity is determined primarily by the free volume. Since the internal mobility is also determined by the free volume, the manifestation of the second-order transition as an isoviscous state in *substances of low molecular weight* is consistent with Eq. (17).

The macroscopic viscosity of a polymer depends not only on the free volume and temperature but also on the length of the polymer chain, Z.[3,4] Equation (17) must be replaced therefore by a relationship of the form

$$\eta = f(v_f)g(T)h(Z), \tag{18}$$

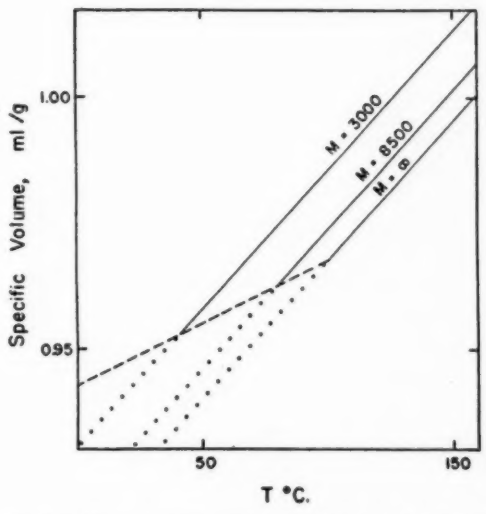

FIG. 7. Specific volume-temperature relations for polystyrene. The parallel lines represent the equilibrium curves, the dotted portions being non-realizable. The dashed line is the v-T curve for polystyrenes in the glassy state.

[20] H. Eyring, J. Chem. Phys. **4**, 283 (1936).
[21] Alfrey, Goldfinger, and Mark, J. App. Phys. **14**, 700 (1943).
[22] A. J. Batschinsky, Zeits. f. physik. Chemie **84**, 643 (1913). D. B. MacLeod, Trans. Faraday Soc. **19**, 6 (1923); **21**, 151 (1925). W. R. Van Wijk and W. A. Seeder, Physica **4**, 1073 (1937); **6**, 129 (1939).

where $h(Z)$ is the statistical factor expressing the required coordination of the motions of *all* segments of the polymer molecule. Since the internal mobility depends only on the first two factors (i.e., the rearrangement of local configurational structure does not require long range cooperation of the segments of a given molecule), it is clear that the macroscopic viscosity for a polymer at its second-order transition will vary with M. This is not true of the viscosity-temperature coefficient. If Eq. (18) is rewritten in the form

$$\ln\eta = F(v_f) + G(T) + H(Z) \tag{19}$$

and differentiated with respect to $1/T$, there is obtained

$$\begin{aligned} E_T &= Rd\ln\eta/d(1/T) \\ &= R[(dF(v_f)/dv_f)(dv_f/d(1/T)) + dG(T)/d(1/T) \\ &\quad + (dH(Z)/dZ)(dZ/d(1/T))]. \end{aligned} \tag{20}$$

For non-polar polymers the last two terms on the right should be very small, and presumably may be neglected for the purpose of the present discussion. The quantity $dv_f/d(1/T)$ is independent of M and is not sensitive to temperature [see Eq. (14)]. Hence, E_T depends predominantly on $dF(v_f)/dv_f$, which is a function of the free volume only, and the dependence of E_T on M must be related primarily to the dependence of v_f on M. The constancy of v_f below T_g requires that the first term on the right of Eq. (20) shall be zero below T_g. Hence, the viscosity of polystyrene below T_g will vary only as a result of the contributions of the second and third terms of Eq. (20). To the approximation that these terms may be neglected, the viscosity of a given polystyrene should remain constant at all temperatures below T_g.

No experimental data are available with which to test this latter prediction with regard to polystyrene. Viscosity measurements of silicate glasses, however, have been extended below their second-order transition temperatures. While the temperature coefficient does not fall to zero, it passes through a pronounced maximum at T_g.[23] This behavior is indeed to be expected, when, as in glass, the intermolecular forces between elementary units are large. The second term in Eq. (20) is then appreciable—perhaps comparable in magnitude with the first. The third term must be small or zero.[24] In other words, viscous flow involves a considerable activation, and the resulting temperature dependence persists below T_g notwithstanding the disappearance of the first term in Eq. (20).

Unpublished measurements that we have made of the specific volumes of polyisobutylene fractions at 217° and at lower temperatures indicate that the "free volume" of this polymer is given by

$$v_f = A_f + BT + 32/M \tag{21}$$

which is the analog of Eq. (14) for polystyrene. Here B, the change in the volume-temperature coefficient at T_g, is estimated as $4.5(\pm1)\times10^{-4}$ from the data of Ferry and Parks.[25] If we assume that the second-order transition occurs at a characteristic free volume, then

$$T_g = T_{g,\infty} - 6.9\times10^4/M. \tag{22}$$

Values of T_g calculated from this equation are approximately equal to the corresponding literature values[6,25] provided $T_{g,\infty}$ is taken as $-63°$. This suggests that the correlations observed here for polystyrene may have general validity.

The second-order transition temperature (100°) that we have observed for high molecular weight polystyrene is somewhat higher than values reported elsewhere (Table VI). It is possible that those previously reported may have been vitiated by the presence in the polymer samples of low molecular weight impurities such as unpolymerized monomer, residual solvent, or degradation products formed from the polymer itself.

The volume-temperature coefficients reported here just above and below T_g correspond to values of the expansion coefficient (α) of 6.0 and 2.7×10^{-4}, respectively. These are in good agreement with most of the previously reported values of these coefficients (Table VI). The slightly lower values obtained by some workers for α below T_g may be due to their use of shorter observation times. The lower values obtained in a few cases for α above T_g are unexplained unless, as has been suggested elsewhere,[26] they are due to the presence of impurities. It should be emphasized that the present values were reproducible (within ±10 percent) over wide ranges in temperature for polymers differing widely in molecular weight.

Since the configuration of complex liquids and their volume-temperature dependence are imperfectly understood, we prefer not to hazard an explanation for the non-linearity of the v-T curves above T_g at this time.

SUMMARY

1. The specific volumes of polystyrene fractions ranging in molecular weight from 2970 to 85,000, and of various mixtures of these fractions, have been measured at 217°. The specific volume at a fixed temperature increases linearly with $1/\bar{M}_n$.

2. Measured values of the specific volume-temperature coefficients for these polystyrenes are 7.0, 5.5, and 2.5×10^{-4} above 160°, between the second-order transition temperature (T_g) and 160°, and below T_g, respectively. The last two coefficients appear to be independent of M; the first increases with decreasing M at low molecular weights. Alternately, the results above T_g may be represented by a line with curvature over a wide range in the neighborhood of 160°.

3. The second-order transition temperature is 100 ±2° for high molecular weight polystyrene, and it decreases linearly with $1/\bar{M}_n$.

[23] H. R. Lillie, J. Am. Ceram. Soc. **16**, 619 (1933).
[24] R. W. Douglas, J. Soc. Glass. Tech. **31**, 74 (1947).
[25] J. D. Ferry and G. S. Parks, J. Chem. Phys. **4**, 70 (1936).
[26] F. E. Wiley, Ind. Eng. Chem. **34**, 1052 (1942).

4. At temperatures 10° or more above T_g volume equilibrium appears to coincide with the attainment of temperature equilibrium. In the vicinity of T_g the specific volume decreases approximately linearly with the logarithm of time. In this range the rate of volume relaxation (as measured by $-dv/d\log t$) decreases rapidly with decreasing volume, attaining a low limiting value about 10° below T_g. This limiting value is independent of molecular weight. The rate of internal relaxation (mobility) appears to depend primarily on the internal configurational structure (and on the associated free volume) and to be otherwise independent of T and M.

5. It has been observed that *the specific volumes of polystyrenes below their transition temperatures are independent of the molecular weight.* Hence, it appears that the same "frozen-in" internal configuration prevails in the glassy state independent of molecular weight as well as temperature. The observed dependence of T_g on M can be deduced as a consequence of this conclusion.

6. Bulk viscosities (η) of the same polystyrene samples have been measured from 217 to 75°. The quantity $\log(\eta_T/\eta_{217})$ may be expressed as the product of two factors, one of which depends only on the absolute temperature (as T^{-6}) and the other on $\bar{M}_n$. This ratio at a fixed temperature decreases exponentially with $1/\bar{M}_n$.

7. Generalized relationships for the viscosity of liquids are suggested which indicate that the second-order transition for simple liquids may represent an isoviscous state but that this concept should fail (as it did here) for polymers differing in M. The molecular weight dependence of the viscosity-temperature coefficient for polystyrene above T_g is related logically to its specific volume-molecular weight relationship; the observed non-dependence of this coefficient on M for polystyrenes at their second-order transition temperatures is shown to be a consequence of the non-dependence on M of the specific volumes of these polymers at (or below) their second-order transition temperatures.

8. It is predicted that the viscosity of polystyrene should become relatively independent of T below T_g. The maximum observed in the viscosity-temperature coefficient for a soda-lime-silica glass is explained on the basis of the above relationships.

9. A relationship between T_g and M for polyisobutylene has been suggested.

TABLE VI. Second-order transition temperature and thermal expansion coefficients for polystyrene.

T_g	$\alpha \times 10^4$ Above T_g	$\alpha \times 10^4$ Below T_g	Reference
≥100°	≥6	0.4 to 2.5	a
100°	6.0	2.7	b
88°	6.47	2.18	c
87°	6.22	2.33	d
82°	6.0	2.6	e
82°	4.63	2.15	f
82°	4.6	2.5	g
82°	—	—	h
—	4.25	2.7	i
—	4.25	2.4	j
78°	5.89	2.11	k

[a] See reference 5.
[b] Present work.
[c] H. J. Kolb and E. F. Izard, J. App. Phys. **20**, 564 (1949).
[d] See reference 2.
[e] W. Patnode and W. J. Scheiber, J. Am. Chem. Soc. **61**, 3449 (1939).
[f] F. E. Wiley, Ind. Eng. Chem. **34**, 1052 (1942).
[g] See reference 21.
[h] R. F. Boyer and R. S. Spencer, J. App. Phys. **15**, 398 (1944).
[i] See reference 13.
[j] R. S. Spencer and G. D. Gilmore, J. App. Phys. **20**, 502 (1949).
[k] R. J. Clash and L. M. Rynkiewicz, Ind. Eng. Chem. **36**, 279 (1944).

Electrical Breakdown in CSF_8

RONALD GEBALLE AND FRED S. LINN
Department of Physics, University of Washington, Seattle, Washington
(Received December 27, 1949)

The breakdown potential of a new gas, CSF_8, has been measured over the range from $p\delta=4$ to 200 mm×cm under conditions approximating plane-parallel geometry. A comparison of breakdown in air Freon-12 and CSF_8 in the same apparatus indicates the ratio of the strengths of these gases to be approximately 1:2:3, respectively. CSF_8 decomposes rapidly during breakdown into CF_4 and SF_4 with a consequent doubling of pressure and appreciable increase in breakdown potential.

INTRODUCTION

THE insulating properties of certain gaseous compounds of carbon or sulfur and the halogens, notably Freon-12 (CCl_2F_2) and sulfur hexafluoride (SF_6) have been discussed recently by several investigators.[1–5] The two substances named above are found to have breakdown strengths of about 2 to 2.5 times that of air under comparable conditions. It is believed that the high breakdown strengths of such compounds result from the large number of electronegative atoms contained in each molecule, together with the existence of many degrees of freedom capable of absorbing energy from electrons in inelastic collisions. The above two compounds are particularly useful as insulators because they possess, in addition to notable breakdown potentials, the rather large vapor pressures of 5.5 and 22 atmospheres at room temperature, respectively. Recently, in connection with certain syntheses of fluorine-containing compounds, a substance with the empirical formula CSF_8 was isolated by Mr. Gene A. Silvey of the Department of Chemistry. This compound is colorless, and chemically inert. It possesses a boiling point of -20°C at atmospheric pressure and a saturation vapor pressure of 4.3 atmospheres at 20°C. Its structure is believed to be F_3C-SF_5. A detailed description of its synthesis and chemical behavior will be discussed elsewhere.[6] In view of the large number of fluorine atoms per molecule and the high vapor pressure of CSF_8 a survey of its insulating properties was felt to be of considerable interest and was undertaken by the present authors. Measurements of the breakdown strength of this gas were made in the range from $p\delta=4$ to 200 mm×cm under conditions closely approximating plane-parallel geometry. A comparison of its strength with those of air and Freon-12 was made under the same conditions. It was found that air, Freon-12, and CSF_8 possess strengths in the approximate ratio 1:2:3 in this range of $p\delta$. It was also found that CSF_8 decomposes in an unusual manner in the course of electrical breakdown. The breakdown products could be separated in relatively pure states and their identity verified.

APPARATUS

The breakdown voltage was measured in a Pyrex discharge vessel containing two plane Monel disks of 7.65 cm diameter and spaced 1.5 cm apart. Because of the limited supply of CSF_8 the volume of the envelope was deliberately made small, about 0.8 liter. To localize discharges on the axis of the electrode system under this condition a hemispherical boss of 1.6 mm radius was mounted at the center of the anode. The small field distortion thus introduced was responsible, in certain cases, as will be seen, for the production of streamer pulses preceding breakdown. The distortion was sufficiently small, however, that no serious alteration in breakdown potential was noticed in standard gases in the range of $p\delta$ under investigation. In computing $p\delta$, the electrode separation, neglecting the boss, was used.

The pumping system consisted of a mercury diffusion pump backed by a mechanical pump. Pressures were determined by the use of appropriate McLeod gauges or a mercury manometer. Traps surrounded by liquid nitrogen were used to eliminate contamination by mercury vapor except during short intervals when pressure measurements were being made.

Direct voltage up to 40 kv was supplied by a half-wave rectifier with sufficient filtering to reduce ripple to 0.1 percent. Small increments in voltage were made possible by the use of a small transformer in series with the high voltage one, each with its own variable input. The voltage was read with the aid of a calibrated multiplier and a potentiometer. The over-all error in voltage readings, due primarily to line voltage fluctuation, amounted to about one percent. A two-megohm resistor was in series with the high voltage to prevent excessive current upon breakdown.

To insure an adequate supply of initiating electrons a radium-containing sample was placed near the discharge chamber.

PROCEDURE

The electrodes were polished and cleaned before assembly of the system performed in an atmosphere of nitrogen. The tube was annealed in hydrogen and baked

[1] H. C. Pollock and F. S. Cooper, Phys. Rev. **56**, 170 (1939).
[2] Trump, Safford, and Cloud, Trans. A.I.E.E. **60**, 132 (1941).
[3] H. H. Skilling and W. C. Brenner, Trans. A.I.E.E. **61**, 191 (1942).
[4] B. Hochberg and E. Sandberg, J. Tech. Phys. U.S.S.R. **12**, 65 (1942); E. Sandberg, J. Tech. Phys. U.S.S.R. **17**, 299 (1947).
[5] Schumb, Trump, and Priest, Ind. Eng. Chem. **41**, 1348 (1949).
[6] Gene A. Silvey and George H. Cady, J. Am. Chem. Soc. (to be published).

out at 400°C while at a pressure of 10^{-5} mm of mercury. Between runs in different gases the tube was well pumped out. In one case, after the run in Freon-12, the system was completely dismantled and cleaned before proceeding.

The air used in this investigation was withdrawn slowly from the room and passed through a trap surrounded by liquid nitrogen. For all the measurements in this gas, except the last, the vapor pressure of oxygen at the temperature of the trap exceeded the total pressure in the apparatus; hence the composition of the air was not appreciably altered. In any case, the breakdown potentials of air and nitrogen are very closely the same in this range of $p\delta$.[3] The more readily condensed gases were admitted from traps after careful drying by redistillation. Hydrogen, used to test the geometry, was obtained from a commercial cylinder, passed through a catalytic purifier and then through a trap immersed in liquid nitrogen.

Breakdown voltages were found by slowly increasing the applied potential in increments of a few volts, with suitable delay between each step in an attempt to eliminate errors due to statistical factors. In general the onset of a visible discharge was taken as the breakdown potential. In certain cases, as described below, observations were made with an oscilliscope connected across a series resistor.

EXPERIMENTAL RESULTS

1. Hydrogen

The breakdown potential of hydrogen was investigated in order to determine the properties of the particular geometrical arrangement employed. The oscilliscope showed small pulses, increasing in size with increased voltage, which suddenly assumed the character of breakdown streamer pulses.[7] A few volts above this the discharge became visible, first pulsating and then steady to the eye. These events took place at well-defined potentials, reproducible within the accuracy of the apparatus. In Fig. 1 the streamer onset voltage thus found is compared with the curve compiled by Druyvesteyn and Penning[8] for breakdown between plane electrodes. All pressures have been reduced to standard conditions. It can be seen that the advent of the large pulses coincided rather closely with the breakdown voltage found under conditions of strictly uniform field.

2. Freon-12

Commercial Freon-12 was used after vapor density measurements indicated its purity was better than 99.5 percent. The oscilliscope gave no hint of impending breakdown in this gas, but merely exhibited preliminary burst pulses as reported by Mohr and Weissler.[9] In contrast to these workers no hysteresis was noted. There were, however, large fluctuations in delay between the time of application of voltage and breakdown when the voltage was applied by closing a switch. The average of these fluctuations is a function of the applied voltage. It decreases, for example, from 30 sec. at 29,700 volts to 2 sec. at 30,900 volts for $p\delta = 275$ mm×cm. Figure 1 shows the breakdown potentials associated with a maximum delay of 1 min. For comparison the curves of Trump, Safford, and Cloud[2] as well as Hochberg and Sandberg[4] are shown. The decomposition products of Freon-12 were found to be exceedingly corrosive, attacking glass, electrodes, and mercury.

3. Air

The breakdown potential of air was determined for use as a reference. The appearance of visible discharge was regarded as breakdown. There was no noticeable fluctuation in delay times and voltages were easily reproducible. No study of the pre-breakdown pulses was made. The data obtained are compared in Fig. 1 with the curve compiled by Whitehead[10] for plane geometry. They agree with the results of Fisher[11] in the range where comparison is possible.

4. CSF_8

No streamer pulses were observed in this gas. The small burst pulses, which in many gases precede streamers, increased in size and frequency until a spark occurred, persisting until the high voltage switch was

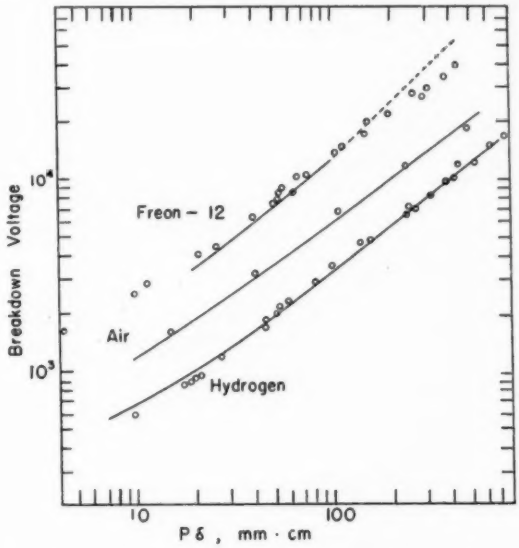

FIG. 1. Breakdown voltages measured in the present chamber as compared with published data. Curves are as follows: H_2, reference 7; air, reference 9; Freon-12, solid portion, reference 4; Freon-12, dashed portion, reference 2. Points are those of the present work. All data reduced to 0°C.

[7] A. F. Kip, Phys. Rev. **55**, 549 (1939).
[8] M. J. Druyvesteyn and F. M. Penning, Rev. Mod. Phys. **12** (April, 1940).
[9] B. A. Mohr and G. L. Weissler, Phys. Rev. **72**, 289 (1947).
[10] S. Whitehead, *Dielectric Phenomena* (D. Van Nostrand Company, Inc., New York, 1927), p. 43.
[11] L. H. Fisher, Ph.D. thesis, Library, University of California, Berkeley, California.

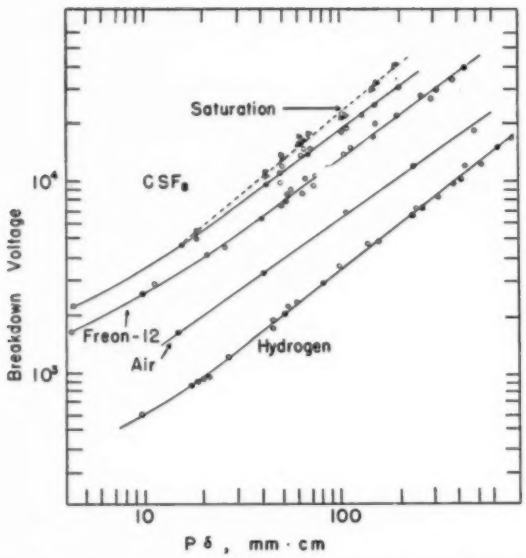

FIG. 2. Comparison of breakdown voltages of CSF_8 with other gases. Curves are drawn through the experimental points. Dashed curve is the saturation voltage discussed in the text. All data reduced to 0°C.

opened. On closing the switch again, the potential remaining constant, breakdown did not recur. When the voltage was increased to a new level it could be reapplied several times to produce sparking. The time lapse between the closing of the switch and the spark increased for each of these breakdowns from an initial value of less than a second to more than five minutes and eventually it was apparent that no more sparks were possible at this level. At higher levels the sequence of events was similar except that the total number of breakdowns at each voltage increased. In addition, the time lag increased less rapidly with the number of breakdowns at a given level. At a level about ten percent above the initial breakdown potential a saturation voltage was attained after which sparking took place with small time lags which fluctuated between zero and about three seconds without steady increase.

It was believed that an investigation of the decomposition products would provide the explanation of these observations. To obtain the products in sufficient quantity for analysis, a continuous discharge of 2 ma was permitted to pass through CSF_8 for 15 min. and the gases collected over liquid nitrogen. This process was repeated several times. During the course of these runs measurements of the pressure indicated an increase to twice the initial value, after which no further change occurred. Analysis of the products by Mr. Silvey provided the following information:

(1) When condensed, the products formed two immiscible phases.

(2) One of the phases was definitely identified through its vapor density and freezing point as CF_4.

(3) The other constituent, because its odor, melting and boiling points agreed closely with those reported by Fischer and Jaenchner,[12] was tentatively identified as SF_4, a compound of hitherto dubious existence.[5]

(4) The average vapor density of the products was correct assuming the above are the sole products.

It appears then that during the course of electrical discharge the CSF_8 is split rapidly into two products, CF_4 and SF_4. The consequent rise in pressure accounts for the behavior of the breakdown potential in the following manner: When the first breakdown took place some of the CSF_8 was decomposed, the pressure rose and no further breakdown was possible at this voltage. When the voltage was increased and reapplied, breakdown occurred immediately, producing further decomposition. At a constant pressure the breakdown potential of the products is considerably less than that of the CSF_8. Hence, because of the slow diffusion rate of the heavy molecules involved, the mixture of gases between the electrodes broke down when the same voltage was again applied, even though the pressure had increased to some extent. With successive applications of voltage the decomposition continued, the mixture of gases became more nearly homogeneous until the pressure increased to such an extent that no further breakdown could take place at this potential. At higher voltages the process was similar. Because the percentage of CSF_8 continually diminished, the lag introduced by diffusion became less pronounced until with complete decomposition the saturation voltage was attained. It should be noted that the lags after reaching saturation were not dependent on voltage in the pronounced manner of Freon-12. To verify the nature of the decomposition products an additional sample of CSF_8 was subjected to discharge. Again the doubling of pressure and rise in breakdown potential were noted. Separation of the two phases and analysis for sulfur and fluorine by Mr. Silvey indicated without doubt that one of the products was SF_4.

The breakdown potential of CSF_8 as well as the saturation voltage characteristic of the completely decomposed gas under conditions of constant volume are shown in Fig. 2 with pressures reduced to 0°C. For comparison, the results obtained under Sections 1–3 are given. It can be seen that in the range of the present investigation the strengths of air, Freon-12, and CSF_8 are in the approximate ratio 1:2:3.

At the conclusion of the discharges in CSF_8 a thin whitish layer, identified as sulfur, coated the glass. The Monel electrodes used in the first set of measurements showed no evidence of corrosion. The vessel used to decompose the gas in the second set contained stainless steel, which became markedly corroded. These effects are probably due to further decomposition during the passage of the current. When allowed to stand for a day or so, the mixture of CF_4 and SF_4 exhibited a constant pressure and breakdown potential.

It is a pleasure to thank Professor George H. Cady and Mr. Silvey of the Department of Chemistry for supplying the CSF_8 and to acknowledge the aid rendered by the latter in performing the various analyses.

[12] J. Fischer and W. Jaenchner, Zeits. f. angew. Chemie **42**, 810 (1929).

The Effect of Cold-Work Distortion on X-Ray Patterns*

B. E. Warren and B. L. Averbach
Massachusetts Institute of Technology, Cambridge, Massachusetts
(Received January 9, 1950)

With modern experimental technique, it is possible to measure a peak shape with sufficient accuracy to justify an interpretation based on the precise shape of the reflection. The corrected shape is represented by a cosine Fourier series and a set of A_n coefficients determined. A plot of the A_n coefficients *vs.* n will distinguish between distortion and particle size broadening. From the A_n coefficients, root mean square values of strain averaged over lengths na_3 are obtained. The decrease in these values for increasing length na_3 is a direct indication of the non-uniform nature of the strains in cold-worked metal. By measuring several orders of a given plane, it is theoretically possible to obtain a distribution function of the strains directly from a Fourier transform of the A_n coefficients.

I. INTRODUCTION

COLD-WORK distortion produces a broadening of powder pattern reflections. Most of the previous work in this field has involved measurements of cold-work broadening as a function of λ and θ, and the use of these breadth measurements to distinguish between various assumed theories of the nature of cold-work distortion.

With modern experimental technique, using focusing curved crystal monochromators and Geiger counter spectrometers, it is possible to measure the shape of a powder pattern line with sufficient accuracy to justify an interpretation based on the precise shape of the line, rather than using just the line breadth.[1] By making full use of the shape of the line, it is possible to get a great deal of information about the nature of cold-work distortion without making any *a priori* assumptions. The theoretical treatment must be carried through for a completely general distortion, so that what we get in the end is given uniquely by the x-ray measurements and is not partly the result of assumptions concerning the nature of the distortion which have been inserted during the treatment.

II. EFFECT OF A GENERAL DISTORTION

We start with the same formulation used by Stokes and Wilson.[2] Only cubic crystals are considered for which it is always possible to adopt a set of orthogonal axes so as to make any reflection of the form (00l). The position of any cell $m_1m_2m_3$ is given by the vector

$$R_m = m_1a_1 + m_2a_2 + m_3a_3 + \delta_{m_1m_2m_3},$$

where δ is an arbitrary displacement, in general different for every cell. Expressed in electron units the intensity from one crystal is

$$I = F^2 \sum_{m_1} \sum \sum \sum \sum \sum_{m_3'} \exp[2\pi i/\lambda (s - s_0)\cdot(R_m - R_{m'})],$$

where s_0 and s are unit vectors giving the directions of the primary and diffracted beams. Let

$$s - s_0 = \lambda(h_1b_1 + h_2b_2 + h_3b_3),$$

where $b_1b_2b_3$ are the reciprocal vectors, and $h_1h_2h_3$ are continuous variables. The intensity per crystal is

$$I(h_1h_2h_3) = F^2 \sum_{m_1} \sum \sum \sum \sum \sum \sum_{m_3'} \exp\Big[2\pi i \Big\{ h_1(m_1 - m_1') + h_2(m_2 - m_2') + h_3(m_3 - m_3') + \left(\frac{s - s_0}{\lambda}\right)\cdot(\delta_m - \delta_{m'})\Big\}\Big]. \quad (1)$$

For a powder pattern, the total diffracted power in a reflection is given by an integration throughout a sufficient volume in the reciprocal lattice to include everything contributing to the reflection.

$$P = \frac{MjR^2\lambda^3}{4v_a} \int\int\int \frac{I(h_1h_2h_3)}{\sin\theta} dh_1 dh_2 dh_3, \quad (2)$$

where M is the number of crystals in the sample, j is the *hkl* multiplicity, R is the sample to film distance, and v_a is the volume of the unit cell. The distribution of power with angle is expressed by $P_{2\theta}$ where

$$P = \int P_{2\theta} d(2\theta). \quad (3)$$

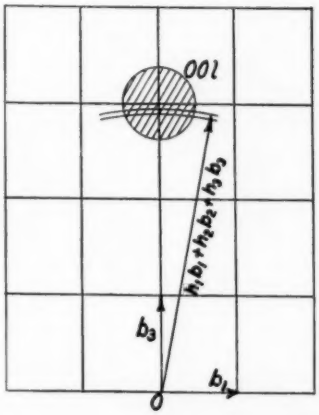

FIG. 1. Approximation of a spherical surface by a tangent plane involved in the integration about 00l.

* Research sponsored by the ONR under Contract N5 ori-07832.
[1] B. L. Averbach and B. E. Warren, J. App. Phys. **20**, 885 (1949).
[2] A. R. Stokes and A. J. C. Wilson, Proc. Camb. Phil. Soc., **38**, 313 (1942); Proc. Phys. Soc. **56**, 174 (1949).

In carrying out the integration about the point $00l$ in Fig. 1, it is assumed that the spreading out of the point due to distortion is small compared to its distance from the origin, so that a spherical layer can be approximated by a horizontal layer

$$|s-s_0| = 2\sin\theta = \lambda|h_1b_1+h_2b_2+h_3b_3| \rightarrow \lambda|b_3|h_3$$

$$dh_3 = \frac{\cos\theta d(2\theta)}{\lambda|b_3|}.$$

The integration with respect to dh_3 in (2) can be expressed in terms of $d(2\theta)$ and from (3) we get $P_{2\theta}$ by leaving out this integration.

$$P_{2\theta} = \frac{MjR^2\lambda^2}{4v_a|b_3|\tan\theta}\int\int I(h_1h_2h_3)dh_1dh_2. \qquad (4)$$

Experimentally we measure the distribution of power per unit length of diffraction line

$$P_{2\theta}' = \frac{P_{2\theta}}{2\pi R\sin 2\theta}.$$

Let

$$K = \frac{MjR\lambda^2F^2}{16\pi v_a|b_3|\sin^2\theta}.$$

The distribution of power is then

$$P_{2\theta}' = K\int\int \sum_{m_1}\sum\sum\sum\sum\sum_{m_3'} \exp\Big[2\pi i\Big\{h_1(m_1-m_1') + h_2(m_2-m_2') + h_3(m_3-m_3') + \left(\frac{s-s_0}{\lambda}\right)\cdot(\delta_m-\delta_{m'})\Big\}\Big]dh_1dh_2. \qquad (5)$$

Represent the displacement δ_m by

$$\delta_m = X_ma_1+Y_ma_2+Z_ma_3 \quad (m=m_1, m_2, m_3)$$

and for computing the scalar product $(s-s_0)\cdot(\delta_m-\delta_{m'})$ use the average position of the vector $(s-s_0)$, $\langle s-s_0\rangle_{Av} = \lambda h_3b_3$

$$\frac{2\pi i}{\lambda}(s-s_0)\cdot(\delta_m-\delta_{m'}) = 2\pi ih_3(Z_m-Z_{m'}).$$

It is only the component of displacement perpendicular to the reflecting planes that is involved. To include everything belonging to point $00l$ we carry out the integration with respect to dh_1 and dh_2 from $-\frac{1}{2}$ to $+\frac{1}{2}$.

$$P_{2\theta}' = K\sum_{m_1}\sum\sum\sum\sum\sum_{m_3'} \frac{\sin\pi(m_1-m_1')}{\pi(m_1-m_1')} \times\frac{\sin\pi(m_2-m_2')}{\pi(m_2-m_2')} \exp[2\pi ih_3\{(m_3-m_3') + (Z_m-Z_{m'})\}]. \qquad (6)$$

The sine functions are zero except for $m_1=m_1'$ and $m_2=m_2'$. This means that we should think of the crystal in terms of columns of unit cells, the columns being parallel to a_3 or perpendicular to the reflecting planes $00l$. The summation with respect to m_3 and m_3' is carried out for all pairs of cells in a given column, and the summation with respect to m_1 and m_2 means summation of the contributions from each column.

Let

$$n = m_3-m_3' \quad Z_n = Z_{m_3}-Z_{m_3'}.$$

Assuming that the number of cells in a column N_3 is large compared to the value of n at which a summation with respect to n will converge

$$\sum_{m_3}\sum_{m_3'} \rightarrow N_3\sum_{n=-\infty}^{+\infty}$$

$$P_{2\theta}' = K\sum_c N_3\sum_{n=-\infty}^{+\infty}\langle\exp[2\pi ih_3(n+Z_n)]\rangle_{Av}, \qquad (7)$$

where $\sum_c$ means summation over the columns, and the average is an average over-all pairs of cells $m_1m_2m_3$ and $m_1'm_2'm_3'$ with $m_1=m_1'$, $m_2=m_2'$ and $m_3-m_3'=n$. Let the total number of cells in the crystal be $N=\sum_cN_3$. Since $Z_{-n}=-Z_n$

$$P_{2\theta}' = KN\sum_{n=-\infty}^{+\infty}\langle\cos 2\pi h_3(n+Z_n)\rangle_{Av}$$

$$P_{2\theta}' = KN\sum_{n=-\infty}^{+\infty}(A_n\cos 2\pi nh_3 + B_n\sin 2\pi nh_3), \qquad (8)$$

where $A_n=\langle\cos 2\pi h_3Z_n\rangle_{Av}$ and $B_n=-\langle\sin 2\pi h_3Z_n\rangle_{Av}$.

The coefficients of the sin terms will vanish if positive and the negative values of Z_n are equally probable for a given n. If they do not vanish their effect is to displace the center of the $P_{2\theta}'$ peak from the position for an undistorted material. This is just another way of recognizing that cold-work distortion may produce an average expansion or contraction of the lattice. Measurements on cold-worked metals to which the theory has been applied so far, show no appreciable shift in peak position, and hence we will confine our attention to the restricted case where the sin terms are negligible.

$$P_{2\theta}' = KN\sum_{n=-\infty}^{+\infty}A_n\cos 2\pi nh_3, \qquad (9)$$

where

$$h_3 = 2a_3(\sin\theta)/\lambda$$
$$A_n = \langle\cos 2\pi lZ_n\rangle_{Av}.$$

In the expression for A_n we have replaced h_3 by its peak value l. From (9) the corrected shape of the peak is represented by a cosine Fourier series, and the coefficients A_n depend only on relative displacements perpendicular to the reflecting planes. By definition a_3Z_n is the change in length of a column of original length na_3.

III. EXPERIMENTAL DETERMINATION OF FOURIER COEFFICIENTS

The coefficients A_n are determined from carefully measured peak shapes from a cold-worked sample and from an annealed sample. The second peak is used to correct the first for all sources of broadening other than that due to cold-work distortion. The correction is carried out by the method of Stokes[3] using the Lipson-Beevers strips. This method delivers directly the desired A_n coefficients. The Fourier analysis is done over the range h_3' from $-\frac{1}{2}$ to $+\frac{1}{2}$ where $h_3'=h_3-l$. Fictitious values of l and a_3 are used where necessary to make the range of the Lipson-Beevers strips cover efficiently the range of 2θ-values in the measured peak.

IV. EFFECT OF PARTICLE SIZE BROADENING

Particle size broadening is represented by a cosine Fourier series similar to that developed for distortion broadening and hence the Fourier coefficients A_n give a very general method of handling either effect. The particle size broadening follows the same treatment used for distortion broadening up to Eq. (6) except that δ and hence Z_m and Z_m' are zero.

$$P_{2\theta}'=K\sum_{m_1}\sum\sum\sum\sum\sum\sum_{m_3'}\frac{\sin\pi(m_1-m_1')}{\pi(m_1-m_1')}\times\frac{\sin\pi(m_2-m_2')}{\pi(m_2-m_2')}\exp[2\pi ih_3(m_3-m_3')].$$

Consider the crystal in terms of columns of unit cells perpendicular to the reflecting planes. Let n_i be the number of columns of length i cells, so that

$$N=\sum_{i=1}^{\infty} in_i$$

is the total number of cells in the sample.

$$P_{2\theta}'=KN\sum_{n=-\infty}^{+\infty}A_n\cos2\pi nh_3, \tag{10}$$

where

$$A_n=\frac{1}{N}\sum_{i=|n|+1}^{\infty}(i-|n|)n_i.$$

Introduce a distribution function $p(i)$ such that $p(i)di$ is the number of columns of length between i and $i+di$ cells.

$$\int_1^{\infty}p(i)di=N_c \qquad \int_1^{\infty}ip(i)di=N,$$

where N_c is the number of columns and N is the number of cells. In terms of the distribution function

$$A_n=\frac{1}{N}\int_{i=|n|+1}^{\infty}(i-|n|)p(i)di.$$

For both distortion and particle size broadening the coefficients A_n have been defined so that A_0 is unity.

$$\frac{dA_n}{dn}=-\frac{1}{N}\int_{i=|n|+1}^{\infty}p(i)di.$$

The initial slope of the A_n *vs.* n curve is

$$(dA_n/dn)_{n=0}=-N_c/N=-1/\bar{N}_3, \tag{11}$$

where $\bar{N}_3a_3$ is the average column length and hence an average particle size in the direction a_3.

$$(d^2A_n)/(dn^2)=(1/N)p(n). \tag{12}$$

If the measurements of particle size broadening are expressed in terms of a plot of the Fourier coefficients A_n *vs.* n the initial slope of the curve gives directly the average column length and the second derivative gives the column length distribution. This important result has already been obtained by M. F. Bertaut[4] by essentially the same method. The treatment given here is one developed by the authors before they were aware of Bertaut's work and it has been included here so as to present the particle size theory in the same notation used for distortion broadening.

V. REPRESENTATION BY FOURIER COEFFICIENTS

The representation of measured peak shapes by a plot of the Fourier coefficients A_n *vs.* n gives a very general and powerful method for representing many different effects in the sample. Three different examples are shown in Fig. 2. For a distortion such as that of cold-work the coefficients are given by

$$A_n=\langle\cos2\pi lZ_n\rangle_{Av}.$$

For small n, we expect the values of $\langle Z_n^2\rangle_{Av}^{\frac{1}{2}}$ to be small and proportional to n and hence A_n *vs.* n should start with the shape of an error curve. The effect of small particle size is to give a finite initial slope whose value is determined by the average particle size. This

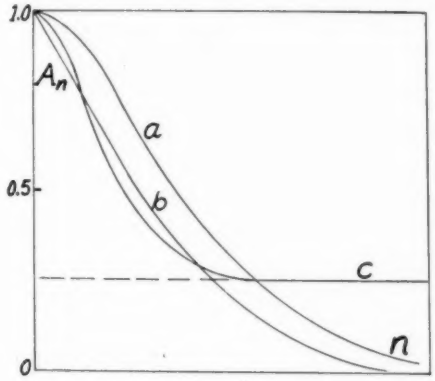

FIG. 2. Difference in shape of the A_n *vs.* n curves. (a) Cold-work distortion. (b) Particle size broadening. (c) Temperature effect.

[3] A. R. Stokes, Proc. Phys. Soc. **61**, 382 (1948).

[4] M. F. Bertaut, Comptes Rendus **228**, 492 (1949).

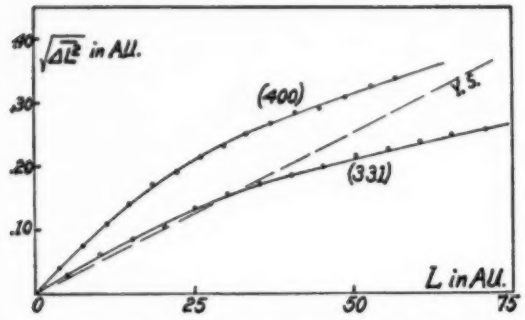

FIG. 3. Relative displacements for cold-worked 70–30 α-brass. ΔL is the change in length of a column of length L, both expressed in angstrom units.

expected difference in the shape of the A_n *vs.* n curves has been confirmed by the experimental measurements which have been made. From precise measurements of the shape of a *single reflection* it is possible to distinguish between particle size and distortion broadening.

The effect of temperature vibration is represented schematically by curve c. For large n, the value of $\langle Z_n^2\rangle_{Av}^{\frac{1}{2}}$ becomes independent of n, and A_n approaches a constant value. If each A_n value is split into the part above and below the horizontal line of curve c, the complete set of values below the line represents the sharp reflection unaffected in breadth but cut down in height, while that part of the coefficients above the line represents a diffuse scattering which peaks at the position of the reflection.

The integral breadth β of a reflection is given by

$$\beta=\frac{1}{(P_{2\theta}')_{\max}}\int P_{2\theta}'d(2\theta)$$

$$\beta=\frac{1}{\sum_{-\infty}^{+\infty}A_n}\int_{-\frac{1}{2}}^{+\frac{1}{2}}\sum A_n\cos(2\pi nh_3)\frac{\lambda}{a_3\cos\theta}dh_3$$

$$\beta=\frac{\lambda}{a_3\cos\theta}\frac{1}{\sum_{-\infty}^{+\infty}A_n}. \qquad (13)$$

From a measurement of a peak breadth β we get only the sum of the Fourier coefficients $\sum A_n$, and hence not nearly as much information as is available in a knowledge of the value of each coefficient.

VI. INTERPRETATION OF MEASUREMENTS ON COLD-WORKED METAL

From the experimental peak shape we determine a set of coefficients A_n which involve the relative displacements Z_n. If the values of Z_n are sufficiently small, or if they follow a Gaussian distribution $p(Z_n)=C\times\exp -\alpha^2Z_n^2$, the average of the cosine can be expressed as an exponential.

$$A_n=\langle\cos 2\pi lZ_n\rangle_{Av}\rightarrow\exp[-2\pi^2l^2\langle Z_n^2\rangle_{Av}]. \qquad (14)$$

From each coefficient A_n we compute a root mean square relative displacement $\langle Z_n^2\rangle_{Av}^{\frac{1}{2}}$.

Figure 3 shows a set of measurements on cold-worked 70–30 α-brass filings. To avoid the confusion resulting from the fictitious a_3 values used in the Fourier analysis, the Z_n values computed by (14) have been changed to distances in angstrom units.† L is a column length and ΔL is the change in length of the column due to cold-work

$$L=na_3 \quad \Delta L=a_3Z_n.$$

The slope of a line from the origin to any point on a curve represents a root mean square strain averaged over columns of length $L=na_3$ perpendicular to the reflecting planes. The initial slopes represent the true root mean square strains for the respective directions. The initial slopes are roughly in the inverse ratio to the values of Young's modulus for the corresponding directions, in agreement with previous studies involving measurements of peak width only.[5,6] For the cold-work involved in preparing filings, the initial slopes are of the same order as the yield strain computed from the yield stress and an average value of Young's modulus.

If strains were constant over appreciable distances in the material, as is usually assumed in the micro stress theory of cold-work broadening, the curves of Fig. 3 should be straight lines. To the extent that the approximation in (14) is justified, the noticeable drooping of these curves at distances as small as 20A is evidence for the non-uniform and localized nature of the strains in cold-worked metal.

The curves of Fig. 3 depend on the approximation that the Z_n values are either small or represented by a Gaussian distribution function $p(Z_n)=C\exp[-\alpha^2Z_n^2]$. In principle it is possible to obtain the distribution function directly from the x-ray data rather than assuming it. By using different wave-lengths it is possible to throw several orders of a particular set of planes into the high angle region. By measuring the A_n coefficients for several values of l and making use of the fact that $A_n=1.0$ for $l=0$, and vanishes for large l, we determine $A_n(l)$ approximately as a function of the variable l. In terms of the distribution function

$$A_n(l)=\langle\cos 2\pi lZ_n\rangle_{Av}=\int_0^\infty p(Z_n)\cos 2\pi lZ_ndZ_n.$$

The distribution function is given directly as the

† In a previous presentation of similar curves (reference 1) the scale of ordinates for the 331 and 222 curves involved fictitious a_3 values different from the cube edge a and the slopes are not comparable.

[5] C. S. Smith and E. E. Stickley, Phys. Rev. **64**, 191 (1943).

[6] Stokes, Pascoe, and Lipson, Nature **151**, 137 (1943).

Fourier transform of the measured $A_n(l)$ values.

$$p(Z_n)=4\int_0^\infty A_n(l)\cos 2\pi Z_n l dl. \qquad (15)$$

In principle we can determine an average strain distribution function for each n and plane (hkl). The plane (hkl) selects a direction in the crystal perpendicular to the planes, the index n selects a distance $L=na_3$ along this direction, and $p(Z_n)$ gives the distribution of strain magnitudes averaged over such lengths na_3. This probably represents as much information about the nature of cold-work deformation in a metal as can be obtained directly from the x-ray broadening data, with no assumptions about the nature of the strains being introduced.

A Quantized Theory of Strain Hardening as Applied to the Cutting of Metals

MILTON C. SHAW
Massachusetts Institute of Technology, Cambridge, Massachusetts
(Received January 18, 1950)

A theory of strain hardening is presented which utilizes the fact that metals deform blockwise rather than continuously. A metal is assumed to possess an orderly array of weak spots through which slip planes pass. The slip displacement which occurs upon a single plane is related to the spacing of weak points and the slip plane inclination. Use of a linear relation between shear plane displacement and resisting shear stress, enables the mean shear stress to be computed.

In the two examples considered it is seen that the influence of normal stress on the shear plane is less important in cutting than has been generally believed. Strain hardening and the short range inhomogeneity of metals is seen to account for most of the dynamic increase in shear strength during cutting, including the increase in shear energy per unit volume with decreased depth of cut. This size effect is akin to the increase in tensile strength with decreased specimen diameter, both phenomena involving strain hardening as influenced by inhomogeneity. The quantity Aa^2 which represents in a single number the strain hardening and short range inhomogeneity characteristics of a metal should prove particularly valuable in analyzing the cutting characteristics of metals which strain harden extensively.

INTRODUCTION

FUNDAMENTAL studies in the field of solid state physics have revealed that, in general, metals do not strain uniformly. When a single metal crystal is loaded, it will first deform elastically and then plastically. The plastic deformation is observed to occur by a process of slip as one section of the crystal slides over another. The direction of this shear deformation in a single crystal is along those planes containing the greatest number of atoms per unit area. Slip planes are clearly evident under the microscope on a polished and etched single crystal that has been plastically deformed. The presence of slip planes of a fairly regular spacing attests the fact that the metal has not been strained uniformly throughout but rather that the deformation is confined to well-defined planes that are many atomic layers apart. It is further found that polycrystalline metals also strain blockwise rather than uniformly.

Energy considerations show that slip does not involve the motion of one layer of uniformly spaced atoms over another en masse. Present theory rather suggests that slip occurs due to the motion of certain types of lattice imperfections called dislocations through a crystal. Dislocations are generally associated with highly localized stress gradients in a metal which may arise from any one of a number of causes (small internal cracks or holes, the mutual interference of adjacent grains at grain boundaries or small inclusions of foreign matter). While the exact physical nature of dislocations is not exactly clear, the properties of dislocations explain a number of characteristics of metals that are not as conveniently explained in other ways. For the purpose of the present discussion the dislocation sources may be considered as weak spots which are present in a piece of metal that has been processed in a particular way. The planes along which slip occurs are those which pass through one or more of these weak spots, the metal between adjacent planes being undeformed.

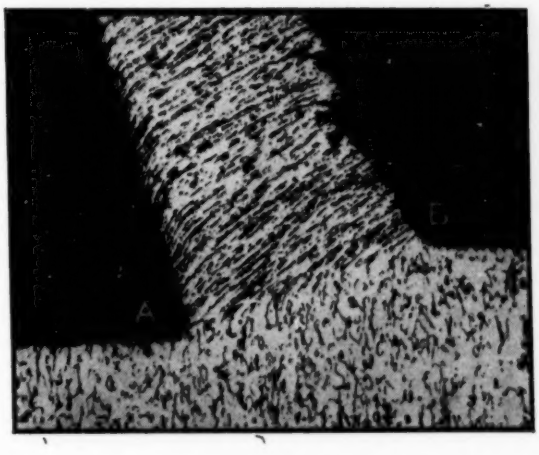

FIG. 1. Photomicrograph of a partially formed chip. Magnification 100×.

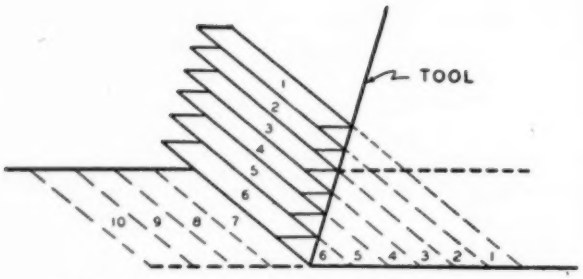

FIG. 2. Schematic representation of cutting process.

Despite the foregoing inhomogeneous picture of plastic deformation, it has been customary to treat the metal as a continuum in quantitative calculations of strain. Consideration of the well-known phenomenon of strain hardening makes it evident that a quantized treatment of strain should be used in place of a treatment involving uniformly distributed strain. The metal cutting process is a convenient one for illustrating the need for adopting such a discontinuous picture of the straining process.

THE METAL CUTTING PROCESS

When metal is cut by a two-dimensional single point cutting tool the material removed is plastically deformed to a considerable extent. Photomicrographs of the chip-tool interface of a partially formed chip, such as that shown in Fig. 1, show that metal is removed in a cutting operation by a process of shear. A distinct line of demarcation in structure (AB) is generally evident in such photomicrographs, below which metal is undeformed plastically and above which it has a deformed structure. The angle which AB, the shear line, makes with the direction of cut is called the shear angle, ϕ.

Piispanen[1] first likened the metal cutting process to the successive displacement of a series of cards as shown in Fig. 2. In this figure portions of the chip numbered 1, 2, 3 etc. originally occupied the similarly numbered positions on the workpiece. In practice the thickness of the individual "cards" is quite small, corresponding to the spacing of the aforementioned weak spots in a piece of metal. The mechanism of cutting shown exaggerated in Fig. 2 forms the basis for the theory of metal cutting that is presented here.

Previous attempts to formulate a quantitative theory of metal cutting have ignored the important tendency of a metal to strain harden. Piispanen[1] has mentioned that metals strain harden and that this factor should be included in a complete analysis of the cutting process. Merchant[2] has also mentioned that strain hardening may occur in cutting but concludes that it plays an insignificant role. Drucker[3] has more recently discussed the possibility of strain hardening in metal cutting and concludes that metal behaves as an ideal plastic when cut, strain hardening not being among the items of interest.

To prove conclusively that strain hardening can play a very significant role in metal cutting, one need only attempt to machine a specimen of austenitic stainless steel. Herbert[4] has presented data for such materials which clearly show the importance of strain hardening when they are machined. The source of the conclusion that strain hardening plays an insignificant role in metal cutting arises from the classical view that strain in a plastically deformed metal is uniformly distributed rather than being confined to certain planes. This matter will be considered in greater detail in the following discussion.

PRESENT THEORY OF METAL CUTTING

Before discussing the manner in which strain hardening may be introduced into cutting calculations, it may be well to review briefly the present theory of metal cutting that has been developed for the most part by Piispanen and Merchant. This theory is for cutting operations which produce a continuous chip with no built-up edge. The forces acting at the point of a two-dimensional cutting tool are shown in Fig. 3. If the chip above the shear plane (shown heavy) is taken as a free body, then forces R and R' must be equal if the negligible inertia force due to the change in velocity of the metal as it flows across the shear plane is ignored. Force R' is shown resolved into two sets of force components F_H and F_V, those which are normally measured with a cutting dynamometer; and F_S and N_S, those along and perpendicular to the shear plane. Force R is shown resolved into the friction and normal components on the tool face, F and N. Attention is drawn to angles α

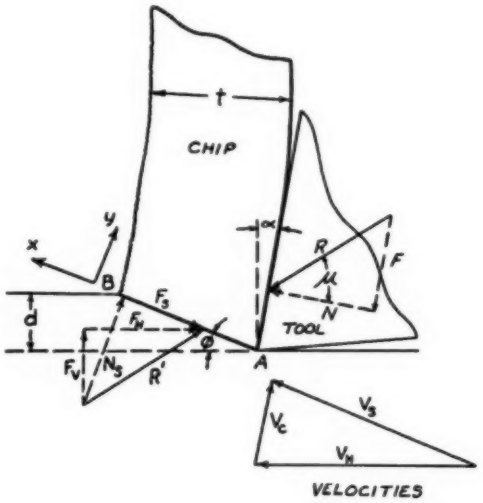

FIG. 3. Force and velocity relations in a two-dimensional cutting operation.

[1] V. Piispanen, "Lastunmuodostumisen Teoriaa" (Theory of Chip Formation), Teknillinen Aikakauslehti **27**, No. 9, 315–322 (1937).
[2] M. E. Merchant, J. App. Phys. **16**, 267–275, 318–324 (1945).
[3] D. C. Drucker, J. App. Phys. **20**, 1013–1021 (1949).
[4] E. G. Herbert, "Work Hardening Properties of Metals," Trans. ASME **48**, 705–748 (1926).

(the rake angle), ϕ (the shear angle), and μ (the friction angle) which are defined in the figure. A velocity triangle is also shown in Fig. 3 where V_H is the absolute velocity of the tool, V_S is the velocity of the chip along the shear plane relative to the stationary work piece, and V_C is the velocity of the chip up the face of the tool.

For purposes of analysis, the shear and normal stresses may be considered constant across the shear plane although actually it is evident that this cannot be the case.[5] We may also ignore the fact that plastic deformation in the vicinity of the tool point may not be along the main shear plane but at a much greater angle of shear as is evident in Fig. 1.

Piispanen[1] and Merchant[2] have suggested that the shear stress to cause slip along the shear plane is influenced by the normal stress on the shear plane and given to a good approximation by the expression

$$\tau=\tau_0+B\sigma \tag{1}$$

where τ_0 is the critical shear stress to cause slip in the absence of normal stress, σ is the normal stress on the shear plane, and B is a constant. Under certain conditions a dependence of critical shear stress or normal stress has been observed experimentally by Bridgman[6] for polycrystalline metals.

Both Piispanen[1] and Merchant[2] have applied the principle of minimum energy to the cutting process in order to relate the shear angle to other known variables. From the geometry of Fig. 3, it is evident that for a cut of unit width

$$F_HV_H=\tau dV_H\frac{\cos(\mu-\alpha)}{\sin\phi\cos(\phi+\mu-\alpha)} \tag{2}$$

where F_HV_H is the rate at which work is expended in the cutting process. Equation (1) may be written

$$\tau=\tau_0+B\tau\tan(\phi+\mu-\alpha) \tag{3}$$

and by combining Eqs. (2) and (3)

$$F_HV_H=\tau_0dV_H\times\frac{\cos(\mu-\alpha)}{\sin\phi\cos(\phi+\tau-\alpha)-B\sin\phi\cos(\phi+\tau-\alpha)}. \tag{4}$$

Applying the principle of minimum energy by differentiating with respect to ϕ (considering μ constant[7]) and equating to zero gives

$$\cot(2\phi+\mu-\alpha)=B. \tag{5}$$

This equation which relates the shear, friction, and rake angles to the slope of the shear stress-normal stress curve (B) will be discussed later.

STRAIN HARDENING

As already mentioned when metal is cut at a temperature sufficiently below its melting point, it shears in blocks rather than uniformly. Under ordinary conditions, the shear planes will be very closely spaced corresponding to the closeness of spacing of the weak spots in the metal. It may be assumed that slip planes are so spaced that a single weak spot is present on each plane. Drucker[3] has recently employed a random array of weak points to qualitatively demonstrate the increase in unit cutting energy with decrease in depth of cut. However, inasmuch as the spacing of weak points is very small compared with usual depths of cut, an orderly array of weak spots seems justified. The dots shown in Fig. 4 represent such an orderly arrangement of weak points to an exaggerated scale. These points have a uniform spacing of a units in each direction.

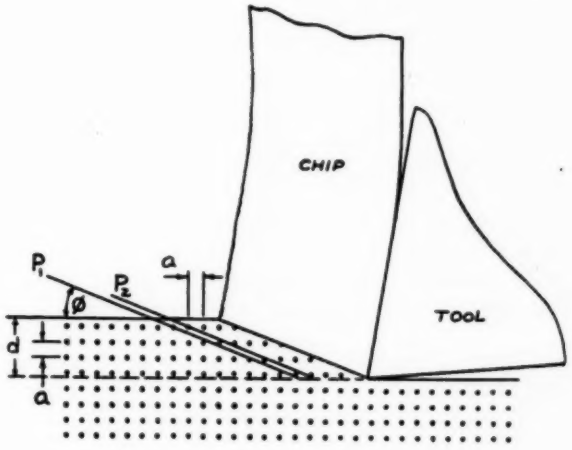

FIG. 4. Specimen with uniform array of weak spots.

Let P_1 and P_2 be two shear planes making an angle ϕ with the direction of cut and passing through adjacent points in the first row below the surface. If the depth of cut is d, then d/a planes may be placed between those at P_1 and P_2 such that a single plane passes through each weak spot in the layer in the process of being cut. The number of planes per inch in a direction perpendicular to the shear plane will be

$$n=\frac{d}{a(a\sin\phi)} \tag{6}$$

or the spacing of successive planes is

$$y=\frac{a^2\sin\phi}{d}. \tag{7}$$

[5] In order that the shear plane correspond to a plane of maximum shear stress, it is necessary that at each point along the shear plane a compressive stress exist that is directed parallel to the shear plane and which is equal to the compressive stress acting normal to the shear plane. The compressive stress parallel to the shear plane will be zero at the free surface of the chip and have its maximum value at the end of the shear plane adjacent to the tool point.

[6] P. W. Bridgman, J. App. Phys. **14**, 273–283 (1943).

[7] Drucker (see reference 3) has pointed out that in this step μ has been considered independent of ϕ but it is not at all clear that this is so.

The total slip on a given shear plane will be

$$x=\frac{a^2\sin\phi}{d}\gamma \tag{8}$$

where γ is the unit uniform strain which from Figs. 1 and 3 may be shown to be

$$\gamma=\cot\phi+\tan(\phi-\alpha). \tag{9}$$

Need now exists for data concerning the manner in which shear stress is related to shear strain. As a guide to the nature of a relation which might be assumed the so-called true stress-strain curves for metals tested in direct tension may be considered. A representative curve of this type is shown in Fig. 5. Such curves are characterized by a linear elastic region from 0 to P_1 and a less steep nearly linear plastic region extending from P_2 to the breaking point P_3. For purposes of analysis involving large strains (as in metal cutting), the curve shown dotted may be substituted for the actual diagram. Thus, according to this approximation, a critical stress σ_0 exists below which there is no plastic flow, and the stress required to produce a given strain increases linearly with the strain. The slope of this curve represents the best known measure of the tendency of a metal to strain harden.

A diagram similar to that of Fig. 5 is obtained if shear stress is plotted against shear strain. Such a diagram is shown in Fig. 6 with total shear strain x as the abscissa rather than unit strain. The critical shear stress to initiate slip is τ_0' while the slope of the curve is represented by the symbol A in the following discussion. Point P_3 is the point at which slip on a given plane ceases. Following Piispanen and Merchant we may assume that τ_0' is influenced linearly by normal stress as follows

$$\tau_0'=\tau_0+B\sigma. \tag{10}$$

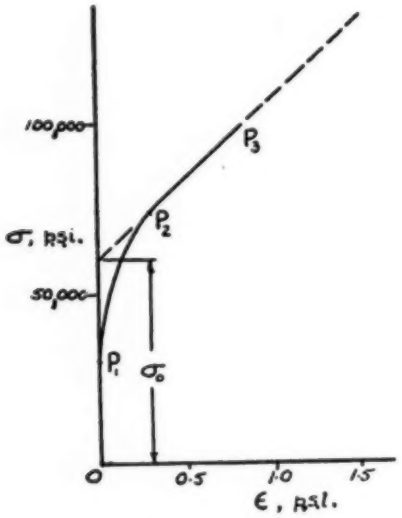

FIG. 5. True stress-strain diagram.

It is then evident that the mean shear stress during slip is

$$\tau=\tau_0+B\sigma+(Ax/2) \tag{11}$$

or from Eqs. (8) and (9)

$$\tau=\tau_0+B\sigma+\frac{Aa^2\sin\phi}{2d}[\cot\phi+\tan(\phi-\alpha)]. \tag{12}$$

This equation differs from that employed by Piispanen and Merchant by the inclusion of the last term on the right which introduces the effect of strain hardening and the inhomogeneity of the metal cut. It is interesting to note that the slope of the stress-strain curve (A) and the spacing of weak points (a) appear in the equation only in the form of the product Aa^2. This product may thus be considered a new constant of the material which measures its tendency to strain harden during shear flow. For a given material the strain hardening effect is seen to increase linearly with the unit uniform strain γ which the chip undergoes (the quantity in brackets in Eq. (12)), and inversely with the first power of the depth of cut d.

The most convenient method of evaluating the constants τ_0, Aa^2, and B for a given metal is from cutting data obtained by use of a tool dynamometer. While theoretically the data from but three different cuts would be sufficient to enable these constants to be determined, actually it is advisable to use from 10 to 20 points so that probability may tend to neutralize the effect of the natural scatter in the data due to long range in homogeneity of metal cut and other causes.

FIRST EXAMPLE

In order to illustrate the method of evaluating the three constants from cutting tests, some data previously published by Merchant[2] will be considered. In these tests a particular specimen of NE9445 steel having a Brinell hardness of 187 was cut with a carbide tool. The workpiece was in the form of a tube so as to give a simple two-dimensional cut when the tool was fed axially against the end of the tube. The chips produced were in the form of a continuous ribbon, the condition on which the foregoing analysis is based. The data obtained for a range of cutting speed, depth of cut and rake angle are summarized in Table I. Merchant plotted these data in accordance with Eq. (1) to obtain Fig. 7. The values of τ and B obtained from this plot were 58,000 lb./in.^{2} and 0.23 respectively, corresponding to the solid line.

These same data may be replotted in accordance with Eq. (12) developed here. For this purpose it is convenient to rearrange the equation as follows

$$\tau-B\sigma=Aa^2[\cot\phi+\tan(\phi-\alpha)]\frac{\sin\phi}{2d}+\tau_0$$

$$=Aa^2\left(\frac{\gamma\sin\phi}{2d}\right)+\tau_0, \tag{13}$$

where it is evident that a straight line of slope Aa^2 and intercept τ_0 will be obtained when the quantity $(\tau - B\sigma)$ is plotted against $(\gamma \sin\phi)/2d$. Such a plot could be readily obtained from the data of Table I if B were known. A procedure which may be followed in the absence of this value is to assume successive values of B and obtain a series of plots. The line best fitting the data points corresponds to the value of B to be adopted. A series of plots obtained in this manner is shown in Fig. 8 for values of B of 0, 0.05, 0.1, 0.2 and Merchant's value of 0.23 which of course should be a horizontal line. The foregoing procedure of plotting a series of curves involves less work than it might appear at first glance due to the ease of obtaining successive curves from the one first plotted.

It would appear from Fig. 8 that the curve best fitting the data points corresponds to a B of 0.05 and the corresponding equation for shear stress may be written

$$\tau = 80{,}000 + 0.05\sigma + 29\frac{\gamma \sin\phi}{2d}, \text{ p.s.i.} \qquad (14)$$

In considering which value of B best fits the data points, special attention should be given those points corresponding to high and low depths of cut. Data corresponding to a greater range of depth of cut will enable a more decisive choice of the correct value of B. The value of B in Eq. (14) is seen to be far less than that in Merchant's analysis and in better agreement with the value of 0.125 directly observed by Bridgman[6] for drill rod. It would thus appear that much of the effect which Merchant has attributed to normal stress on the shear plane is actually due to strain hardening and the inhomogeneity of the metal cut.

Merchant[2] has plotted directly measured values of ϕ against the quantity $(\mu - \alpha)$ from Eq. (5) in which B is taken equal to 0.23. This plot corresponds to the solid line in Fig. 9. If Eq. (12) including the effect of strain hardening is substituted for Eq. (1) in the derivation leading to Eq. (5) it is found that for minimum energy

TABLE I. Data for NE9445 steel.[2]

Depth of cut in. ×1000	Cutting speed V_H ft./min.	Rake angle α, deg.	ϕ deg.	γ	tan μ	σ psi ×10⁻³	τ psi ×10⁻³	W_S in. lb./in.³ ×10⁻³
3.70	197	10	17.0	3.4	1.05	115	85	292
3.70	400	10	19.0	3.1	1.11	137	88	266
3.70	642	10	21.5	2.7	0.95	129	90	248
3.70	1186	10	25.0	2.4	0.81	130	93	224
3.70	400	−10	16.5	3.9	0.64	153	89	342
3.70	637	−10	19.0	3.5	0.58	152	90	311
3.70	1160	−10	22.0	3.1	0.51	154	94	289
1.09	542	10	19.0	3.1	1.12	164	103	308
2.34	542	10	18.5	3.1	1.08	140	92	287
3.70	542	10	21.5	2.7	0.96	131	91	248
7.88	542	10	25.0	2.4	0.76	116	89	214
1.09	542	−10	12.5	5.0	0.78	179	103	523
2.34	542	−10	16.0	4.0	0.70	172	96	385
3.70	542	−10	19.0	3.5	0.60	164	94	306
7.88	542	−10	22.5	3.1	0.46	138	90	270

(again considering μ to be independent of ϕ)

$$\cot[\cot^{-1}(B) - \phi - \mu + \alpha] = \cot\phi - \frac{\tan(\phi-\alpha)\tan\phi\sin(2\phi-\alpha)}{\cos\alpha\left(1+\dfrac{2d\tau_0}{Aa^2}\right)}. \qquad (15)$$

This is seen to reduce to Eq. (5) if strain hardening is ignored (i.e., when $Aa^2 = 0$). For most applications the last term on the right side of Eq. (15) is negligible and Eq. (15) reduces to Eq. (5). The strain hardening term will be important only when the quantity $(d\tau_0)/(Aa^2)$ is small, i.e., if Aa^2 is large, the depth of cut is very small as in grinding, or the material has a low critical shear stress τ_0.

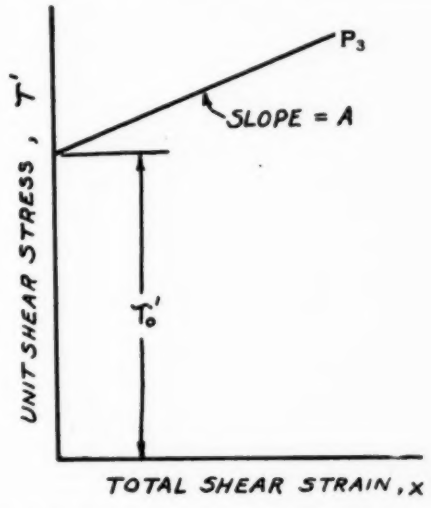

FIG. 6. Unit shear stress-total shear strain diagram.

Equation (15) has been used to obtain the dotted curve shown in Fig. 9. In this instance the second term

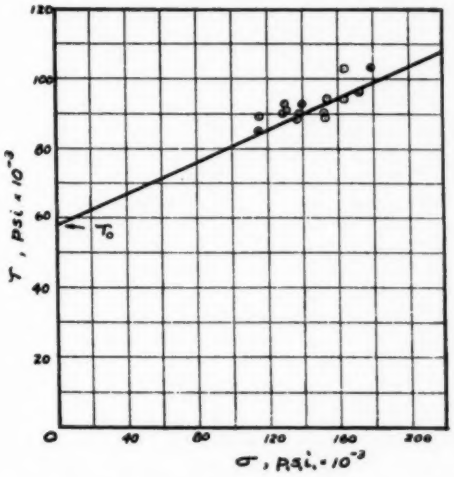

FIG. 7. Relation between shear strength and normal stress for cutting data of Table I.

on the right is negligible. It is evident that the dotted curve does not fit the data as well as the solid curve but this observation is not thought very significant in view of the following approximations of the theory leading to Eqs. (5) and (15).

1. The influence of temperature upon τ_0 has been ignored. This effect is apt to be quite significant since in practice the mean temperature along the shear plane is quite high. The effect of temperature is to cause a decrease in the value of ϕ obtained from Eqs. (5) or (15). The inclusion of the temperature effect would thus tend to lower both curves of Fig. 9, bringing the dotted line into better agreement with the experimental points but the solid line into poorer agreement.

2. The coefficient of friction has been considered independent of the shear angle in the foregoing analysis. It is not known how significant this approximation is but it may be observed that a decrease in the coefficient of friction that accompanies the use of an effective cutting fluid causes an appreciable increase in the angle ϕ. Conversely, it is to be expected that a change in ϕ will be accompanied by a change in μ. This point

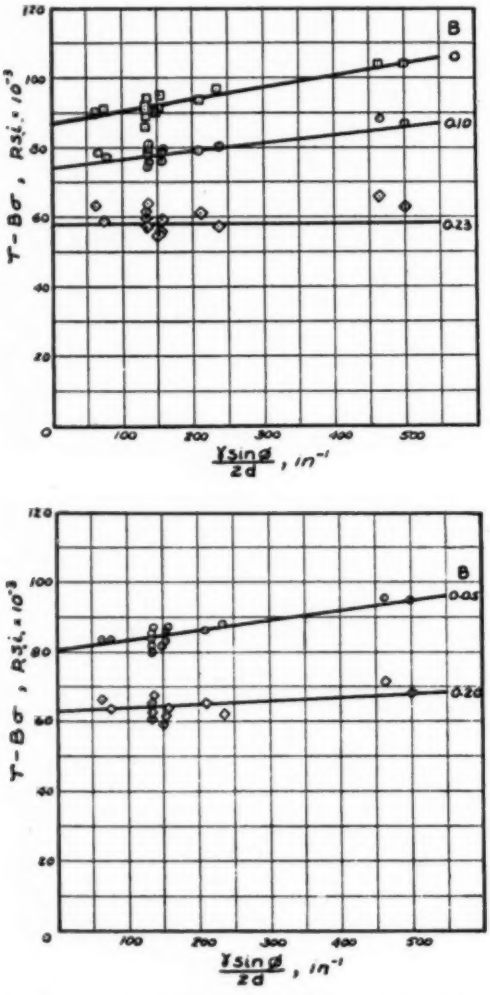

FIG. 8. Plots of $\tau - B\sigma$ against $(\gamma \sin\phi)/2d$ for data of Table I.

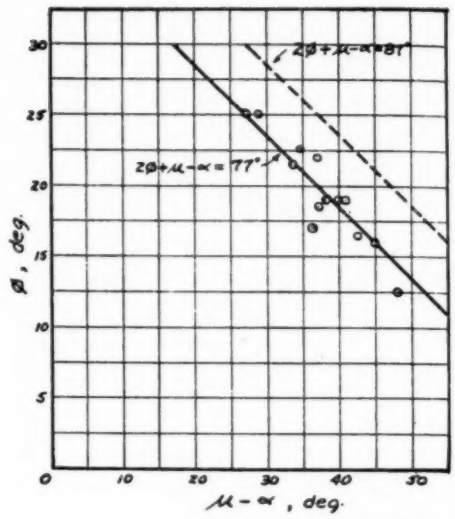

FIG. 9. Plot of ϕ against $\mu - \alpha$ for data of Table I.

places the portion of the analysis leading to Eqs. (5) and (15) in question.

3. The effect upon τ_0 of the change in the rate of strain with ϕ has been ignored in the derivation of Eqs. (5) and (15). If this effect were included, it would also cause the dotted and solid curves of Fig. 9 to be lower. However, it is unlikely that this effect would be significant inasmuch as the rate of strain is always at a very high level in metal cutting. As is evident in Fig. 1, the metal goes from an essentially unstrained condition to the fully strained condition in the very short time it takes to traverse the shear plane. Theoretically this would correspond to an infinite rate of strain were the shear plane a truly mathematical surface of zero thickness.

The position of the solid curve in Fig. 9 is significantly influenced by the choice of curve in Fig. 7. In this instance it would appear that the points in Fig. 7 call for a line of considerably less slope which would tend to shift the solid line of Fig. 9 in the direction of the dotted line.

SECOND EXAMPLE

Results of a series of tests were recently published[8] in which seamless tubing of 6 inch diameter and 0.475 inch wall thickness was cut using two-dimensional high speed steel tools having rake angles ranging from 25 to 45°. The steel was cut under conditions to prevent the formation of a built-up edge at a speed of 90 feet per minute. It is interesting to examine these data which are summarized in Table II from the point of view of the foregoing theory.

In accordance with Merchant's theory, the relation of shear strength to normal stress is first considered (Fig. 10). In this instance it is quite difficult to know

[8] Lapsley, Grassi, and Thomsen, "Correlation of Plastic Deformation during Metal Cutting with Tensile Properties of the Work Material, ASME Preprint No. 49-A-121 (December, 1949).

just where to draw the line, there being apparently two possibilities—the line shown solid and that shown dotted. The data are next shown plotted in Fig. 11 in accordance with the strain hardening theory presented here. Only the curve corresponding to $B=0$ is shown inasmuch as other values of B investigated gave points which fitted a straight line less closely than that for $B=0$. The solid line shown corresponds to the equation

$$\tau = 52{,}000 + 153(\gamma \sin\phi)/2d, \text{ p.s.i.} \qquad (16)$$

In the third figure of this series (Fig. 12) the observed values of ϕ are shown plotted against the quantity $(\mu-\alpha)$. Equation (15) again reduces to Eq. (5) since the strain hardening term is negligible. The relation based on strain hardening theory is given by the dash line in Fig. 12 while the relation predicted by Merchant's theory (corresponding to the solid line in Fig. 10) is shown solid. If the dotted line in Fig. 10 is used, the dotted line of Fig. 12 is obtained. The line in Fig. 12 corresponding to strain hardening theory is seen to be in good agreement with the data for tools of high rake angle, but the data for the 25° rake angle tool lies below the curve as in the example of the previous section and probably for the same reasons.

DISCUSSION

Drucker[3] has considered the fact that essentially all of the strain which occurs in the cutting process takes place as the material crosses the shear plane at approximately a constant shear stress to be a paradoxical result. He concludes that this can only mean that the metal behaves as an ideal plastic which strains without strain hardening ($A=0$). This is a natural conclusion when viewed from the classical point of view where the metal is considered to strain uniformly. However, while there is no appreciable spatial change in shear stress in the vicinity of the shear plane, there is a significant temporal change. The shear stress on the shear plane is not constant with time but increases as slip proceeds due to strain hardening. This variation in shear stress would give rise to a variable shearing force which could be detected with a very sensitive dynamometer of high frequency response were it not for the fact that the process of slip is in varying phases of completion at different points across the chip. This may be seen by examining the back surface of a chip where the edges of certain slip planes are evident as wavy rather than straight lines extending across the chip in a direction perpendicular to the direction of cut. The slip process is thus not quite as simple as the sliding of cards one over the other, but the actual process appears to involve the propagation of screw type as well as edge type dislocations.

The stress concentration associated with a sharp tool point is largely responsible for the fact that strain occurs essentially on only one plane at a time. In this

TABLE II. Data for mild steel.*

Depth of cut in. ×1000	Cutting speed V_H ft./min.	Rake angle α, deg.	ϕ deg.	γ	tan μ	σ psi ×10⁻³	τ psi ×10⁻³	Ws in. lb./in.³ ×10⁻³
2.5	90	25	20.9	2.55	1.46	104	82.8	209
3.5	90	25	21.5	2.48	1.46	96.0	74.6	180
5	90	25	24.0	2.23	1.375	100	75.5	169
6	90	25	20.1	2.65	1.36	86.5	65.8	175
8.5	90	25	22.4	2.38	1.38	83.6	66.5	159
2.5	90	35	31.6	1.56	1.53	96.0	71.4	112
3.5	90	35	31.9	1.55	1.52	84.0	61.2	96.4
5	90	35	32.0	1.55	1.48	82.9	62.4	96.5
6	90	35	32.2	1.54	1.425	88.6	61.8	95.5
8.5	90	35	32.0	1.55	1.38	80.9	58.5	91.3
2.5	90	40	35.7	1.32	1.54	94.5	72.0	94.0
3.5	90	40	35.4	1.33	1.50	84.3	66.5	87.8
5	90	40	37.5	1.26	1.44	87.0	66.1	83.1
6	90	40	37.2	1.27	1.42	90.0	63.5	81.1
8.5	90	40	37.2	1.27	1.35	83.1	61.5	78.1
2.5	90	45	41.9	1.06	1.83	114.6	71.1	74.8
3.5	90	45	41.9	1.06	1.74	98.8	64.2	68.5
5	90	45	40.2	1.10	1.64	87.2	63.8	69.6
6	90	45	39.6	1.01	1.60	80.8	61.7	62.7
8.5	90	45	39.9	1.11	1.51	73.6	58.7	65.0

* See reference 8.

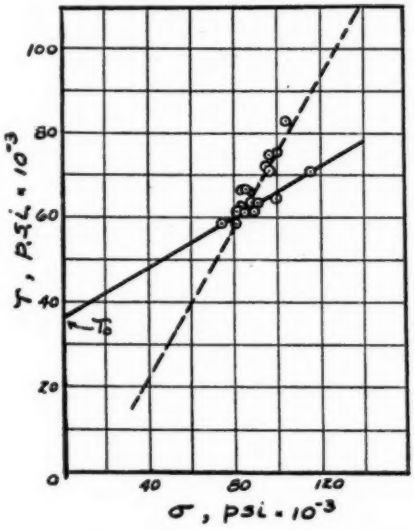

FIG. 10. Relation between shear strength and normal stress for cutting data of Table II.

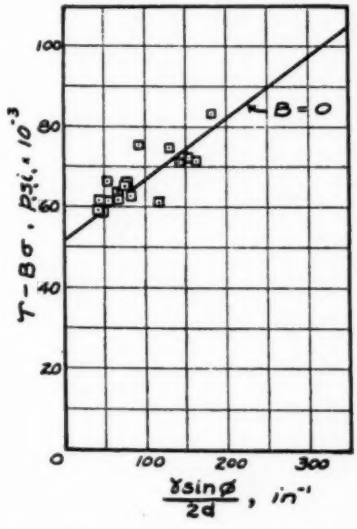

FIG. 11. Plot of $\tau - B\sigma$ against $(\gamma \sin\phi)/2d$ for data of Table II.

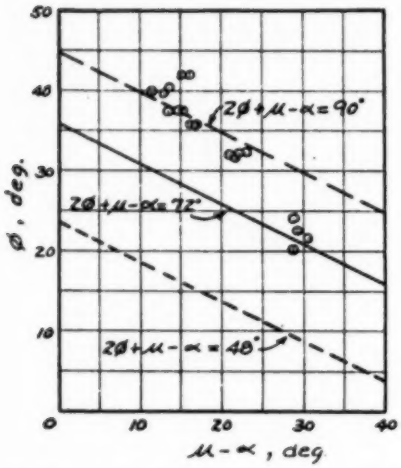

FIG. 12. Plot of ϕ against $\mu-\alpha$ for data of Table II.

respect the cutting process differs from all others in the field of plastic flow. For example, in the ordinary tensile test, strain occurs simultaneously upon many planes as the load is progressively increased. The concept of a homogeneous strain is not so serious in such applications as in the case of the cutting process. However, it would appear that even in such problems it is advantageous to adopt the quantized picture of strain which will enable a size effect to be included in the quantitative theory just as the effect of the depth of cut was included in the foregoing theory of metal cutting.

In Table II it is evident that the shear work to remove a cubic inch of metal increases with decreased depth of cut. This is particularly true for the data obtained with the 25° rake angle tool. The strain hardening theory explains this observation. The shear work for this metal may be obtained by use of Eq. (16) as follows

$$W_S = \tau\gamma = 52{,}000\gamma + 153(\gamma^2 \sin\phi)/2d, \text{ in.-lb./in.}^3. \quad (17)$$

From this expression it is evident that the specific shear work is increased with an increase of shear strain γ or a decrease of depth of cut d. The experimental values of W_S given in Table II are in agreement not only with the observation concerning the influence of depth of cut but also shear strain. The specific work is seen to increase as the rake angle α is decreased, the main reason for this being the increase in strain associated with the decrease in rake angle.

CONCLUSIONS

As the basic metal cutting process becomes better understood, the gap between our well-known materials tests and the metal cutting operation is narrowed. The simple two dimensional machining operation is seen to provide means for conducting materials tests that are now carried out only with considerable difficulty. Specifically the cutting test offers a very convenient method for determining the dynamic shear strength of metals since the inherent feature of this process is to allow shear on approximately one plane at a time thus naturally providing very high rates of strain. Correspondingly high rates of strain are obtained in the ordinary tensile test only with considerable difficulty and uncertainty due to inertia effects. Furthermore the characteristics of the cutting process enable tests to be carried to strains that are considerably higher than those in the usual tensile test. The simplicity of the test apparatus and the fact that a specially shaped specimen need not be prepared are additional factors of interest. While the tensile test has a superficial appearance of simplicity, a little study will reveal that this process may even at present be less completely understood than the cutting process. It would therefore not be surprising to one day find the simple two-dimensional cutting process in use in materials laboratories engaged not alone in machinability studies but also in use in evaluating the basic physical properties of metals.

Mechanical and Electrical Properties of Plasticized Vinyl Chloride Compositions*

LAWRENCE E. NIELSEN, ROLF BUCHDAHL, AND RITA LEVREAULT
Plastics Division, Monsanto Chemical Company, Springfield, Massachusetts

(Received January 24, 1950)

The temperature dependence of the dynamic mechanical and a.c. electrical properties of a given polyvinyl chloride plasticizer composition can be characterized by two quantities: (a) the transition temperature which is defined as the temperature of maximum dissipation factor and (b) the half-widths of the loss factor-temperature curve. A simple relationship exists between the transition temperature determined mechanically or electrically and the volume fraction of a compatible plasticizer. The modification of this relationship for non-compatible plasticizer has been indicated. The half-width is a function of the volume fraction of the plasticizer, although this relationship is not as simple as the one obtained for the transition temperature. A simple correlation exists between the electrical and mechanical half-width. The compliance measured in tensile creep has been found to be a function of the applied load and the compliance-load relationship varies depending on the region in which the material finds itself. The shape of the creep curve at different temperatures has been correlated with the dissipation factor-temperature curve. The shape of the stress-strain curve has been related to the modulus-temperature curve and a correlation between the initial Young's modulus and the ultimate elongation and breaking strength has been established. It has been shown that the relaxation theory is not sufficient to explain certain features of the modulus (or dissipation factor) temperature relationship. The limited significance of the μ-value and of the viscosity of plasticizers with respect to plasticizer efficiency has been demonstrated.

INTRODUCTION

THE mechanical properties of plasticizer-polymer systems in the solid state have been the subject of several investigations.[1–4] As a result of such work, it has been possible to draw the following conclusions concerning the effect of plasticizer concentration and type of plasticizer on these properties: (1) the addition of plasticizer always lowers and broadens the transition or softening region compared to the unplasticized resin; (2) plasticizers differ in their effectiveness to lower and broaden the transition region.** Several attempts have been made to interpret these data in terms of other physical quantities. For example, Jones[5] tried to show that the viscosity and the viscosity temperature coefficient of the plasticizer are significant quantities determining plasticizer efficiency, or the transition range of plasticizer-polymer systems. On the other hand, Boyer and Spencer[6] have derived an expression for the flex or second-order transition temperature as a function of polymer concentration, assuming that this temperature corresponds to an isoelastic or isoviscous state of this system, and second, making use of the Flory equation of viscous flow. The same authors have also suggested[6] that the reason for the difference in kind of plasticizers might be due to the difference in μ-value for different plasticizers in various polymers. The importance of plasticizer-resin interaction has also been pointed out by Aiken[4] in interpreting the very different creep curves which one obtains for polyvinyl chloride-plasticizer systems. Alfrey[7] has tried to show that the creep data support in general his relaxation theory of viscoelastic deformations of linear high polymers. However, the experimental data available until now are neither extensive nor precise enough to permit a proper evaluation of the proposed mechanism of plasticizer action. It was, therefore, one of the major objectives of this work to undertake a systematic study of various mechanical properties, such as the dynamic modulus and dissipation factor, stress-strain relationships and creep, over a wide temperature range as a function of plasticizer concentration and type of plasticizer, in order to obtain more definite information concerning the dependence of these properties on the above-stated variables. In Table I are shown the various plasticizers used, and it will be noted that all of them, with the exception of di-lauryl phthalate, are commonly referred to as solvent-type plasticizers; such generalizations, which will be permissible on the basis of the results obtained, apply, therefore, primarily to this type of plasticizer, although some characteristic effects of non-solvent type plasticizers will be considered. In order to study the significance of the μ-value on plasticizer action, without changing the functional groups of the molecule, five different phthalate plasticizers were chosen, covering a μ-value range in polyvinyl chloride from -0.1 to $+1.4$.[8]

The a.c. electrical properties of plasticizer-polymer systems have been studied by several investigators;[9–11]

* Presented in parts at the American Physical Society Meeting, New York City (January, 1949) and at the High Polymer Forum of the A.C.S. Atlantic City Meeting (September, 1949).

[1] R. Lawrence and E. B. McIntyre, Ind. Eng. Chem. **41**, 689 (1949).

[2] N. C. Read and Harding, Ind. Eng. Chem. **41**, 675 (1949).

[3] Rider, Sumner, and Myers, Ind. Eng. Chem. **41**, 709 (1949).

[4] Aiken, Alfrey, Janssen, and Mark, J. Polymer Sci. **2**, 178 (1947).

** The transition region has, in the past, been characterized by some arbitrary temperatures, such as the flex or brittleness temperature or the apparent second-order transition temperature; the significance of the transition region lies in the fact that it is in this range where all mechanical properties undergo a considerable change in magnitude and kind over a rather limited temperature range.

[5] H. Jones, J. Soc. Chem. Ind. **67**, 415 (1948).

[6] R. F. Boyer and Spencer, J. Polymer Sci. **2**, 157 (1947).

[7] T. Alfrey, Jr., *Mechanical Behavior of High Polymers* (Interscience Publishers, Inc., New York, 1948).

[8] W. G. Bagley (unpublished data).

[9] Davies, Miller, and Busse, J. Am. Chem. Soc. **63**, 361 (1941).

[10] Würstlin, Kolloid Zeits. **105**, 9 (1943).

[11] R. Fuoss, J. Am. Chem. Soc. **61**, 2334 (1939); **63**, 2401, 2410, 2832 (1941); **64**, 283 (1942).

TABLE I.

1	2	3	4	5	6	7	8	9	10	11
		Concentration		Transition temp. °C		Half-width °C				
Composition	Density	c_v	c_m	Mech.	Elec.	Mech.	Elec.	$\left(\frac{E_i}{G'}\right)_{25°C}$	ΔE (kcal.)	30°C $\eta(c\rho)$
Polyvinyl chloride	1.41*	0	0	86	105	7(?)	15–21	2.09	—	—
PVC-dimethyl phthalate	1.19	0.291	0.10	28	42	13	38	—	14.3	9.8
PVC-diethyl phthalate	1.12	0.254	0.07	35	50	13	40	2.09	7.6	10.0
PVC-DEP		0.336	0.10	22	32	17(?)	45	1.24	15.2	—
PVC-DEP		0.443	0.15	−6	15	17	46	2.67	26.9	—
PVC-dibutyl phthalate	1.045	0.158	0.03	57	70	12	26	1.93	—	10.4
PVC-DBP		0.313	0.07	25	39	42	—	2.68	9.6	—
PVC-DBP		0.400	0.10	4	21	13	45–51	2.14	8.4	—
PVC-DBP		0.526	0.15	−20	3	12(?)	45	1.59	14.9	11.5
PVC-*n*-dioctyl phthalate	0.986	0.402	0.07	5	21	46(?)	61	2.62	—	—
PVC-*n*-DOP		0.501	0.10	−15	3	32	74	2.22	12.6	—
PVC-dilauryl phthalate	0.943	0.368		—	68	—	85	—	—	—
PVC-tricresyl phosphate	1.16	0.351	0.069	29	45	15(?)	37	—	15.5	15.4
PVC-TCP		0.443	0.10	12	30	15	42	2.86	34.0	—
PVC-dibutyl sebacate	0.935	0.250	0.042	34	46	56	20	1.87	—	7.6
PVC-DBS		0.458	0.10	−27	−7	62	31	1.52	—	—

* Density values are for resin and plasticizer and not for the mixture.

the work of Fuoss,[11] in particular, has given us extensive data concerning the dependence of the dielectric constant and the power factor on temperature, on plasticizer concentration and type of plasticizer. However, the theoretical interpretation of such data on the basis of a simple relaxation mechanism has not been too successful.[12] It was hoped, therefore, that a simultaneous investigation of the electrical and mechanical properties *on identical samples* might aid in the clarification of the plasticizer mechanism in general, particularly as a close qualitative correlation between the electrical and mechanical properties of plasticizer systems had been suggested in the past.[13]

EXPERIMENTAL DETAILS

Preparation and Composition of Specimens

A polyvinyl chloride of fine particle size, having an intrinsic viscosity of about one in cyclohexanol, was used in the preparation of all specimens. The volume and mole fractions of all the compositions used and the density of the resin and the plasticizers are given in Table I, columns 3, 4, and 5, respectively. The preparation of all test specimens was carried out according to the following procedure. The resin, the plasticizer, and a small amount of tribase stabilizer (two percent based on the amount of the resin used) were weighed out separately and mixed together by hand. The mix was then transferred to a two-roll mill and was milled for not longer than 10 min. at a temperature varying between 265° and 280°F. The mix was taken off the mill, cut into small pieces, and specimens of various thickness were compression-molded to the required dimensions using, as much as possible, the same molding cycle throughout.

Instruments and Testing Procedures

The dynamic mechanical properties were measured using a torsion pendulum, with the exception of a few measurements on unplasticized polyvinyl chloride, which were carried out with a vibrating reed-type instrument.[14] The rectangular test strip ($2\times\frac{3}{8}\times0.025$ in.) is part of the pendulum, see Fig. 1. The dynamic modulus is calculated from the frequency of the free vibration and the dimensions of the specimens, and the damping is determined from the logarithmic decrement of the vibration. Actually, the frequency and the damping are measured as a function of the load attached to the lower end of the specimen and all data given are extrapolated to zero load. The temperature of the instrument is controlled by an air bath, having a temperature variation of about ±0.5°C. The frequency of the vibration can be varied by a factor of 10, using different disks giving the system different moments of inertia. The precision of the shear modulus and logarithmic decrement values is ±5 and ±10 percent, respectively, provided the damping is not too high; as the damping increases the precision of the measurement decreases.

The tensile creep was measured by clamping both ends of the strip, applying a fixed load to the lower clamp and following the separation of two inked lines on the sample with a cathetometer as a function of time. The sample, but not the load, was surrounded by an air bath, controlled within ±0.5°C. A difference of 0.005 cm in length could be measured with the cathetometer. In general, the creep data could be reproduced within ±5 percent, except in the transition region, provided a new sample was used in the repeat run. It was found that the previous history definitely affected the absolute value of the creep and the shape of the creep

[12] F. G. Kirkwood and R. Fuoss, J. Chem. Phys. **9**, 329 (1941).
[13] H. Roelig and Heidemann, Kunststoffe **7**, 125 (1948).
[14] W. Kuhn and O. Künzle, Helv. Chim. Acta **30**, 839 (1947); and M. Mooney and R. Gerke, Rubber Chem. Tech. **14**, 35 (1941).

curves; however, no systematic study was made of this phenomenon.

The stress-strain properties were measured on an Instron machine† at 25°C and 50 percent relative humidity. For each composition five separate runs were made; the variations in Young's modulus, determined graphically from the initial slope of the stress-strain curve, and the tensile strength are less than 10 percent, but the variations in elongation at break were at times as much as 100 percent for the same composition.

A 5-sec. modulus was measured with a torsional instrument, first described by Clash and Berg.[15] The specimen, which consists of a narrow strip immersed in a liquid bath of constant temperature, is held rigidly at the lower end, whereas the upper end is attached to a rod to which a known torque can be applied. The angular deflection after 5 sec. is noticed and Young's modulus is calculated knowing the torque, the angle of twist, and the dimension of the specimen, using a Poisson ratio of 0.5 to convert from shear to Young's modulus. Shore hardness was measured by the indentation and/or the penetration of a needle-type point under usually variable load into the surface of the plastic composition. The viscosity of the plasticizers was measured with a capillary viscosimeter of the Ostwald-Fenske type. The viscosimeters were immersed in a liquid bath controlled to ±1°C.

The dielectric constant and power factor were measured for all compositions at 1000 c.p.s. as a function of temperature. The measurements were made with a General Radio capacitance bridge using circular specimens, and the surfaces of each specimen was painted with a du Pont silver electrode paint. For a few compositions measurements were also made at 500 and 10,000 c.p.s. The d.c. resistance was measured with a General Radio resistance bridge using General Electric type electrodes. The precision of these measurements was at best ±15 percent, but in many cases it was much poorer because of the high resistance of the samples, which approached frequently the upper limit of sensitivity of the instrument. For all electrical measurements the samples were immersed in an air bath controlled to ±0.5°C.

RESULTS

Figures 2 and 3 show some typical log modulus and dissipation factor data as a function of temperature for various plasticized compositions. Within a certain temperature range the modulus is high, of the order of magnitude of 10^{10} dynes/cm², whereas in the higher temperature range the modulus is low, of the order of magnitude of 5×10^{7} dynes/cm². These two regions, the hard and the rubbery one, are joined by a third one where the modulus changes strongly in a relatively narrow temperature range and this range can be called the transition region. The dissipation factor, or damping,‡ also changes with temperature in a characteristic manner; the damping is low and fairly insensitive to temperature in the hard and the rubbery region, and goes through a definite maximum in the transition region. In the hard and rubbery region the modulus and the damping factor approach a constant value which is fairly independent of plasticizer and plasticizer concentration. It is clear, therefore, that these curves can be characterized quite satisfactorily by two constants, the transition temperature and the half-width.[16] The transition temperature is defined as the temperature where the dissipation factor has its maximum, or where the log modulus-temperature curve goes through an inflection point. The use of transition temperature, as defined above, to characterize the transition region is to be preferred to other temperatures (flex temperature, brittleness, etc.) for the following reasons: (a) it is not an arbitrarily defined quantity, as many of the other temperature values; (b) it is independent of the half-width, and (c) it leads to a simpler relationship with the amount of plasticizer than do the other quantities. The half-width is defined as the temperature difference in degrees centigrade where the dissipation factor has reached half its maximum value. Columns 5

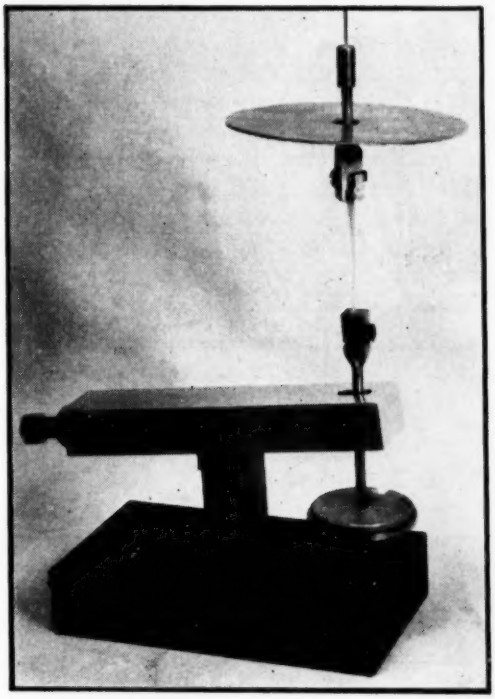

FIG. 1. Torsion pendulum for measurements of dynamic mechanical properties.

† We wish to thank Dr. Hamburger of the Fabrics Research Laboratories for the use of this instrument. A description of this instrument is given by G. S. Burr, Electronics **22**, No. 5, 101 (1949).

[15] R. F. Clash and Berg, Ind. Eng. Chem. **34**, 1218 (1942).

‡ δ = logarithmic decrement = $\pi\frac{G''}{G'}$; $\frac{G''}{G'} = \frac{\text{imaginary modulus}}{\text{real modulus}}$ = dissipation factor.

[16] Dienes and Dexter, Ind. Eng. Chem. **40**, 2319 (1948).

and 7 of Table I give the transition temperature and the half-width of all compositions. In a few cases it was not possible to determine the half-width with any degree of reliability, because the absolute value of the maximum could not be determined. In these cases the half-width given is the best estimate possible. Figure 4 shows the dielectric constant and loss factor as a function of temperature for various plasticized compositions. Here again it is possible to characterize these curves by two constants, namely the transition temperature and the half-width. Columns 6 and 8 of Table I show these two quantities for all compositions.

The dependence of the mechanical and electrical transition temperature on plasticizer concentration turns out to be a very simple one, as can be seen from Figs. 5 and 6. For all the plasticizers investigated, with the exception of dilauryl phthalate, which will be discussed later, the transition temperature is a linear function of the volume fraction (c_v) of the plasticizer. For four members of the phthalate homologous series the slope of the $T_t - c_v$ curve is the same, whereas the slope is different for tricresyl phosphate and dibutyl sebacate. The concentration dependence of T_t is independent of frequency, but the absolute value of T_t is dependent on frequency. Finally, it should be pointed out that the transition temperature as a function of the mole fraction of the plasticizer yields a non-linear relationship between these two quantities and also different curves for each plasticizer.

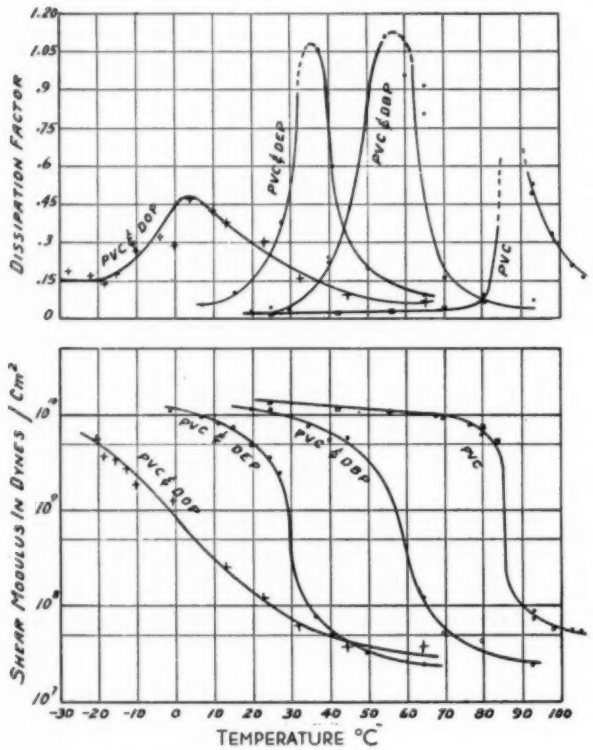

FIG. 2. Dynamic shear modulus and dissipation factor as a function of temperature. 0.158 DBP+PVC; 0.254 DEP+PVC; 0.402 DOP+PVC; PVC without plasticizer (number gives volume fraction).

The dependence of the half-width of the electrical power factor-temperature curve on plasticizer and plasticizer concentration is shown in Fig. 7. The half-width first increases with plasticizer concentration, goes through a maximum at about 0.5 c_v, and then appears to decrease again. For a given plasticizer concentration the half-width increases with increasing chain lengths of the mechanical dissipation factor. It was not possible to determine the relationship between the mechanical half-width and plasticizer concentration with the same accuracy as in the electrical case. However, a correlation between the electrical and mechanical dissipation factors shown in Fig. 8 suggests very strongly that the same conclusions arrived at in the electrical case also hold for the mechanical dissipation factor. It should also be noted that the mechanical dissipation factor is always smaller than the corresponding electrical dissipation factor.

The most interesting feature of stress-strain curves of plasticized polyvinyl chloride compositions (Fig. 9) is the wide difference in the shape of the stress-strain curve as a function of plasticizer and plasticizer concentration. Some stress-strain curves show a definite yield point; in other cases the stress increases rapidly and then remains almost constant over a considerable elongation range before the sample breaks. A more careful analysis of the data shows that the shape of the curves is closely related to the region in which the sample finds itself: in the hard region the slope of the stress-strain curve is very steep and frequently followed by a yield value before break; in the transition region the stress-strain curve slopes strongly, followed by a very flat region with an indefinite yield point, whereas in the rubbery region the stress-strain curve has a small slope which changes little over a very wide range of elongation. The relationship between initial Young's modulus and (a) elongation at break and (b) the tensile strength is shown in Fig. 10. Figure 11 shows the ultimate elongation as a function of the volume fraction of plasticizer; although a slight difference seems to exist for various plasticizers, the number of tests and the precision of the elongation measurement do not justify putting too much emphasis on these differences, and, to a first approximation, one can conclude that the ultimate elongation is very small up to a critical plasticizer concentration at a given temperature and then increases linearly with concentration, irrespective of the type of plasticizer employed. Column 9, Table I gives the ratio of the initial Young's modulus, obtained from the stress-strain curve, to the corresponding dynamic shear modulus obtained with the torsion pendulum, both measured at 25°C.

In studying the creep properties of the various compositions listed in Table I, it was found (a) that repeated creep and recovery runs on the same sample

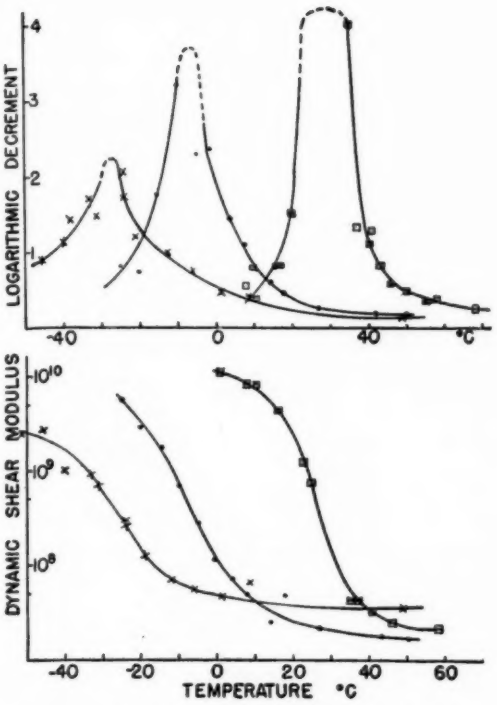

FIG. 3. Dynamic shear modulus and dissipation factor as a function of temperature. ● −0.443 DEP; × 0.458 DBS; ⊡ 0.351 TCP.

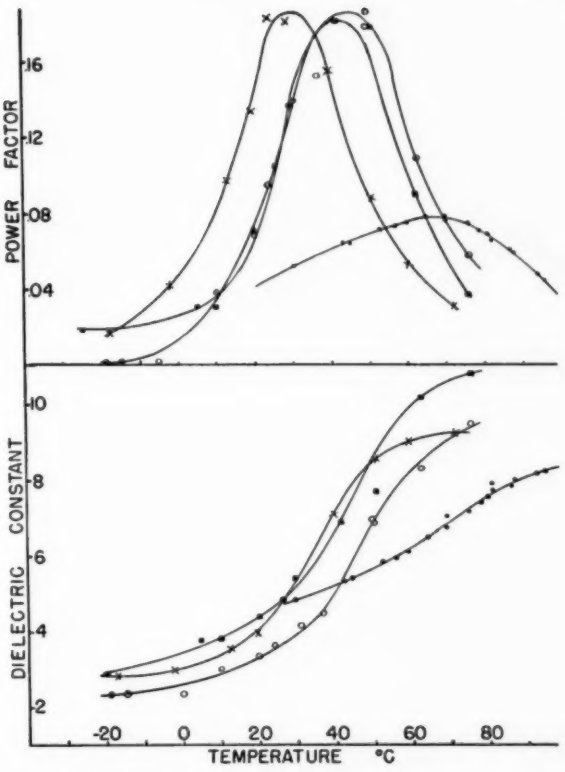

FIG. 4. Dielectric constant and power factor as a function of temperature at 1000 c.p.s. ⊙ .443 TCP; ■ 0.291 DMP; ○ 0.351 TCP; ● 0.368 DLP.

changed the creep properties of the specimen[17] and (b) that the compliance is a function of the applied stress.[4] As a matter of fact, the relationship between load and compliance appears to show significant differences depending on the region in which the material finds itself. In the hard region an increase in the load shifts the compliance-log time curve along the compliance axis toward higher values. In the transition region the slope of the compliance-log time curve decreases with increasing load and in the rubbery range the reverse appears to be true. For these reasons, it seemed more reasonable to study the creep at small and similar elongations by varying the load correspondingly. Some typical results obtained in this manner are shown in Figs. 12 and 13. In the rubbery region the initial elongation is very large, and then changes only slightly with time.§ As one approaches the transition region, the initial elongation becomes less and the change in elongation with time is quite pronounced. In the hard region the change of elongation with time becomes very small, although very few reliable experiments were carried out in this range. In other words, "the curvature" of the elongation-time curve increases as the material proceeds from the rubbery to the transition range and then decreases again going from the transition to the hard region and does not seem to depend very much on the type or amount of plasticizer. Therefore, if one plots the difference in delayed and instantaneous creep as a function of temperature, which was first suggested by Conant and Liska,[18] one obtains a curve very similar to the dissipation factor-temperature curve shown previously and the temperatures of the maxima of both curves are identical. It is believed that the similarity of these two sets of data is more than a coincidence.

The d.c. resistance of the plasticized compositions and of some of the plasticizers was measured as a function of temperature. Over a rather limited temperature range the dependence of the resistance on temperature can be represented by the usual exponential relationships and the slopes of the $\log R - 1/T$ curves which can be represented as an energy of activation, are given in column 10 of Table I. It will be noticed that this quantity increases in all cases with plasticizer concentration, and shows wide variations for different plasticizers at about equal concentration. It should be pointed out, however, that the experimental precision of these measurements was not good enough to establish whether or not the resistance changed in a similar manner as the modulus with changing temperature.

Clash-Berg data and Shore hardness values were

[17] Alfrey, Wiederhorn, Stein, and Tobolsky, J. Colloid Sci. **4**, 211 (1949).

§ The initial elongation at a given temperature correlates satisfactorily with the dynamic modulus at the corresponding temperature.

[18] F. S. Conant and J. W. Liska, J. App. Phys. **15**, 767 (1944).

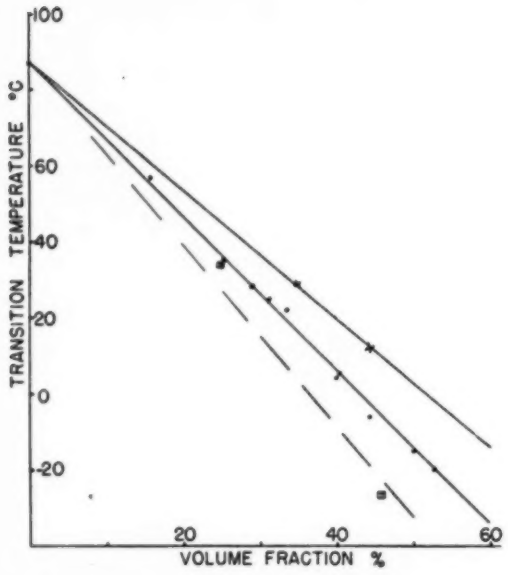

FIG. 5. Dynamic mechanical transition temperature as a function of plasticizer concentration. ● phthalate plasticizers; ⊙ tricresyl phosphate; ⊡ dibutyl sebacate.

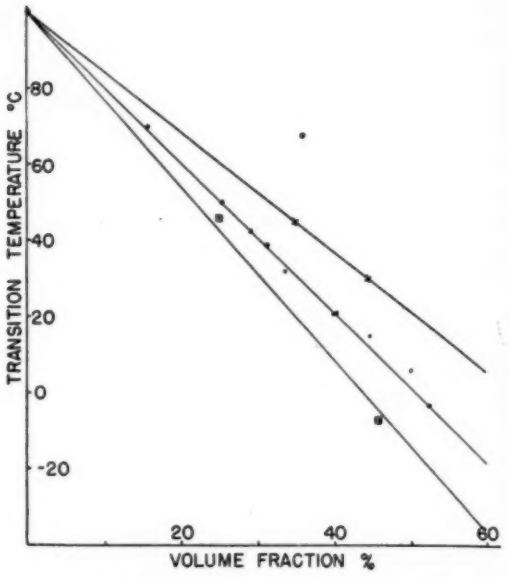

FIG. 6. A.c. electrical transition temperature as a function of plasticizer concentration at 1000 c.p.s. Symbols as in Fig. 5.

obtained as a function of temperature. The shape of the static 5-sec. modulus temperature curve is the same as that for the dynamic modulus temperature curve and the $T_t - c_v$ curves are identical with those shown in Fig. 5, but the absolute values differ by a constant factor. The correlation between Shore hardness and moduli data is not very satisfactory. This is in agreement with previous work on similar compounds[19] and shows the limited usefulness of Shore hardness data to determine moduli of plasticized compositions.

DISCUSSION

During the last few years, several suggestions have been made concerning the mechanism of plasticization; in most cases, these considerations have been concerned with plasticizer efficiency as measured, for example, by the transition temperature, whereas the half-width, or range of plasticization, has not been considered to any great extent. It is the purpose of this section to consider these theoretical attempts in the light of the data presented above.

It has been suggested that the viscosity[5] and the temperature coefficient of the viscosity of plasticizers are of major importance with respect to plasticizer efficiency. However, if the plasticizer efficiency is measured in terms of the transition temperature, then the data given above certainly do not support this contention; see also column 11, Table I. Furthermore, no significant correlation could be established between the temperature coefficient of the viscosity and the temperature dependence of the modulus (or the half-width of the damping curve) in the transition region. Other investigators[6] have tried to show a correlation between the compatibility and plasticizer efficiency; they suggest that the efficiency goes through a maximum as a function of the thermodynamic μ-value. However, it has been shown here that, at least for the first eight members of the homologous phthalate series, the transition temperature is completely independent of the μ-value of the different plasticizers. Furthermore, it is not possible to establish a satisfactory correlation between the μ-value and the slope of the transition temperature-volume fraction curve, not only for the plasticizers studied in this investigation but also for other plasticizer-resin systems reported by other investigators. Nevertheless, the deviation of dilauryl phthalate from the $T_t - c_v$ relationship for all other phthalate plasticizers suggests that the compabitility has some bearing on the transition temperature. Recent investigations[20,21] have brought out rather clearly the relationship between compatibility and plasticizer efficiency: to the extent that the plasticizer is compatible

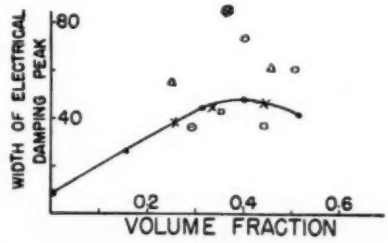

FIG. 7. Half-width of electrical power factor-temperature curve as a function of plasticizer concentration. ■ unplasticized PVC; ⊙ DMP; × DEP; ● DBP; ⊙ DOP; ⊗ DLP; △ DBS; □ TCP; (curve drawn for DBP).

[19] K. H. Reiss, Rubber Chem. Tech. **18**, 398 (1945).

[20] W. R. Richards and P. A. S. Smith, J. Chem. Phys. **18**, 230 (1950).

[21] Merz, Buchdahl, and Nielsen, High Polymer Forum, ACS Meeting (February, 1949).

with the resin, the dependence of the transition temperature on the volume fraction of the plasticizer is within the same range as the data given above. Beyond, what might be called a critical concentration, the transition temperature then remains essentially unchanged as more of the incompatible plasticizer is added to the resin. In other words, as the plasticizer becomes incompatible with the resin it has only a negligible effect on lowering the transition temperature, that is the plasticizer efficiency approaches zero.|| Neither does there exist a close correlation between the half-widths, at equal volume concentration, and the μ-value; it rather appears, on the basis of the data shown in Fig. 7 that the half-width increases with increasing chain length of plasticizers belonging to a homologous series.

Based on the analogy between the a.c. electrical properties and the dynamic mechanical properties, it has been suggested at various times that the mechanical properties of plasticized polymeric systems can be interpreted on the basis of a simple relaxation theory. Assuming such a mechanism, Alfrey[22] has derived an

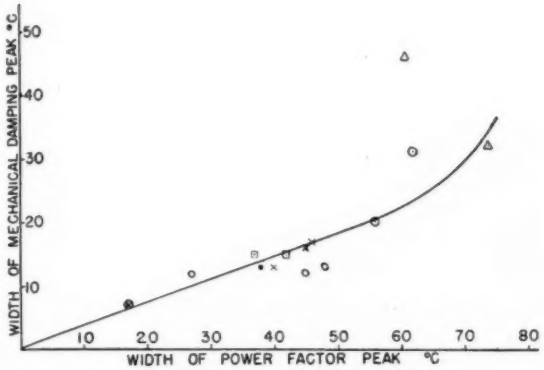

FIG. 8. Correlation between mechanical and electrical half-widths.

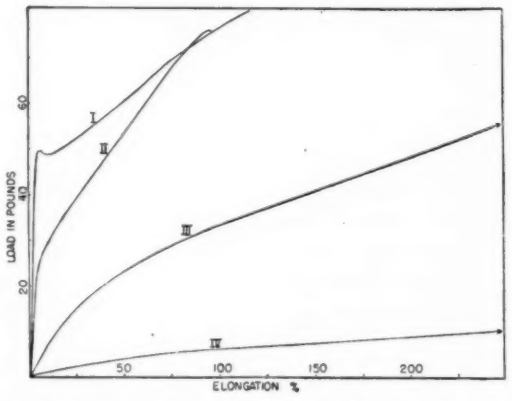

FIG. 9. Typical stress-strain curves of plasticized polyvinyl chloride. I—0.254 DEP; II—0.250 DBS; III—0.402 DOP; IV—0.526 DBP.

|| The μ-value still retains its significance with respect to the compatibility of plasticizers and resins.

[22] T. Alfrey, Jr., J. Chem. Phys. **12**, 374 (1944).

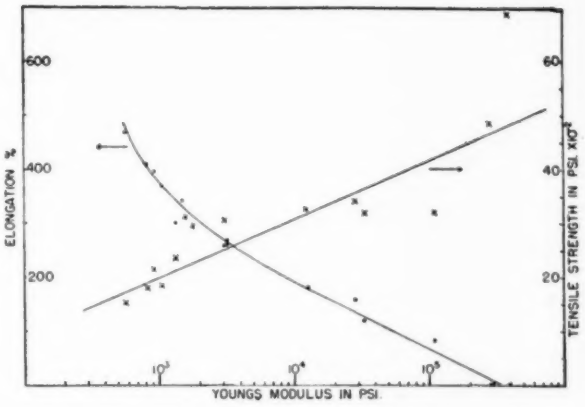

FIG. 10. Ultimate elongation and breaking strength as a function of initial Young's modulus.

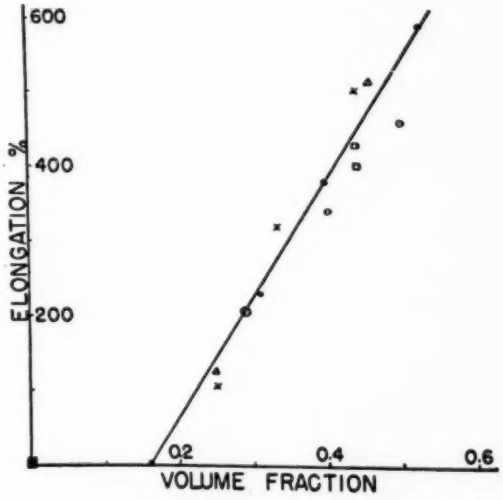

FIG. 11. Ultimate elongation as a function of plasticizer-concentration. ■ unplasticized PVC; ● DBP; ○ DOP; × DEP; ⊙ DMP; □ TCP; △ DBS (curve drawn for DBP).

expression for the compliance as a function of time (or frequency) and molecular weight. If one now considers the transition temperature as an indication of an isoelastic state, one can then derive an expression for the transition temperature as a function of plasticizer concentration, with the result that the reciprocal of the absolute transition temperature must be proportional to the square root of the weight average molecular weight of the mixture. The same relationship has been obtained by Boyer and Spencer,[6] without using Alfrey's compliance equation, by applying Flory's equation of viscous flow of liquid polymers[23] to the transition region in the solid state. A plot of the reciprocal of the absolute transition temperature as a function of the square root of the weight fraction (w_f)** shows that the relationship is more or less linear, although the value for the unplasticized resin does not fall on the linear portion of

[23] P. J. Flory, J. Chem. Phys. **17**, 223 (1949); J. Am. Chem. Soc. **62**, 1057 (1940).

** W_f is proportional to $\bar{M}w$ over a very wide concentration range for polymers of $\bar{M}w > 100{,}000$.

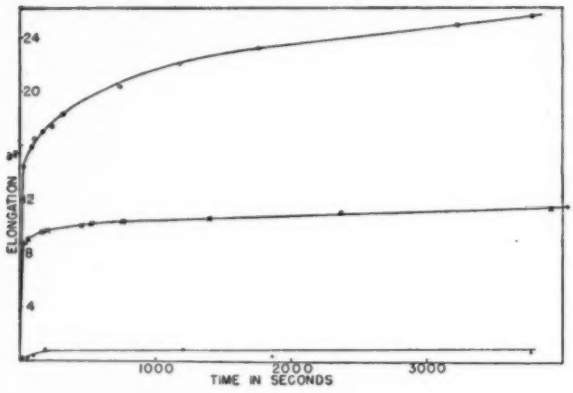

FIG. 12. Elongation as a function of time. Top curve: PVC +0.33 DBP 32°C lower transition range. Middle curve: PVC +0.526 DBP 32°C rubbery range. Bottom curve: PVC+0.158 DBP 22°C hard range.

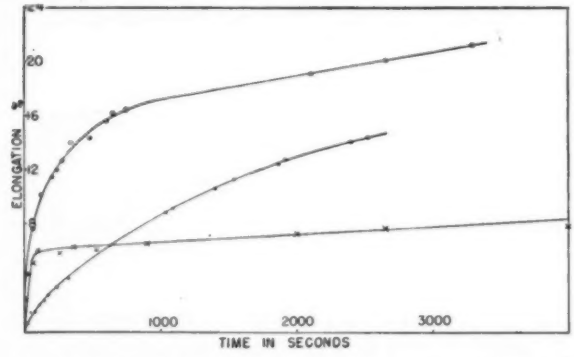

FIG. 13. Elongation as a function of time for PVC+0.254 DEP. Top curve: 32°C lower transition range. Middle curve: 23°C upper transition range. Bottom curve: 45°C rubbery range.

the curve. The square root dependence is due, in both cases, to the use of Flory's equation which, as a result of recent investigations on polystyrene and polyisobutylene, will require some modification.††

Figure 14 shows the transition temperature as a function of the frequency in c.p.s. for several plasticized compositions; the transition temperature changes slowly with frequency, as would be expected on the basis of the relaxation theory. The shape of the curve suggests a very broad relaxation spectrum which has been found to exist for rubber compounds,[24] when investigated over a wide frequency range. However, the frequency dependence of T_t is smaller in the mechanical case than in the electrical.

By and large then, these data could be used to argue in favor of the validity of a relaxation theory were it not for another very important experimental fact, which is the very strong temperature dependence of the modulus or the loss factor in the transition region. It will be recalled that the modulus changes by a factor of 500 to 1000 over a temperature range of 20° to 30°C. This would correspond to an activation energy of the order of 100 kcal. or more, and it is very difficult, if

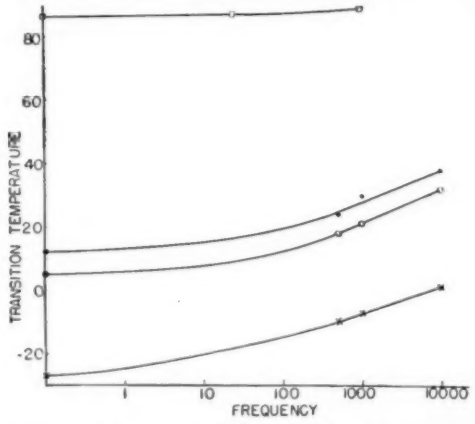

FIG. 14. Transition temperature as a function of frequency. □ unplasticized PVC; ● 0.443 TCP; ○ 0.403 DOP; ⊙ 0.458 DBS.

not altogether impossible, to explain such a high activation energy in terms of a relaxation mechanism. In this connection it seems worth while to point out that the half-width, which is a measure of the temperature dependence in the transition region, is always larger in the electrical case than in the mechanical and on the basis of a relaxation theory one would, at first hand, expect the reverse to be true.

Recently, experimental evidence has been presented in support of the existence of crystalline structure in polyvinyl chloride compositions.[25] One might, therefore, interpret the transition temperature as a melt temperature, and we have tried to fit our data to the equations given by Flory concerning the melting point of polymers.[23] The agreement is not too good using the simplified equation and becomes worse when the more exact equations are being used.‡‡ Furthermore, the existence of a similar transition temperature in completely amorphous polymers, such as polystyrene requires an explanation which is independent of the presence or absence of detectable crystallites. Nevertheless, it seems inescapable to assume some sort of a transition, if for no other reason than to explain the high temperature coefficient of the modulus and loss factor. The nature of this transition is not yet well understood, but it seems to be peculiar to any polymeric or network system.

†† Some years ago, Fuoss (see reference 11) suggested that the product of the mole fraction and a characteristic length of the plasticizer molecule would be a useful quantity to characterize the efficiency of a given plasticizer. When the data given above are treated in this manner, one finds that the transition temperatures of most of the phthalate plasticizers fall on a single curve, but the transition temperature for tricresyl phosphate and dibutyl sebacate fall on a different curve, unless an arbitrary factor is being used to change the length of the plasticizer molecule. This treatment of the data is, therefore, not more advantageous than the treatment given above on the basis of volume fraction.

[24] Witte, Mrowca, and Guth, J. App. Phys. **20**, 481, 486 (1949).

[25] Alfrey, Wiederhorn, Stein, and Tobolsky, Ind. Eng. Chem. **41**, 701 (1949).

‡‡ The dependence of the transition temperature on the volume fraction instead of mole fraction also argues against the application of a simple melting theory.

Letters to the Editor

X-Ray Tube Producing a Beam of X-Rays Convergent to a Point

C. H. Bachman and S. J. Silverman
Department of Physics, Syracuse University, Syracuse, New York
February 9, 1950

A TUBE has been developed which produces a convergent beam of X-radiation in the form of a hollow cone, the apex of which forms a crossover point in space for the radiation. The radiation density at this crossover point is much greater than at any region in space before or after it.

Figure 1 shows the basic idea of operation of the tube. A filament C is arranged coaxial with target T which is in the shape of a truncated cone. Electrons from the cathode are drawn outward radially to strike the interior face of the cone. X-radiation is emitted in all directions. Much of it is cut off by the shape of the tube. In cross section, that which escapes the tube from the right side is shown as D', that from the left side is D''. Region A is more intense since it has overlapping contributions. No radiation appears at B.

The point F is the region of interest. This point, the apex of the projected conical target, contains like the rest of region A, contributions from all portions of the target area. However, a collimating block may be so placed as to remove all radiation from A and consequently D' and D'' except for a sheath of radiation of controlled thickness. This sheath, a hollow cone of radiation, passes through F, crosses over and diverges beyond.

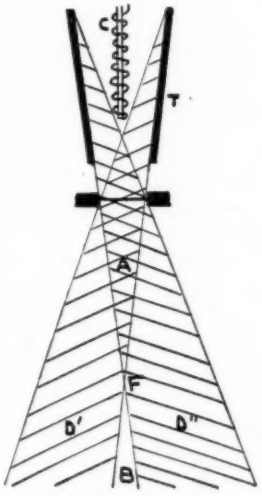

FIG. 1. Schematic ray diagram.

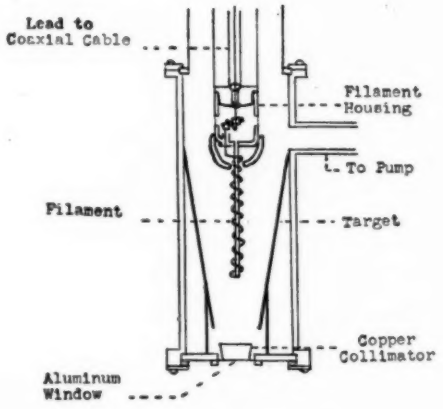

FIG. 2. Tube construction.

FIG. 3. Beam cross sections. Distance from window: (a) 2.5 cm (before crossover); (b) 7.5 cm (near crossover); (c) 11 cm (after crossover).

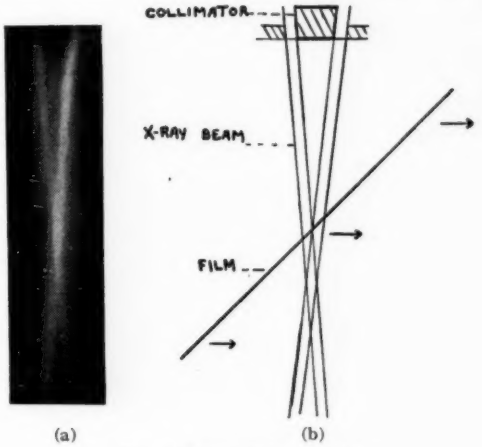

FIG. 4. Crossover presentation.

Figure 2 shows the design features of such a tube and Fig. 3 shows pictures of the beam cross section at several distances from the window. The clover leaf pattern in the scattered outer radiation is due to three radial spacing pins which cross the collimating gap.

Figure 4 was taken by placing a film at 45° to the beam axis and drawing it through the beam. The increased beam density in the crossover region is easily apparent in the negative.

It will be noted that in the tube design no electron focusing problem is encountered; all electrons contribute regardless of where they hit the cone. The very large target area eliminates the customary anode cooling problem or stated conversely, tremendous energy may be used in the tube without being limited by the cooling problem. Also the power rating and x-ray output may be increased by extending the axial length of the conical target since all target areas contribute to the crossover point.

Present efforts are toward explaining some unpredicted radial distribution effects and determining the radiation density distribution in the vicinity of the beam before and after crossover. Other target geometric and methods of utilizing them are also being investigated. More complete results will be published in a future paper.

On Turbulent Jet Mixing in Two-Dimensional Supersonic Flow

D. Bershader and S. I. Pai
Institute for Fluid Dynamics and Applied Mathematics, University of Maryland, College Park, Maryland
February 16, 1950

At the present time techniques for the measurement of turbulent fluctuations in a supersonic stream are still in the developmental stage and our knowledge of turbulent supersonic flow is correspondingly meager. This note reports a preliminary attempt to investigate the problem by comparing a phenomenological theory of turbulence, extended to the supersonic regime, with some experimental results on the density distribution in such flows. Both the phenomenological type of approach and the measurements in this case deal with the mean properties of the turbulent supersonic flow and lead to some information on the general characteristics of supersonic turbulent flow such as the value of the coefficient of eddy kinematic viscosity and the divergence of jets.

Distributions of mean density in several sections of the mixing region of a rectangular, uniform, fully expanded jet of Mach number 1.7,[1] discharging into the atmosphere, have been calculated from measurements made with the Mach-Zehnder interferometer.* The results thus obtained have been compared with predicted density distributions, calculated by use of a theory developed by the second author in reference 2, which makes use of Reichardt's theory of free turbulence.[2]

In the theory, the coefficient of eddy kinematic viscosity ϵ is assumed to be constant over each cross section of the zone of mixing. Its dependence on X, the distance along the axis of the jet, is found by dimensional analysis to be

$$\epsilon = \epsilon_0 X/L \tag{1}$$

where ϵ_0 is a proportionality constant having the same dimensions as ϵ, and L is a reference length.

The theory further predicts that the density ρ, in terms of the free stream density ρ_1, i.e., ρ/ρ_1 is a function of y/X, y being the coordinate normal to the flow axis. Hence if we plot ρ/ρ_1 *vs.* $\sigma y/X$, the experimental results for all sections must lie on one curve. σ is an experimentally determined scale factor whose value depends on the divergence or spreading of the mixing region. The larger the value of σ, the smaller the divergence of the jet. Comparison with the theory shows that

$$\sigma = (U_1 L/2\epsilon_0)^{\frac{1}{2}} \tag{2}$$

where U_1 is the free stream velocity. Other conditions remaining the same, the divergence of the jet decreases with increasing stream velocity.

Figure 1 is a plot of the experimental results for four sections at distances 2, 3, 5, and 7 mm, respectively from the exit of a nozzle approximately 1 by 2 cm in cross section. Superimposed on this is the theoretical curve corresponding to (2). In comparing the experimental data with theory, the following points arise.

(1) Width of the boundary layer at the orifice. The theory assumes zero width of the mixing region at the orifice. In the experiments there exists a 1-mm boundary layer at this point, so extrapolation was employed to obtain the "virtual orifice." This was found to be 10 mm upstream of the actual nozzle exit so that the four test sections were then at X 12, 13, 15, and 17 mm, respectively.

(2) Choice of X axis. Due to the finite dimensions of the nozzle, one would expect a shift of the mixing zone density profile toward the side of the air at rest with increasing X. This is in contrast with a semi-infinite free stream for which a line through the starting point of the jet and parallel to the main flow is an axis of symmetry for the mixing zone and in the present theory corresponds to a density value $\rho/\rho_1 = 0.75$. In the present case, the line $\rho/\rho_1 = 0.75$, chosen as X axis, was found to make an angle θ with the direction of the free stream given by $\theta = 1° 28'$. Gooderum, Wood, and Brevoort,[3] in a similar type of experiment on a jet of Mach number 1.6 found that $\theta = 1\frac{1}{4}°$.

(3) Scale factor. A value of scale factor $\sigma = 17$ was found to give best agreement between theory and experiment. The value of σ in low speed subsonic flow is about 12,[4] showing the smaller divergence of the jet in the present case. (Gooderum *et al.* find $\sigma = 15$.)

From Fig. 1 we see that the experimental points show fairly good agreement with the general shape of the theoretical curve, the deviations becoming more pronounced at the outer edge of the mixing region, which is explained by the fact that in all probability the turbulence is less developed in this region, a phenomenon also found in the case of low subsonic flow.[5]

The calculation of ϵ_0 from the data gives $\epsilon_0 = 7.92$ cm²/sec. To calculate a typical value of ϵ, we find at $X = 17$ mm and $L = 1$ mm that $\epsilon = 134.7$ cm²/sec. which is 1950 times larger than typical values obtained for the laminar coefficient of kinematic viscosity. This is of the same order of magnitude as the ratio of eddy kinematic viscosity to laminar kinematic viscosity for the case of an incompressible fluid.

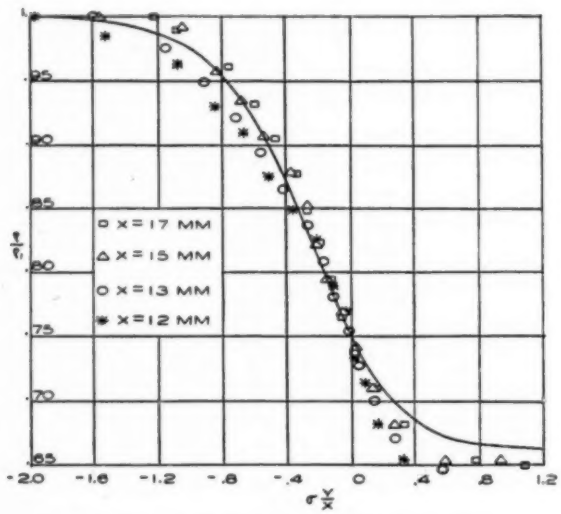

Fig. 1. Density distribution in turbulent mixing region.

[1] D. Bershader, "An interferometric study of supersonic channel flow," Rev. Sci. Inst. 20, 260–275 (April, 1949).
* The experimental data used herein was obtained by the first author in research performed with R. Ladenburg at Princeton University.
[2] S. I. Pai, "Two-dimensional jet mixing of a compressible fluid," J. Aero. Sci. 16, 463–469 (August, 1949).
[3] Gooderum, Wood, and Brevoort, "Investigation with an interferometer of the turbulent mixing of a free supersonic jet," N.A.C.A. Tech. Note 1875 (April, 1949).
[4] H. W. Liepmann and J. Laufer, "Investigations of free turbulent mixing," N.A.C.A. Tech. Note 1257 (August, 1947).
[5] S. Corrsin, "Investigation of flow in an axially symmetrical heated jet of air," N.A.C.A. Wartime Report W-94 (December, 1943).

Use of Brightness Temperatures in Richardson Plots

Henry F. Ivey
Westinghouse Electric Corporation, Bloomfield, New Jersey
February 27, 1950

Quite frequently in experimental investigations it is desired to study the thermionic emission from a material whose spectral emissivity is unknown. In this case the brightness temperature, as determined with an optical pyrometer, cannot be corrected to give true temperature values. It is therefore of interest to investigate the errors in the values of work function, ϕ, and emission constant, A, which result from using brightness

temperatures in making a Richardson plot. The writer is not aware of a published discussion of this kind.

An indication of the magnitude of the effect considered was obtained in the following manner. The emission to be expected from tungsten was calculated at 100° intervals in the temperature range 1200–2800°K, using the constants $\phi=4.52$ volts and $A=60$ amp./cm² deg.². The brightness temperatures corresponding to these points were then determined from the known temperature scale for tungsten.[1] A Richardson plot constructed from these data for emission as a function of brightness temperature showed negligible curvature and yielded values of the constants, as determined by the usual least-squares method, of $\phi'=4.57$ volts and $A'=698$ amp./cm² deg.². It is seen that the apparent work function differs from the true value by only a small amount but the apparent value for the emission constant has been increased by an order of magnitude.

The effect on the emission constants can be predicted theoretically as follows. The brightness temperature, T_B, and true temperature, T, are related by the expression

$$(1/T)-(1/T_B)=(\lambda \log e_\lambda)/c_2=p \log e_\lambda, \tag{1}$$

where e_λ is the spectral emissivity at the wave-length λ used in the pyrometers and natural logarithms are used. The value of the constant p is 4.553×10^{-5} deg.$^{-1}$ for $c_2=1.4385$ cm-deg. and $\lambda=6550$A. When relation (1) is substituted in the Richardson emission equation,

$$J=AT^2e^{-b/T}, \tag{2}$$

the result is

$$J=\frac{AT_B^2e_\lambda^{-bp}}{(1+T_Bp \log e_\lambda)^2}e^{-b/T_B}. \tag{3}$$

It is desired to find the constants b' and A' in the Richardson equation in terms of brightness temperature,

$$J=A'T_B^2e^{-b'/T_B}. \tag{4}$$

The constant b' is given by the relation

$$b'=-\frac{d[\log(J/T_B^2)]}{d(1/T_B)}=T_B^2\frac{d}{dT_B}\log(J/T_B^2), \tag{5}$$

or

$$b'=b-2T_B\left[\frac{T_Bp \log e_\lambda}{1+T_Bp \log e_\lambda}\right]-\frac{T_B^2p}{e_\lambda}\left[b+\frac{2T_B}{1+T_Bp \log e_\lambda}\right]\frac{de_\lambda}{dT_B}. \tag{6}$$

The constant A' can be expressed in terms of b' by elimination between Eqs. (3) and (4).

$$A'=\frac{Ae_\lambda^{-bp}}{(1+T_Bp \log e_\lambda)^2}e^{-(b'-b)/T_B}. \tag{7}$$

In Eqs. (6) and (7), T_B is to be interpreted as the mean of the temperature range over which the measurements are made.[2]

When it is recalled that $e_\lambda<1$, it is seen that the result of the first bracketed term in Eq. (6) is to make the apparent work function ($\phi'=b'/11{,}606$) slightly greater than the true value. The effect of the second term will depend on the sign of de_λ/dT_B and will further increase ϕ' if this quantity is negative (as is the case for tungsten). The effect of the de_λ/dT_B term will be greater the greater the work function. The magnitude of both terms increases for higher values of the measuring temperature and lower values of the emissivity.

In expression (7) for A', the predominant factor is the term

$$e_\lambda^{-bp}=e_\lambda^{-0.528\phi}. \tag{8}$$

It is seen that the apparent emission constant will always be larger than the true value and that the ratio will be larger the higher the work function and the lower the emissivity. From the complete expression (7) it can also be seen that A' increases with increasing values of the measuring temperature.

A check on the numerical example discussed earlier can be obtained by substituting the values of the spectral emissivity (i.e., 0.438) and of de_λ/dT_B (i.e., 2.32×10^{-5} deg.$^{-1}$) for tungsten[1] at 2000°K ($T_B=1860$°K) in Eqs. (6) and (7). The results are $\phi'=4.58$ volts and $A'=746$ amp./cm² deg.², in good agreement with the values $\phi'=4.57$ volts and $A'=698$ amp./cm² deg.² obtained numerically. If the de_λ/dT_B term is neglected in the expression for ϕ', one obtains $\phi'=4.54$ volts and $A'=578$ amp./cm² deg.². In general, therefore, the effect of this term is not negligible.

In conclusion it may be said that the use of brightness temperatures instead of true temperatures in the construction of Richardson plots will result in apparent work functions which differ only slightly from the true value, but the apparent emission constant obtained from such a plot may be greater than the real value by more than an order of magnitude. These errors will be greater the higher the measuring temperature and the lower the spectral emissivity of the material in question. In the case of the emission constant the error will also be greater the higher the work function. The variation of the emissivity with temperature also contributes an appreciable effect.

[1] Symposium (sponsored by American Institute of Physics), *Temperature. Its Measurement and Control in Science and Industry* (Reinhold Publishing Corporation, New York, 1941), p. 1318.

[2] In terms of true temperature, Eqs. (6) and (7) may be written

$$b'=b-2T\left[\frac{Tp \log e_\lambda}{1-Tp \log e_\lambda}\right]-(b+2T)\frac{(T^2p/e_\lambda)(de_\lambda/dT)}{1+(T^2p/e_\lambda)(de_\lambda/dT)}, \tag{6'}$$

$$A'=A(1-Tp \log e_\lambda)^2e_\lambda^{(b'-2b)p}e^{-(b'-b)/T}. \tag{7'}$$

Stroboscopic Mapping of Time-Variable Fields

L. Marton and D. L. Reverdin
National Bureau of Standards, Washington, D. C.
March 8, 1950

SEVERAL publications appeared[1–3] on the mapping of steady electrostatic or magnetic fields using the deflections of a viewing electron-beam. We have contemplated for some time the possibility of extending the method to include time-varying fields by the use of a stroboscopic technique. A need for this modification arose in an extensive series of studies of the static field of a cut-off magnetron.[4] In these experiments an electron beam was sent axially through the static magnetron in order to view the space-charge field. The filament heating current, however, generated a magnetic field which masked the space-charge field completely. To eliminate the effect of the filament heating current, the heating

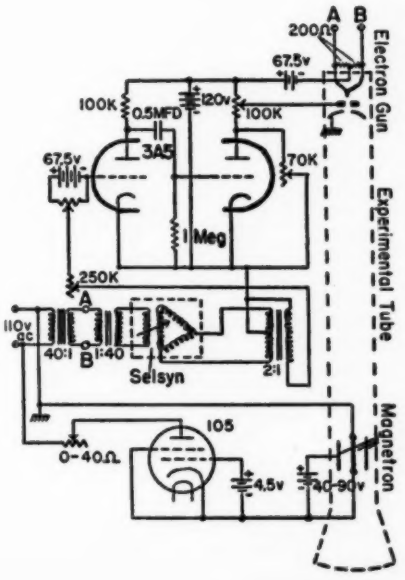

FIG. 1.

was produced by a half-wave rectifier, and the observation of the space-charge distribution was restricted to the other half-cycle.

Figure 1 shows a schematic circuit diagram. Pulse operation of the observing electron beam was achieved by a square-wave modulation of the electron gun bias potential.

An interesting observation while carrying out these experiments was that the image appeared considerably sharper when the stroboscopic method was used than in a steady-state observation. No complete explanation for the sharpening of the image can be offered at this time, but there is good indication that the pulsing of the observing beam reduced the effect of 60-cycle stray fields always present in the laboratory.

The stroboscopic method is applicable in principle to the observation of any repetitive, time-variable fields up to very high frequencies. At very high frequencies there are two serious limiting factors. One is the speed with which the current of the observing beam can be modulated; the second is due to the transit time of the electrons in the field to be observed. The first limitation is the less serious one, since by beam deflection methods instead of biasing of a control electrode, very high frequency pulses can be generated. The second limitation is the more serious one because it requires an increasingly stiff electron beam to keep the transit time low while the sensitivity of the method varies inversely with beam stiffness. A vague estimate of the practical upper frequency limit at which the method can be applied without undue experimental difficulties can be set at about 300 Mc, the present upper limit of oscillograph operation.

[1] L. Marton, J. App. Phys. **19**, 687 (1948).
[2] L. Marton, J. App. Phys. **19**, 863 (1948).
[3] L. Marton and S. H. Lachenbruch, J. App. Phys. **20**, 1171 (1949).
[4] Doctoral dissertation submitted in February, 1950 by D. L. Reverdin to the George Washington University, Washington, D. C. Part of it is scheduled to be published in an early issue of this Journal.

Announcement

From time to time, the Institute has received inquiries from subscribers for information as to where and how they may have their copies bound. After investigation the Institute has found that this may be best accomplished by selecting a capable bindery that will work to our specifications and produce a well-bound volume at as low a price as possible. The necessary arrangements have been completed with the Book Shop Bindery, 308 West Randolph Street, Chicago 6, Illinois.

The volumes will be bound in the best grade of washable buckram with facsimile gold stamping on the spine and the subscriber's name in gold on the front cover. A distinctive color for each of the Journals has been selected as listed below. Advertising matter and covers are removed before binding. The price of $3.00 per volume applies to any of these journals regardless of size. Issues, comprising complete volumes, should be sent by prepaid express or parcel post to the Book Shop Bindery. Bound volumes will be shipped approximately 30 days after receipt. Return transportation will be prepaid when remittance accompanies order.

No deviation in color or specification can be allowed in view of the favorable price.

Physical Review	Green
Reviews of Modern Physics	Orange
Journal of the Optical Society	Brown
Journal of the Acoustical Society	Orange
American Journal of Physics	Black
Review of Scientific Instruments	Grey
Journal of Chemical Physics	Blue
Journal of Applied Physics	Red
Physics Today	Purple